Elastic Constants of Architectural Fabrics for Design Purposes

Von der Fakultät für Ingenieurwissenschaften, Abteilung Bauwissenschaften,
der Universität Duisburg-Essen
zur Erlangung des akademischen Grades

Doktor-Ingenieur

genehmigte Dissertation

von

Dipl.-Ing. Jörg Uhlemann
aus Oberhausen

Referentin:	Univ.-Prof. Dr.-Ing. habil. Natalie Stranghöner
Korreferent:	Univ.-Prof. Dr.-Ing. Kai-Uwe Bletzinger
Eingereicht:	16. Oktober 2015
Mündliche Prüfung:	02. März 2016

Abteilung Bauwissenschaften der Fakultät für Ingenieurwissenschaften
Institut für Metall- und Leichtbau
Univ.-Prof. Dr.-Ing. habil. Natalie Stranghöner

Abstract

Architectural tensile surface structures – often made from coated woven fabrics – carry external loads only by activating tensile stress in the membrane plane, typically in the form of biaxial stress states. One important and challenging aspect of structural fabric analysis is the determination of stiffness parameters that sufficiently model the stress-strain behaviour for these stress states. The particular difficulty is that coated woven fabrics exhibit very complex stiffness behaviour. In general, it is nonlinear, nonelastic and considerably anisotropic. Nevertheless, current membrane structure design practice is based on a simplified orthotropic linear-elastic plane stress relationship, where the elastic constants are “tensile modulus” and “Poisson’s ratio”. The elastic constants must be determined for each material using biaxial tensile tests.

The intention of the present work is to develop principles for determining elastic constants that closely approximate the actual fabric stress-strain response for any fabric structure and all common types of coated woven fabrics. The focus lies on the most commonly utilised materials: PVC coated polyester fabrics and PTFE coated glass fibre fabrics.

The foundation of the present work is a comprehensive survey of the structural behaviour of all types of membrane structures – anticlastic, synclastic and plane – as well as of the stiffness properties of coated woven fabrics for architectural applications. Discussion of the mechanical background to the constitutive law for orthotropic linear-elastic plane stress provides the frame of application for elastic constants, particularly in relation to the boundaries of the Poisson’s ratios. An analysis of internationally established biaxial test and evaluation procedures identifies the strengths and weaknesses of current practice. Gaps in knowledge are closed with experimental investigation into the full range of commonly used architectural fabrics.

Combining all insights, principles for refined biaxial test and evaluation procedures are stated with the objective of determining elastic constants for design purposes. As a basic principle, procedures for anticlastic structures and for synclastic or plane structures are developed separately. Their commonality lies in the fact that they are based on what is defined as the stable state of the fabric. Using stable state elastic constants makes it possible to calculate with the nominal prestress in the fabric structure analysis.

Example application of the refined procedures illustrates that deviations between the measured and calculated strain on a specific evaluation stress level are low throughout. This is striking evidence that linear elastic constitutive law can actually be very useful in approximating the stress-strain behaviour of all common PVC coated polyester fabrics and PTFE coated glass fibre fabrics.

Kurzfassung

Membrantragwerke – häufig hergestellt aus beschichteten Geweben – tragen externe Lasten nur durch Zugspannungen in der Membranebene ab, typischerweise in Form von biaxialen Spannungszuständen. Ein wichtiger und herausfordernder Aspekt der Tragwerksberechnung ist die Bestimmung von Steifigkeitsparametern, die das Spannungs-Dehnungs-Verhalten der Gewebe in diesen Spannungszuständen in geeigneter Weise modellieren. Dies gestaltet sich für beschichtete Gewebe wegen ihres sehr komplexen Steifigkeitsverhaltens äußerst schwierig. Im Allgemeinen verhalten sich Gewebe nichtlinear, nichtelastisch und deutlich anisotrop. Gleichwohl basiert die aktuelle Membranbaupraxis auf einem vereinfachten orthotropen, linear-elastischen, ebenen Materialgesetz, das auf den elastischen Konstanten “Verformungsmodul” und Querkontraktionszahl beruht. Die elastischen Konstanten müssen für jedes Material in biaxialen Zugversuchen bestimmt werden.

Das Ziel der vorliegenden Arbeit ist die Entwicklung von Prinzipien zur bemessungsorientierten Bestimmung elastischer Konstanten derart, dass sie das tatsächliche Spannungs-Dehnungs-Verhalten von allen üblichen Architekturgeweben für alle Tragwerksformen gut approximieren. Der Fokus liegt dabei auf den gebräuchlichsten Produkten: PVC-beschichtete Polyestergewebe und PTFE-beschichtete Glasfasergewebe.

Das Fundament der vorliegenden Arbeit ist sowohl eine umfassende Studie des Tragverhaltens aller typischen Membranbauformen – antiklastisch, synklastisch und eben – als auch der Steifigkeitseigenschaften der Architekturgewebe. Eine Erörterung des mechanischen Hintergrunds zum orthotropen, linear-elastischen Materialgesetz bei Anwendung auf den ebenen Spannungszustand liefert die Randbedingungen für die Anwendung der elastischen Konstanten, besonders im Bezug auf Grenzwerte für die Querkontraktionszahlen. Eine Analyse internationaler Biax-Versuchs- und Auswerteprozeduren identifiziert die Stärken und Schwächen der aktuellen Praxis. Vorhandene Wissenslücken werden durch experimentelle Untersuchungen an der ganzen Bandbreite der gebräuchlichen Gewebetypen für die textile Architektur geschlossen.

Aus der Kombination aller Erkenntnisse werden Prinzipien für fundierte Biax-Versuchs- und Auswerteprozeduren abgeleitet. Das Ziel ist die Bestimmung von elastischen Konstanten, die als Eingangsparameter in der Bemessung dienen. Grundsätzlich wird zwischen Prozeduren für antiklastische und synklastische bzw. ebene Strukturen unterschieden. Beiden ist allerdings gemein, dass sie den “eingespielten Zustand eines Gewebes” nutzen. Erst die Nutzung von elastischen Konstanten im eingespielten Zustand ermöglicht es, die Strukturberechnungen auf den nominellen Vorspannungszustand zu gründen.

Beispielhafte Anwendungen der weiterentwickelten Prozeduren verdeutlichen, dass die Abweichungen zwischen gemessenen und berechneten Dehnungen auf einem

zuvor für die Auswertung definierten Spannungshorizont durchweg klein sind. Dies zeigt eindrucksvoll, dass das linear-elastische Materialgesetz durchaus sehr geeignet ist, auch das Spannungs-Dehnungs-Verhalten aller typischen PVC-beschichteten Polyester- und PTFE-beschichteten Glasfasergewebe zu beschreiben.

Preface and Acknowledgements

This work has been prepared and written during my work as research associate at the Institute for Metal and Lightweight Structures at the University of Duisburg-Essen. It would not have been possible without the great support of many people.

First I would like to thank my doctoral supervisor Professor Natalie Stranghöner for giving me her overwhelming support, technically and personally. Her straightforward, powerful and winning leadership of the institute is a source of strength and confidence and makes conducting research there a great pleasure. I am additionally grateful to Professor Kai-Uwe Bletzinger for acting as co-supervisor and Professor Jörg Schröder in his capacity as chairman of the examination board.

Professor emeritus Herbert Schmidt first inspired this topic and made fundamental contributions to it in the early stages of the project.

However, this work would not have been possible without the generous support of Klaus Saxe, until recently head of the Essen Laboratory for Lightweight Structures (ELLF). He shared with me his vast experimental experience and immense knowledge of tensile membrane structures and architectural fabrics during many scientific discussions.

I am thankful too for the valuable support of our ELLF team, consisting of Thomas Homm, Stefanie Schülpen and Thomas Hens, as well as Christian Schoedon from our steel structures laboratory. They all helped me very much with the execution of the numerous experimental tests and measurements.

To my colleagues at the institute I wish to express my gratitude for the wonderful working atmosphere and for keeping me free from other tasks whenever I needed it in the final phase of this work. My thanks similarly go to my former and current student assistants Amin Jejji, Sebastian Lattberg and Kerstje vom Hofe for all the helpful calculations, evaluations, programmings, drawings etc. they carried out for me over the years, and to Amanda Dixon El Hachem for her excellent proofreading.

It is a pleasure also to extend sincere thanks to the material producers who so generously provided me with material for experimental testing. In alphabetical order they are: Mehler Texnologies GmbH, Hückelhoven, Germany, Sattler AG, Gössendorf, Austria, Serge Ferrari S.A.S, La Tour du Pin Cedex, France and Verseidag-Indutex GmbH, Krefeld, Germany. They made it possible for me to ensure the serviceability of the refined biaxial test procedures for the full range of commonly used architectural fabrics.

Finally, I wish to thank my parents Rolf and Helga Uhlemann for wholeheartedly supporting me in everything I do, and my unique life companion Stefanie Riedel for her patient, tender and loving care and for keeping my mind free.

Oberhausen, in March 2016 Jörg Uhlemann

Contents

List of Figures

List of Tables

Symbols

Latin

E Young's modulus for material in [N/mm^2] or
tensile modulus for a structural component such as the composite coated fabric, here in [kN/m], or
error in conjunction with the correlation analysis routine [%]

f tensile strength [kN/m] or

deflection

G shear modulus [kN/m]

n load cycle number [-]

p prestress [kN/m]

Greek

$\Delta\varepsilon$ strain difference between final strain and starting strain during a loading sequence or within a chosen stress interval [%]

$\Delta\sigma$ stress increment or stress interval [kN/m]

ε strain [%]

σ membrane stress, given in force per unit width [kN/m] as no defined section height exists

ν_{xy} warp Poisson's ratio describing strain in warp direction due to stress in fill direction [-], assuming that warp is aligned with x and fill is aligned with y

ν_{yx} fill Poisson's ratio describing strain in fill direction due to stress in warp direction [-], assuming that warp is aligned with x and fill is aligned with y

Indexes

Latin

c	carrying direction in anticlastic structures
d	design value
e	evaluation level
f	fill direction
i	initial
irr	irreversible
k	characteristic value
m	mean value
r,del	delayed reversible (viscoelastic)
r,spon	spontaneous reversible (elastic)
s	supporting direction in anticlastic structures
t	tensile
w	warp direction
x,y,z	coordinate directions
	x-direction in the mechanical model is aligned with the warp direction in the fabric, y-direction in the mechanical model is aligned with the fill direction in the fabric

Greek

ε	strain
ξ,η,ζ	coordinate directions

Numerical

23	room temperature 23°C

Abbreviations

LSM	Least Squares Method
PA	polyamide
PE	polyethylene
PES	polyester
PET	polyethylene terephthalate
PTFE	polytetrafluoroethylene
PVC	polyvinylchloride
SIR	stress increment ratio
THV	tetrafluoroethylene-hexafluoropropylene-vinylidene-fluoroide
UV	ultraviolet

1 Introduction

1.1 Topic

Both architecture and aerospace applications use tensile membrane elements as structural components. Stiffened by a combination of form and prestress, tensile membranes are increasingly being built as wide-span, architecturally appealing and sustainable lightweight structures. The shape is traditionally characterised by spatial curvature. This allows for large, column-free spans in roofing structures. But today low-curvature or even plane membrane elements are becoming increasingly common, e. g. for facades or billboards.

Structural tensile membranes are always prestressed. Prestress is essential in order to stiffen the membrane and thus reduce its inherent large deflections and prevent wrinkling. The required prestress level is defined by the structural engineer. A distinction is basically made between two types of prestress relating to specific shapes: one is mechanical prestress induced by spanning the membrane over a supporting structure, e. g. by applying tension flanges. This technique is used for flat and anticlastic (e. g. saddle-shaped) structures; the other is pneumatic prestress by inflation, used in synclastic structures like air domes, cushions or inflated beams.

Materials used for structural membranes are essentially fabrics and foils, see Figure 1. Fabrics for membrane structures are made primarily of woven or laid yarns, the latter also known as non-crimp fabric or scrim. In exceptional cases, knitted and warp-knitted fabrics can be employed, e. g. for indoor, low-span or temporary structures, but their large strain limits opportunities for architectural application.

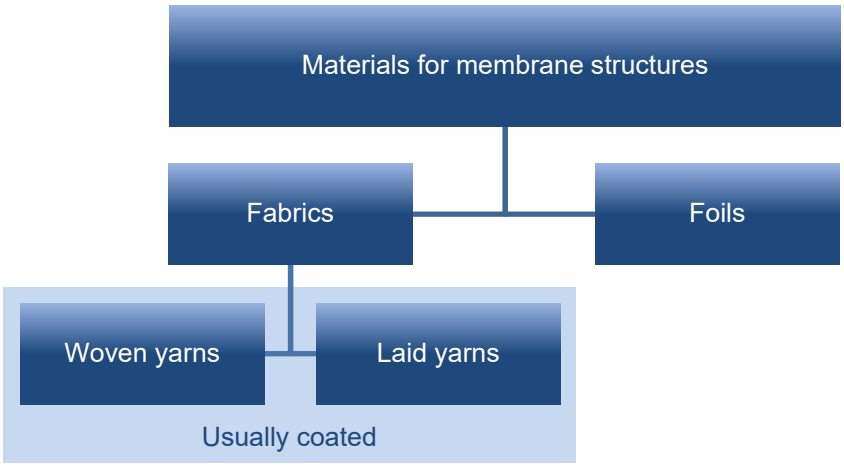

Figure 1 Materials for membrane structures

For outdoor applications, woven and laid fabrics are usually coated to enhance properties like weather resistance, protection against environmental impacts, weldability etc. Coated woven fabrics are mainly used in the typical outdoor fields of application in textile architecture: light wide-span roofs, air-supported structures and facades. Fabrics can also be left uncoated. However, except where special yarn

material is used, uncoated fabric is more suitable for indoor structures like exhibition stands or acoustic membranes, or for outdoor structures such as awnings, which have lower requirements for life span or degree of protection. To improve the watertightness, uncoated fabric products can be supplied with a water repellent finish.

Coated fabrics are available with a waterproof, closed surface or with an open mesh. In the open mesh the coated yarns are arranged with spacing, which increases translucency and offers permeability. Foils are usually applied in smaller span structures like cushions. Large-surface structural elements can be achieved by assembling several cushion elements.

The present work focuses on coated woven fabrics for architectural applications. Examples of membrane structures made of coated fabrics are illustrated in Figure 2. On the left it shows a mechanically prestressed roofing structure with a sequence of saddles (top) and a facade made of plane frames spanned with coated open mesh fabrics (bottom). On the right, spherical air-supported domes carried directly by the air pressure (top) and a dome carried by inflated beams (bottom) are shown as pneumatically prestressed structures.

Mechanically prestressed structures **Pneumatically prestressed structures**

Source: formTL ingenieure für tragwerk und leichtbau GmbH, © Michele D'Ottavio

© CENO Membrane Technology GmbH

© J. Uhlemann

© J.-C. Thomas

Figure 2 Left: mechanically prestressed membrane structures: saddle-shaped roof structure (top), plane facade structure (bottom); right: pneumatically prestressed membrane structures: air-supported domes (top), inflatable beam structure (bottom)

One important and challenging aspect of the design process for tensile membrane structures is determining the material stiffness parameters. As structural membranes are stressed biaxially, biaxial stiffness parameters are required in the design process. Coated technical textiles for use as architectural fabrics display highly nonlinear, viscoelastic and anisotropic stress-strain behaviour under biaxial tensile stresses in the main fabric directions. These are the directions of the (usually) orthogonally arranged yarns. Nevertheless, the inhomogeneous coated textiles are modelled as a homogeneous continuum in state-of-the-art structural analyses. Herein the nonlinear and viscoelastic behaviour of these composites is simplified as linear-elastic within a plane stress state in which the elastic constants are the “tensile modulus” and the “Poisson’s ratio”. The elastic constants are determined for each material using biaxial tensile tests. They are known to depend on the stress ratio and – as different stress ratios occur in structures with different shapes – hence are correlated to the structural shape.

Several – more or less standardised – biaxial test protocols with related evaluation procedures have been published internationally in the last two decades. Moreover, numerous unpublished concepts created by design offices are applied in daily design practice. However, the various approaches differ considerably, and so too do the resulting sets of elastic constants. This situation is unsatisfactory and leaves the design engineer with no guideline for optimal and safe modelling of material behaviour within the simplified linear-elastic approach.

Approximating the complex stress-strain behaviour of coated architectural fabrics using anisotropic linear-elastic material law is likely to remain in design practice, even when more refined methods are developed in the future. There are three reasons why:

1. Material linear analysis today ensures short computation time and robust computation;
2. Determining elastic constants is easy compared to more refined methods which partially require numerous material parameters; and
3. Elastic constants will always be needed for simplified and approximated "manual" structural control.

The last aspect will remain an important tool in design.

1.2 Objective and method

Various aspects of the material behaviour of coated woven fabrics and the optimal way to model it with elastic constants have not been studied to date. The aim of the present work is to close these gaps in knowledge and – bringing together the state of the art and the latest findings – to establish principles for determining so called “design elastic constants”. “Design elastic constants” are referred to as one or more sets of elastic constants that are determined in order to sufficiently model the

material behaviour in a specific membrane structure as part of the structural analysis. Linear elastic modelling has been known up to now to provide a rather rough approximation of the highly nonlinear stress-strain behaviour of fabrics. However, it will be demonstrated in this work that a good approximation of the stress-strain paths is possible under certain conditions. This will be made possible by the inter-coordinated development of a biaxial test protocol. Hence, the final objective of this thesis is to derive principles for refined biaxial test protocols together with related evaluation procedures. The biaxial test protocols should be able to cover the structural behaviour of the most important typical structural forms in the field of membrane structures. The aim of the evaluation procedures is to determine the design elastic constants from the measured stress-strain paths.

To achieve this objective, a thorough investigation and consolidation of the material behaviour, methods of material testing and evaluation, and the mechanical fundament of the material model used is necessary. This comprehensive knowledge has not existed up to now in relation to membrane structures made from coated fabrics.

Elastic constants can only describe the gradient of the stress-strain paths of a linear-elastic material. But coated woven fabrics are well known to also display nonlinear and inelastic behaviour. Therefore, any method for the determination of design elastic constants must be embedded in an overall concept that also considers the handling of nonlinearity and residual strains or prestress, respectively, in the design process.

Chapter 2 provides a brief introductory description of the design and the load-bearing behaviour of typical membrane structures made particularly from coated woven fabrics. Emphasis is given especially to the importance of stress ratios in a fabric structure and the influence of transverse strain of fabrics on the distribution of stress ratios.

The fundamentals of coated woven fabrics are presented in Chapter 3 together with current knowledge of their stress-strain behaviour.

Chapter 4 gives a detailed state-of-the-art report on possibilities for modelling the material behaviour and the relevant parts of the theory of anisotropic elasticity. One main concern is the demonstration of restrictions on elastic constants for the most relevant material classes related to the modelling of coated woven fabrics: orthotropic, transversely isotropic and isotropic materials. Further discussion considers the restriction of the theory of elasticity to small strain.

The experimental part of this work begins with a survey of the investigated fabrics in Chapter 5, which provides a basic characterisation of the materials.

The subsequent chapter 6 documents the results of experimental investigations into the uniaxial and biaxial material behaviour as well as the structural behaviour of

orthogonally loaded prestressed membrane strips. Indepth knowledge of the fundamental stress-strain characteristics of the materials under consideration and the interrelations between load cycles, prestress, maximum stress and maximum deflection in a membrane structure are taken as a basis for assessing existing procedures in the determination of stiffness parameters as well as for developing more refined methods.

In Chapter 7, established biaxial test procedures (including test protocols and evaluation procedures) are analysed, compared and discussed with regard to their applicability for design purposes. This is primarily done by means of experimental validation.

Finally, based on the findings of the previous chapters, refined biaxial test protocols, one for anticlastic and one for synclastic or plane fabric structures, are developed in Chapter 8. The documentation is accompanied by development of an evaluation methodology. Numerical recommendations are provided. Application of the new procedures is demonstrated in examples.

Chapter 9 provides the conclusions and an outlook on further research issues with regards to modelling the stiffness behaviour of architectural fabrics within the structural analysis.

Some parts of the present work were already published in various papers. In the event that entire chapters are reproduced, the reference is marked in the heading. Other verbatim quotations are marked with quote signs and the reference is provided.

2 Characteristics of membrane structures

2.1 General

The basic principles of tensile structures are double curvature, i. e. a curved shape in two orthogonal structural directions, and prestress. The combination of curvature and prestress enables equilibrium states under external loads in all directions with only tensile stresses in the structural membrane. The curvature furthermore contributes to the geometrical stiffness of tensile structures. A distinction is made between two types of doubly curved shapes: those with a positive Gaussian curvature, called synclastic, and those with a negative Gaussian curvature, called anticlastic, see Figure 3. The Gaussian curvature at one point of a curved surface is defined as the product K of the principal curvatures k_i in the two orthogonal principal directions i at the given point: $K = k_1 \cdot k_2$, where k_i is the reciprocal of the radius R_i of an actual or approximate circular segment. The product is positive if the origins of both radii are on the same side of the membrane and negative if on opposite sides.

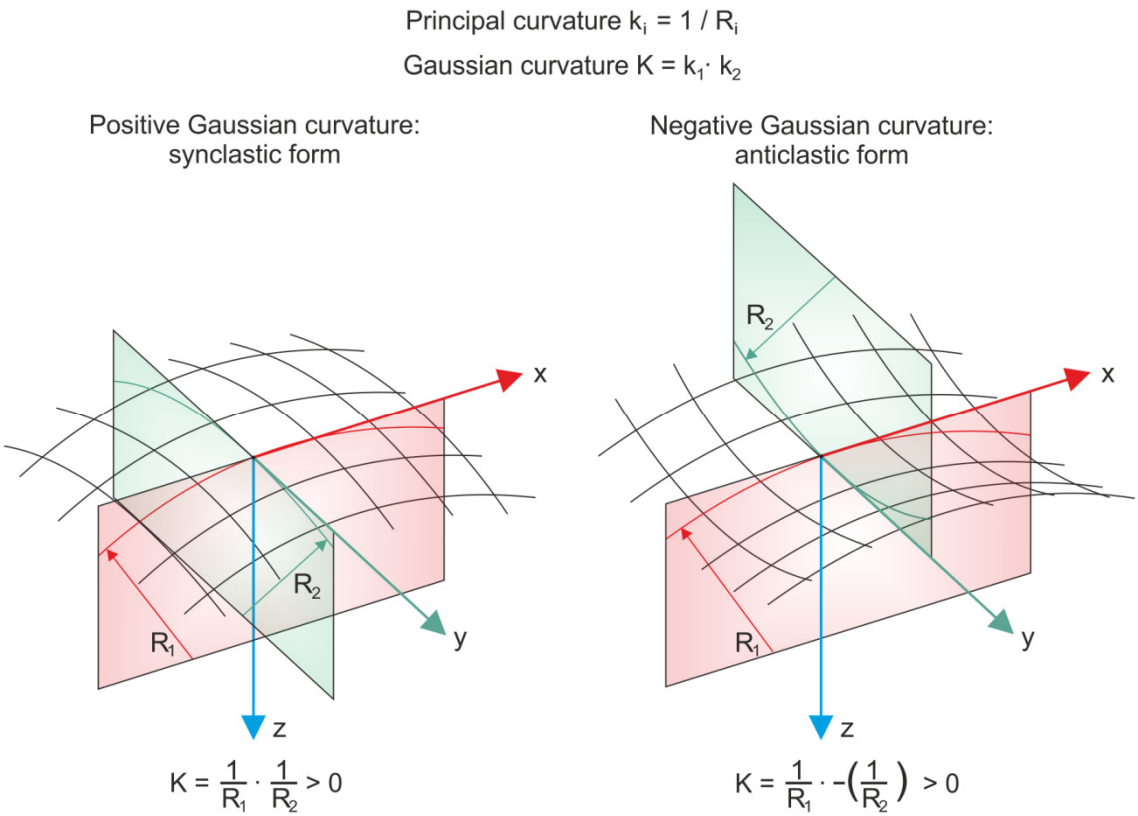

Figure 3 Positive and negative Gaussian curvature, for synclastic and anticlastic forms respectively

Prestress is essential as it enables the creation of the planned shape. Moreover, prestress introduces stiffness and thus reduces deformation and vibration. Biaxial prestress prevents wrinkles.

Only a few types of membrane structures diverge in some way from the above stated principle of (double) curvature. Inflatable beams, for instance, usually have a

cylindrical section, i. e. a single curvature. Flat membranes are also increasingly being built today, e. g. for facade structures, which have a synclastic shape under external load. This is because equilibrium of forces in a tensile structure with a load perpendicular to the membrane plane is only possible with curvature. If the very low geometrical stiffness is taken into account, flat membranes are entirely suitable for structural use.

Synclastic forms are prestressed pneumatically, i. e. by inflation. Anticlastic forms are prestressed mechanically. With a few exceptions, the terms “synclastic” and “pneumatically prestressed” can be used as synonyms. The same applies for the terms “anticlastic” and “mechanically prestressed”. One exception to be mentioned here is the plane. The plane which is neither synclastic nor anticlastic can only be prestressed mechanically.

Most membrane structures consist of a primary and secondary structure, see Figure 4. The primary structure is the structural part over which the membrane is spanned. This part is mostly constructed from steel beams or steel cables. The secondary structure is the structural membrane itself. Some membrane structures, mainly pneumatically prestressed structures such as air-supported domes or inflatable structures, do not require a primary structure.

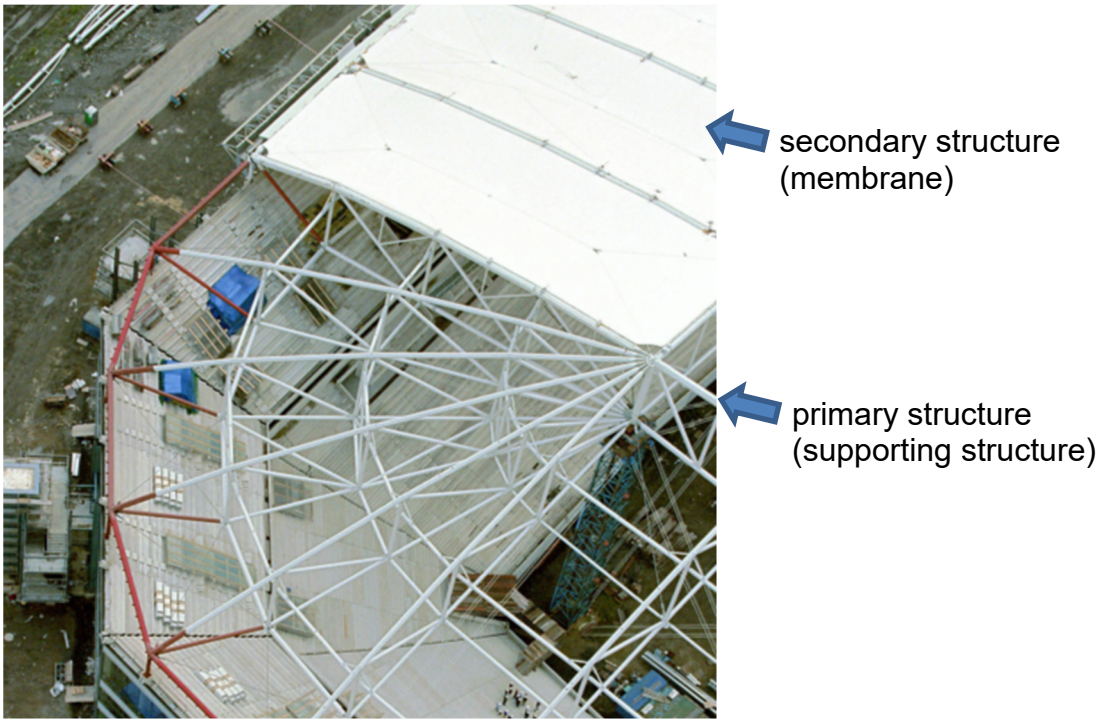

Figure 4 Example of primary and secondary structure for a membrane stadium roof (©FC Schalke 04)

2.2 Design and compensation

Membrane structures carry external loads only via tensile stresses in the membrane surface. Architectural fabrics are flexible, i. e. they have no bending stiffness, and they do not exhibit compression rigidity. For this reason, the design process for

membrane structures differs significantly from that for bending stiff structures, see Figure 5. A form-finding process is the first step. The aim is to determine the equilibrium shape depending on the geometry of the boundaries and the prestress level – or, to be more precise, the ratio of the prestress levels in the main structural directions. The resulting structure is the basis for all subsequent structural analyses. During this procedure the required nominal prestress level is defined by the design engineer, possibly together with the architect and with assistance from the manufacturer and the material producer.

As a doubly curved membrane surface is assembled from strips of plane fabric, cutting patterns must be generated and the curved surface developed. In order to ensure for the entire lifetime that the prestress does not fall below the nominal value defined by the design engineer, the cutting patterns are compensated. Compensation means determining the required undersize of the plane unstressed patterns by reducing the pattern dimensions so that the desired initial prestress level is achieved after straining the material to the nominal geometry during installation. After a period of time and several load incidents, the initial prestress will tune down to the nominal prestress. The design procedure is completed by the construction engineering. The design flow presented here is a simplification. It may be iterative in practice.

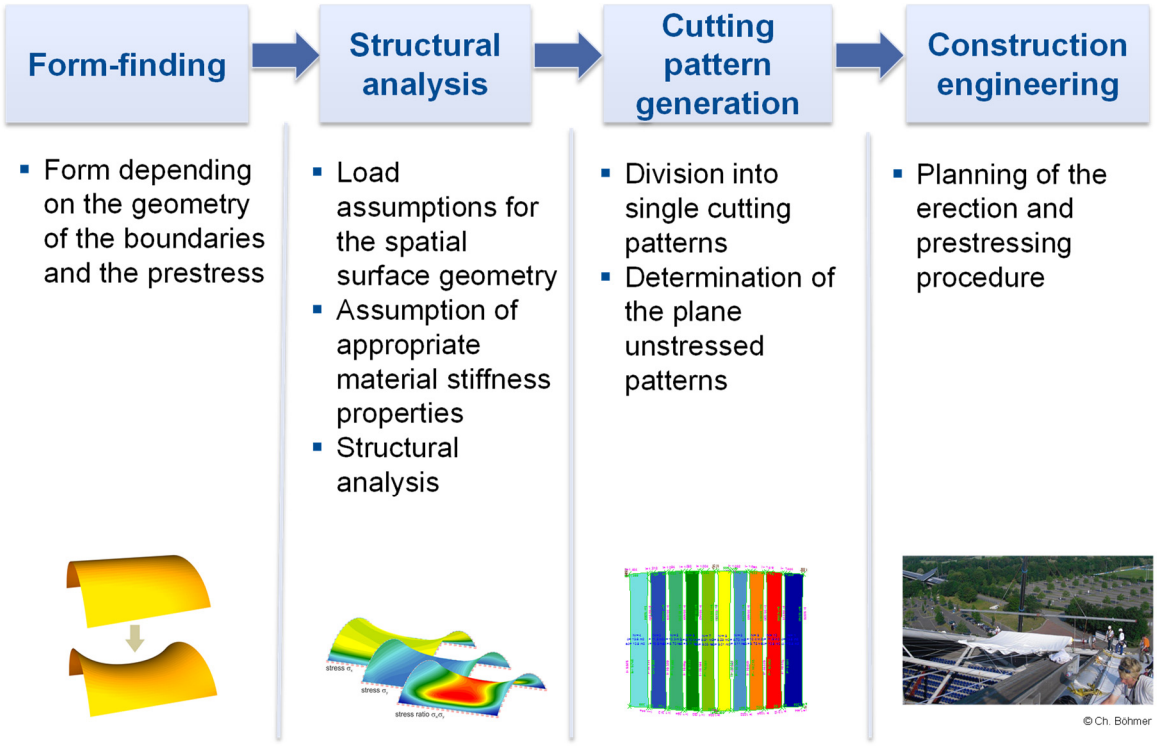

Figure 5 Design steps for the design of membrane structures [SaP15]

In the present context it is important to distinguish between material stiffness properties for the design, i. e. for the structural analysis and compensation planning. In both design steps, the required values are determined for every project by means

of experimental biaxial tests for each material batch to be installed. But both values aim at different stress levels.

Biaxial tests to determine design elastic constants for the structural analysis focus on the stress interval between the prestress level and the design strength as the maximal upper limit of the design stress. Commonly, the design strength of an architectural fabric is referred to as the tensile strength divided by a global stress factor. The stress factor contains safety factors and strength reduction factors. The latter consider the actual loss of fabric strength due to diverse impacts such as long-term loads, high temperature or environmental impacts [SaP15]. Stress factors used in tensile membrane design have a magnitude of usually four to five, see [Go13b], [PWB13], [USS14] for recent comparisons of stress factors.

The determination of compensation values focuses mainly on the initial stressing of the virgin material, but it also considers stress under external loads. This is necessary to prevent the prestress falling (significantly) below the nominal prestress level after external load incidents. The nominal prestress level should be ensured over the entire lifetime of the structure. The procedure basically leads to an initial prestress level which is higher than the nominal prestress level. It compensates the expected loss of prestress due to the viscoelastic effects of creep and relaxation as well as the enduring loss of yarn crimp.

2.3 Principles of load-bearing behaviour of typical membrane structures

Figure 2 illustrates some typical forms of membrane structures and both methods of prestressing: mechanical and pneumatic. Figure 6 onnects these forms to the structural behaviour and related stress ratios in the main structural directions. The stress ratios are examined for the prestress state and the state under uniform external loads. The examined forms and stress ratios are to be understood as examples. The stress ratios can change for specific geometries. For instance, a rectangular plane membrane with a high aspect ratio, i. e. the long edge being much longer than the short edge, might reasonably be prestressed uniaxially.

Assuming an isotropic material, pneumatically prestressed structures exhibit stress ratios in the prestress state of approximately 1:1 (e. g. a square cushion) to 2:1 (circumferential:longitudinal in cylindrical form). These stress ratios do not change significantly in basic load scenarios such as snow or uniform wind suction. The stress ratio under external loads for plane structures depends mainly on the aspect ratio.

Inflatable beams are an exception. These cylindrical, pneumatically prestressed structures exhibit a stress ratio of 2:1 (circumferential:longitudinal) under prestress. But under an external load which leads to pure bending the stresses in longitudinal direction can increase/decrease on the tension/compression side of the circumference maximally by the magnitude of the prestress in longitudinal direction.

This leads to a stress ratio of 1:1 on the tension side and 1:0 on the compression side – but only at the location of the maximum bending moment. As inflated beams are a speciality rather than a commonly built membrane structure, the stress ratio of 1:0 is disregarded in Figure 6 for pneumatically prestressed structures under external loads. The given stress ratios of 1:1 to 2:1 reflect the more typical air-supported domes.

Forms/ Main structural directions / Characteristic features	Synclastic forms	Plane	Anticlastic forms
	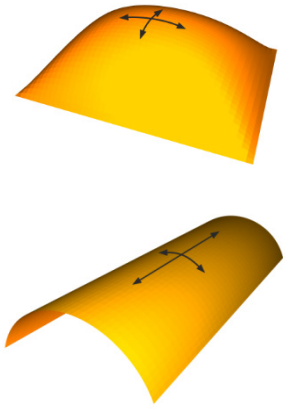		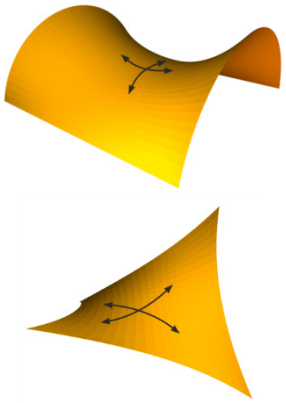
Prestress	Pneumatic	Mechanical	
Stress ratios for prestress	Biaxial with stress ratios 1:1 to 2:1		Biaxial
Stress ratios for external loads			Biaxial with stress ratios of approx. 2:1 and higher, uniaxial limit 1:0

Figure 6 Examples of forms and structural behaviour of membrane structures [US13]

In mechanically prestressed structures, a distinction must be made for the main structural directions between the “carrying” direction and the “supporting” direction. The carrying direction refers to the structural direction that carries an external load by activating positive stress increments, i. e. tensional increments. Hence, what is the carrying and the supporting direction in a structure depends on the load direction, see Figure 7.

For a saddle-shaped membrane spanning two arches, see Figure 6 top right, a gravitation load is carried primarily by means of tensile stresses between the arches. Following the classical membrane theory derived from a cable net, the prestress in the transverse direction is reduced. The prestress reduction contributes to the load-bearing behaviour. Assuming a growing external load, the prestress reduction can proceed until the prestress is used up, i. e. equals zero. At this point the load-bearing behaviour suddenly changes as if the structural system had been changed. This is referred to as the “point of system change”. If the external load is increased beyond this point, load bearing changes: the additional load is carried by additional tensile stresses in the carrying direction only. This makes the structure more compliant than when the prestress plays a role. This behaviour actually occurs in a cable net. In

contrast, for a material whose characteristics include transverse strain, the decrease in prestress is reduced, see the detailed examination in Chapter 2.4.

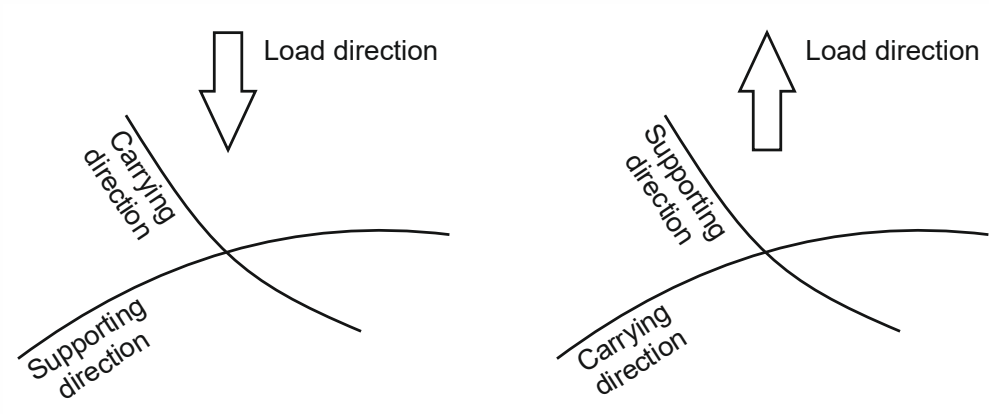

Figure 7 Definition of carrying and supporting direction in a mechanically prestressed anticlastic structure

2.4 Impact of transverse strain on the stress state

Most materials show transverse strain under uniaxial stressing. In the theory of elasticity, the transverse strain is described by Poisson's ratio ν. It is defined as the ratio of the strain in transverse direction to the strain in the direction of uniaxial stress. Using an x,y-coordinate system and applying the uniaxial stress in x-direction, a transverse strain would be measured in y-direction and the Poisson's ratio would become: $\nu = -\varepsilon_y/\varepsilon_x$, see Figure 8. Most materials exhibit transverse shrinkage under uniaxial tensile stress, i. e. a negative transverse strain. In this case the Poisson's ratio becomes positive. For instance, woven fabrics are known to exhibit positive Poisson's ratios – sometimes of surprisingly considerable magnitude.

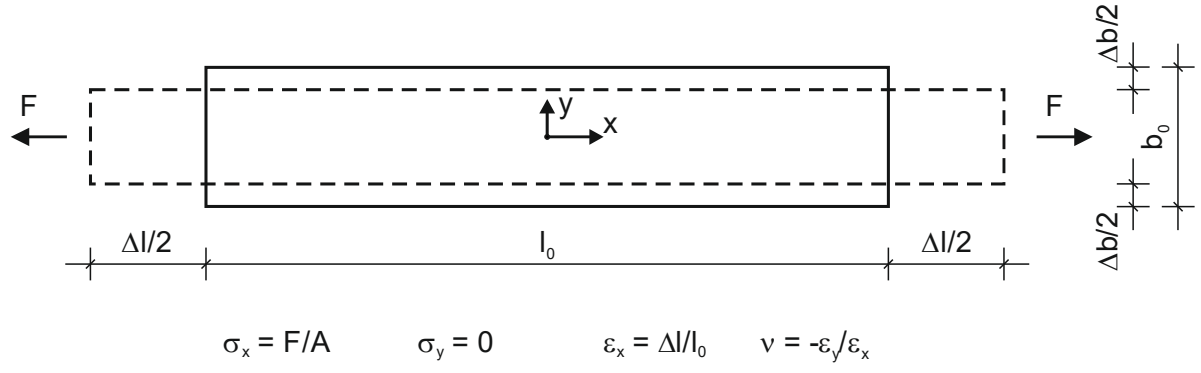

Figure 8 Transverse strain and Poisson's ratio of a transversely unrestrained material strip under uniaxial tensile stress

In general, the effect of transverse shrinkage without any transverse stress can be expressed thus: a contraction $\varepsilon_y = -\nu \cdot \varepsilon_x$ in transverse direction is not associated with compressive stress in transverse direction. If compression and reduction of prestress are the same, for a prestressed material it can be stated that a contraction $\varepsilon_y = -\nu \cdot \varepsilon_x$ in transverse direction is not associated with reduction in prestress.

The impact of transverse strain on the development of stresses and stress ratios in a prestressed anticlastic structure can be explained by means of an example. The first step is to examine a cable net structure. To do this, a prestressed saddle-shaped cable net with cables in the main structural directions is assumed, see Figure 9 top for a section. The cable net exhibits a prestress state $\sigma_{\xi,0}$, $\sigma_{\eta,0}$ and a correlated prestrain state $\varepsilon_{\xi,0}$, $\varepsilon_{\eta,0}$. A uniform gravity load in ζ-direction is applied. This leads to a downward displacement f_ζ of the centre point of the structure, see Figure 9 bottom. The cable net undergoes elongation (or stretching) in the carrying direction ξ under this load, i. e. positive incremental strain $\Delta\varepsilon_\xi$. Naturally, a positive incremental stress $\Delta\sigma_\xi$ starting from the prestress level $\sigma_{\xi,0}$ is related to the positive incremental strain. Presuming potential local displacements are disregarded, i. e. the initial negative Gaussian curvature of the structure remains negative overall, the centre cable in the supporting direction is shortened simultaneously. The shortening equals a loss of prestrain, i. e. a negative incremental strain $\Delta\varepsilon_\eta$. This is due to the geometrical restraint at the centre point. A decrease in tensile stress, i. e. a negative incremental stress $\Delta\sigma_\eta$, starting from the prestress level $\sigma_{\eta,0}$ is undoubtedly related.

In a second step, the cable net is substituted theoretically by a membrane made from a woven fabric which exhibits transverse strains, described by a positive Poisson's ratio. Given the event that the incremental strain ratio $-\Delta\varepsilon_\eta/\Delta\varepsilon_\xi$ equals the strain ratio $-\varepsilon_y/\varepsilon_x$ of the above mentioned material strip in Figure 8, i. e. $-\Delta\varepsilon_\eta/\Delta\varepsilon_\xi = \nu$, no stress change occurs in the supporting direction, analogous to the situation in the material strip: $\Delta\sigma_\eta = \sigma_y = 0$. A stress reduction in transverse direction only occurs if shortening in η-direction is great enough, that is $|\Delta\varepsilon_\eta| > \nu \cdot \Delta\varepsilon_\xi$. Three cases can thus be identified:

- $-\Delta\varepsilon_\eta/\Delta\varepsilon_\xi = \nu$: $\Delta\sigma_\eta = 0$,
- $-\Delta\varepsilon_\eta/\Delta\varepsilon_\xi < \nu$: $\Delta\sigma_\eta > 0$,
- $-\Delta\varepsilon_\eta/\Delta\varepsilon_\xi > \nu$: $\Delta\sigma_\eta < 0$.

The greater the Poisson's ratio, the less distinct the reduction of prestress in the supporting direction. This can be illustrated by a comparison: for the same strain decrease in the supporting direction of a cable net and a woven fabric, the woven fabric is expected to have the higher stress in transverse direction at the end of the straining process. This means that the uniaxial stress ratios commonly understood to be characteristic of anticlastic structures are hardly reached with materials which exhibit considerable transverse strains – and considerable transverse strains are indeed observed for some woven fabrics.

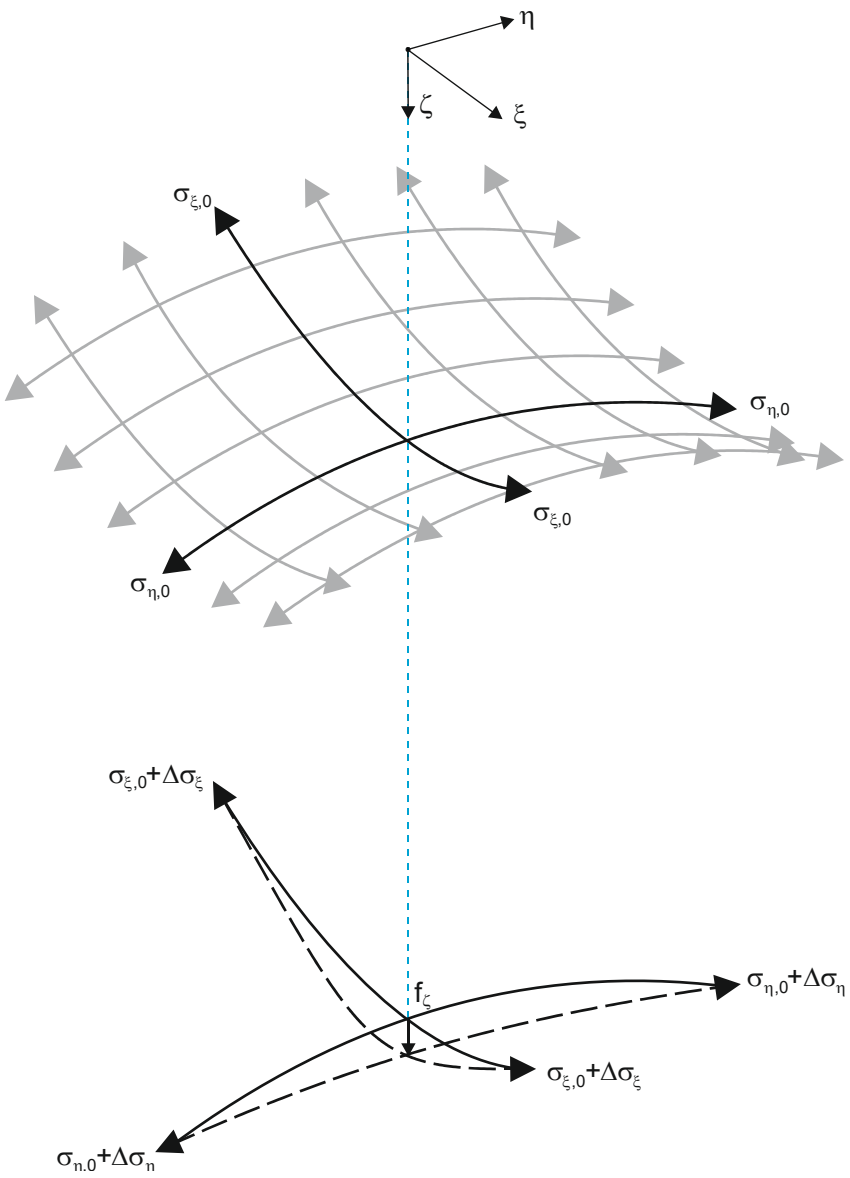

Figure 9 Stress change in a prestressed spatially curved structure under external load

2.5 Stress ratios in the structure and their distribution over the surface

In most load cases, stresses are not uniform over a membrane surface, hence neither are the stress ratios. Bearing this in mind, it is important to be precise about the given stress ratios in Figure 6: they are meant as the stress ratios at the characteristic location of the membrane surface. In this context, the characteristic location is the decisive location for the verification of the structural membrane, i. e. the location of maximum membrane stress.

This is illustrated by the example of a barrel vault structure, see Figure 10. The dimensions are 10 m x 10 m in the ground plot and an arch height of 2.5 m. The prestress is taken to be isotropic at p = 2.0 kN/m. The membrane is modelled as an isotropic material with a tensile modulus of E = 1300 kN/m and no transverse strain.

The structure is loaded externally with a uniform surface load of q = 0.60 kN/m^2. A geometrical non-linear structural analysis is performed using the FE software package Sofistik [Sof14].

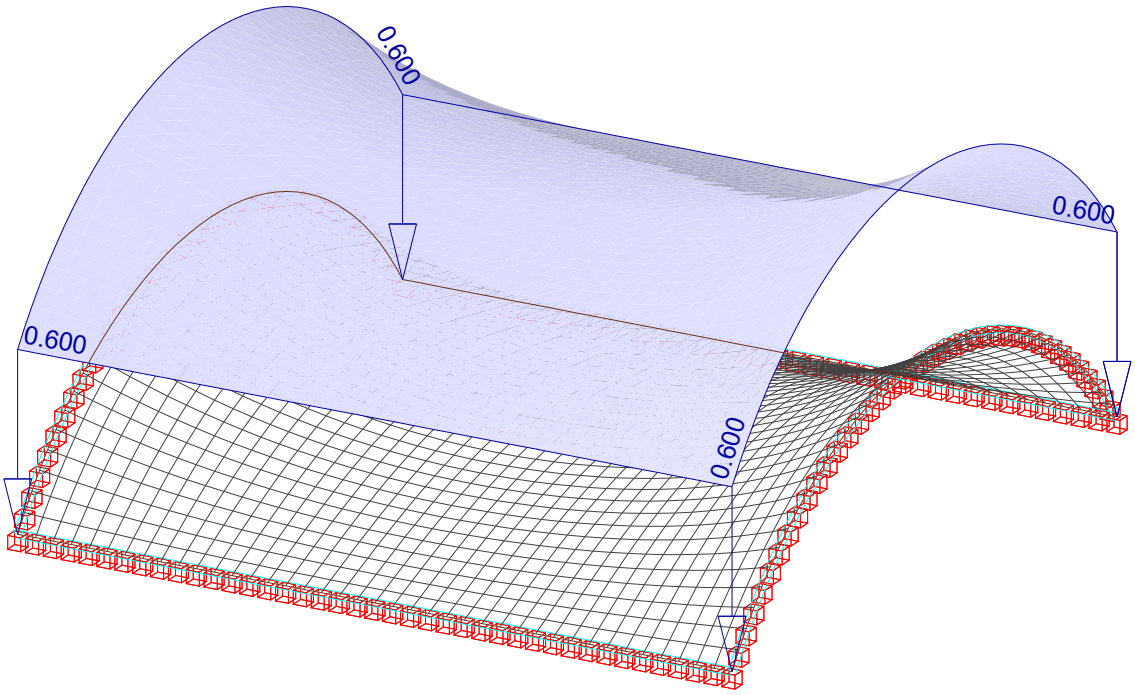

Figure 10 Structural FE model of the investigated barrel vault structure with a uniform external surface load in gravitational direction of q = 0.60 kN/m^2

Results are given for this configuration in Figure 11. As the barrel vault is a double symmetrical structure, it is sufficient to present the results for one quarter of the structure. This quarter is shown in the geometry diagram in Figure 11 top left. The stress ratio for the membrane stresses under prestress and the external load σ_x/σ_y is plotted against the x,y-plane for the quarter in Figure 11 top right. This map shows a non-uniform distribution of stress ratios. Very high stress ratios σ_x/σ_y are apparent for most of the membrane surface. This indicates that the external load is carried by the x-direction almost uniaxially. The plots in Figure 11 below demonstrate the stress increments in x- and y-direction, i. e. the differences between the maximum absolute stress in one direction at one location and the corresponding prestress in the same direction at the same location. This highlights the large positive stress increments in x-direction, while in y-direction the stress level diminishes significantly over the majority of the x,y-plane. This is the “typical” behaviour of anticlastic membrane structures discussed in the previous chapter. It was produced by modelling a material with no transverse strain properties. The location – or rather region in this case – of highest stress σ_x is the characteristic location of the membrane surface. It can be identified in the $\Delta\sigma_x$-plot as the ridge parallel to approximately y = -4 m.

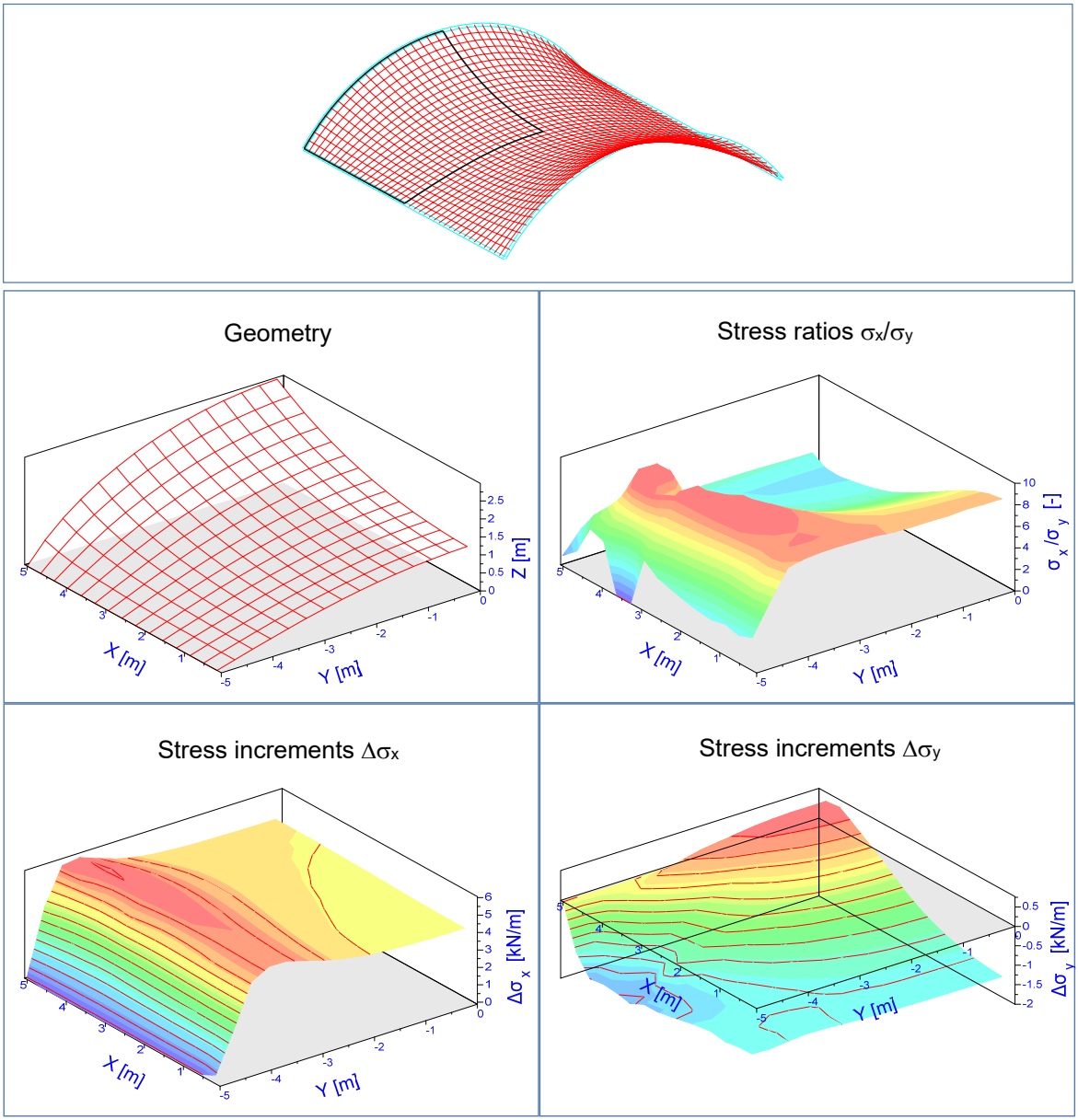

Figure 11 Geometry of one quarter (mid-left) of the investigated barrel vault structure (top), stress ratios σ_x/σ_y (mid-right) and stress increments $\Delta\sigma_x$ and $\Delta\sigma_y$ (below) plotted against the quarter x,y-plane

Of course, the stresses and stress ratios depend on the utilised set of elastic constants that is precisely the object of investigation in the present work. Therefore, the presented stress distribution in Figure 11 must be understood as an example.

2.6 Conclusions

The basic principles for tensile membrane structures with “double curvature” and “prestress” as well as exceptional cases with single or no curvature – cylindrical and plane forms – have been presented. Typical forms and their structural behaviour, mainly the development of stresses starting from the prestress level and distribution of stress ratios in the main structural directions, have been discussed. It has been emphasised that transverse strain in the material may have a significant impact on the resulting stresses and stress ratios. Up to now, this has been completely

disregarded in the theory of membrane structures based on the behaviour of a cable net.

Focussing on biaxial tests, it was shown that a distinction must be made between procedures in order to determine stiffness parameters for the structural analysis and compensation values.

3 Coated woven fabrics and their stress-strain behaviour: state of the art

3.1 Construction and production of the material

Coated woven fabrics are composites. The function of the yarns is to carry the loads, while the primary function of the coating is to make the membrane waterproof and protect the weave from environmental impacts such as UV rays. The yarns today are usually composed of polymeric or glass filaments. Alongside the anorganic synthetic glass fibres, many different organic synthetic yarn materials are available for technical textiles, together with many different organic synthetic coating materials. A great variety of combinations of yarn and coating materials exists. Yarn materials linked to textile architecture are e. g. polyester (PES) – in the form of the subcategory polyethylene terephthalate (PET) –, fibreglass, polytetrafluorethylene (PTFE), polyethylene (PE) and polyamide (PA). Coatings can be made of plasticised polyvinylchloride (PVC), fluoropolymers like polytetrafluoroethylene (PTFE) or tetrafluoroethylene-hexafluoropropylene-vinylidene-fluoride (THV), silicone, polyolefins like polyethylene (PE) and many others [Kn10], [Se09], [Be15]. The fabric has a major influence on the mechanical properties strength and stiffness. But also the coating can influence the stiffness behaviour in specific situations. Furthermore, topcoats or lacquers are often applied, e. g. thermoplastic fluoropolymers like polyvinylidene fluoride (PVDF), as the topcoat on a PVC main coat. The intention is to positively influence technical properties like weldability or self-cleaning of the membrane. As these layers are very thin, however, they do not have a significant impact on the stiffness behaviour [Se09] and are disregarded in this work.

For architectural outdoor applications two material combinations are mostly utilised:

- polyester (PES) fibres coated with a plasticised polyvinylchloride (PVC) matrix (short: PES-PVC) and
- glass fibres coated with a polytetrafluoroethylene (PTFE) matrix (short: glass-PTFE).

Other material combinations may be much more suitable in situations with particular demands. For instance, for high-quality foldable structures, crease fold-resistant materials like uncoated or fluoropolymer-coated PTFE fabrics are used. For particularly high strength requirements, aramid fabric – a polyamide – coated with PVC or PTFE could be employed [Kn10]. Neither are mass products, primarily due to their high price. In the past, the development of new products was driven by other physical, chemical and/or environmental requirements. For example, the PVC coating of a PES fabric can be substituted by polyolefins to improve environmental impact. A rather new development is to substitute PVC with fluoropolymers to increase weathering resistance, life span and translucency [Kn10], [SSU14]. Both combinations feature good processability but up to now have not become widely

accepted, which could be a matter of price [SSU14]. Glass fibre fabrics are also available with a silicone coating. Silicone is relatively cost effective and has high flexibility, high light transmission and good fire resistance [Kn10], [SSU14], [Be15]. However, it is today not very widespread in this capacity due to comparable low strength of connections and a rather high affinity to dirt – disadvantages, which might be eliminated by future developments. Numerous composites with the above mentioned or several other material combinations are available on the market. Despite the confusingly large variety, the vast majority of market share in textile architecture is held by PES-PVC and glass-PTFE fabrics. Compared with other materials, they provide the best combination of many key features, like high strength of the base material, weldability and high strength of connections, a suitable stiffness, i. e. not too stiff to be installed and not too compliant to prevent wide-span structures, good resistance to environmental impacts and thus a long life span, low affinity to dirt, good fire behaviour, high translucency, printability (only PES-PVC) and not least affordability. For that reason, these two types are the main focus of the present work.

Woven fabrics are produced as webs on the weaving loom. They consist of a weave of two orthogonal yarn directions. The yarns in the longitudinal direction of a web are called the warp yarns, those in perpendicular direction the fill (or weft) yarns. The warp yarns are drawn, i. e. prestressed, on the weaving loom. On industrial looms the fill yarns are literally “shot” through in perpendicular direction.

Different weaves are commonly used for architectural fabrics. The main ones are plain weave and panama weave 2/2 or panama weave 3/3, see Figure 12. The panama weaves are double or triple-thread woven fabrics. All these weaves are tightly woven so that the yarns touch each other [Go13a]. Loosely woven fabrics are possible, too, in the form of mesh fabrics, see also Figure 12, which are coated fabrics with spacing between adjacent yarns. This construction increases translucency.

For structural membranes which are normally for outdoor applications like roofing or facade elements, coated fabrics are required to protect the yarns from environmental impacts. A coated plain weave fabric and a coated mesh fabric are illustrated as rendered isometric views in Figure 13. The spacings between the coated yarns in the mesh fabric can be left open or they can be closed with a transparent laminate (“laminated mesh”). While the former enables high translucency and permeability for wind and humidity, the latter combination largely preserves translucency while achieving a waterproof membrane. The seal can be a transparent PTFE or ETFE-foil laminate on both sides or a coating with transparent plasticised PVC. The possibility for a transparent seal is indicated in Figure 13 by the sub-section of grey transparent surface.

The fabric webs are rolled up in the weaving mill for transport to the coating. During the subsequent coating process, the fabric is rolled off the fabric roll and the coating

spread onto it as it passes (“spread coating” used for PES-PVC) or – more simply – drawn through a bath of liquid synthetic (glass-PTFE). The coating adheres to the fabric and hardens. When the coating has hardened, the coated fabric is rolled up again for shipment to the manufacturer, who assembles a complete membrane panel from single cutting patterns.

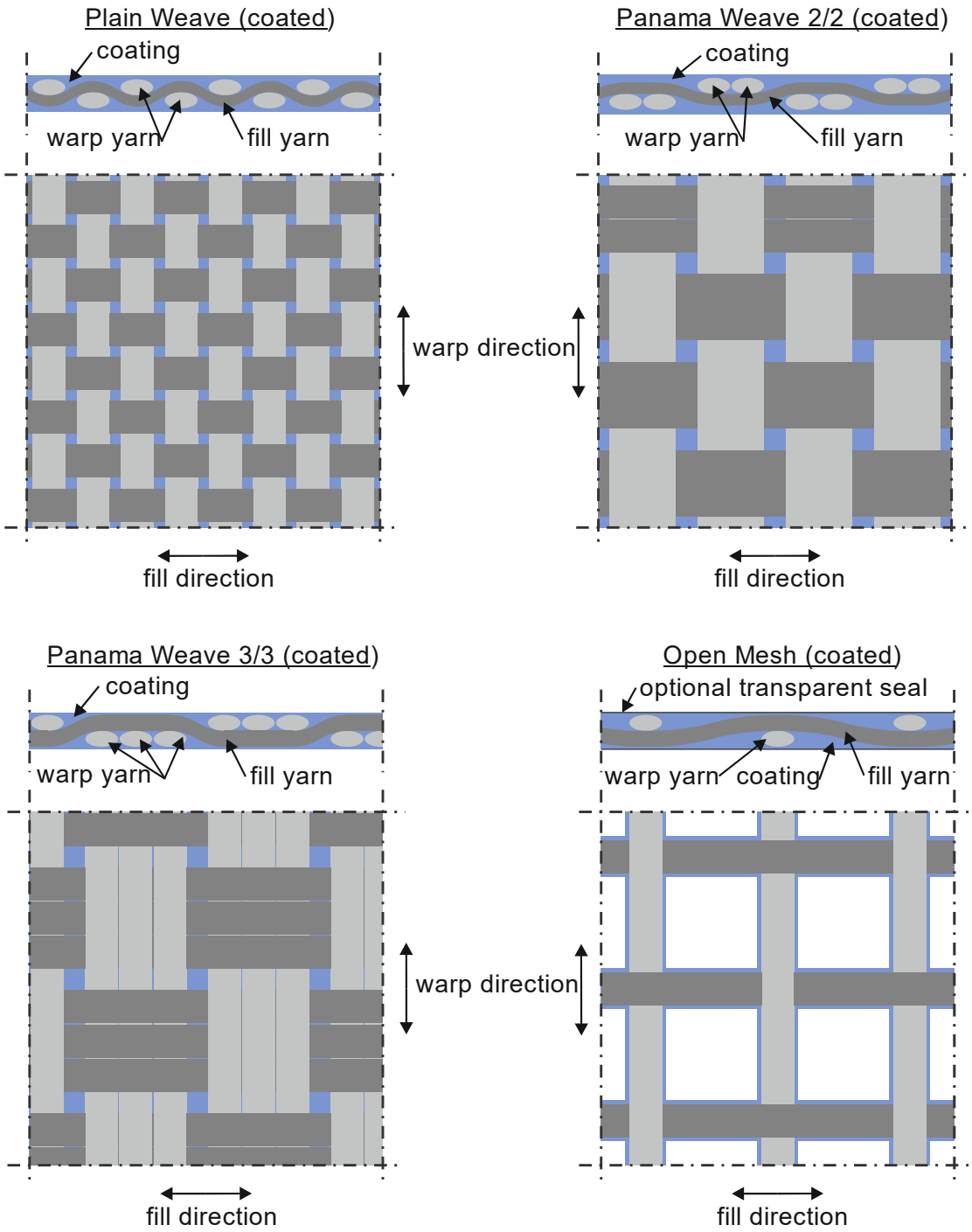

Figure 12 Schematic construction of coated fabrics with typical weaves (©IML/ELLF)

Because the fabric web is drawn in longitudinal direction during the coating process, the warp yarns are under tension when the coating matrix hardens. In the “traditional” coating process the fill yarns are not stressed during coating. This was the process

used at the beginning of technical textiles. It creates different yarn crimp in the main warp and fill directions of the fabric. This is one reason for the considerable anisotropic stress-strain behaviour.

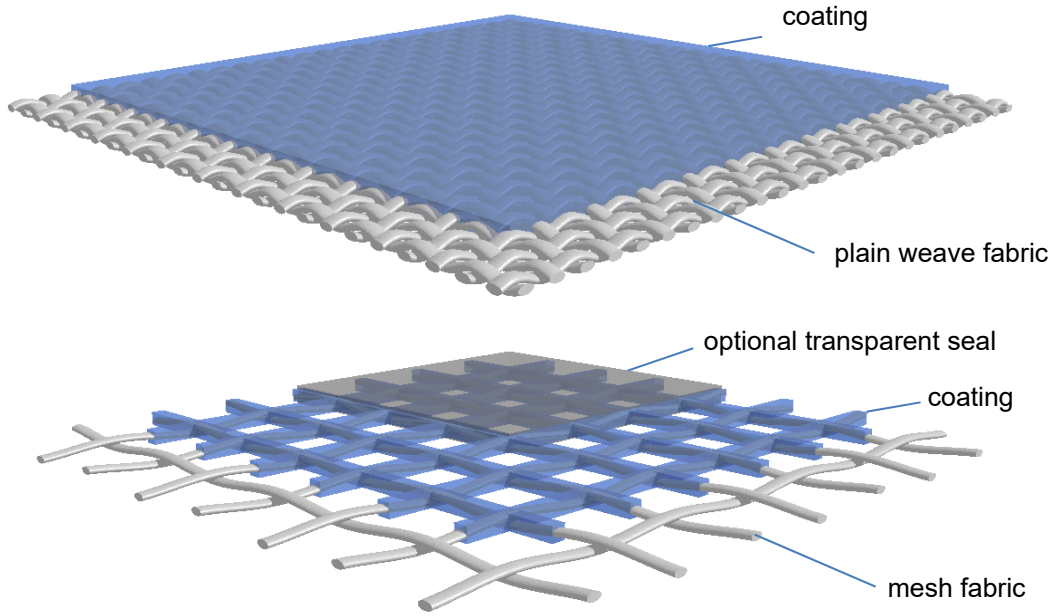

Figure 13 Rendered isometric view on a coated plain weave fabric (top) and a coated open mesh fabric (bottom) with optional transparent seal

In an advanced coating procedure developed later for PES-PVC fabrics, controlled stress is applied during coating not only to the warp yarns but also to the fill yarns. This technique is referred to as “biaxially prestressed coating system” in this work. The procedure can be used to reduce the anisotropic properties of the fabric as the fill crimp approaches the warp crimp. When the fill stress equals the warp stress during coating and hardening and the fill crimp approximately equals the warp crimp, roughly equal mechanical properties can be achieved in the warp and fill direction of the fabric. This in particular means a higher fill stiffness and a lower warp stiffness compared to traditionally coated fabrics. Both techniques, traditional and biaxially prestressed coating, are commonly used for PES-PVC fabrics today. Neither technique is better a priori. The engineer should be aware of the differences and decide on one material at an early project stage [GB09], depending e. g. on the structural requirements or the envisaged installation procedure. The biaxially prestressed coating system is not available for PTFE-coated fabrics. After the fabric has passed through the liquid PTFE bath, the PTFE is sintered at approx. 400°C – a temperature at which even high-temperature steels suffer significant strength reduction [EN 13084-7]. This circumstance prevents the fabric from clamping in fill direction.

The magnitude of the yarn crimp depends on the weave, e. g. mesh fabrics with spaced yarns have a lower degree of crimp than fabrics with a tight weave. This and many other weaving and coating parameters can influence the stress-strain

behaviour of the ready-made composite. For this reason, the mechanical behaviour cannot be completely generalised for one product type – although some characteristics appear to be typical.

3.2 Base materials [USS15c]

With regard to the base materials of the yarns, it is known that the stress-strain behaviour of E-glass – the type of glass from which glass fibres are made – is linear elastic, see Figure 14 (a).

The base material for polyester fibres is polyethylene terephthalate (PET), a subcategory of polyester. Polyester and usually also polyethylene terephthalate are denoted by the general fibre code PES according to [DIN EN ISO 2076]. Polyester filaments – consisting of macromolecules that constitute semicristalline and amorphous regions – show the viscoelastic behaviour typical of all polymeric materials. Furthermore, their behaviour is non-linear, see Figure 14 (b). The characteristic stress-strain path consists of two inflexion points or three sections respectively. Section I is characterised by alignment of the macromolecules during initial application of stress. During further stressing, the initially aligned macromolecules undergo drawing. This process reduces the entropy and is accompanied by a stiffening of the material (section II). This part of the stress-strain behaviour is usually known as the “entropy elasticity”. When most macromolecules undergo drawing, the number of additional molecules that take part in the transmission of force decreases. This is accompanied by a decreasing tangent modulus (section III) [Me78].

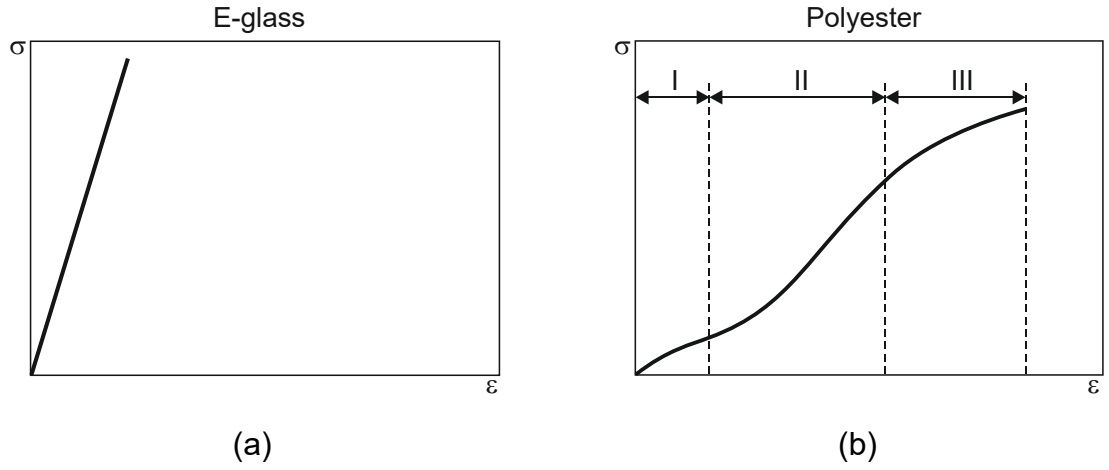

Figure 14 Schematic stress-strain diagrams of E-glass (a) and polyester (b) [USS15c]

Young’s moduli for polyester – given as tangent modulus – and E-glass are presented in Table 1, together with the Young’s moduli of the coating materials, plasticised PVC and PTFE.

The Young’s modulus of glass filaments is many times higher than that of polyester filaments. Nonetheless, this does not necessarily mean that the modulus of

deformation of twisted multifilament yarns, and particularly the woven (coated) fabric made from glass fibres, is consequently higher than for yarns and fabric made from polyester fibres. Regarding the yarns, the stiffness depends on the yarn size and the spinning details. Regarding the fabric, the stiffness depends on the yarn density as well as the weave type and the coating process.

Table 1 Young's moduli for yarn and coating materials [USS15c]

Material	**Young's modulus [N/mm²]**
Yarn material	
PET filaments [Kn10], [Ko08]	10000 – 21000
E-glass filaments [Ba02], [Kn10], [Ko08]	72000 – 90000
Coating material	
Plasticised PVC [Me78]	10
PTFE [Ba02]	400

3.3 Interaction of materials and constructional properties [USS15c]

Yarns for use in technical textiles are composed of numerous filaments; they are so-called multifilament yarns. The stress-strain behaviour of a yarn can be influenced significantly by varying the spinning details, e. g. varying the number of twists per unit length. Basically, the yarn is less stiff than the single filaments. The yarn exhibits a "constructional stretch": during the first loading cycles the yarns' individual filaments align themselves. The more the filaments are inclined against the longitudinal direction of the yarn, the greater is the constructional stretch that can be expected.

Constructional stretch is also observed in woven fabrics. During the first loading cycles (particularly during the very first cycle) the yarn crimp decreases and adapts to the applied stress and warp:fill stress ratio when the fabric is stressed biaxially, as is typical in an *in situ* fabric structure. The magnitude of constructional stretch of a fabric depends mainly on the magnitude of yarn crimp. The yarn crimp in turn depends mainly on the yarn density. The more tightly the fabric is woven, the higher is the "frequency" of the yarns' wave form.

The constructional stretches described can be recognised in measured stress-strain paths of woven fabrics. *Grosberg* [Gr69] distinguishes between three sections of the stress-strain path of a woven fabric, see Figure 15. The first section is characterised by inter-fibre friction, which initially prevents the yarn from bending. Once the friction is overcome, the yarn's, and mainly the fabric's, constructional stretch dominate the deformation behaviour (both are strainless deformations of the fabric). The last section is characterised by material strain in the yarn.

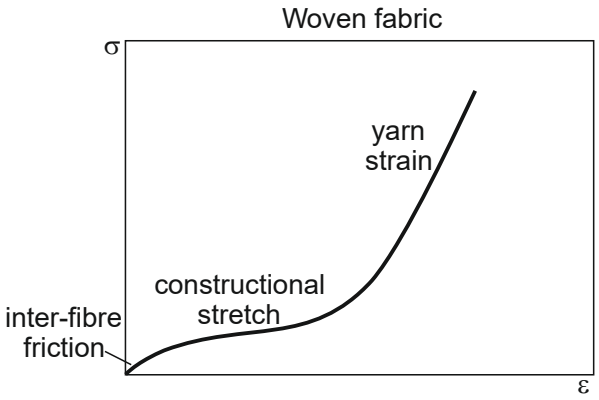

Figure 15 Sections of the stress-strain paths of woven fabrics (schematic) according to *Grosberg* [Gr69] [USS15c]

“Crimp interchange” describes the mechanism that a change in the yarn crimp of one weave direction affects the crimp of the orthogonal yarn: if the yarns in one direction are straightened due to applied force the yarns in the perpendicular direction are forced to increase their crimp. This is a key feature that influences the stress-strain behaviour of fabrics. It also explains, in part, the inelasticity of materials [USS15a].

With regard to the stiffness share of the coating materials in the composite, it can be seen from Table 1 that the coating materials exhibit only a fraction of the stiffness of the yarn materials, particularly plasticised PVC. This leads to the assumption that the influence of the coating tends to be negligible. By estimating the coating thickness, the stiffness share of the coating in the composite can be determined approximately. *Meffert* [Me78] has estimated the stiffness share for a PES-PVC fabric to be max. 3 %; this magnitude is indeed negligible. But at least for the fill direction in glass-PTFE fabrics the coating can play a significant role during the installation of a structural membrane. Regarding the lower stress range of glass-PTFE fabrics, *Saxe & Kürten* [SK92], based on an investigation into the temperature-dependent stress-strain behaviour of glass-PTFE fabrics, concluded that exactly this effect can only be explained by the impact of the PTFE coating because the stiffness of glass is basically independent of the temperature in the investigated range between 3°C and 28°C.

3.4 Basic principles of the biaxial stress-strain behaviour of fabrics

The stress-strain behaviour of coated fabrics depends on many factors. Figure 16 gives an overview of aspects relating to the stress-strain behaviour of coated woven fabrics and their interactions. The figure does not claim to be complete, but it does demonstrate the diversity and thus the complexity of the topic. Some of these aspects are preconditioning aspects that can be manipulated by the material supplier, e. g. prestress during weaving and coating which influences the initial crimp of the yarns. The behaviour of the yarn itself can be influenced by the spinning. The mechanical properties of the coating can be influenced by chemical and physical

handling. Preconditioning aspects which can be manipulated by the material supplier are shown in orange.

Figure 16 Aspects relating to the stress-strain behaviour of coated woven fabrics and their interactions

Fabrics made from synthetics or coated with synthetics – which always exhibit viscous effects – are well known for their viscoelastic stress-strain behaviour. Viscoelasticity includes creep, revertive creep, stress relaxation, hysteresis loops under cyclic loading, a possible specific amount of residual strain and rate-dependency of the stiffness.

Traditionally coated materials are shown to be distinctly anisotropic. Furthermore, coated fabrics are described as nonlinear materials. Some of the nonlinearity

originates from the stress-strain behaviour of synthetic yarn materials and some from the crimp interchange. The nonlinear stress-strain paths can be concave or convex over the working stress range. A clearly recognisable concave curvature may appear for polyester fabrics. The origin is the base material behaviour found in “Section I” in Figure 14 (b).

3.5 PVC-coated polyester fabric

3.5.1 General

The following chapters explore in detail current knowledge of the complex stress-strain behaviour of PVC-coated PES fabrics. Investigations are presented which look at the importance of the single aspects mentioned in Figure 16 to the stress-strain behaviour of coated woven fabric and how they can be handled in a simplified linear-elastic design approach. The objective is to identify the principal characteristics in order to enable the establishment of appropriate biaxial test protocols and evaluation procedures.

The first systematic study of the stress-strain behaviour of a coated fabric is provided by *Reinhardt* [Re75] in what is still the most important and comprehensive basic scientific report on this topic. This very elaborate study accompanied the planning of a specific building. It therefore took as an example for its investigation the material intended for the project: a mesh polyester fabric, the yarns of which were encased with PVC in a dipping bath for UV protection and subsequently covered with a transparent plasticised PVC coating which completely sealed the mesh. The mesh itself consisted of 2.2 warp yarns/cm and 3.4 fill yarns/cm. The transparent PVC coating had a thickness in the spacings between the yarns of ca. 0.7 mm and of ca. 0.2 mm on the nodes of the weave. The total weight was 995 g/m^2, of which 256 g/m^2 was accounted for by the base fabric. Load histories of repeat uniaxial and biaxial loading were investigated in particular, including different loading velocities, recovery times and hold times on different stress levels in order to explore the creep behaviour. Moreover, the cross-shaped, long-arm test specimen with slits in the arms near the centre of the cross was developed which was the basis for the later refined specimen form developed in the Essen Laboratory for Lightweight Structures (ELLF) at the University of Duisburg-Essen, see Figure 32.

The following report into the state of the art is largely based on the basic scientific findings of *Reinhardt* and gives the most relevant results related to the present work, complemented by the work of additional researchers.

3.5.2 Uniaxial loading

3.5.2.1 Uniaxial cyclic loading

The first aspect in *Reinhardt’s* investigation [Re75] was uniaxial cyclic loading – which at that time was conducted with up to 40% of the tensile strength. The loading

of 40% of the tensile strength was justified at the time as the highest assumed working stress, related to a stress factor of 2.5. It yielded the following fundamental results, see also Figure 17:

- The investigated fabric had clear anisotropic stress-strain behaviour; the fill direction was much more compliant than the warp direction;
- As a tendency the slopes of the stress-strain paths increased with every load cycle, but
- There was a major difference between the stress-strain behaviour of the first load and all following load cycles. The second cycle already behaved approximately like the 10^{th} cycle.

Moreover, the dependency of the loading rate on the stiffness was not clear, but its relevance was minor compared to the impact of the number of the load cycle. A moderate rate dependency for a PES-PVC fabric is also reported by [GL11] (and for glass-PTFE fabrics of various types by [SK92]). The rate dependency can therefore be neglected for practical applications.

As coated woven fabric even on macroscopic scale is a component or a construction in itself rather than a construction material, the “modulus of tensile deformation” E – termed the tensile modulus E in the present work – is determined instead of the “Young’s modulus” E, which is introduced as a constant of a base material. The tensile modulus was determined by *Reinhardt* as a secant within an arbitrary stress interval. This is illustrated for the first load cycle in Figure 17. The reason for establishing secants within an arbitrary stress interval rather than between the reversal points of the hysteresis loops was of a technical nature related to the evaluation procedure employed analogously. However, the selected stress interval was of minor significance, as the objective was merely to illustrate the tendency towards the initial strong increase in stiffness with cumulation of the first load cycles and the converging stiffness during the subsequent load cycles. This can be illustrated by a rapidly converging curve in a diagram where the tensile modulus E_n of load cycle n related to the tensile modulus E_1 of the first load is plotted against the number of load cycles, see Figure 18.

Moreover, the stress-strain paths in Figure 17 also justified the suggestion that the nonlinearity of the deformation behaviour decreases with an increasing number of load cycles. This was confirmed by *Reinhardt* when he determined tensile moduli for different stress intervals. For the first load cycle the moduli for the different stress intervals varied significantly, which illustrates the nonlinearity of the stress-strain path. For the 10^{th} load cycle the moduli for different stress intervals were almost the same, which proved almost linear behaviour.

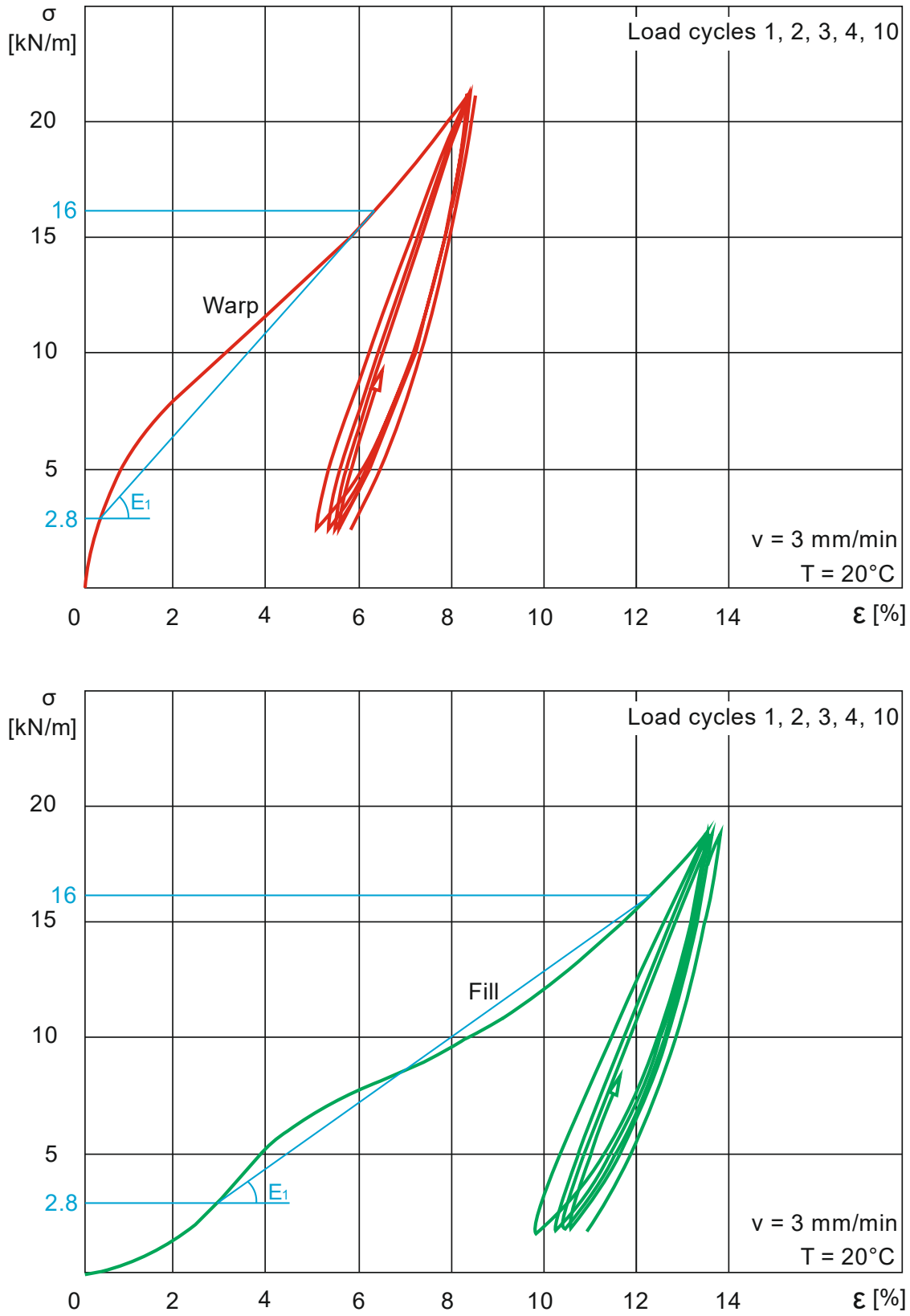

Figure 17 Stress-strain hysteresis in warp and fill direction for a PES-PVC mesh fabric, each under a uniaxial load according to [Re75]

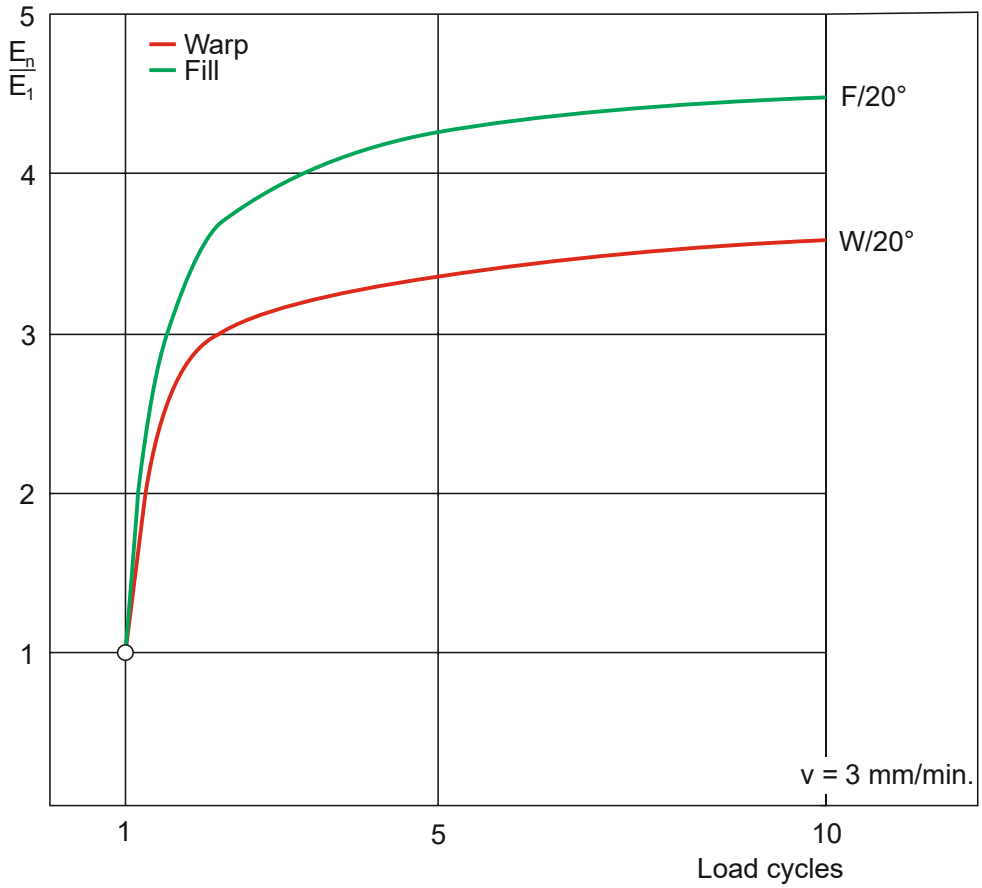

Figure 18 Development of the tensile modulus E for a PES-PVC mesh fabric dependent on the number of load cycles under uniaxial load according to [Re75]

From *Reinhardt's* point of view, the determined tensile modulus had no practical relevance unless its determination was based on realistic stress levels for the prestress and the working stress.

Meffert [Me78] remarked that the stress-strain characteristic in warp direction of the composite PES-PVC under uniaxial warp load resembles very much the stress-strain characteristic of a single polyester yarn. This can be observed from Figure 19, which illustrates the tensile strain measured in a uniaxial tensile test conducted until fracture. This test was performed on a PES-PVC type III in the Essen Laboratory for Lightweight Structures (ELLF) at the University of Duisburg-Essen. *Meffert* supposed that the similarity of fabric to yarn is due to the low yarn crimp in warp direction in a virgin PES-PVC fabric. The more compliant behaviour of the fill direction under uniaxial fill load – particularly in the initial phase – is then due to the higher yarn crimp. Note that the stress-strain paths in Figure 17 reflect a section of the "full" stress-strain paths in Figure 19: they only show the behaviour in a certain working stress interval up to a stress level far below the tensile strength. Today, approximately one quarter of the tensile strength is used for the working stress range. This is indicated in Figure 19. The concave curvature of the warp path in this stress range marks the softening behaviour of the polyester yarns, see "Section I" in Figure 14 (b).

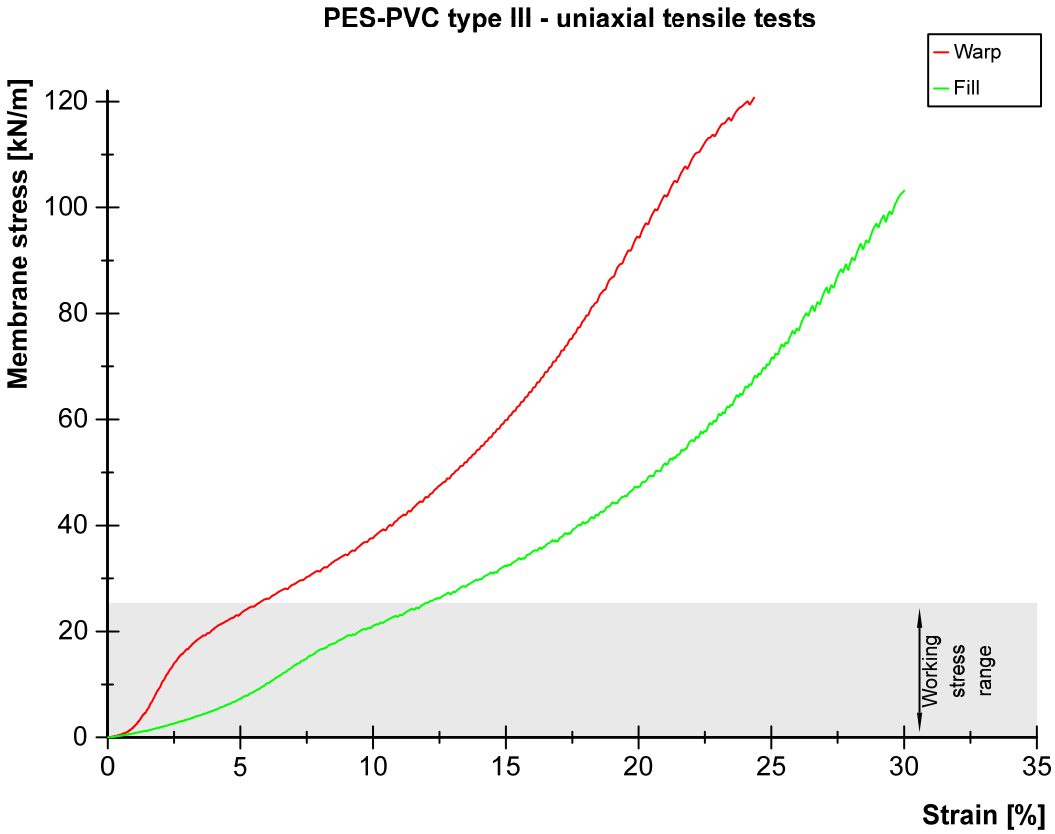

Figure 19 Stress-strain paths in warp and fill for a PES-PVC fabric type III in uniaxial tensile tests of virgin material conducted until fracture

Meffert [Me78] also reports that the deformation behaviour of the fill yarns themselves varies from that of the warp yarns – even though the same material is used for the warp and fill yarns. This is supposed to be due to different stresses during the weaving process and – clearly to a much greater extent – to different stresses during the coating process. The high temperature of up to approximately 120°C-180°C during the coating process, which is not far from the melting temperature of polyester, leads to a reorientation of the chain molecules in the yarns. This process is reported to be more distinctive in the yarns with lower stress, which are the fill yarns in a traditional coating process. Reorientation actually means a loss of orientation towards yarn longitudinal direction. This process was already supposed by [Re75].

3.5.2.2 Repeated uniaxial loading with recovery times

In order to investigate the effect of a recovery time, *Reinhardt* conducted uniaxial tensile tests with repeated loading and long recovery times in between. A load was applied to the specimens once each day in the first five days and afterwards loaded on the 18th, 32nd, 45th and 121st day. The specimens were relieved of the full load after each loading procedure. Disregarding irreversible strains in the first step, only strain differences $\Delta\varepsilon$ for each loading sequence are plotted in Figure 20. During these tests, the relative stiffness, i. e. the gradient of the respective loading stress-strain paths, increased in the initial phase under daily loading and decreased again slightly

in the following phase with recovery times of longer than one day. The example in Figure 20 demonstrates this for the warp direction, but the fill direction behaves very similarly, only it is more compliant. However, the initial stiffness differed significantly from the stiffness during all subsequent load sequences.

Unfortunately, the gradients of these stress-strain paths cannot be compared directly to those of the uninterrupted cyclic loading described above because different stress intervals were employed during testing. For direct comparison purposes, experimental tests at the same stress intervals with and without recovery times will be described for PES-PVC in Chapter 6.2.

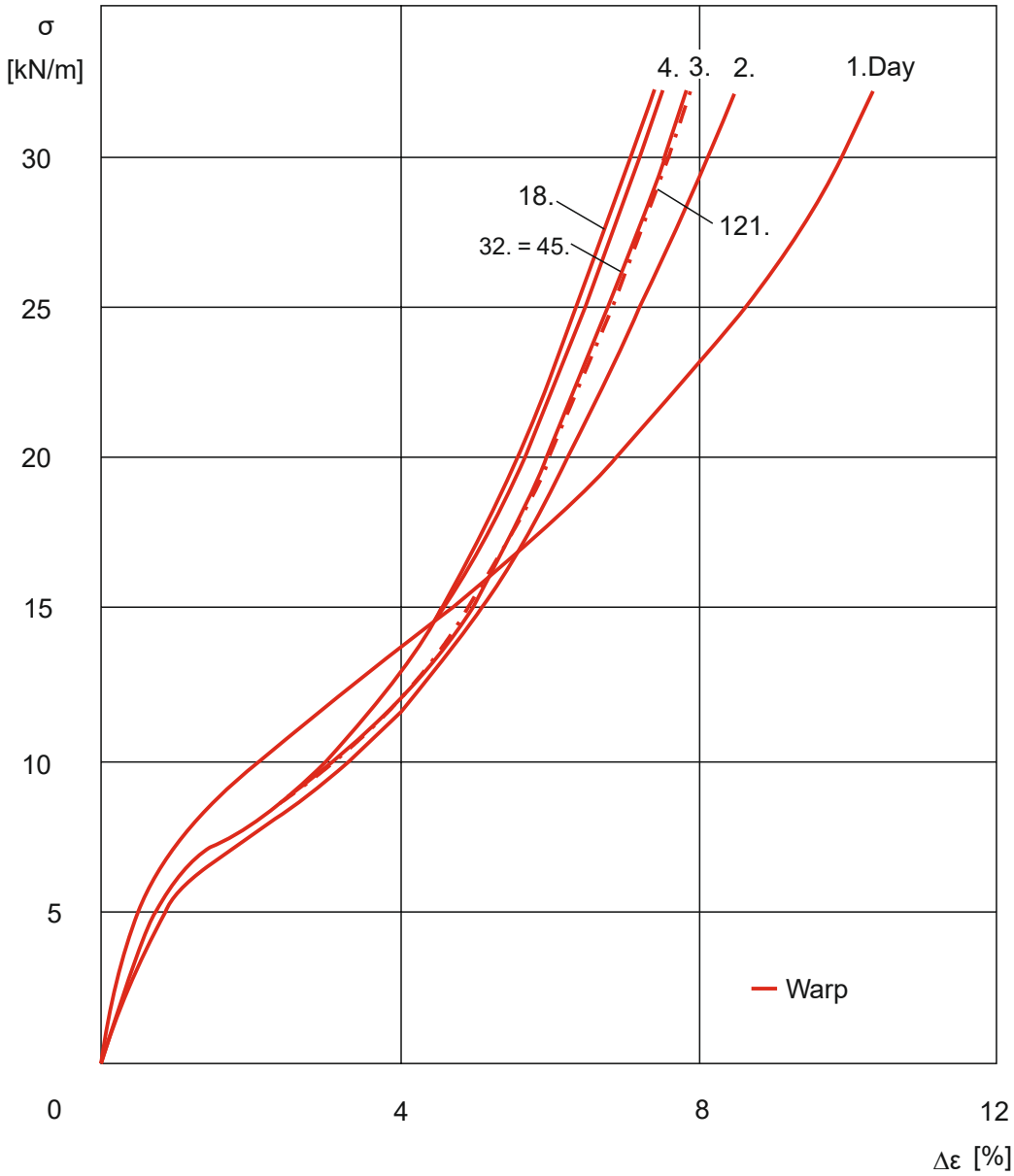

Figure 20 Stress-strain paths in warp direction for repeated uniaxial loading with recovery times of at least one day between single loads for a PES-PVC mesh fabric according to [Re75], each stress-strain path beginning at the point of origin

When considering the irreversible strains, the stress-strain diagram for the warp direction is as shown in Figure 21. *Reinhardt* divided the total strain ε_{tot} due to initial loading into

- spontaneous reversible strain $\varepsilon_{r,spon}$,
- delayed reversible strain $\varepsilon_{r,del}$ and
- irreversible strain ε_{irr}.

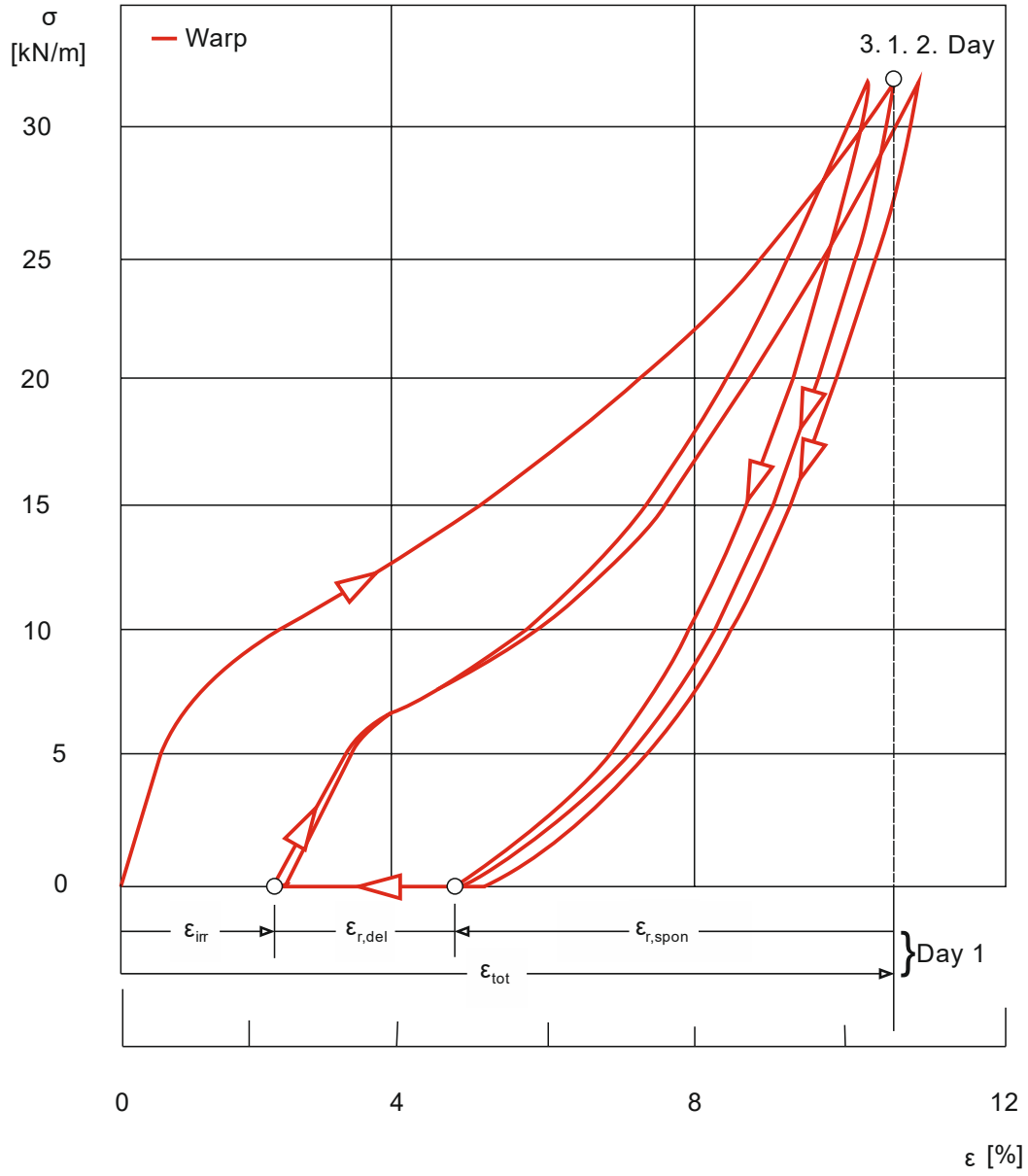

Figure 21 Stress-strain paths in warp direction for repeated uniaxial loading with recovery time, including irreversible strains for a PES-PVC mesh fabric according to [Re75]

He recognised that the irreversible strain ε_{irr} mainly resulted from the first and second loading and stayed almost constant afterwards. The irreversible strain was interpreted as a viscous or plastic yield. This was superimposed by viscoelastic strain. The delayed reversible strain can be understood as “revertive creep”. Overall, these tests confirmed that the material characteristics change in the first load cycles

– due to molecular and structural transformation – but stay constant afterwards. Irreversible strain occurs only in the first two load cycles, and mainly in the first. The material fully recovers after all subsequent loading, as long as the recovery time is sufficient.

3.5.2.3 Uniaxial testing with hold times at different stress levels

Reinhardt's investigations also included uniaxial tensile tests with hold times of 30 minutes at different stress levels [Re75]. The next stress level was introduced immediately after each hold time. The resulting stress-strain paths are illustrated in Figure 22.

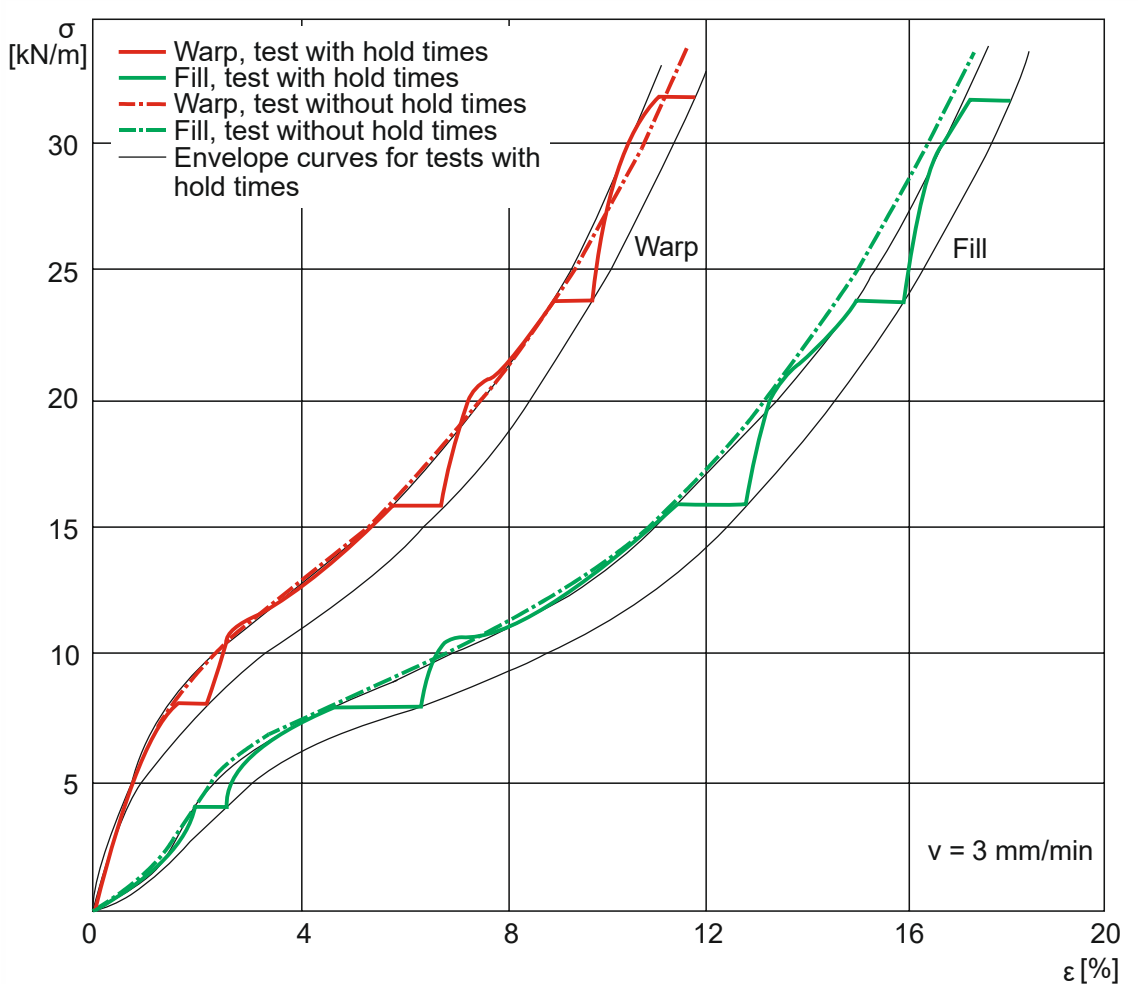

Figure 22 Stress-strain paths for stepwise uniaxial loading and hold times of 30 minutes for a PES-PVC mesh fabric according to [Re75]

The bold curves represent the measured strains for warp and fill direction during the tests with hold times. The increasing strains during the hold times with constant stress can be recognised clearly in the staircase-shaped curves. For comparison purposes, the stress-strain paths resulting from uninterrupted loading are given as a reference, see the dot-and-dashed lines. It can be observed very clearly from the thin black envelope curves that the stress-strain paths including hold times roughly accompany the nearby reference lines. During the hold time stages they proceed

locally in a “zigzag” around the reference lines. The difference of the rough path to the reference line is not significant.

Creep is not of the same magnitude in both fabric directions and is dependent on the stress level. At the stress levels of 4 kN/m and 8 kN/m, the highest creep rates related to the respective strain increments at these stress levels were observed.

3.5.3 Biaxial loading

3.5.3.1 Biaxial cyclic loading

For the biaxial tests, *Reinhardt* [Re75] employed the test rig developed by *Losch* [Lo71] using plane test specimens with a homogeneous stress state in the centre measurement field, which is free of constraint forces. As already mentioned above, *Reinhardt* enhanced the test specimen geometry with the aim of also enabling biaxial strength tests. The resulting cruciform test specimen with long arms and slits adjacent to the centre field was used for all biaxial tests. The applied forces were parallel to the fabric yarns. The following warp:fill stress ratios were applied: 1:1, 2:1, 10:1 and 1:2, 1:10. It should be mentioned that during the very high and very low stress ratios 10:1 and 1:10, the lower load could not be adjusted exactly in the low stress range. The target stress ratios were achieved only for higher stresses. The loads were applied stepwise. The only reason for this was to gain time for the optical strain measurement, which was based on photo documentation of the measurement field at the centre of the test specimen.

Ten load cycles were applied for each stress ratio in an initial test. A secant modulus was determined for each measured stress-strain path, independently for the warp and fill direction. With regard to the development of the secant modulus over the ten load cycles, the same behaviour as observed for the uniaxial tests was apparent: usually, the stiffness in the first or first two load cycles differed significantly from the stiffness in all other load cycles. It was only for two stress ratios (1:1 and 1:10) that this development was not completely finished in fill direction when the 10^{th} load cycle was reached. *Galliot & Luchsinger* [GL11] report a stabilised stress-strain behaviour after four load cycles for a PES-PVC material during loading with a stress ratio of 1:1.

A principal result was that the gradients of the stress-strain paths were higher the higher the perpendicular membrane stress was, i. e. 1:1 biaxial stress leads to the stiffest material response, whereas almost uniaxial stress (10:1 and 1:10) shows the most compliant response [Re75], [RM79]. This is not surprising and was to be expected because of the structural composition of woven fabrics leading to the effect of crimp interchange. What is surprising, however, is that the mesh fabric – i. e. low yarn density with related low yarn crimp – investigated by *Reinhardt* [Re75] showed approximately the same crimp interchange effect as the tightly woven fabric – i. e. high yarn density with related high yarn crimp – investigated by *Rehm & Münsch* [RM79]. A considerably higher impact of biaxial loading, i. e. a greater increase in the

1:1 stress-strain path slopes compared to the uniaxial ones, might have been expected for the fabric with higher yarn crimp, see also [Me78].

Unfortunately, the transverse strains could not be documented by *Reinhardt* for the almost uniaxial stress ratios 10:1 and 1:10. The reason was reported to be the great measurement deviations resulting from the equipment. *Rehm & Münsch* [RM79] reported transverse strains for uniaxial stress. Almost no transverse strain in fill direction was recognised for warp stress. By contrast, the transverse strain in warp direction for fill stress was extensive. From these different observations they concluded that the transverse strains in a PES-PVC fabric do not result from the PVC coating but from the weave structure only.

Further yarn-parallel biaxial tests on a PES-PVC fabric have been reported by *Rehm & Münsch* [RM79]. They used an advanced version of *Losch*'s biaxial test rig. Stress ratios of 1:1, 2:1, 5:1 and 1:2 and 1:5 were applied with 20 load cycles each. The strain measurement was taken in the main fabric directions with displacement transducers. This technique made it possible to apply the biaxial loads without hold times. The authors also mentioned that, given the equipment employed, the stress measurement in the low stress range up to 1.5 kN/m contained "certain mistakes". As results they reported that the slope of the stress-strain paths grew with an increasing load cycle number. The fill path slopes approximate the warp paths during this process. The behaviour moreover approximates elastic behaviour, which can be recognised from the decreasing difference between loading and unloading paths. Finally, the stress-strain paths approach linear behaviour.

3.5.3.2 Biaxial testing with hold times at different stress levels

In biaxial tests with hold times at different stress levels, creep was observed to be dependent on the fabric direction and the stress level [Re75]. To this extent it was the same result as for the analogous uniaxial tests described above. Creep was also found to change with the stress ratio, but no unambiguous relation was detected. As the measured absolute creep values were of the same magnitude as in the uniaxial tests, *Reinhardt* suggested uniaxial tests to be sufficient for the measurement of creep.

3.5.4 State of independence from previous load history

It is often postulated that the stress-strain behaviour of a coated fabric depends on the load history previously applied. As the results presented above show, this is true to some extent. A virgin material naturally shows different behaviour from a previously loaded material. Every time the stress ratio changes, the state of the material changes too, which is mostly associated with the change of yarn crimp. But the findings presented above can also suggest that the yarn crimp no longer changes after a certain number of load cycles. In fact, *Galliot & Luchsinger* [GL11] showed for a PES-PVC material that the stress-strain behaviour depends only on the stress ratio

and the number of load cycles in this stress ratio – and not on the complete previous load history. To do this, they applied blockwise five cycles of 1:1 stress ratio alternating with load blocks consisting of five cycles of other stress ratios than 1:1. Comparison of all the resulting fifth stress-strain paths of the different 1:1 load blocks showed them to be very similar – independent of the previous load history. This very clearly illustrates that the influence of a previous load history can be removed by repeating loads in the same stress ratio.

3.5.5 Influence of prestress level on the slope of the stress-strain paths

Any long-term load generates creep. Based on the experimental results discussed in Chapter 3.5.2.3, a stress-strain path due to application of a load after a hold time can be expected to be steeper for many stress levels. This effect is less distinct in the low stress regions, which are usually linked to prestress. However, prestress as the lowest long-term load can be expected to have some amount of impact on the slope of the stress-strain paths. Investigations by *Galliot & Luchsinger* [GL11] for a tightly woven PES-PVC fabric with a tensile strength of 60 kN/m confirmed this expectation – at least for fill. They exposed two biaxial test specimens to different prestress levels, 1.3 % and 4 % of the tensile strength, each over a duration of six hours. After this prestress hold time, both specimens were loaded with a 1:1 stress ratio up to a stress level equal to 1/5 of the tensile strength. In warp direction practically identical stress-strain response was measured. By contrast, in fill direction the stress-strain path was initially considerably steeper for the specimen with the higher prestress. However, the results also show that the stress-strain path flattens subsequently. Idealising both fill stress-strain paths over the entire investigated working stress range between prestress and 1/5 of the tensile strength with secants, it is revealed that the secant gradient is identical for both prestress variations. The results confirm the findings of *Reinhardt*, as presented in Chapter 3.5.2.3, that interrupted and uninterrupted loads both lead to identical stress-strain paths on the whole. It can be concluded that the prestress level has no significant influence on the secant modulus when the entire working stress range is evaluated as it was here.

3.6 PTFE-coated glass fibre fabrics

Whereas PVC-coated polyester fabrics are investigated thoroughly, test data for PTFE-coated glass fibre fabrics are rarely published. The available investigations into the material behaviour are not as detailed as those by *Reinhardt* for PES-PVC described above. What can be observed from the existing publications is summarised in the following.

The stress-strain behaviour of glass-PTFE fabrics is also considerably anisotropic, nonlinear and nonelastic. Many characteristics are similar to those of PES-PVC. However, while the stress-strain behaviour of PES-PVC in many load situations shows a softening behaviour with increasing stress – at least for the warp direction in the working stress range, which is a consequence of the “Section I” behaviour, see

Figure 14 (b) – glass-PTFE fabrics are characterised by a stiffening behaviour, see e. g. [Ba02], [Mi06], [Me95]: the material is initially very compliant at low stress and under the first load – particularly in fill direction – but the stress-strain path rises sharply when the initial yarn crimp diminishes.

Measured stress-strain paths are documented e. g. in [Mi06], [Me95]. They are given for five different warp:fill stress ratios, which are 1:1, 2:1, 1:2, 1:0 and 0:1. *Minami* [Mi06] shows paths for initial load, whereas the commentary of the Japanese standard MSAJ/M-02-1995 [Me95] shows paths picked from a subsequently conducted load history including all five mentioned stress ratios. In this procedure the single stress ratios are each separated by three 1:1 load cycles. Stress-strain paths of a glass-PTFE fabric type III tested with the biaxial test protocol according to MSAJ/M-02-1995 in the Essen Laboratory for Lightweight Structures (ELLF) are displayed in Figure 23. With the exception of the 1:1 stress ratio, all paths display the behaviour of the first load in the corresponding stress ratio after the previous 1:1 load cycles and the further previous loads respectively. The 1:1 stress-strain paths reflect the third load cycle at the beginning of the test.

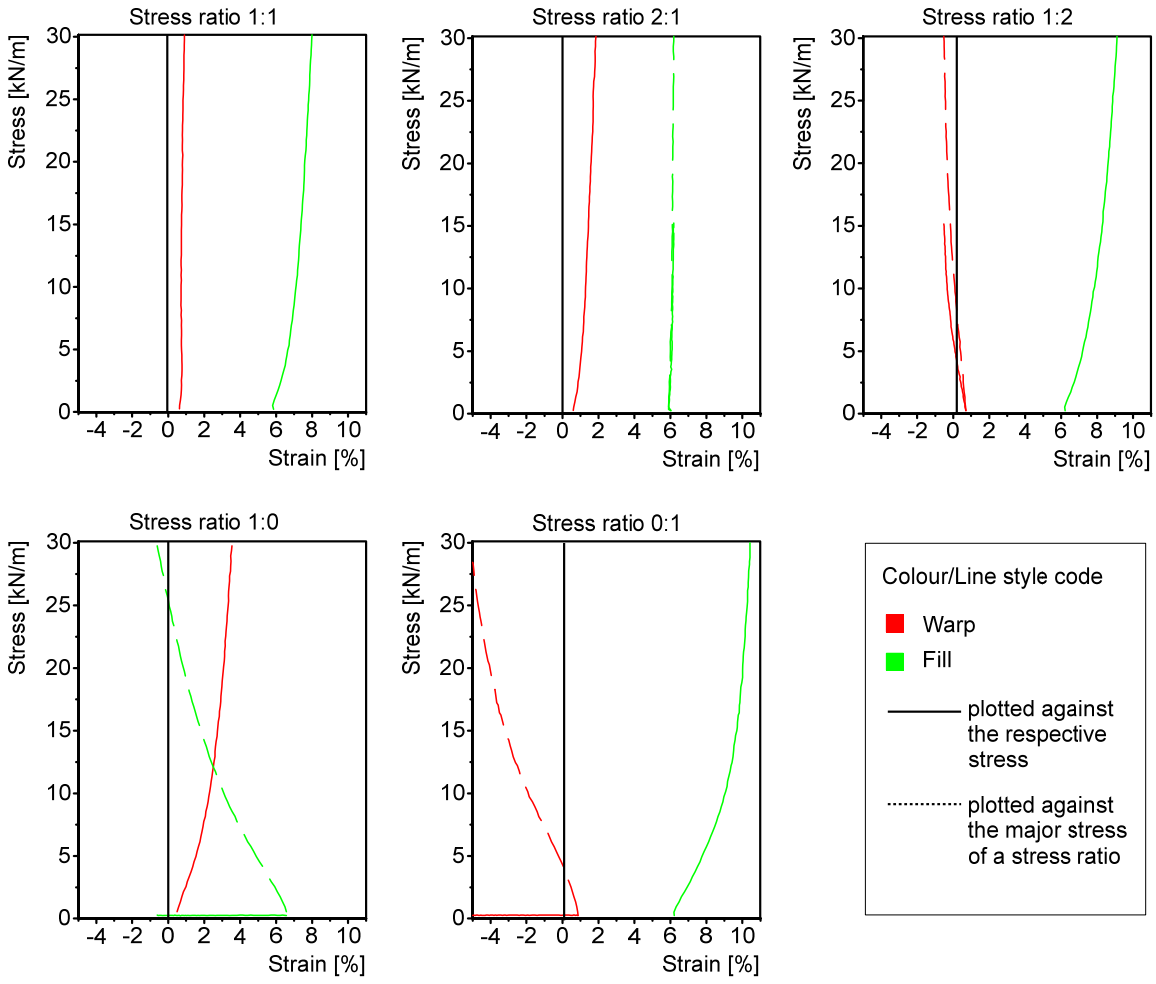

Figure 23 Stress-strain paths for glass-PTFE fabric tested biaxially according to MSAJ/M-02-1995

The continuous lines show stress-strain paths where the strain is plotted against the respective stress of a stress ratio, while the dashed lines show stress-strain paths where the strain is plotted against the major stress of a stress ratio. The major stress refers to the greater stress in a stress ratio. The latter representation has the main advantage that the “zero-stress” paths in the stress ratios 1:0 and 0:1 do not appear as horizontal lines near the strain-axis but as clearly visible and interpretable curves.

The nonlinearity is stronger in the lower stress region. After initial high strains (constructional stretch), the composite behaviour tends towards linear behaviour like that of the glass material used for the fibres. This becomes apparent when conducting uniaxial tests with stresses up to the tensile strength such as those of *Schmidt* [Sc12]. The nonlinearity furthermore depends on the stress ratio. For instance, the warp direction at 1:1 stress ratio shows a visible change of gradient at very low stress but almost linear behaviour beyond that stress level. Essentially, the paths are considerably nonlinear when fill stress predominates.

3.7 Conclusions

Various yarn and coating materials for architectural fabrics have been presented alongside typical and new combinations. Emphasis was placed on the most frequently utilised combinations for architectural outdoor applications: PVC-coated polyester fabrics and PTFE-coated glass fibre fabrics. Fabrication and construction details for these materials were discussed.

As a general rule, the stiffness behaviour of coated woven fabrics has been shown to be nonlinear, nonelastic and anisotropic. It is important to note that two different coating techniques exist for PES-PVC fabrics: a traditional process in which only the warp yarns are stressed during the coating process, and a biaxially prestressed coating system in which the fill yarns are also stressed. The latter technique makes it possible to influence the magnitude of anisotropy.

The stress-strain behaviour of the base materials is quite different. While E-glass behaves in a linear manner, the polymeric synthetic polyester is highly nonlinear. In many stress states this leads to a considerable softening behaviour of polyester fabrics in the working stress range, particularly in warp for the first load in a uniaxial tensile test. The stress-strain behaviour of woven fabrics is characterised by initial constructional stretch, i. e. considerable compliance during the first or first two load cycles in a specific stress ratio. The constructional stretch is essentially responsible for the inelasticity: it does not diminish unless stress is applied in another stress ratio.

In addition to the nonlinearity of polyester itself, it is again mainly the constructional stretch that leads to the nonlinearity of woven fabrics. This can be observed very clearly for glass-PTFE fabrics where the base yarn material is linear. The linearity prevails when the constructional stretch diminishes either after several load cycles in one and the same stress ratio or under high stress levels in general.

Another important aspect governing the stiffness behaviour of woven fabrics is the crimp interchange: yarns in one fabric direction are subject to stronger crimp when the yarns in the orthogonal direction are pulled and straightened. Extensive transverse strain is one major result of this mechanism; another is that the material appears to be most compliant under uniaxial stress and considerably stiffer under uniform biaxial stress, i. e. a warp:fill stress ratio of 1:1.

Generally, viscoelastic behaviour is observed for coated woven fabrics. Creep, revertive creep and stress relaxation are key characteristics. This means that load duration and recovery time are of importance. The above mentioned inelasticity is limited to the first load cycles. The material appears to recover fully after all following load cycles as long as the recovery time is sufficient. Biaxial creep is of the same magnitude as in uniaxial tests. Researchers agree that rate dependency exists but is moderate and negligible compared to other influences.

The stress-strain behaviour under initial load in a specific stress ratio varies considerably from the stress-strain behaviour of all subsequent load cycles in the same stress ratio in that it is much more compliant. The stress-strain behaviour usually stabilises at the latest after five load cycles. The material approximates linear as well as elastic behaviour with an increasing number of load cycles. These processes can be observed for both uniaxial and biaxial tensile stress.

The influence of previous load history can be removed by applying repeat loads in an unaltered stress ratio. The prestress level as the lowest long-term load has no significant influence on the overall slope of stress-strain paths; nor does the hold time on any other stress level.

PES-PVC and glass-PTFE fabrics behave in a similar way in principle. One difference is that glass-PTFE stiffens over the typical working stress range, whereas PES fabric often softens as mentioned above. Another is that the PTFE coating can have a substantial impact on the stiffness of the glass-PTFE composite, while the impact of plasticised PVC on PES-PVC is negligible. To be precise, this is limited to initial loading in fill direction at low stress range. However, it can have a significant influence on installation at low temperature as it is responsible for the temperature dependence of glass-PTFE.

4 Modelling of the material behaviour: state of the art

4.1 General

There are essentially two ways of modelling the behaviour of a coated woven fabric, which itself is in fact a structure rather than a material [Lo71], [Ba07]:

- Phenomenological modelling: the inhomogeneous composite is idealised as an anisotropic homogeneous continuum, see e. g. [Lo71], [RM79], [Me95], [MR95], [BBN04], [So09], [Am10], or
- Microstructural modelling: to model the macrostructure behaviour, i. e. the behaviour of the entire “coated woven fabric” composite, the microstructure is modelled with a discrete mechanical model including the yarns, the matrix etc. as single mechanical elements like beams and springs, see e. g. [Me78], [BB87], [CJS03], [Bö04], [Ba07], [PLI07], [IBG13].

The quality of both approaches depends strictly on the appropriate determination of the material parameters. These material parameters can be e. g. elastic constants in a linear-elastic phenomenological model or the stress-strain behaviour of the yarns, the yarn crimp and the contact data at the yarn intersections in a microstructural model. In order to be adjusted to a specific fabric product, both approaches require experimental testing: the first method requires biaxial testing of the overall fabric, while the latter requires uniaxial testing of the yarns and precise measurement of the section geometry using microscopic images and potential further parameters for the various proposed models. For instance, the constraining effect of the coating could be modelled with spring elements, for which the spring stiffness then has to be estimated.

The strength of microstructural modelling lies more in its scientific benefit to basic research than its usefulness in everyday structural design [Ba07], [MR95]. The phenomenological approach dominates the practical engineering of membranes today. It can be combined with different constitutive laws [SU12], see Figure 24:

- linear-elastic, e. g. [RM79], [MM84], [MR95], [Me95], [BBN04], [Am10],
- multilinear-elastic, e. g. [Me95], [Mi06], [AK14b],
- nonlinear (e. g. hyperelastic), e. g. [Lo71], [BG04], [GL09], [SBS11].

The main objective of the present work is to refine current practical engineering methods in the short term. Hence it is based on phenomenological modelling combined with a linear-elastic constitutive law. The latter is the only one in use in current design practice. Given that it is fast, robust and, furthermore, a firmly established engineering method and thus easy to interpret for many involved in the construction process, it is implemented in every commercial or in-house design software for practical membrane structure design. A deep understanding of the possibilities and limitations of the linear-elastic model applied to coated woven fabrics

combined with a target-oriented determination of the related material parameters delivers the most benefits to structural engineers in the short term [SU12].

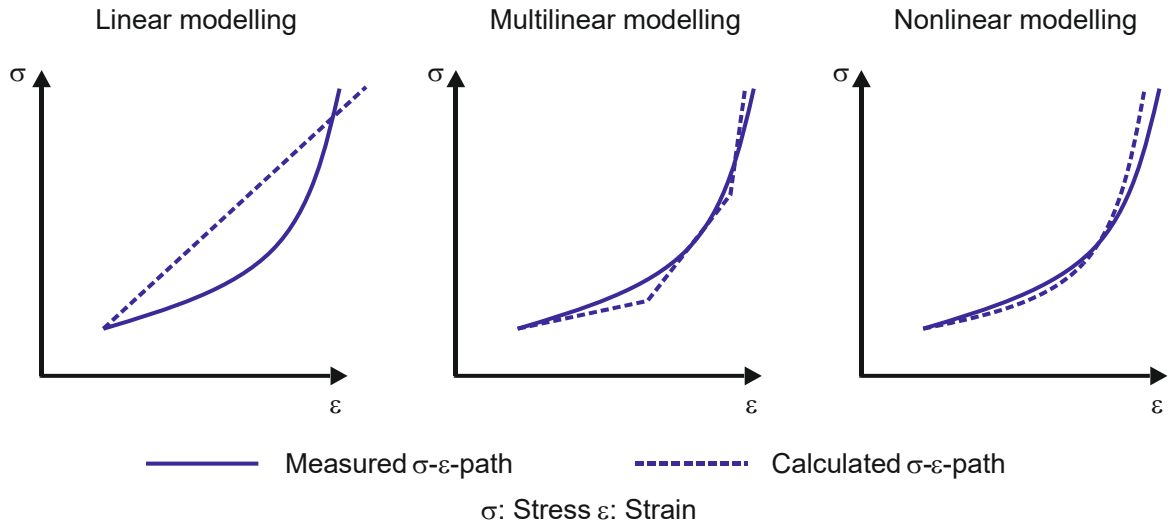

Figure 24 Three phenomenological modelling approaches to nonlinear stress-strain behaviour [SU12]

Linear modelling of a nonlinear stress-strain path may prove to be a somewhat approximate approach depending on the degree of nonlinearity. Nevertheless, it can perfectly model the slope of the path at (1) a specific location with a tangential modulus or (2) within a specific stress or strain interval with a secant modulus.

Going a step further, *Galliot & Luchsinger* [GL09] have proposed an extension of the linear-elastic model with variable secant moduli which depend on the current stress ratio of a membrane element. This procedure has actually made it possible to establish a “simple” nonlinear model.

Chapters 4.2 to 4.5 give a state-of-the-art report on the mechanical background to modelling elastic behaviour of anisotropic materials, particularly for the most relevant material classes related to orthogonally woven fabrics: orthotropic, transversely isotropic and isotropic materials. The main objectives are to demonstrate the limits for the Poisson’s ratios, to show that common fabrics satisfy the restriction to small strain and that different mathematical formulations of the plane stress state are connected with membrane structure analysis. Because woven fabrics often exhibit large Poisson’s ratios, see Chapter 6.2, this topic requires special attention. Considering these boundaries is fundamental when establishing a procedure to determine elastic constants from experimental biaxial tests.

4.2 Fundamentals of anisotropic elasticity

4.2.1 General

The term “elastic” describes a material behaviour in which

- the deformation completely returns to zero after full removal of the load and

- a particular stress state is unambiguously related to a particular strain state, independent of the deformation or loading history and independent of the time [GHW11].

The strain resulting from uniaxial stress in longitudinal direction σ_ℓ applied to an elastic medium can be described with Hooke's law in the form

$$\varepsilon_\ell = \frac{\sigma_\ell}{E_\ell} \tag{4.1}$$

where E_ℓ is the "Young's modulus" in longitudinal direction. The transverse strain ε_t (ε_y in Figure 8) can be described with "Poisson's ratio", which is defined as

$$\nu = -\frac{\varepsilon_t}{\varepsilon_\ell}. \tag{4.2}$$

Originally, the Young's modulus and the Poisson's ratio were defined for the uniaxial stress state. For isotropic materials they are conventionally determined from measured stress-strain results of one single uniaxial (tensile) test.

For a general three-dimensional, homogeneous, linear-elastic continuum with small strains, the stress-strain relation can be modelled with Hooke's law in the form

$$\varepsilon = C \cdot \sigma \quad \text{or} \tag{4.3}$$

$$\sigma = S \cdot \varepsilon. \tag{4.4}$$

The stress σ is linearly linked to the strain ε by the compliance matrix C or the stiffness matrix S respectively. The strain and stress can be given in engineering terms by the vectors

$$\varepsilon = \begin{bmatrix} \varepsilon_x & \varepsilon_y & \varepsilon_z & \gamma_{yz} & \gamma_{xz} & \gamma_{xy} \end{bmatrix}^T, \ \sigma = \begin{bmatrix} \sigma_x & \sigma_y & \sigma_z & \tau_{yz} & \tau_{xz} & \tau_{xy} \end{bmatrix}^T \tag{4.5}$$

where γ and τ are the shear strain and shear stress respectively.

Using terms from "generalised Hooke's law", the compliance matrix $C = \{C_{ij}\}$ for a general anisotropic three-dimensional solid takes the form

$$C = \begin{bmatrix} C_{11} & C_{12} & C_{13} & C_{14} & C_{15} & C_{16} \\ & C_{22} & C_{23} & C_{24} & C_{25} & C_{26} \\ & & C_{33} & C_{34} & C_{35} & C_{36} \\ & & & C_{44} & C_{45} & C_{46} \\ & \text{sym.} & & & C_{55} & C_{56} \\ & & & & & C_{66} \end{bmatrix}, \tag{4.6}$$

and analogously the stiffness matrix $S = \{S_{ij}\}$ becomes

$$S = \begin{bmatrix} S_{11} & S_{12} & S_{13} & S_{14} & S_{15} & S_{16} \\ & S_{22} & S_{23} & S_{24} & S_{25} & S_{26} \\ & & S_{33} & S_{34} & S_{35} & S_{36} \\ & & & S_{44} & S_{45} & S_{46} \\ & \text{sym.} & & & S_{55} & S_{56} \\ & & & & & S_{66} \end{bmatrix}. \tag{4.7}$$

These 6x6 matrices each contain 36 elastic coefficients. Following *Maxwell's* theorem, the matrices are presumed to be symmetrical, i. e. only 21 of the coefficients are independent [RR05], [PW92], see the upper right part of the matrices.

Both matrices are elasticity matrices and contain only the elastic stiffness or compliance. They should not be confused with the stiffness matrix of a finite element, which additionally contains the share of geometric stiffness.

4.2.2 Orthotropic materials

In relation to anisotropic elasticity, different classes of materials are defined employing different states of symmetry. For an "orthotropic" material, i. e. an orthogonal anisotropic material, three orthogonal planes of elastic symmetry exist. This is represented in Figure 25 by different arrow lengths for the Young's moduli in the main coordinate directions. Introducing the elastic coefficients in terms of engineering constants, the compliance matrix for an orthotropic material becomes

$$C = \begin{bmatrix} \frac{1}{E_x} & -\frac{\nu_{xy}}{E_y} & -\frac{\nu_{xz}}{E_z} & 0 & 0 & 0 \\ -\frac{\nu_{yx}}{E_x} & \frac{1}{E_y} & -\frac{\nu_{yz}}{E_z} & 0 & 0 & 0 \\ -\frac{\nu_{zx}}{E_x} & -\frac{\nu_{zy}}{E_y} & \frac{1}{E_z} & 0 & 0 & 0 \\ 0 & 0 & 0 & \frac{1}{G_{yz}} & 0 & 0 \\ 0 & 0 & 0 & 0 & \frac{1}{G_{xz}} & 0 \\ 0 & 0 & 0 & 0 & 0 & \frac{1}{G_{xy}} \end{bmatrix}. \tag{4.8}$$

Here the first index of the Poisson's ratio refers to the direction of the transverse strain and the second refers to the direction of stress that causes the transverse strain [Le68]. For instance, ν_{xy} describes the transverse strain in x-direction due to a stress in y-direction. G is the shear modulus.

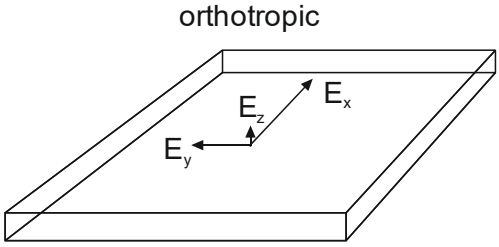

Figure 25 Orthotropic material behaviour, represented by different arrow lengths for the Young's moduli in the main coordinate directions

The requirement for a symmetrical compliance matrix leads directly to

$$\frac{\nu_{xy}}{E_y} = \frac{\nu_{yx}}{E_x} \tag{4.9}$$

and analogously for the other elements along the main diagonal of the matrix. The term in eq. (4.9) is referred to as the "reciprocal relationship". Assuming that E_x is larger than E_y, ν_{yx} is larger than ν_{xy}. For this reason ν_{yx} is also referred to as the "major Poisson's ratio" in this usual case and ν_{xy} as the "minor Poisson's ratio" [Ans14]. With regard to symmetry and considering that for orthotropic materials the shear modulus is independent from the Young's modulus and the Poisson's ratio [RR05], the compliance matrix in eq. (4.8) shows that an orthotropic material is defined by nine independent elastic constants: six to describe the normal stress-normal strain relations and three to describe the shear stress-shear strain relations.

Inverting the compliance matrix leads to the stiffness matrix

$$S = C^{-1} = \begin{bmatrix} \frac{(1-\nu_{yz}\nu_{zy})}{E_y E_z \Delta} & \frac{(\nu_{xy}+\nu_{xz}\nu_{zy})}{E_y E_z \Delta} & \frac{(\nu_{xz}+\nu_{xy}\nu_{yz})}{E_y E_z \Delta} & 0 & 0 & 0 \\ \frac{(\nu_{yx}+\nu_{yz}\nu_{zx})}{E_x E_z \Delta} & \frac{(1-\nu_{xz}\nu_{zx})}{E_x E_z \Delta} & \frac{(\nu_{yz}+\nu_{yx}\nu_{xz})}{E_x E_z \Delta} & 0 & 0 & 0 \\ \frac{(\nu_{zx}+\nu_{yx}\nu_{zy})}{E_x E_y \Delta} & \frac{(\nu_{zy}+\nu_{xy}\nu_{zx})}{E_x E_y \Delta} & \frac{(1-\nu_{xy}\nu_{yx})}{E_x E_y \Delta} & 0 & 0 & 0 \\ 0 & 0 & 0 & G_{yz} & 0 & 0 \\ 0 & 0 & 0 & 0 & G_{xz} & 0 \\ 0 & 0 & 0 & 0 & 0 & G_{xy} \end{bmatrix} \tag{4.10}$$

where

$$\Delta = \frac{(1-\nu_{xy}\nu_{yx}-\nu_{yz}\nu_{zy}-\nu_{zx}\nu_{xz}-2\nu_{xy}\nu_{yz}\nu_{zx})}{E_x E_y E_z}. \tag{4.11}$$

4.2.3 Transversely isotropic materials

Transversely isotropic materials have *one* isotropic plane [RR05]. Assuming the xy-plane is the isotropic plane, the following equations can be stated:

$$E_x = E_y = E\,, \tag{4.12}$$

$$E_z = E'\,, \tag{4.13}$$

$$\nu_{xy} = \nu_{yx} = \nu\,, \tag{4.14}$$

$$\nu_{xz} = \nu_{yz} = \nu'\,, \tag{4.15}$$

$$G_{yz} = G_{xz} = G'\,, \tag{4.16}$$

$$G_{xy} = G\,. \tag{4.17}$$

This is represented in Figure 26 by different arrow lengths for the Young's moduli in the plane and through-thickness direction. With these six elastic constants the compliance matrix becomes

$$C = \begin{bmatrix} \frac{1}{E} & -\frac{\nu}{E} & -\frac{\nu'}{E'} & 0 & 0 & 0 \\ & \frac{1}{E} & -\frac{\nu'}{E'} & 0 & 0 & 0 \\ & & \frac{1}{E'} & 0 & 0 & 0 \\ & & & \frac{1}{G'} & 0 & 0 \\ & \text{sym.} & & & \frac{1}{G'} & 0 \\ & & & & & \frac{1}{G} \end{bmatrix}. \tag{4.18}$$

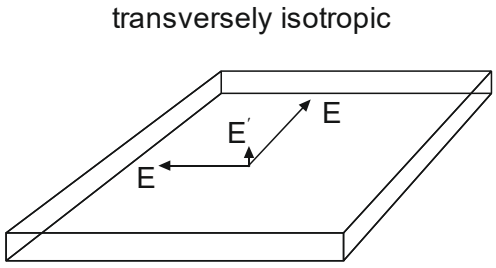

Figure 26 Transversely isotropic material behaviour, represented by equal arrow lengths in the plane coordinate directions and a different arrow length for the Young's modulus in the through-thickness direction

For transversely isotropic materials, the following dependence for the shear modulus in the isotropic plane applies, which is well known from isotropic materials [RR05]:

$$G = \frac{E}{2(1+\nu)}. \tag{4.19}$$

As one of the six elastic constants is dependent on the others, five independent constants remain to characterise a transversely isotropic material.

4.2.4 Isotropic materials

Isotropy can be interpreted as a special form of anisotropy. The stress-strain relations in all three coordinate directions are the same. See Figure 27 for the symbols used.

$$E_x = E_y = E_z = E, \tag{4.20}$$

$$\nu_{xy} = \nu_{xz} = \nu_{yz} = \nu, \tag{4.21}$$

$$G_{xy} = G_{xz} = G_{yz} = G. \tag{4.22}$$

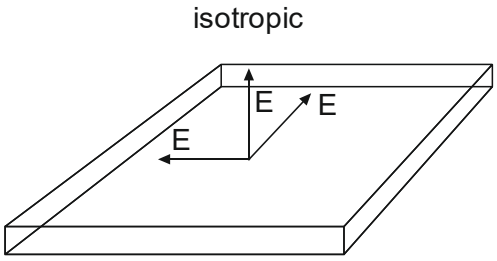

Figure 27 Isotropic material behaviour, represented by equal arrow lengths for the Young's moduli in the main coordinate directions

The compliance matrix becomes

$$C = \frac{1}{E}\begin{bmatrix} 1 & -\nu & -\nu & 0 & 0 & 0 \\ & 1 & -\nu & 0 & 0 & 0 \\ & & 1 & 0 & 0 & 0 \\ & & & 2(1+\nu) & 0 & 0 \\ & \text{sym.} & & & 2(1+\nu) & 0 \\ & & & & & 2(1+\nu) \end{bmatrix} \tag{4.23}$$

and the stiffness matrix

$$S = \frac{E}{(1+\nu)(1-2\nu)}\begin{bmatrix} 1-\nu & \nu & \nu & 0 & 0 & 0 \\ & 1-\nu & \nu & 0 & 0 & 0 \\ & & 1-\nu & 0 & 0 & 0 \\ & & & \tfrac{1}{2}-\nu & 0 & 0 \\ & \text{sym.} & & & \tfrac{1}{2}-\nu & 0 \\ & & & & & \tfrac{1}{2}-\nu \end{bmatrix}. \tag{4.24}$$

From the demoninator in eq. (4.24) the familiar limits of ν can be observed: ν cannot be equal or smaller than -1 nor equal to or greater than 0.5. Otherwise, this would

result in infinite or negative stresses for a positive strain state, both of which are implausible.

4.2.5 Restrictions on elastic constants

In the previous chapters it was shown for isotropic materials and transversely isotropic materials in the isotropic plane that the shear modulus has a dependence on the Young's modulus and the Poisson's ratio. The shear modulus is thus fixed via these two constants. This is not the case for orthotropic materials.

More interesting information is forthcoming from the investigation into boundaries for the Poisson's ratios. This is because they are known to attain very high values for composite materials, see e. g. [Le68], [CS88], [Pe07]. As mentioned above, limit values for the isotropic solid are known to be $-1 < \nu < 0.5$. These values can be derived from the "thermodynamic requirement of positive strain energy". Positive strain energy is a requirement for plausibility: more simply, it ensures that the constitutive equations lead for a medium under tensile stress to positive strain (expansion) in the direction of the tensile stress.

Orthotropic materials

Lempriere appeared to be the first to investigate the implications of the thermodynamic requirement of positive strain energy for orthotropic materials. He derived limit values for the Poisson's ratios of orthotropic and transversely isotropic materials and demonstrated the transition of the limit values to those of isotropic solids when a transversely isotropic material approaches full isotropy [Le68]. This work is reflected here for a better understanding of the context.

In order to ensure positive strain energy, a positive-definite compliance and stiffness matrix is required. The term "positive-definite" means that the determinant of the matrix and all submatrices is positive. The first submatrix of the compliance matrix is $1/E_x$, see eq. (4.8). This value must be positive, which gives

$$E_x > 0 \,. \tag{4.25}$$

The same applies for all other diagonal elements of the compliance matrix: Young's moduli and shear moduli. All must be positive in order to ensure the above mentioned plausibility. Analogously, the diagonal elements of the stiffness matrix must also be positive. Considering eq. (4.10) this leads to

$$\left(1-\nu_{yz}\nu_{zy}\right),\left(1-\nu_{xz}\nu_{zx}\right),\left(1-\nu_{xy}\nu_{yx}\right) > 0 \tag{4.26}$$

and

$$\Delta = 1-\nu_{xy}\nu_{yx}-\nu_{yz}\nu_{zy}-\nu_{zx}\nu_{xz}-2\nu_{xy}\nu_{yz}\nu_{zx} > 0 \,. \tag{4.27}$$

The expression in eq. (4.26) can also be written in the form

$$\nu_{yz}\nu_{zy},\nu_{yz}\nu_{zx},\nu_{xy}\nu_{yx} < 1 \tag{4.28}$$

or – using the symmetry conditions eq. (4.9) –

$$\begin{aligned} |\nu_{xy}| &< \sqrt{\frac{E_y}{E_x}} \qquad |\nu_{yx}| < \sqrt{\frac{E_x}{E_y}} \\ |\nu_{yz}| &< \sqrt{\frac{E_z}{E_y}} \qquad |\nu_{zy}| < \sqrt{\frac{E_y}{E_z}} \\ |\nu_{zx}| &< \sqrt{\frac{E_x}{E_z}} \qquad |\nu_{xz}| < \sqrt{\frac{E_z}{E_x}} \end{aligned} \tag{4.29}$$

and the expression in eq. (4.27) can be written as

$$\nu_{xy}\nu_{yz}\nu_{zx} < \frac{1-\nu_{xy}^2\left(\frac{E_x}{E_y}\right)-\nu_{yz}^2\left(\frac{E_y}{E_z}\right)-\nu_{zx}^2\left(\frac{E_z}{E_x}\right)}{2} < 1/2 . \tag{4.30}$$

The latter condition clearly shows that the Poisson's ratio in the xy-plane ν_{xy} is subject to more stringent limitation for all values $\nu_{yz} \neq 0$, $\nu_{zx} \neq 0$ than in eq. (4.29).

Transversely isotropic materials

Assuming an isotropic xy-plane, eqs (4.12 – 4.15) apply. In this case eq. (4.29) reduces to

$$-1 < \nu < 1 \tag{4.31}$$

as well as

$$-\sqrt{\frac{E'}{E}} < \nu' < \sqrt{\frac{E'}{E}} \tag{4.32}$$

and eq. (4.30) reduces to

$$\nu < 1 - 2\nu'^2\left(\frac{E}{E'}\right) \tag{4.33}$$

which is more restrictive than the upper constraint of eq. (4.31). Hence, the limits for the in-plane Poisson's ratio of a transversely isotropic material can be given as

$$-1 < \nu < 1 - 2\nu'^2\left(\frac{E}{E'}\right). \tag{4.34}$$

Isotropic materials

Assuming E' = E and ν' = ν, the last constraint leads to

$$-1 < \nu < 1/2 . \tag{4.35}$$

It is clear that the familiar limit for isotropic materials of ν < 0.5 can only be obtained when the conditions are examined in the three-dimensional space. This is important when considering a plane stress state as is usual in the field of membrane structure analysis.

4.3 The plane stress state

Membrane materials are thin, i. e. the through-thickness dimension is much smaller than the typical in-plane dimensions. Hence, when it comes to the analysis of structural membranes, a plane stress state is presumed in design practice, i. e. $\sigma_z = 0$ and also $\tau_{yz} = \tau_{xz} = 0$. As woven fabrics are normally orthogonally anisotropic in the plane, the shear modulus is not dependent on the Young's modulus and the Poisson's ratio (see previous chapter). Thus it can be treated independently and is disregarded in the following. Using eq. (4.3) with the compliance matrix eq. (4.8) and assuming a plane stress state with $\sigma_z = 0$ leads to the following set of equations for the strains

$$\begin{aligned}
\varepsilon_x &= \frac{1}{E_x}\sigma_x - \frac{\nu_{xy}}{E_y}\sigma_y + 0 \\
\varepsilon_y &= -\frac{\nu_{yx}}{E_x}\sigma_x + \frac{1}{E_y}\sigma_y + 0 \\
\varepsilon_z &= -\frac{\nu_{zx}}{E_x}\sigma_x + \frac{\nu_{zy}}{E_y}\sigma_y + 0
\end{aligned} \tag{4.36}$$

which demonstrates that the strain in through-thickness direction ε_z does not disappear. However, as the deformation of a membrane in through-thickness direction is not restrained, the strain ε_z does not lead to stresses in the membrane [HM01]. It can therefore be treated independently. Eq. (4.36) – again written as matrices – reduces to:

$$\begin{bmatrix} \varepsilon_x \\ \varepsilon_y \end{bmatrix} = \begin{bmatrix} \frac{1}{E_x} & -\frac{\nu_{xy}}{E_y} \\ -\frac{\nu_{yx}}{E_x} & \frac{1}{E_y} \end{bmatrix} \begin{bmatrix} \sigma_x \\ \sigma_y \end{bmatrix}. \tag{4.37}$$

In terms of stresses these relations become

$$\begin{bmatrix} \sigma_x \\ \sigma_y \end{bmatrix} = \frac{1}{1-\nu_{xy}\nu_{yx}} \begin{bmatrix} E_x & \nu_{xy}E_x \\ \nu_{yx}E_y & E_y \end{bmatrix} \begin{bmatrix} \varepsilon_x \\ \varepsilon_y \end{bmatrix}. \tag{4.38}$$

Indeed, the same constraints for the Poisson's ratio apply as examined in the chapters above, derived from the requirement for a positive-definite compliance and stiffness matrix respectively [Jo75], [AG93]. Thus eqs. (4.28) and (4.29) reduce to

$$\nu_{xy} \cdot \nu_{yx} < 1 \text{ or } \left|\nu_{xy}\right| < \sqrt{\frac{E_y}{E_x}}. \tag{4.39}$$

A comparison with eq. (4.27) or eq. (4.30) reveals that the terms of eq. (4.39) correspond to a three-dimensional material with Poisson's ratios in the through-thickness direction of $\nu_{yz} = \nu_{xz} = 0$. Moreover, the right-hand side inequality of

eq. (4.39) shows that the limit for the minor Poisson's ratio ν_{xy} decreases with an increasing orthotropy ratio E_x/E_y (while the limit for the major Poisson's ratio ν_{yx} increases at the same time). When the orthotropy ratio approaches $E_x/E_y = 1$ – which means transverse isotropy – the minor Poisson's ratio approaches its maximum limit of $\nu_{xy} < 1$.

When the independent shear modulus is omitted – which is done in the present work throughout – and when the reciprocal relationship of eq. (4.9) is considered, a plane orthotropic elastic material is fully characterised by one set of three elastic constants: typically E_x, E_y and one of the Poisson's ratios. In this work the minor Poisson's ratio ν_{xy} will be used preferentially. The only reason for this is the fixed maximum limit value of one. The fixed maximum limit allows for a useful valuation of a concrete Poisson's ratio.

4.4 Direct stiffness formulation

In addition to the formulation of the constitutive law presented in the preceding chapters – the "inverse stiffness" formulation according to [SaP15] –, another mathematical formulation for the stress-strain relations in the plane stress state is widely used in the field of structural membrane analysis. This is known as the "direct stiffness" formulation [SaP15]:

$$\begin{bmatrix} \sigma_x \\ \sigma_y \end{bmatrix} = \begin{bmatrix} E_x^d & E_{xy}^d \\ E_{yx}^d & E_y^d \end{bmatrix} \begin{bmatrix} \varepsilon_x \\ \varepsilon_y \end{bmatrix} \tag{4.40}$$

where E_x^d, E_y^d is the direct stiffness in x- and y-direction and E_{xy}^d, E_{yx}^d is the interchange stiffness in x- and y-direction. In fabric structures the latter is often referred to as the crimp interchange stiffness. The superscript "d" particularly marks the "direct stiffness" constants. This is important since direct stiffness E_x^d, E_y^d and inverse stiffness E_x, E_y do not exhibit the same values in the usual case where the crimp interchange stiffness or the Poisson's ratio are not equal to zero.

Essentially, both formulations – inverse or direct stiffness – are equivalent. The inverse stiffness formulation is used in the present work, but the elastic constants are convertible. Transformation from inverse to direct stiffness can be done by

$$E_x^d = \frac{E_x}{\left(1 - \nu_{xy} \cdot \nu_{yx}\right)}, \tag{4.41}$$

$$E_y^d = \frac{E_y}{\left(1 - \nu_{xy} \cdot \nu_{yx}\right)}, \tag{4.42}$$

$$E_{xy}^d = \nu_{xy} \cdot E_x^d, \tag{4.43}$$

$$E_{yx}^d = \nu_{yx} \cdot E_y^d. \tag{4.44}$$

Reverse conversion can be done by

$$E_x = E_x^d \cdot \left(1 - \nu_{xy} \cdot \nu_{yx}\right), \tag{4.45}$$

$$E_y = E_y^d \cdot \left(1 - \nu_{xy} \cdot \nu_{yx}\right), \tag{4.46}$$

$$\nu_{xy} = \frac{E_{xy}^d}{E_x^d}, \tag{4.47}$$

$$\nu_{yx} = \frac{E_{yx}^d}{E_y^d}. \tag{4.48}$$

4.5 Restriction to small strains in the theory of elasticity

In order to achieve an acceptable level of accuracy, the classical theory of elasticity restricts strains $\varepsilon = \Delta\ell/\ell_0$ to “small strains” – independent of whether the inverse stiffness or the direct stiffness formulation is applied. For conventional materials like metals, glass, stone or timber, a maximum strain smaller than 1% can be presumed [PW92].

Strains of higher order need to be negligibly small [GHW11]. In more simple terms: to ensure acceptable accuracy, the square of the strain must be negligible in comparison to the strain itself: $\varepsilon^2 << \varepsilon$.

While small strain is sometimes restricted to 5%, see e. g. [Aba14], in the field of composites – which often exhibit considerably greater strains than 1% – it is common to consider strains of up to 10% acceptable for small strain theory, see e. g. [Pe07].

The common polyester and glass fibre fabrics investigated in the present work exhibit a strain increment of no more than approximately $\Delta\varepsilon = 8\%$ in the stress range that is aimed to be modelled using the linear theory of elasticity. This value reflects a strain increment correlated to the fabric state at which the constructional stretch is eliminated. This is referred to as the stable state of the fabric, see Chapter 6.2.2 for details and definitions. This chapter also presents experimental results proving the measured strain difference to be a maximum of $\Delta\varepsilon = 7.7\%$. This maximum occurs for a high-strength PES material type V under uniaxial fill stress. The given value of 8% is a representation of this experimental result. No higher strain increment is expected at any time for the entire range of investigated PES-PVC and glass-PTFE materials. Quite the contrary can be expected, in fact, with considerably smaller strain increments apparent for the usual biaxial stress states. Overall, limit values for small strains are met in every case. The analysis results can be expected to have acceptable accuracy for all common PES-PVC and glass-PTFE fabrics in all usual civil engineering applications.

4.6 Conclusions

General possibilities of material modelling – linear, multilinear or nonlinear phenomenological and basically nonlinear microstructural modelling – were presented and discussed at the beginning. With regard to linear-elastic modelling, the fundamental principles of anisotropic elasticity were reflected by means of the most relevant material classes: orthotropic, transversely isotropic and fully isotropic. The limit values for the Poisson's ratios have been stated for these materials. Moreover, it was shown that the shear modulus is completely independent from the Young's modulus and the Poisson's ratios for orthotropic materials. For transversely isotropic materials, the dependence known for fully isotropic materials applies in the isotropic plane.

The stress-strain relations for plane stress were given in terms of the inverse stiffness formulation – which is used throughout this work – and the direct stiffness formulation. Emphasis was placed on the fact that the elastic constants in both formulations usually do not exhibit the same values. Numbers must therefore be used with caution in practice. When numbers are given, it is advisable to clearly indicate the formula for which they are valid. In the frame of the present work, direct stiffness elastic constants are marked with the superscript "d". The different sets of elastic constants resulting from the different mathematical formulations can be interconverted, for which equations were also presented. Essentially, both formulations are equivalent in their capacity to describe the physical behaviour of an elastic material.

Furthermore, both are limited to small strain. It was shown that the small strain restriction applies for all common PES-PVC and glass-PTFE fabrics in all typical design situations.

5 Survey of materials investigated

Several material producers were requested to provide material for experimental research purposes within this work. Four producers sent materials; in alphabetical order they are: Mehler Texnologies GmbH, Hückelhoven, Germany, Sattler AG, Gössendorf, Austria, Serge Ferrari S.A.S, La Tour du Pin Cedex, France and Verseidag-Indutex GmbH, Krefeld, Germany. The following materials were provided for experimental testing:

- PES-PVC materials, traditionally coated from three different material producers, plus materials with a biaxially prestressed coating system from one material producer, ranging overall from type II to type V,
- glass-PTFE materials type II, III and IV from one material producer.

A total of 15 different materials were provided, 12 PES-PVC fabrics and three glass-PTFE fabrics. Table 2 gives an overview. The producers remain anonymous in the following investigations, each being assigned a number in random order. The aim is to emphasise the material-dependent characteristics as far as possible. One producer submitted PES-PVC as well as glass-PTFE fabrics. The “glass-PTFE producer” is assigned number 5 in order not to reveal which of the four PES-PVC producers it is. The given type classification reflects the classification of the material producers. Tensile test results presented hereafter show that the producers’ classifications actually align well with the uniform classification provided in [SaP15].

Table 2 Materials provided for experimental investigations and type classification as given by the material producers

Material producer	Coating technique	Material class			
		Type II	Type III	Type IV	Type V
PVC-coated polyester fabric					
1	Traditional	+	+	+	-
2	Traditional	+	+	-	+
3	Traditional	+	+	+	-
4	Biaxially prestressed	+	+	+	-
PTFE-coated glass fibre fabric					
5	Traditional	+	+	+	-

+: provided
-: not provided

For all the materials the most important mechanical properties associated with the stiffness behaviour were measured in the Essen Laboratory for Lightweight Structures (ELLF) at the University of Duisburg-Essen: tensile strength according to

[DIN EN ISO 1421:1998-08], total mass according to [DIN EN ISO 2286-2:2015-04], thickness according to [DIN EN ISO 2286-3:2015-04] and yarn density according to [DIN EN 1049-2:1994-02]. The weave structure was identified. The yarn size – which could not be measured in the ELLF – was provided by the material producers.

Thirty tensile test series – 15 fabrics each in warp and fill – were performed on the 50 kN Zwick/Roell static testing machine of the ELLF, see Figure 28. Each test series comprises five tensile tests. Among other recorded characteristics, the tensile test results are provided in Table 3 for all materials as mean values $f_{m,23}$ derived from five tensile tests per material at room temperature T = 23°C.

Figure 28 50 kN Zwick/Roell static testing machine of the Essen Laboratory for Lightweight Structures (ELLF) at the University of Duisburg-Essen with a tensile test specimen

Figure 29 presents force-strain paths recorded during the tensile tests as examples of PES-PVC type III from material producer 2 and 4 as well as glass-PTFE type II. These three fabrics are of similar tensile strength. The membrane stress is derived from the force data by dividing the measured force by the test specimen width of b = 5 cm.

The deviations in tensile strength results in the single test series were found to be very low. While the mean value of coefficients of variation of all test series was only

V_x = 2.1 %, the maximum coefficient of variation in one test series was found to be max V_x = 4.9 %. This confirms published values of max V_x = 6 % [Mi81] to max V_x = 8 % [Ho79] (cited in [Mi81]) as an upper boundary. No significant differences in deviation between the three different material groups - traditionally coated PES-PVC, biaxially prestressed coated PES-PVC, and glass-PTFE - were observed. Overall, the low deviations demonstrate high production quality of all the investigated materials.

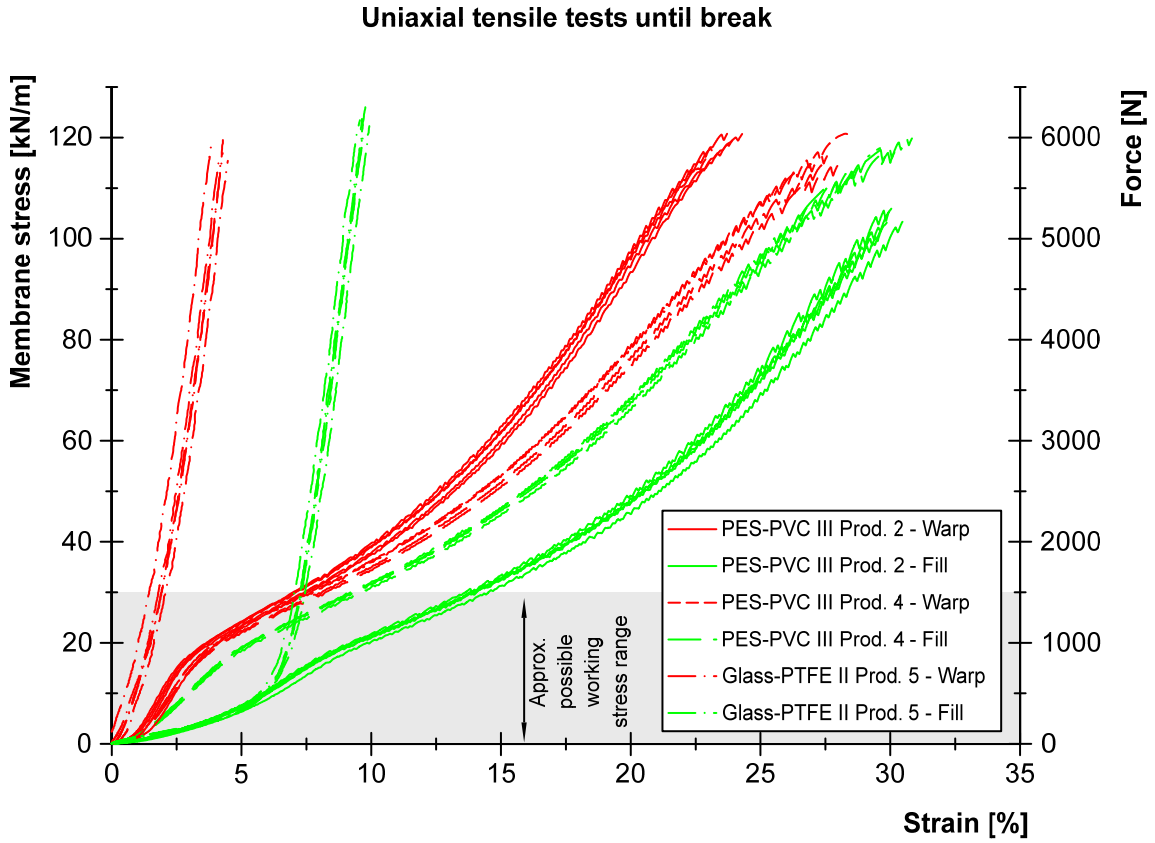

Figure 29 Force-strain paths recorded during the tensile tests and derived stress-strain paths for PES-PVC type III from material producer 2 and 4, as well as glass-PTFE type II

The 5%-fractiles of the tensile strength $f_{k,23}$ were calculated for every test series according to [EN 1990:2002] with the following equation:

$$f_{k,23} = f_{m,23} \cdot (1 - k_n \cdot V_x) \qquad (5.1)$$

where

$f_{m,23}$ mean value of the test results for n tests [kN/m], assuming a normal distribution,

k_n characteristic fractile factor given in Table D.1 of EN 1990, Annex D, depending on the numbers of tests and whether the coefficient of variation is known or unknown [-],

V_x coefficient of variation [-].

The fractile factor k_n = 2.33 was picked from Table D.1 of EN 1990, Annex D, for a test series of n = 5 single tests and the condition “V_X unknown”. The results are given in Table 3.

Similar results were found for the deviations in the strain at break. While the mean value of coefficients of variation of all 30 test series was V_x = 2.1 %, the maximum coefficient of variation was found in two test series to be max V_x = 5.8 %. But these maxima appear rather as outliers, see Figure 30. The results are otherwise very even, with low deviations. Again, no significant differences in deviation between the three different material groups traditionally coated PES-PVC, biaxially prestressed coated PES-PVC and glass-PTFE were observed. The very uniform test data promise reliable results for the stress-strain investigations in the following chapters.

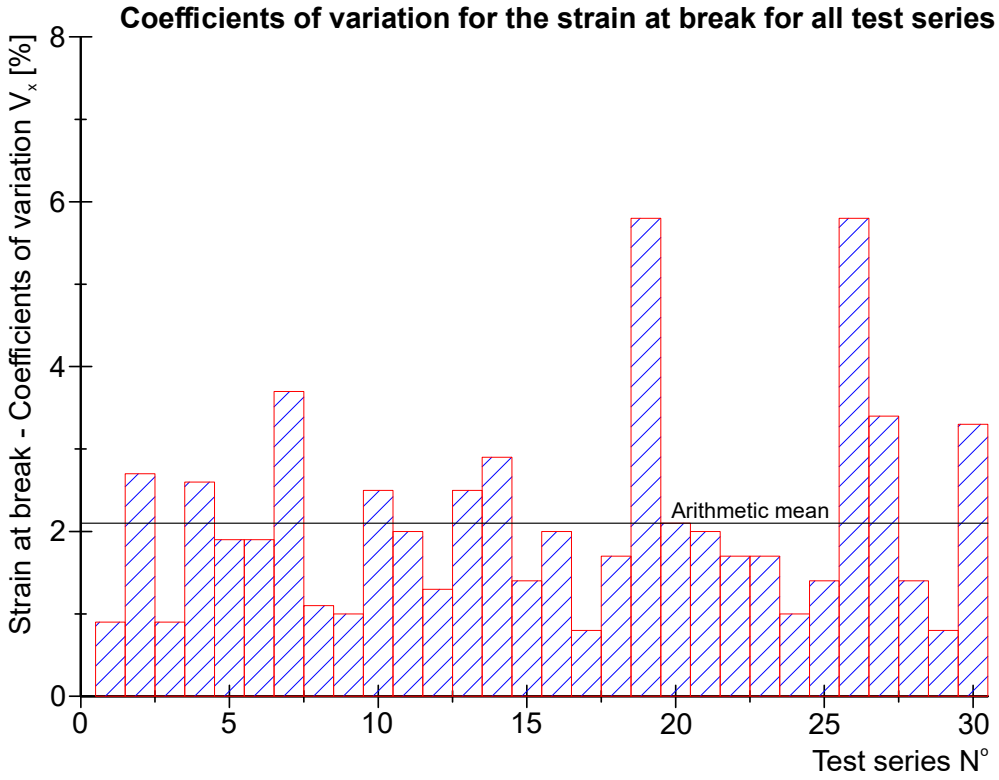

Figure 30 Coefficients of variation V_x for the strain at break for all 30 tensile test series

Tensile strength and the other recorded physical characteristics such as total weight and thickness are fairly even within one material class. This statement applies for PES-PVC types II, III and IV, for which several material producers can be compared. Only single exceptions are apparent. For instance, producer 2 provides a PES-PVC type III with more coating thickness than the other producers for their type III fabrics: the total weight and the thickness stand out from the average. Material producer 4 uses not only a different coating technique but also different weaves than the others.

The glass-PTFE fabrics are considerably thinner than the PES-PVC fabrics of similar tensile strength. They nevertheless exhibit much more yarn crimp.

Table 3 Summary of all measured and recorded material properties

Material producer	$f_{m,23}$ warp/fill [kN/m]	$f_{k,23}$ warp/fill [kN/m]	Total weight [g/m²]	Thickness [mm]	Weave	Yarn density warp/fill [yarns/cm]	Microscopic cross-section	
							Cut through fill yarns	Cut through warp yarns
PES-PVC type II								
1	95.5 / 93.3	89.0 / 90.0	911	0.75	2/2	12.3 / 13.0		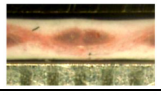
2	91.4 / 84.1	89.9 / 79.9	913	0.76	2/2	11.6 / 12.0	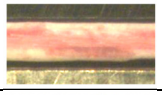	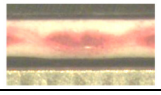
3	87.5 / 92.6	80.1 / 82.0	902	0.77	2/2	11.3 / 12.4	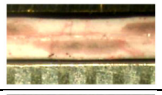	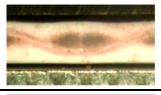
4	87.6 / 83.8	82.7 / 75.0	1051	0.84	2/1	11.4 / 5.8	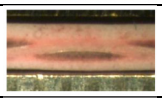	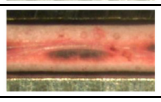
PES-PVC type III								
1	127.3 / 113.6	124.6 / 110.4	1036	0.85	2/2	10.8 / 10.4	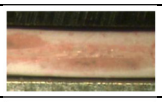	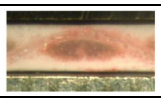
2	118.9 / 104.1	113.9 / 100.4	1266	1.00	2/2	10.2 / 9.8	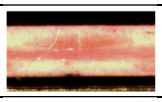	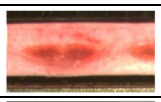
3	129.4 / 120.2	126.0 / 113.7	1078	0.95	2/2	10.8 / 10.5	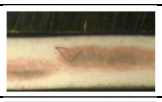	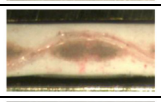
4	116.4 / 118.2	110.4 / 114.9	1053	0.86	2/1	9.6 / 8.0	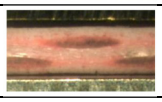	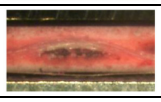
PES-PVC type IV								
1	167.4 / 162.0	164.2 / 160.1	1317	1.08	3/3	13.6 / 13.9	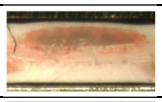	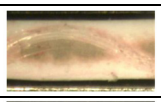
3	167.9 / 160.6	161.2 / 152.7	1329	1.16	3/3	14.1 / 14.0	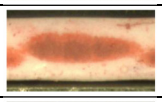	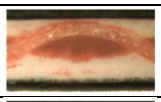
4	169.1 / 144.2	164.3 / 135.8	1355	1.08	4/1	23.0 / 4.9	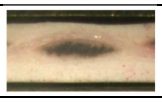	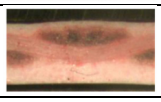
PES-PVC type V								
2	208.7 / 188.8	198.4 / 176.4	1594	1.37	3/3	13.8 / 13.5	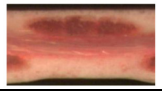	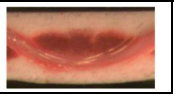

Table 3 continued

Material producer	$f_{m,23}$ warp/fill [kN/m]	$f_{k,23}$ warp/fill [kN/m]	Total weight [g/m²]	Thickness [mm]	Weave	Yarn density warp/fill [yarns/cm]	Microscopic cross-section	
							Cut through fill yarns	Cut through warp yarns
Glass-PTFE type II								
5	117.2 / 122.8	113.3 / 116.5	752	0.46	1/1	14.0 / 12.4	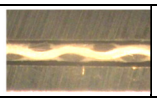	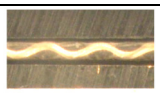
Glass-PTFE type III								
5	142.9 / 120.3	129.9 / 110.2	1195	0.72	1/1	12.2 / 10.1	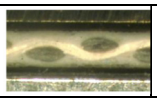	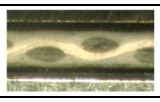
Glass-PTFE type IV								
5	201.6 / 172.7	196.4 / 163.8	1585	0.94	1/1	10.1 / 6.7	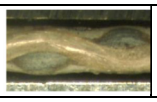	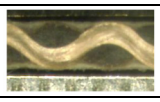

All basic characteristics of the investigated materials are also summarised in Annex A, ordered by material producer and including full microscopic cross-section pictures in warp and fill direction as well the yarn size provided by the manufacturer.

6 Experimental investigations into the structural behaviour of coated architectural fabrics

6.1 General

In order to achieve a complete picture of the principal stiffness characteristics of the most commonly used coated architectural fabrics to date, the objective is to confirm and expand on the latest test results as presented in Chapter 3 for the full range of PES-PVC and glass-PTFE materials. For this reason, the first step was to perform uniaxial tensile tests with and without recovery times for a great variety of material types. In addition to the first step, tests with hold times at maximum test stress level were performed as well as tests with alternation of warp and fill stressing. Secondly, orthogonally loaded membrane strip tests were planned and conducted in order to work out and demonstrate the application of elastic constants in a membrane structure analysis. The tests simulate a uniaxially prestressed membrane strip between fixed boundaries to which an external load is applied orthogonally to the undeformed membrane plane. These tests deliver a deep understanding of the structural behaviour which – as one aspect – depends heavily on the material stiffness behaviour. The investigations show the development of membrane stress and deflections over several load cycles. The main aim is to clarify the load cycle on which an elastic constant determination should be based for safe and accurate design. It is essential to close all these gaps in knowledge in order to develop principles of biaxial testing and determine design elastic constants.

A great number of biaxial experimental tests directly linked to and derived from established biaxial test procedures were also conducted. The results are presented in Chapter 7. They are used to analyse the strengths and weaknesses of existing procedures with regard to different materials.

All measurements and tests described in the following chapters were performed in the Essen Laboratory for Lightweight Structures (ELLF) at the University of Duisburg-Essen. Only virgin materials supplied direct from the material producers were used. All investigations were made at room temperature T = 23°C. The tests were performed force controlled and if not stated otherwise the loading rate was 0.2 (kN/m)/s.

6.2 Uniaxial tensile tests

6.2.1 General

Uniaxial tensile tests are very well suited for the investigation of principles because of their relative simplicity compared to biaxial tests. The knowledge gained from uniaxial tests makes it possible to understand the principles of the material stiffness behaviour and in that way to develop biaxial testing procedures in a further step. One objective of the uniaxial tensile tests is to prove or disprove the principles described

in Chapter 3, which were based mainly on one type of a PES-PVC mesh fabric. For this purpose, the range of tested materials is extended to include all common types of current PVC-coated PES-fabrics and PTFE-coated glass fibre fabrics. The second objective is to investigate the transverse strain properties of common woven architectural fabrics. Thirdly, the load direction is altered between warp and fill direction in order to investigate if and when independence from a previous load history occurs for all common materials. The last two analyses have not been undertaken in this depth in work to date. To enable these investigations, the uniaxial tensile tests were conducted with cruciform test specimens on the 50 kN servohydraulic biaxial test rig of the Essen Laboratory for Lightweight Structures (ELLF) at the University of Duisburg-Essen, see Figure 31.

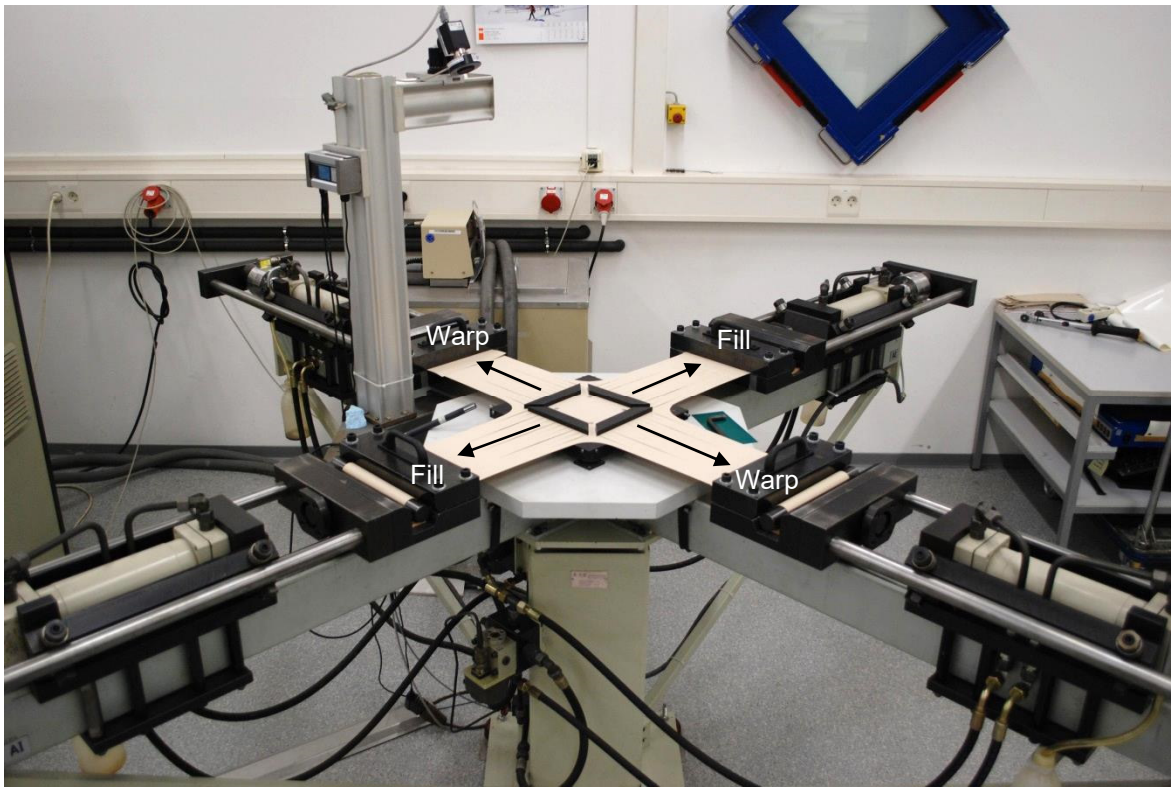

Figure 31 50 kN servohydraulic biaxial test rig of the Essen Laboratory for Lightweight Structures (ELLF) at the University of Duisburg-Essen

The biaxial tensile testing machines at ELLF use plane cruciform test specimens with yarn-parallel long, slit arms. On the 50 kN machine, the testing area at the centre of the specimen has a size of 200 mm x 200 mm, see Figure 32. Forces are applied by two hydraulic actuators in each main axis. A precise optical strain measurement is taken using an industrial digital camera and infrared lighting equipment. Four markers are arranged at the corners of a square: this is the measurement field within the test bay. Movements of the four markers during the test are traced via the camera system by an image processing software developed at the University of Duisburg-Essen [PS10]. The strains in both main directions are derived from the relative movement between the markers. The standard deviation in the measurement

error after calibration of the system is < 12 μm in relation to the size of the testing area.

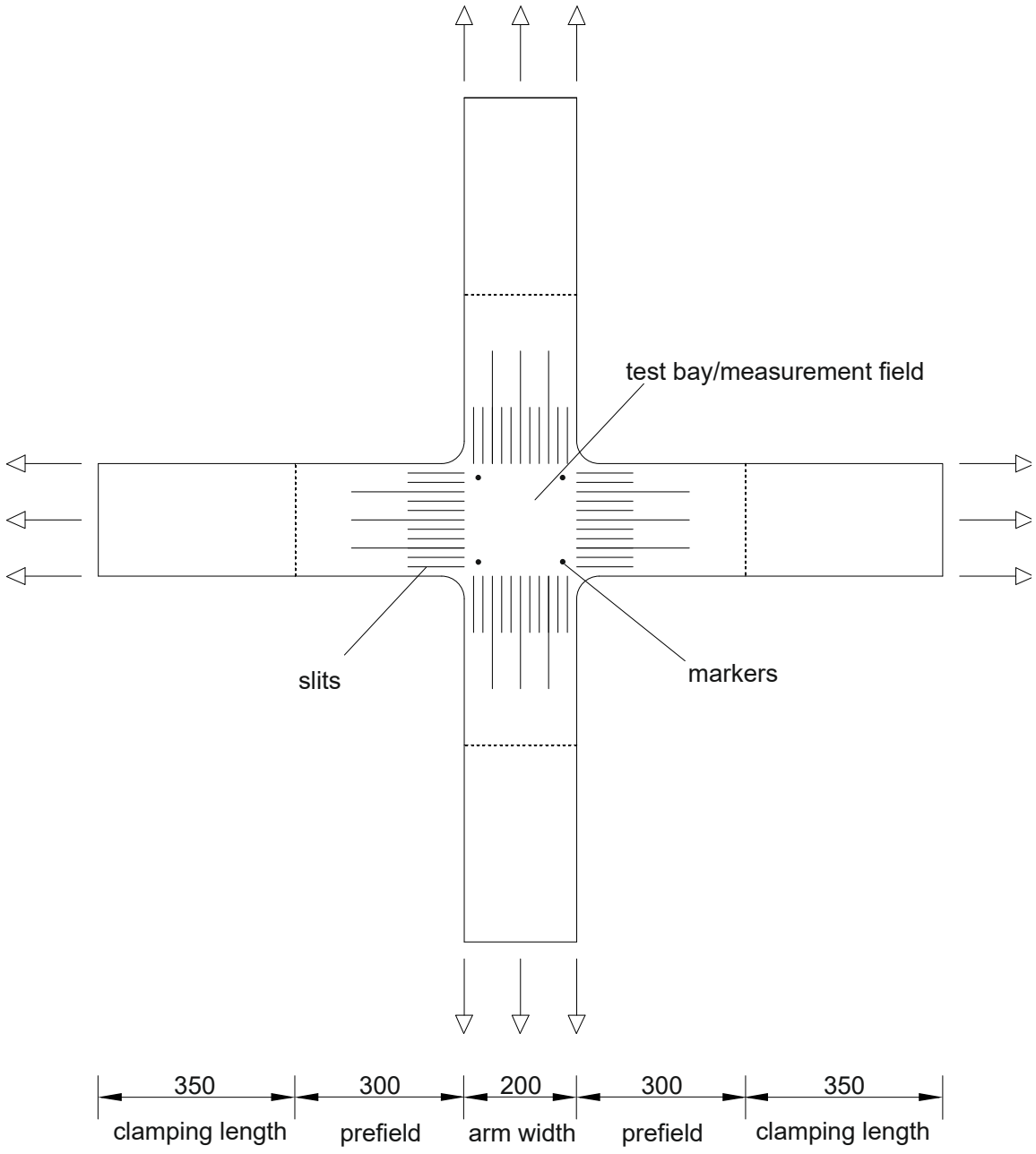

Figure 32 Biaxial test specimen used at the Essen Laboratory for Lightweight Structures (ELLF)

The uniaxial load tests deliver the uniaxial tensile moduli and Poisson's ratios in warp and fill direction. They furthermore provide test data for planning the compensation of the orthogonally loaded membrane strips presented in Chapter 6.3 and the associated comparative finite element analyses.

Short term stress with a magnitude of ¼ of the minor tensile strength given in the manufacturer data sheet was applied in warp or fill direction. A separate virgin test specimen was used for each test in warp or fill direction. In order to investigate

changes in the tensile moduli and Poisson's ratios with an increasing number of load cycles, the loads were repeated five times.

The tests were first performed with a recovery time of 60 minutes between the single load cycles. This simulates natural loading of a membrane structure. Neither significant snow nor significant wind loads appear to be repeated without a considerable time interval inbetween. This allows the material to recover or to regain prestress. The duration of 60 minutes was chosen because the recovery mechanism – revertive creep – can be expected to be largely complete after that period of time.

The tests were performed with traditionally coated PES-PVC material from mainly one producer (material producer 2) but of different types: type II, III and V. The missing type IV was filled with tests on material from producer 1. A repetition of the tests with material from other producers was not necessary. A comparison of stiffness results between the materials from different producers presented in Chapter 7 revealed that the stiffness behaviour of the delivered batches is very similar in the working stress range. Materials of type II, III, IV with biaxially prestressed coating system and glass-PTFE materials of type II, III and IV were also tested.

The second step was to investigate to what extent omitting the recovery times between the single load cycles has an influence on the measured tensile moduli and Poisson's ratios. The complete test series was repeated without recovery times.

6.2.2 Tests with recovery times between single load cycles

The load history for the uniaxial tests with recovery times is illustrated in Figure 33 for both warp and fill stress, based on the example of the stress magnitude for PES-PVC material type III. A recovery time of 60 minutes at zero stress was scheduled after each load cycle.

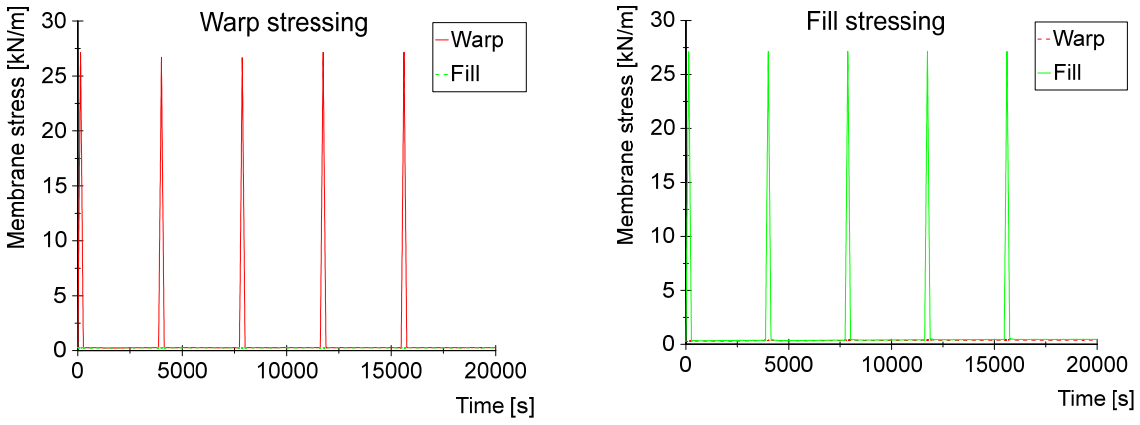

Figure 33 Load history for the uniaxial load tests with 60-minute recovery times, based on the example of PES-PVC material type III, left: load applied in warp direction, right: load applied in fill direction

Together with the warp load history, the measured strains under warp stress is plotted against time in Figure 34 for PES-PVC material type III. It is shown that the

maximum warp strain rises with every load cycle but the increase decays after the fourth load cycle. At the fourth and fifth load cycle the maximum warp strain approaches $\varepsilon_w = 5.5$ % strain. The fill strain becomes negative and shows the same magnitude of approximately $\varepsilon_f = -0.2\%$ at every load cycle. The constant final strains indicate that a stable state of the material is reached approximately after four load cycles. Within the present work, the stable state of a woven fabric is known as the state with a fixed pair of values (max $\sigma \mid \varepsilon$) after repetitive loading with one stress ratio, where max σ is the maximum membrane stress in the test and ε is the correlated strain. In the stable state of the fabric the yarn crimp has adjusted to the applied stress and the stress ratio.

With regard to the unloading behaviour, it can be observed that for each load cycle the warp strain largely diminishes spontaneously. Subsequently, during the 60-minute recovery times, the delayed reversible strain $\varepsilon_{r,del}$ is largely removed – but not completely. This can be observed from the warp strain curve, which approaches but does not completely turn into a horizontal line during the recovery times.

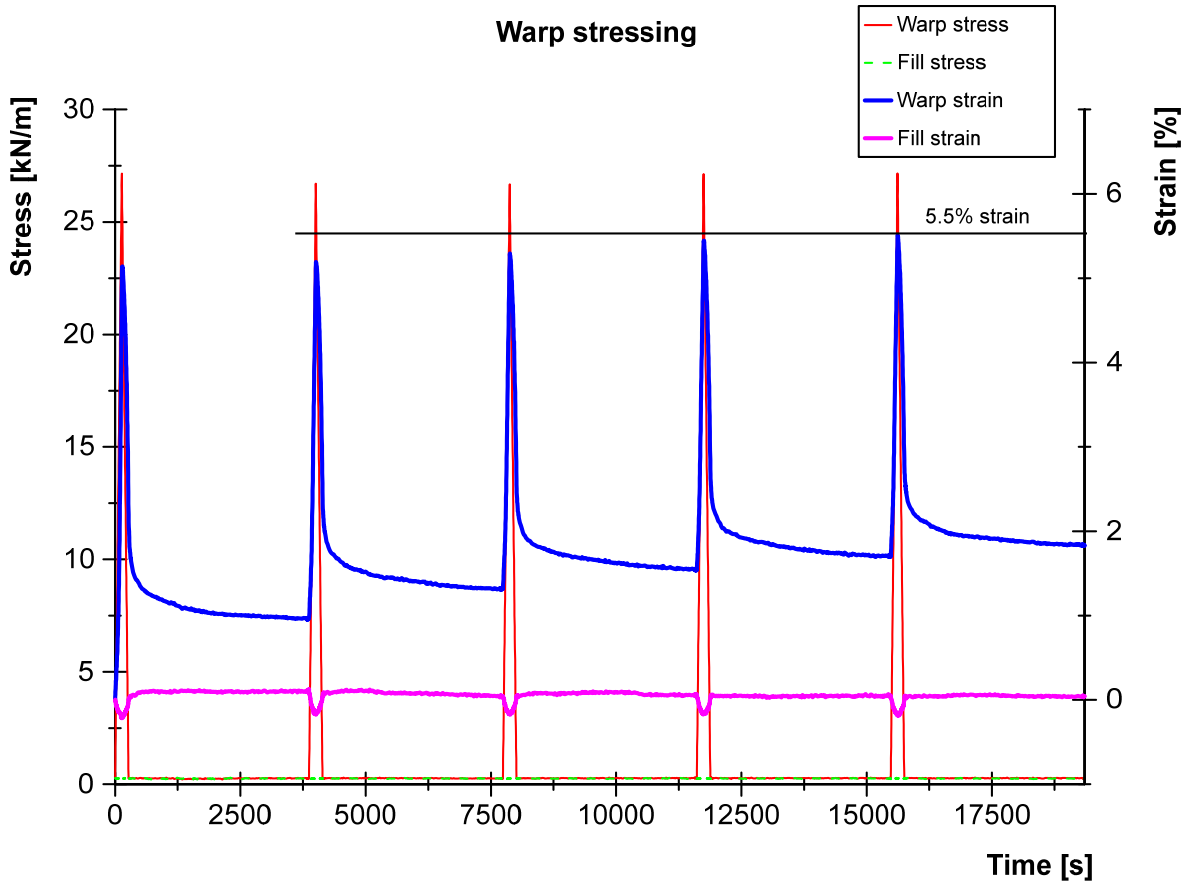

Figure 34 Load history for warp stressing and measured strain against time, based on the example of PES-PVC material type III

Figure 35 presents the results as a stress-strain diagram for uniaxial warp stressing. In order to make the fill stress-strain paths visible as curves – and not only as horizontal lines – the fill strain is plotted against the warp stress.

The warp paths show the initially stiff and subsequently softer behaviour typical of PES, which is expressed by the concave stress-strain paths. The slopes of the first and fifth loading paths are marked by blue secants. Warp tensile moduli are determined as secant moduli: $E = \Delta\sigma / \Delta\varepsilon$. They are attached to the blue lines: E = 532 kN/m for the first load and E = 699 kN/m for the fifth load. The evaluation was performed in the stress interval $\Delta\sigma$ between 1 kN/m and the maximum test stress. This is done following a recommendation in the commentary to the Japanese standard MSAJ/M-02-1995 [Me95]. Applying 1 kN/m as the lower limit of the evaluation stress interval is reasonable insofar as usual prestress values only fall below that value in exceptional cases (e. g. small span facade or billboard membranes). The respective Poisson's ratios $\nu_{yx} = \Delta\varepsilon_y / \Delta\varepsilon_x$ yield as $\nu_{yx} = 0.04$ for the first load and $\nu_{yx} = 0.05$ for the fifth load. This means that warp tensile modulus in the stable state of this specific material is approximately 30% higher than the initial modulus. Poisson's ratio increases by 25% in this example; this may sound high, but from an engineering point of view it is not a significant change because of the low absolute values.

Figure 36 illustrates the results for uniaxial fill stressing. In contrast to the paths for warp stressing, almost all curves are convex for both fill and warp direction – only the first loading fill path has an inflexion point. The convex curvature illustrates the predominant constructional stretch as the counterpart to the stress-strain behaviour of the yarn material. The initial tensile modulus in fill direction – again determined as a secant modulus in the stress interval 1 kN/m to maximum stress – is E = 251 kN/m and in the stable state it is E = 398 kN/m, which is approximately 60% higher. The respective Poisson's ratios are much higher than for warp stressing: $\nu_{xy} = 0.38$ for the first load and $\nu_{xy} = 0.58$ for the fifth load, an increase of 53%. It is comprehensible that the transverse strains are higher when the more highly crimped fill yarns are pulled "straight", which forces the warp yarns to crimp heavily. This inevitably leads to a considerable shortening in warp direction – or a considerable warp stress if warp would be restraint.

Figure 35 and Figure 36 plot the full hysteresis loops. In order to prevent the zero stress paths appearing as horizontal lines, the transverse strains are generally plotted against the "major stress" of a stress ratio: warp stress for uniaxial warp stressing and fill stress for uniaxial fill stressing. Both figures provide evidence that the minimum transverse strains do not change significantly during the load cycles.

Particularly fill stressing in Figure 36 shows that the variation of the secant moduli is not due to a significant variation in maximum strain. The variation originates rather from significantly varying "starting" strains at zero stress or from the lower boundary of a specific stress interval. This mechanism is the reason why the material is known to become stiffer from cycle to cycle. Simultaneously, the maximum or "final" strain increases for each successive cycle of identical stress, albeit not in large steps. This

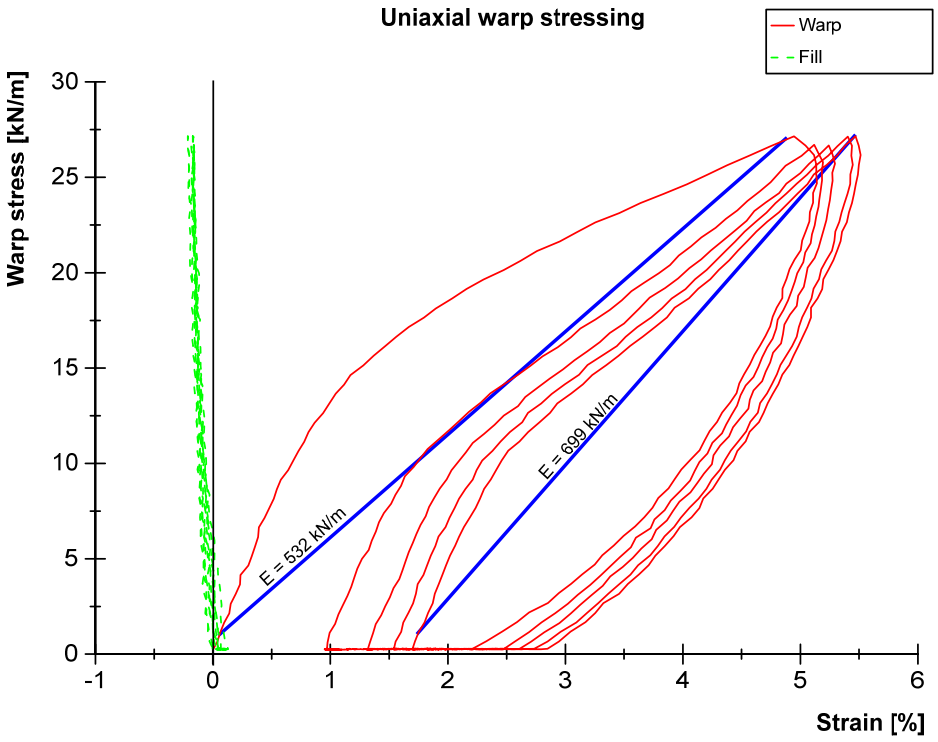

Figure 35 Stress-strain plot for uniaxial warp stressing, based on the example of PES-PVC material type III

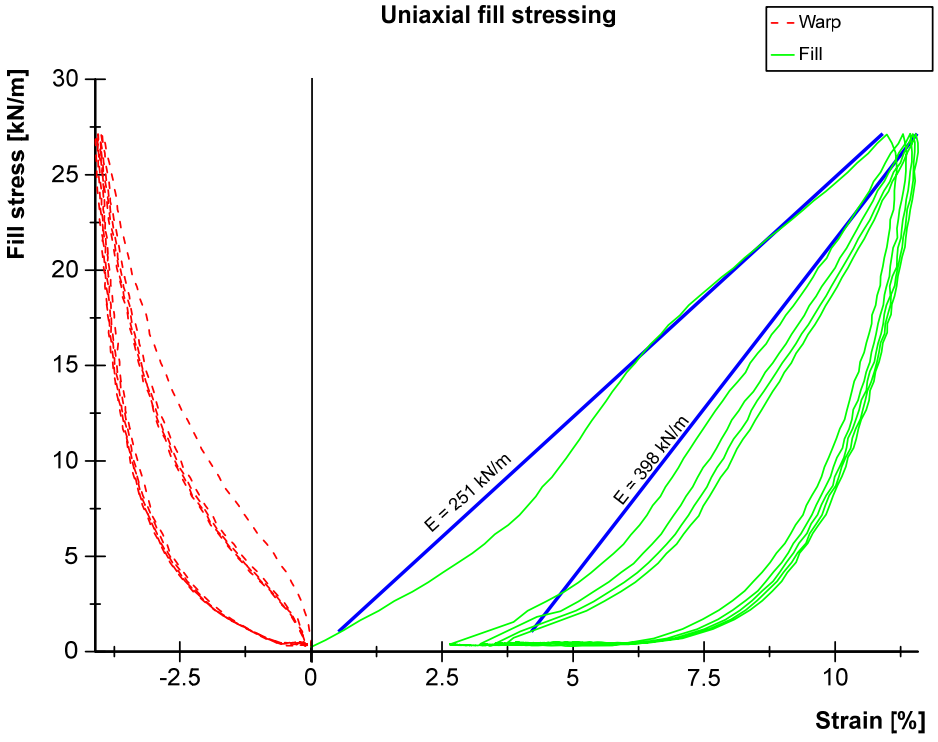

Figure 36 Stress-strain plot for uniaxial fill stressing, based on the example of PES-PVC material type III

means that the material becomes globally more compliant from cycle to cycle. A clear distinction between the two different definitions of stiffness is beneficial. In the present work a distinction is made between

- the “relative” stiffness determined from a secant within a specific stress interval connecting the starting strain in a specific load cycle (“relative zero”) with the maximum strain in the same load cycle and
- the “global” stiffness determined from a secant connecting zero strain (“global zero”) with the maximum strain in a given load cycle.

Figure 37 graphically illustrates these definitions for the stiffness in the stable state of the material after n = ∞ load cycles.

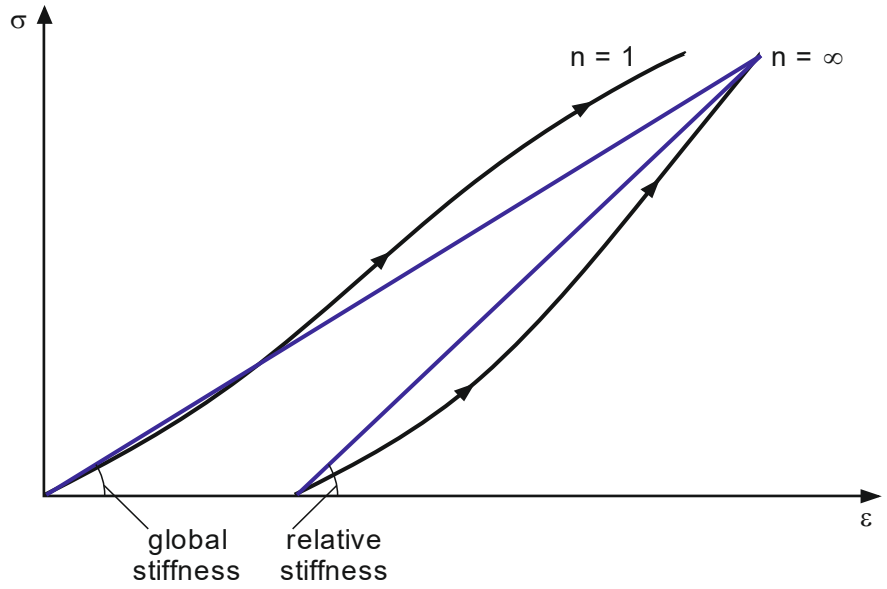

Figure 37 Relative and global stiffness in the stable state (n = ∞)

The complete sets of results for all tested materials are presented in Table 4, including traditionally as well as biaxially prestressed coated PES-PVC fabrics and glass-PTFE fabrics. The given values reflect the relative stiffness in the specified load cycles. The compiled results show that Poisson’s ratio can become very large for some materials and load scenarios. While traditionally coated PES-PVC type II and III have very similar Poisson’s ratios at very low to moderate magnitude, type IV and particular type V show much higher values. The investigated biaxially prestressed PES-fabrics type II and III exhibit much greater fill Poisson’s ratios ν_{yx} than the comparable traditionally coated fabrics. However, with maximum $\nu_{yx} = 0.25$ the values are overall on a moderate level. Warp Poisson’s ratio can be quite large at max. $\nu_{xy} = 0.71$. Type IV is unusual: first because of the comparable height of the Poisson’s ratios at up to 1.00, and second because the fill Poisson’s ratio is greater than the warp Poisson’s ratio.

Remarkably, all glass-PTFE fabrics show Poisson’s ratios greater than one in the stable state; type II even approaches two (fill direction) or exceeds it (warp direction). A value greater than one means that the transverse strain becomes greater than the strain in the direction of the tensile stress: the material shrinks more in the unloaded perpendicular direction than it stretches in the loading direction. Concurrently,

stresses in transverse direction greater than the stresses in tensile direction would follow if the transverse direction would be restrained. This effect should be kept in mind during compensation and installation planning.

Table 4 Uniaxial elastic constants determined from tests with 60-minute recovery times between the single load cycles, reflecting the relative stiffness in the specified load cycles

Uniaxial elastic constants/ material	Virgin material (first loading)				Stable state (fifth loading)			
	Uniaxial warp stressing		Uniaxial fill stressing		Uniaxial warp stressing		Uniaxial fill stressing	
	E_x [kN/m]	ν_{yx} [-]	E_y [kN/m]	ν_{xy} [-]	E_x [kN/m]	ν_{yx} [-]	E_y [kN/m]	ν_{xy} [-]
Traditionally coated PES-PVC (material producer 2 if not indicated otherwise)								
Type II	423	0.05	220	0.38	524	0.01	332	0.55
Type III	532	0.04	251	0.38	699	0.05	398	0.58
Type IV*	824	0.17	354	0.51	971	0.19	510	0.68
Type V	844	0.30	361	0.63	1198	0.46	586	0.92
PES-PVC with biaxially prestressed coating system (material producer 4)								
Type II	331	0.23	304	0.30	421	0.25	405	0.36
Type III	416	0.14	356	0.54	602	0.18	503	0.71
Type IV	558	0.88	493	0.48	703	1.00	688	0.55
Glass-PTFE (material producer 5)								
Type II	1416	1.90	305	1.27	1976	1.97	896	2.22
Type III	939	0.69	273	0.59	1986	1.06	974	1.16
Type IV	1782	1.02	288	0.68	2756	1.28	902	1.19

* Material producer 1

Following the generally accepted presumption, the crimp interchange causes these high transverse strains in the inhomogeneous composite, see also Chapter 3.5.3.1. The Poisson's ratios are partly much greater than typically known for homogeneous solids where the transverse strain results from the molecular structure. A comparison of the measured Poisson's ratios with the microscopic cross-sections (see Table 3) confirm this presumption in most cases. For instance, a very low fill Poisson's ratio is measured for traditionally coated PES fabrics type II and III, and the cross-sections actually show that the warp yarn is almost straight in both fabrics. Hence, this result could be expected. But the conventional explanation appears not to fit for the investigated glass-PTFE materials type II and type IV. The cross-sections show much higher magnitude of fill yarn crimp, particularly for type IV. From this

observation a higher warp Poisson's ratio would be expected, yet a higher fill Poisson's ratio is measured under the first load. While it admittedly changes to a slightly higher warp Poisson's ratio up to the fifth load, the considerably higher warp Poisson's ratio in the first load puts a question mark over whether crimp interchange is the only or major influence on the transverse strain behaviour. This insight does not affect the application of phenomenological elastic constants, but it could lead to difficulties for microstructural approaches, see also Chapter 4.

The Poisson's ratios increase with an increasing load cycle number almost throughout. The reason for this can be very well observed from Figure 38, where stress-strain paths for five load cycles of uniaxial fill stressing are displayed for a PES-PVC fabric type V. Each path is normalised to the strain at the fill stress level $\sigma_f = 1$ kN/m. Hence, the strain difference $\Delta\varepsilon$ rather than the absolute strain ε occurs on the x-axis. These σ–$\Delta\varepsilon$ paths illustrate the slope of the stress-strain curves very clearly, which is precisely the characteristic elastic constants are intended to describe. While the transverse strain difference in warp direction $\Delta\varepsilon_x$ changes little over the load cycles, the strain difference in tensile stress direction $\Delta\varepsilon_y$ decreases considerably. In other words, while the numerator in the term $\nu_{xy} = \Delta\varepsilon_x / \Delta\varepsilon_y$ is quasi stable, the denominator decreases. This leads to growth of the Poisson's ratio. With regard to PES-PVC fabric with a biaxially prestressed coating system, Poisson's ratio has another effect. Taking only the tensile moduli in x- and y-direction, all three tested materials could be classed as approximately isotropic – or transversely isotropic to be more precise, since it can be presumed that the through-thickness properties differ considerably from the in-plane properties. But $E_x = E_y$ is not the only condition for a transversely isotropic material, see Chapter 4.2.3: the transverse strain properties in both directions must be equal as well, i. e. $\nu_{xy} = \nu_{yx}$. This condition is not satisfied, particularly in the case of type III and type IV. Strictly speaking, the investigated PES-PVC fabrics with a biaxially prestressed coating system are not transversely isotropic.

Uniaxial stressing, and particularly uniaxial fill stressing, is known to lead to the softest stress-strain behaviour among all stress ratios. Type V is a high-strength material. The high possible stresses are associated with great strain. Thus, greater strain than presented in Figure 38 for fill stressing of a type V material is not expected for any typical architectural PES or glass fibre fabric. The greatest strain difference for first loading observed from Figure 38 is max. $\Delta\varepsilon_y = 13\%$ and for the fifth load cycle max. $\Delta\varepsilon_y = 7.7\%$.

Comparing polyester and glass fibre fabrics, the numbers in Table 4 suggest that glass fibre fabrics are generally stiffer and exhibit higher transverse strain properties throughout. The first assumption needs to be examined in greater detail by directly comparing materials with similar tensile strength values. This comparison is presented in Chapter 6.2.3.

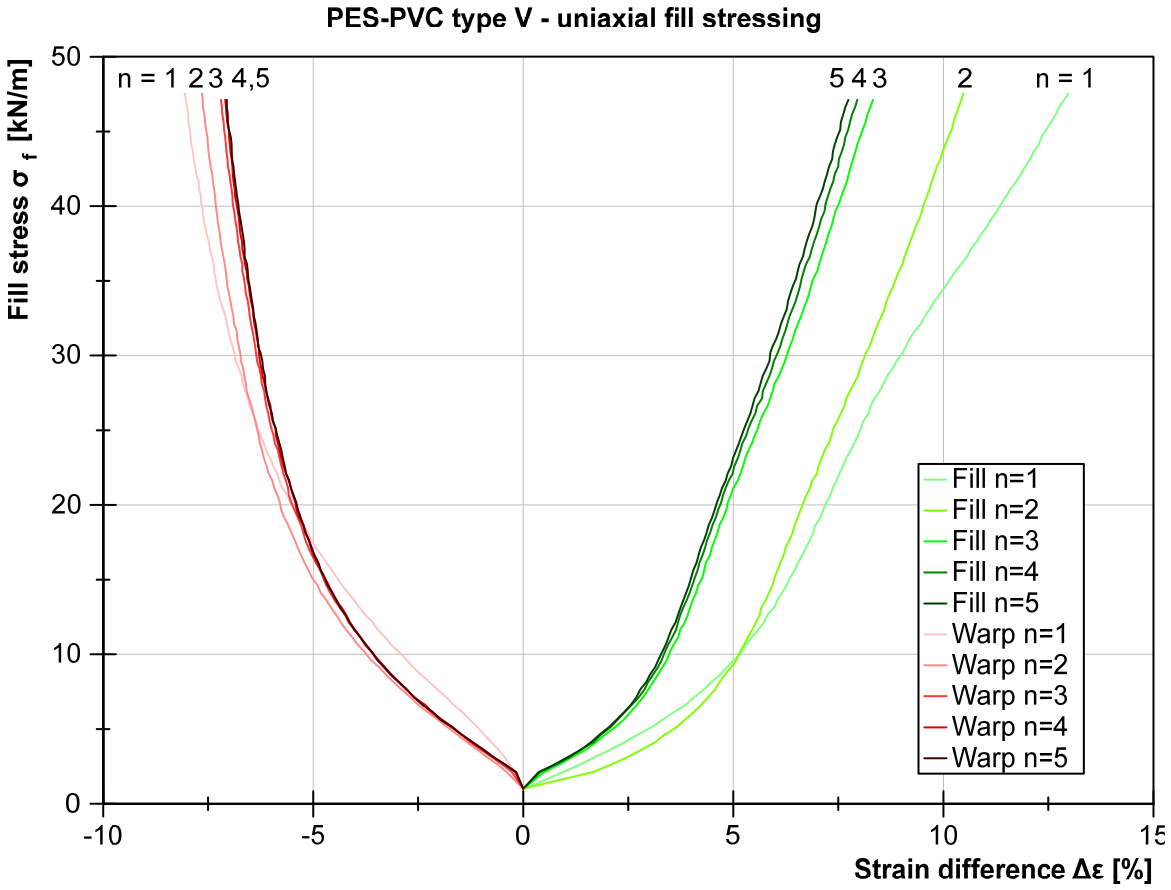

Figure 38 Stress-strain paths over progressive load cycles, based on the example of uniaxial fill stress on a traditionally coated PES-PVC fabric type V

Mircoscopic images of PES-PVC sections [Lo71], [Me78], [BG10] and of glass-PTFE sections [Ba02], [Mi06], [BG10] show different yarn crimps of the virgin material. Here, the yarn crimp of the glass-PTFE materials appears to be higher than that of the PES-PVC materials throughout. Analysis of all the cross-sections prepared in the frame of the present work indicates that this cannot be confirmed without exceptions, especially not for the fill direction. For instance, the fill yarn of PES-PVC type IV (material producer 1 or 3) shows similar yarn curvature to the fill yarn of glass-PTFE type III – although the polyester fabrics of type IV are Panama 3/3 weaves, while the glass fibres are woven with plain weave. Indeed, all these fabrics exhibit similar warp Poisson's ratios for the first load. As far as the warp yarns are concerned, it is apparent that those of the glass-PTFE fabrics exhibit more crimp than most of the PES-PVC warp yarns. The latter have noticeably very low crimp and approach a straight line in the initial state. Only biaxially prestressed fabric type IV is a clear exception to this rule. However, the glass-PTFE fabrics indeed exhibit slightly to considerably higher transverse strain overall.

Furthermore, it can be observed from the nonlinearity of the stress-strain paths in Figure 35, Figure 36 and Figure 38 that tensile moduli would be different for different stress intervals. As the stress-strain paths in transverse direction are simultaneously

more linear, see particularly Figure 35, it can be suggested that Poisson's ratios are noticeably different for different stress intervals, too.

The typical development of uniaxial elastic constants over progressive load cycles is displayed in Figure 39. This diagram shows for the example of a PES-PVC material type V that the development of all stiffness parameters slows significantly after three load cycles. This confirms the observation by [Re75] and others. Certainly from a practical point of view, the stable state of the material can be presumed to occur with sufficient accuracy after n = 5 ≈ ∞ load cycles.

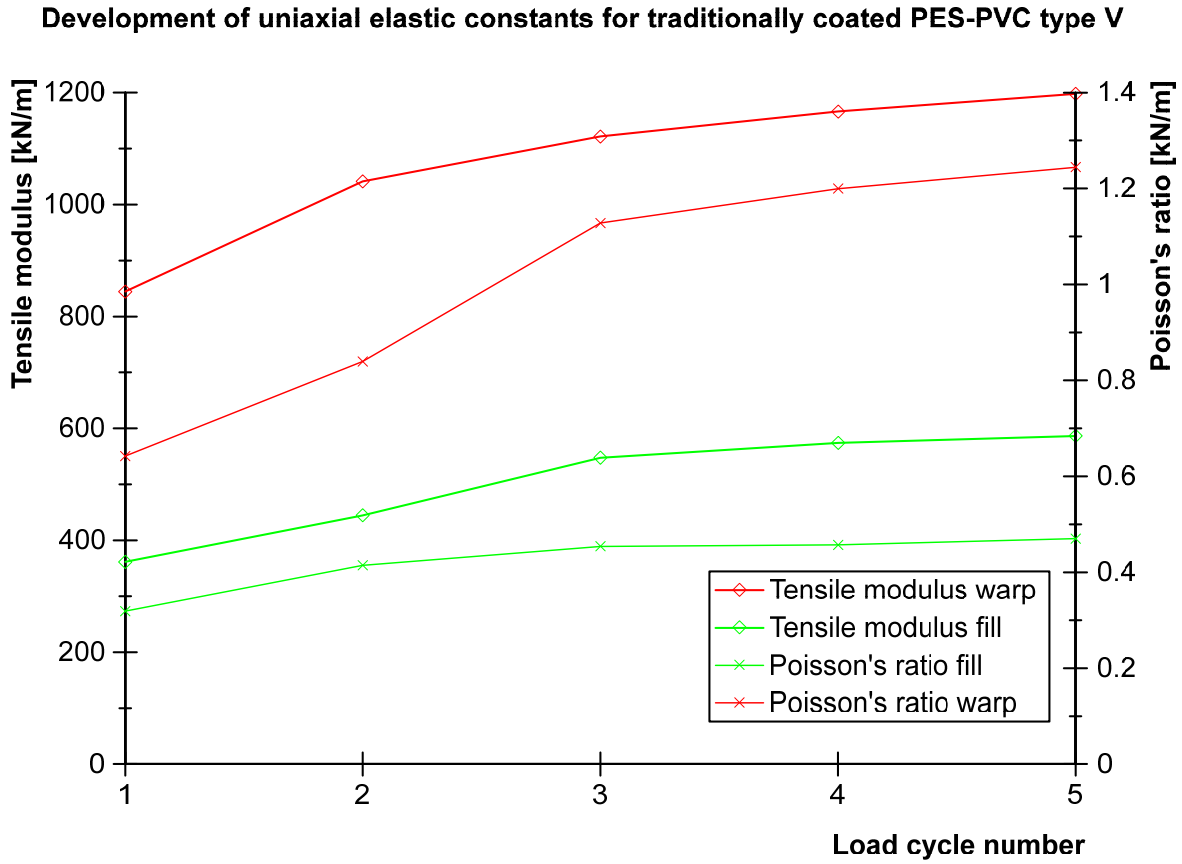

Figure 39 Typical development of uniaxial elastic constants over progressive load cycles, based on the example of traditionally coated PES-PVC fabric type V

6.2.3 Tests without recovery times between single load cycles

Natural loading scenarios like wind and snow are characterised by considerable times without significant load magnitudes between individual significant load incidents. The test procedure with recovery times discussed above is thus a good simulation. For daily laboratory and design practice, however, short test procedures are preferred. The aforementioned tests with recovery times are therefore repeated without recovery times in order to study possible changes in the stiffness behaviour. Figure 40 illustrates the load history for warp and fill stressing. The test duration is reduced from over five hours for the tests with recovery times to approximately half an hour.

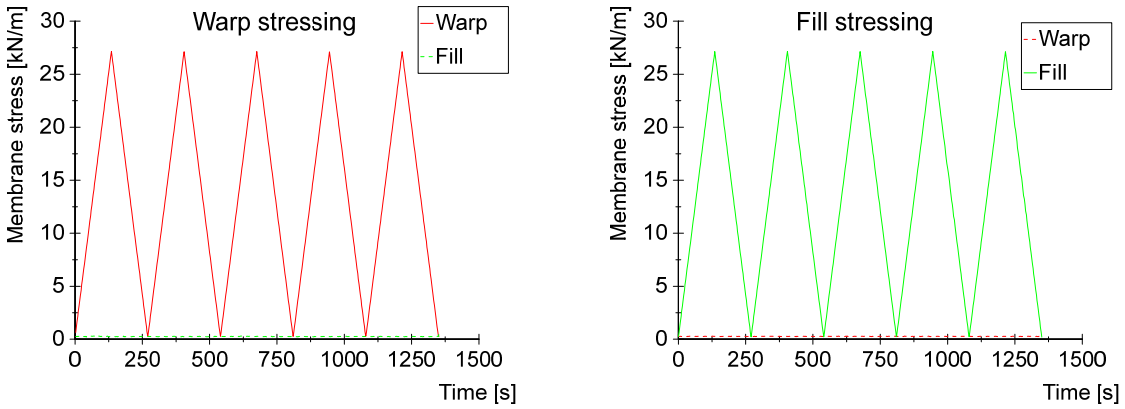

Figure 40 Load history for the uniaxial load tests without recovery times, based on the example of PES-PVC material type III, left: loading in warp direction, right: loading in fill direction

Together with the warp load history the measured strains under warp stressing are plotted against time in Figure 41 for PES-PVC material type III. It can be recognised that the development of the maximum warp strain with every load cycle equals the development in the tests with recovery times, compare Figure 34. In the fourth and fifth load cycle the maximum warp strain approaches 5.5 % strain. Again, the fill strain becomes negative with approximately the same magnitude every time.

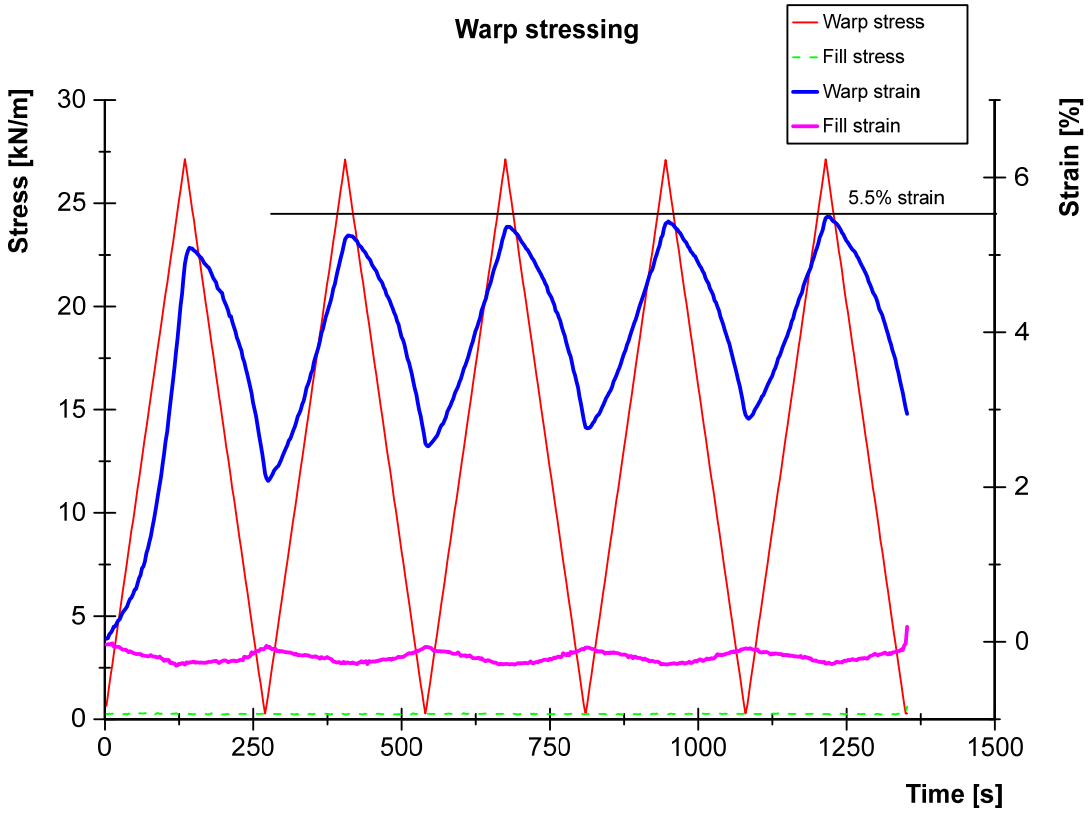

Figure 41 Load history for warp stressing and measured strain over time, based on the example of PES-PVC material type III

Figure 42 and Figure 43 show the test results for warp stressing and fill stressing as stress-strain diagrams. Again, the slopes of the first and fifth loading paths are marked by blue secants.

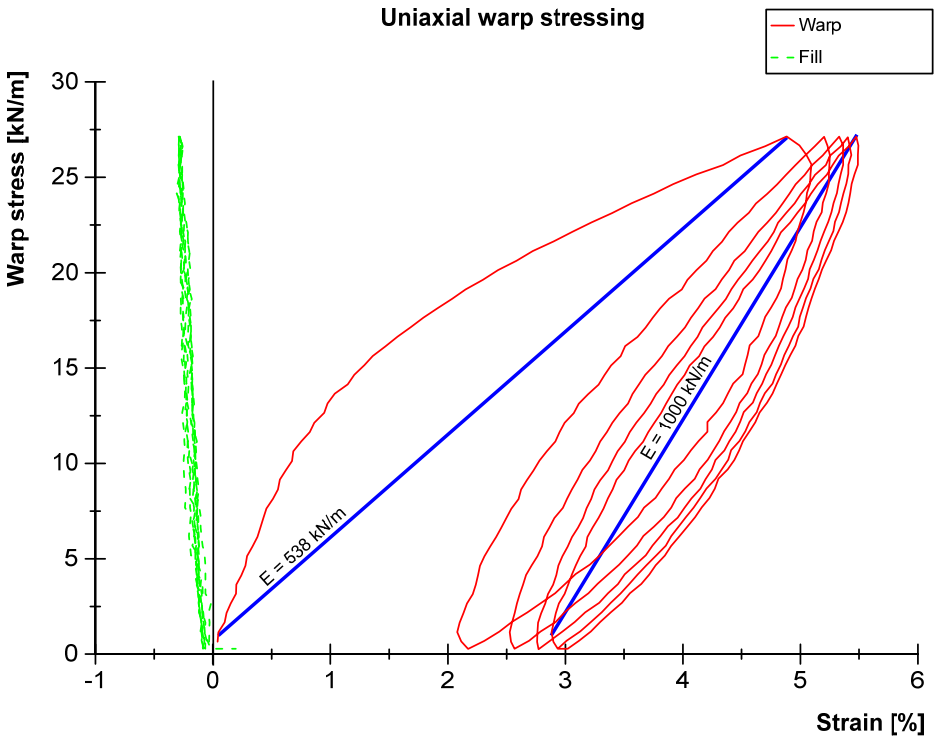

Figure 42 Stress-strain plot for uniaxial warp stressing without recovery times, based on the example of PES-PVC material type III

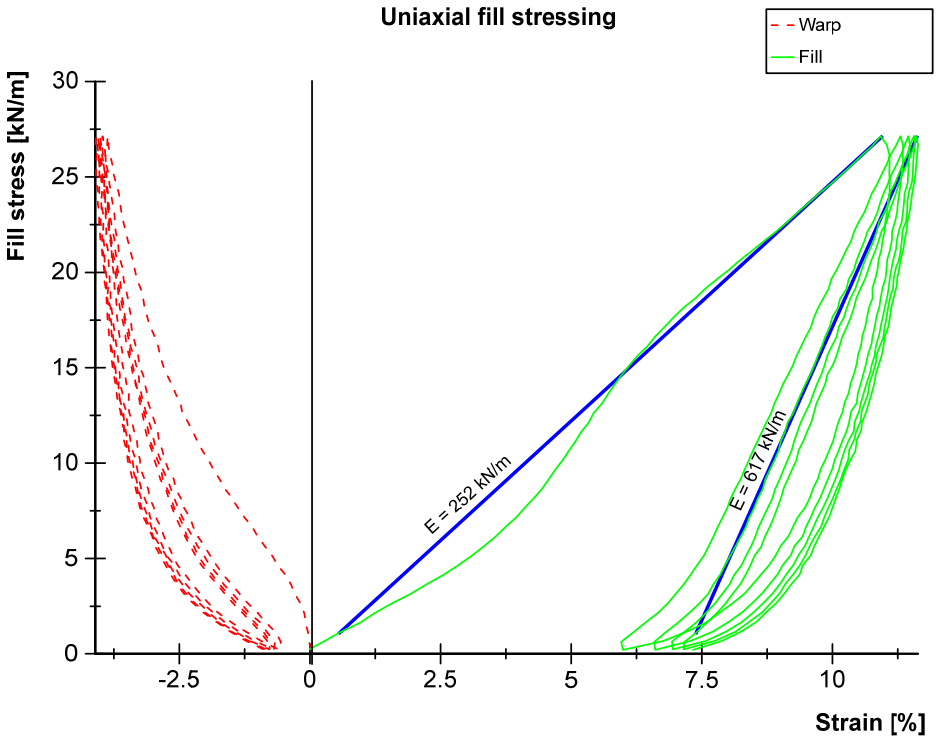

Figure 43 Stress-strain plot for uniaxial fill stressing without recovery times, based on the example of PES-PVC material type III

Tensile moduli are determined using the same procedure as in Chapter 6.2.2. Warp tensile moduli are given in Figure 42 as E = 538 kN/m for the first loading and E = 1000 kN/m for the fifth loading. Of course the stiffness of the first loading does

not differ from that in the tests with recovery times because the change in the test protocol only becomes apparent subsequently. Generally, a comparison of the similar elastic constants for first loading in Table 4 and Table 5 demonstrates the consistency and high reproducibility of the test results.

Table 5 Uniaxial elastic constants determined from tests without recovery times between the single load cycles, reflecting the relative stiffness in the specified load cycles

Uniaxial elastic constants/ material	Virgin material (first loading)				Stable state (fifth loading)			
	Uniaxial warp stressing		Uniaxial fill stressing		Uniaxial warp stressing		Uniaxial fill stressing	
	E_x [kN/m]	ν_{yx} [-]	E_y [kN/m]	ν_{xy} [-]	E_x [kN/m]	ν_{yx} [-]	E_y [kN/m]	ν_{xy} [-]
Traditionally coated PES-PVC (material producer 2 if not marked otherwise)								
Type II	418	0.03	218	0.39	754	0.06	522	0.72
Type III	538	0.05	252	0.37	1000	0.07	617	0.75
Type IV*	804	0.22	350	0.51	1315	0.25	825	0.85
Type V	850	0.31	359	0.62	1705	0.44	930	1.15
PES-PVC with biaxially prestressed coating system (material producer 4)								
Type II	335	0.23	305	0.30	608	0.30	602	0.41
Type III	425	0.15	366	0.55	866	0.19	744	0.83
Type IV	572	0.88	522	0.46	999	1.06	1022	0.55
Glass-PTFE (material producer 5)								
Type II	1417	1.98	317	1.30	2223	1.83	1333	2.39
Type III	869	0.64	297	0.63	2641	1.12	1891	1.53
Type IV	1743	0.98	286	0.69	3464	1.30	1609	1.49

* Material producer 1

For the following stress-strain paths it is apparent that the relative stiffness is considerably higher than for the results with recovery times. For the fifth load cycle, the tensile modulus at E = 1000 kN/m is over 40% higher than for the variant with recovery times, where it is E = 699 kN/m. The reason is that the starting strain when loading begins is greater during the test procedure without recovery times. As already mentioned above, the final strain does not vary at the same time. This leads to a smaller strain difference $\Delta\varepsilon$. This applies in the same way for uniaxial fill stressing, where the increase of tensile modulus from the first to the fifth load cycle constitutes over 30%.

The fact that the final strain does not vary shows that a fixed pair of values (max $\sigma \mid \varepsilon$) exists in the stable state of the material, independently of whether recovery times are included in or omitted from the test protocol.

With regard to the Poisson's ratios, it can be observed for fill stressing in the stable state of the material that the warp Poisson's ratios ν_{xy}, see last row in Table 5, are considerably greater compared to the tests with recovery times, see last row in Table 4. The difference is 25% to 30% for the traditionally coated PES-PVC fabrics and the glass-PTFE fabrics with the higher strength. For the other materials there is no great impact of omitting recovery. The fill Poisson's ratio ν_{yx} during warp stressing is not significantly affected by omitting the recovery time.

As for the tests with recovery time, the Poisson's ratios increase with increasing load cycle number almost throughout. The reason can be very well observed from Figure 44, where – analogous to Figure 38 – stress-strain paths for five load cycles of uniaxial fill stressing are displayed for the example of a PES-PVC fabric type V.

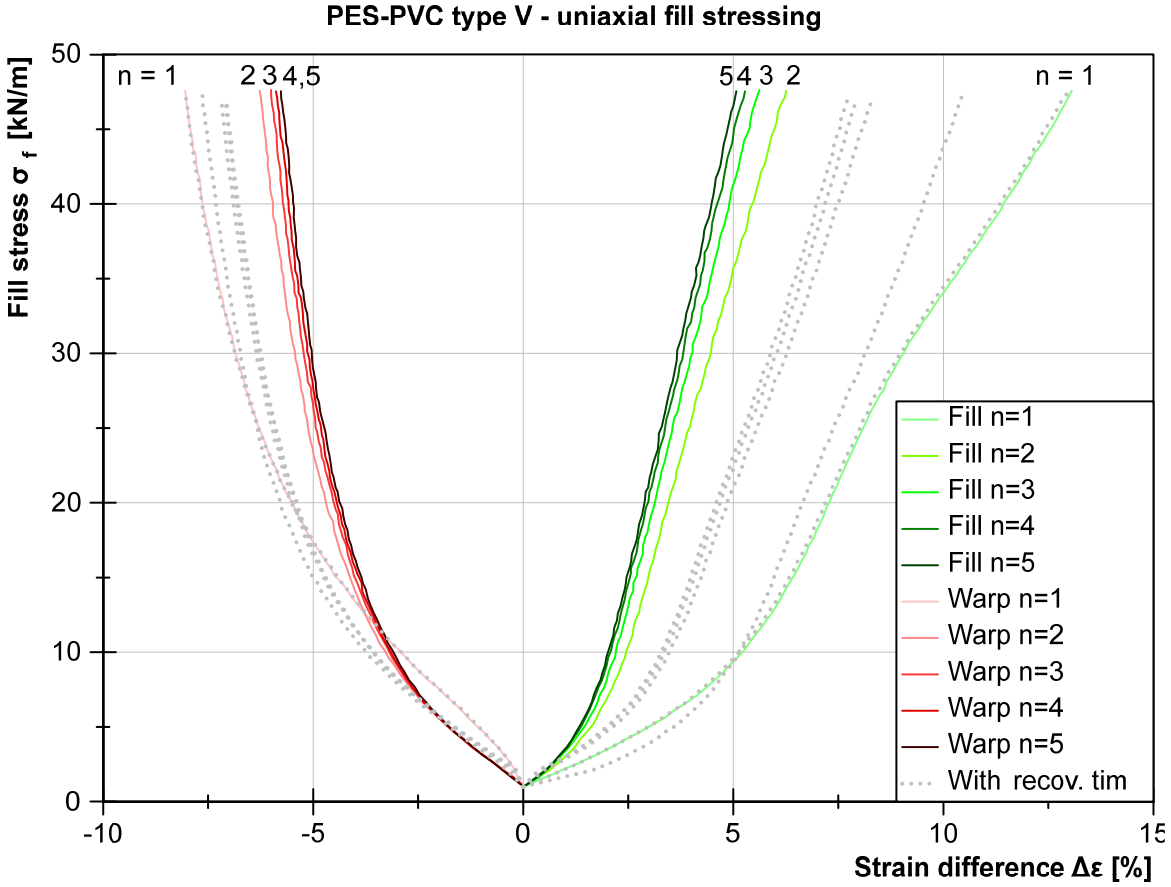

Figure 44 Stress-strain paths for test without recovery times over progressive load cycles, based on the example of uniaxial fill stressing of a traditionally coated PES-PVC fabric type V, compared to stress-strain paths for the test with recovery times

The same mechanism as described for the tests with recovery times leads to the increase in Poisson's ratio. For direct comparison, Figure 44 also shows the paths of the test with recovery times already given in Figure 38, see grey dotted lines. The

comparison reveals that both strain increments in the tensile stress direction and the transverse direction appear to be less when recovery times are omitted in the test protocol. This “artificial strain increment reduction” turns out to be greater in the tensile stress direction. Finally, the same mechanism applies as described above: while the transverse strain difference in warp direction $\Delta\varepsilon_x$ changes little as a result of omitting recovery times, the strain difference in the tensile stress direction $\Delta\varepsilon_y$ decreases considerably. The denominator in the ratio $\nu_{xy} = \Delta\varepsilon_x / \Delta\varepsilon_y$ decreases more strongly than the numerator. For that reason, Poisson’s ratio appears greater for the tests without recovery times. In the end, the comparison shows that omitting recovery times in the test protocol leads to an “artificial stiffening” with regard to the relative stiffness of the tested fabric, both in tensile stress direction and in transverse direction. Directly related to this are greater tensile moduli and greater Poisson’s ratios – the latter at least in warp direction. The absence of recovery time in a membrane structure with fixed boundaries would be linked to a lower prestress level. This is because not all strain is spontaneously reversible after a load incident. If that were the case, prestress would spontaneously recover after unloading. But in fact, part of the reversible strain is delayed. For a membrane structure with fixed boundaries this means that the recovery of prestress is delayed. It eventually becomes apparent that, applying “artificial high” elastic constants from tests without recovery times must be coupled with a lower prestress level in the structural model. Using the nominal prestress would be safe sided with regard to the membrane stress but unsafe with regard to the deflection. The experimental proof of this relation will be described in Chapter 6.3.3.

As far as the stiffness of polyester and glass fibre fabrics is concerned, it is frequently indicated among membrane structure experts that glass-PTFE fabrics are “stiffer” than PES-PVC fabrics. The numbers in Table 4 and Table 5 seem to confirm this statement. But these values reflect only the “secant stiffness” in the investigated stress interval. They should therefore be viewed with caution when it comes to assessing other stress intervals, particularly for initial loading where the stress-strain response is very nonlinear. To make an accurate statement, a direct comparison of two materials with similar tensile strength properties is demonstrated here. This comparison was first published in [USS15c].

“From the huge market for textile fabrics, one PES-PVC fabric and one Glass-PTFE fabric with similar tensile strength properties were identified and chosen for the presented experimental investigations for a direct comparison: PES-PVC fabric type III, material producer 2, and Glass-PTFE fabric type II, material producer 5. They exhibit almost identical tensile strength values in warp direction of $f_{m,23}$ = 118.9 kN/m and $f_{m,23}$ = 117.2 kN/m, respectively. In fill the strength values are at least of similar magnitude: $f_{m,23}$ = 104.1 kN/m and $f_{m,23}$ = 122.8 kN/m.

Determining the stiffness of a structural component in the direction of an axial force requires the longitudinal stiffness EA, where E = Young's modulus and A = cross-sectional area. An estimate of the cross-sectional area of the fabrics investigated can be derived by dividing the yarn size by the mass density of the yarn material. To approximate the longitudinal stiffness of the two fabrics investigated, this operation was conducted assuming the densities of polyester and glass fibre as follows: ρ = 1.4 g/cm^3 for polyester and ρ = 2.5 g/cm^3 for glass fibre [Ko08]. This yields A = 1670 [dtex] / 1.4 [g/cm^3] = (1670 [g] / 10^6 [cm]) / 1.4 [g/cm^3] = $12 \cdot 10^{-4}$ cm^2 per yarn for the investigated PES fabric. The used yarn size reflects manufacturers data, see Annex A. Considering, as an example, the warp direction only and assuming 10.2 yarns/cm as stated in Table 3, this results in A = $12 \cdot 10^{-3}$ cm^2/cm for the fabric. The glass yarns exhibit A = 1360 [dtex] / 2.5 [g/cm^3] = $5 \cdot 10^{-4}$ cm^2 and the fabric with 14 yarns/cm in warp direction A = $7.6 \cdot 10^{-3}$ cm^2/cm. This means that the glass fibre fabric requires only approximately 3/5 of the cross-section of the PES fabric in order to reach the same tensile strength.

The glass fibre fabric/polyester fabric stiffness ratio can be estimated with the data presented. Using the maximum tangent modulus for polyester E = 21,000 N/mm^2 and the lower limit of the Young's modulus presented for E-glass E = 72,000 N/mm^2, see Table 1, the longitudinal stiffness is EA = 21,000 N/mm^2 · 1.20 mm^2/cm = 25,200 N/cm for the polyester fabric and EA = 72,000 N/mm^2 · 0.76 mm^2/cm = 54,720 N/cm for the glass fibre fabric. This is known as the 'base material-related' longitudinal stiffness within the scope of the present work, disregarding any constructional stretch impacts. Assuming the yarns are parallel strands (rovings), i. e. no yarn constructional stretch appears, and the fabric is a laid instead of a woven fabric, i. e. no fabric constructional stretch appears, the glass fibre fabric would be at least 54,720 / 25,200 = 2.2 times stiffer than the polyester fabric with the same strength. But for fabrics that are actually (coated) woven fabrics made of twisted and crimped yarns, this statement is not that simple, at least not for initial loading and low stress ranges where constructional stretch is dominant. In fact it can be expected that for high stress ranges or advanced load cycles where the constructional stretch has less or no impact, the glass fibre fabric behaves significantly stiffer. On the other hand, owing to the greater magnitude of yarn crimp in the glass fibre fabric compared with the polyester fabric, see Figure 45, the glass fibre fabric is expected to show considerably higher constructional stretch. This softening impact on the stiffness behaviour can only be investigated experimentally.

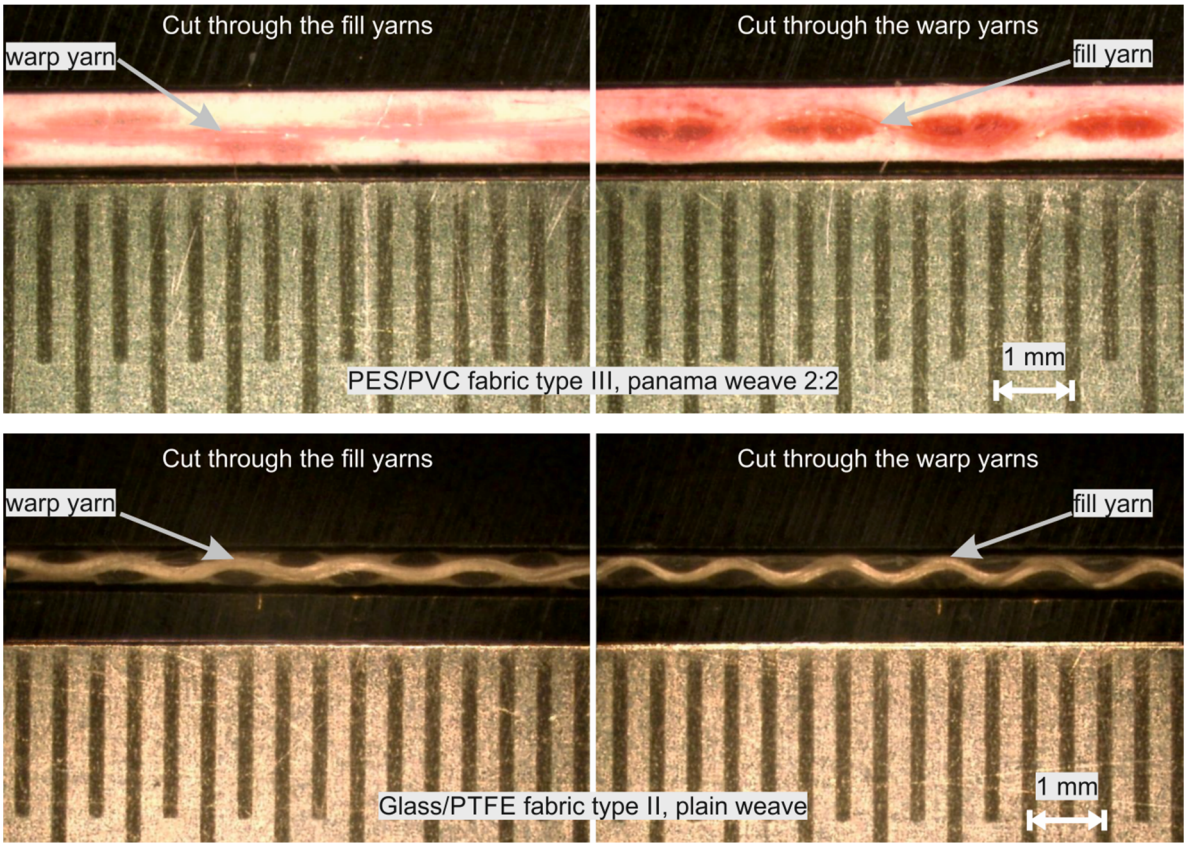

Figure 45 Sections through the materials investigated: PES-PVC type III (top) and glass-PTFE type II (bottom) [USS15c]

Figure 46 shows the measured stress-strain paths for both materials under uniaxial loading during the initial load cycle on the virgin material. Surprisingly, for warp stressing, the strain in the direction of the tensile stress, called “tensile strain”, is almost equal for both materials up to a stress level of approximately σ = 15 kN/m. Only very low constructional stretch was detectable (see the almost linear paths in Figure 46, left). However, the fact that the glass fibre fabric actually appears to be even a little softer up to approximately σ = 15 kN/m, even though it exhibits a much higher base material-related longitudinal stiffness EA than the polyester fabric, reveals the constructional stretch of this material. A softening of the polyester fabric is recognisable beyond the stress level σ = 15 kN/m. This point marks the change from section I to section II, cf. Figure 14 (b). Owing to this behaviour, the glass fibre fabric appears to be considerably stiffer when the whole stress range is evaluated with a secant modulus. The polyester fabric’s transverse strain is much smaller than that of the glass fibre fabric.

During uniaxial fill stressing, it is most remarkable that the glass fibre fabric is clearly softer than the PES fabric up to a quite high stress level of σ = 17 kN/m. This feature can be advantageous in the installation process since it makes it easier to pull the membrane into the prestressed configuration. The stress-strain paths in the tensile direction reveal a very obvious constructional stretch for both materials during stressing the fill direction, see Figure 46, right. The glass fibre fabric stiffens during

stressing and passes over to the linear behaviour of E-glass at approximately σ = 13 kN/m. This point strikingly reveals the transition from constructional stretch to yarn strain, see Figure 15. The same behaviour can be observed for the polyester fabric up to approximately σ = 12 kN/m. But the fabric softens beyond that level. Apparently, the stress-strain characteristic of the yarn material dominates the stiffness behaviour of the fabric beyond that stress level, again indicating the changeover from section I to section II. When evaluating the full design stress range σ = 0-20 kN/m, the glass fibre fabric seems to be somewhat stiffer than the PES fabric. For fill stressing, too, the glass fibre fabric exhibits much higher transverse strain.

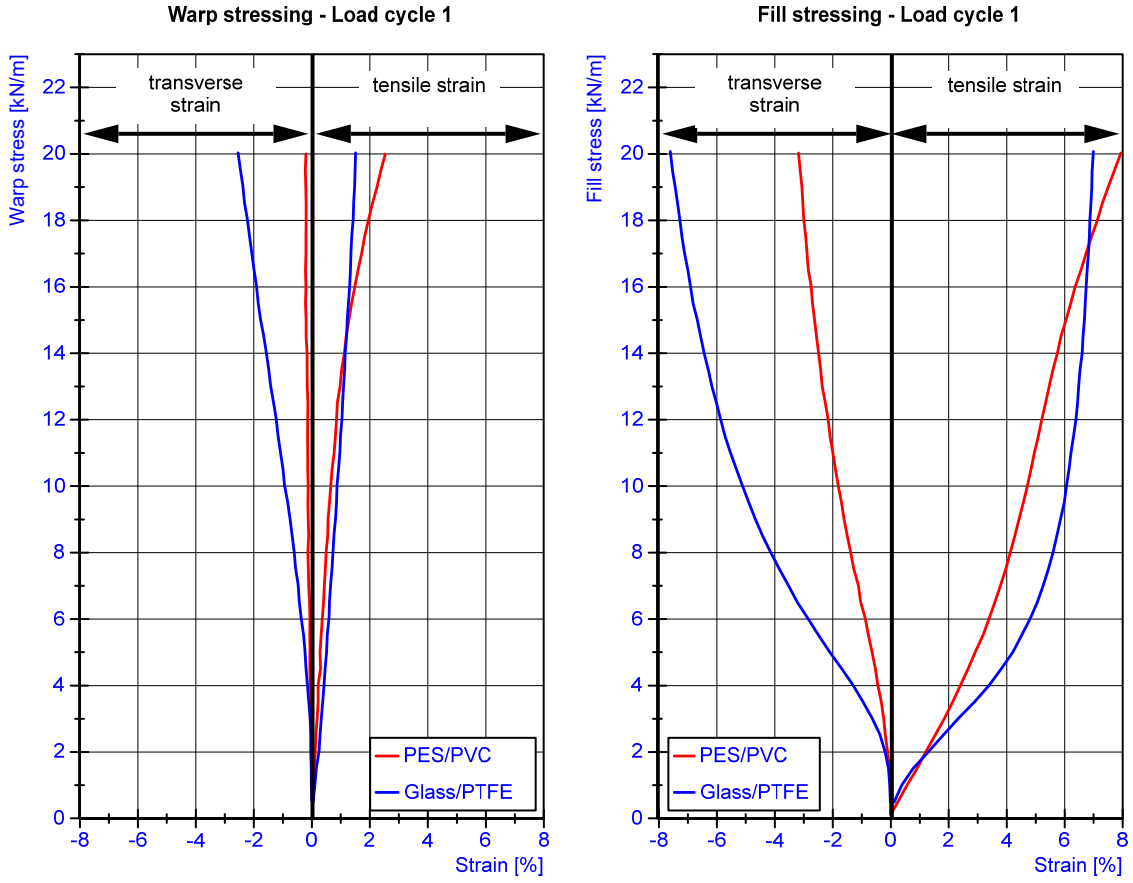

Figure 46 Comparison of stress-strain paths of PES-PVC and glass-PTFE of similar tensile strength for uniaxial warp and uniaxial fill stressing, initial load cycle [USS15c]

As the first load cycle has rather important for the installation of the membrane, it is advantageous to evaluate stiffness properties for use as input data for the structural analysis in an advanced load cycle. For this reason, the comparison of stiffness properties is demonstrated for the 5th load cycle in Figure 47. The stress-strain paths have become almost linear. For both stressing directions, the glass fibre fabric is shown to be distinctly stiffer in the tensile direction than the PES fabric when evaluating the complete design stress range. For warp stressing, the transverse strain of the glass fibre fabric is clearly higher and for fill stressing only a little higher.

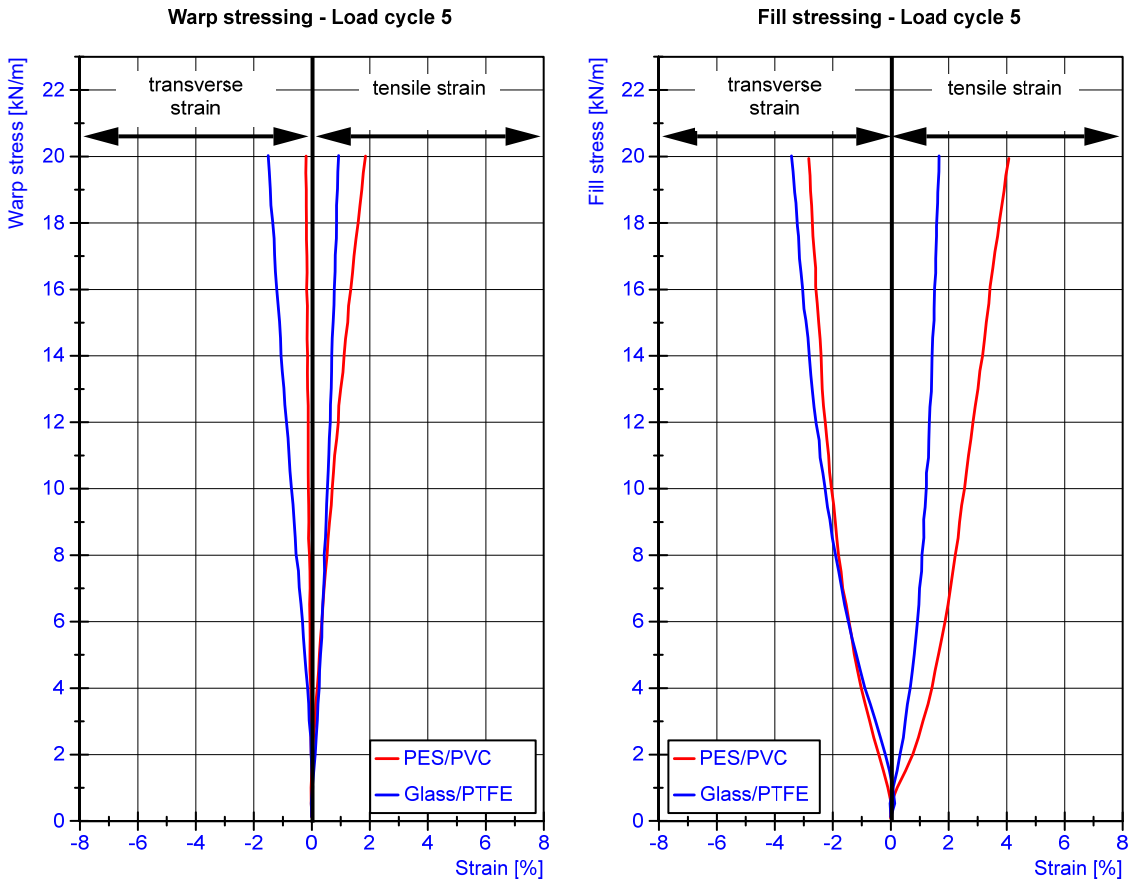

Figure 47 Comparison of stress-strain paths of PES-PVC and glass-PTFE of similar tensile strength for uniaxial warp and uniaxial fill stressing, 5th load cycle [USS15c]

Concluding, uniaxial tensile tests revealed that the glass fibre fabric exhibits considerably higher tensile stiffness when the complete working stress range was evaluated by a secant modulus, irrespective of the load cycle. On the other hand, the results also showed that for large stress ranges, the glass fibre fabric is actually identical to or even less stiff than the comparable polyester fabric, especially during initial loading. This behaviour is caused by higher constructional stretch which originates in a higher magnitude of yarn crimp. This can be advantageous for the installation process. It should be mentioned that material producers can influence the stiffness behaviour by varying constructional details. Moreover, the investigations revealed considerably higher transverse strains for the Glass-PTFE fabric, also linked to the higher yarn crimp magnitude. This characteristic can be beneficial for the installation process, too, but it will be a challenge to consider this specific material behaviour in the material modelling of the structural analysis." [USS15c]

6.2.4 Tests under long-term loads

Two uniaxial tensile tests with long-term loading were conducted with the aim of investigating in particular the strain response in transverse direction. Creep behaviour in tensile direction has been examined extensively. Tests which explore the creep behaviour in transverse direction are unknown, however.

In order to study only the principal material response, two uniaxial tensile tests were performed on one PES-PVC material type III: once with warp stressing and once with fill stressing. Both directions were stressed in these tests with a magnitude of ¼ of the minor data sheet's tensile strength, that is σ = 27 kN/m. A hold time at maximum test stress level of 60 minutes was chosen, and a subsequent recovery time of 60 minutes was applied.

A detailed analysis is given for the test with fill stressing. The initial strain ε_{inst} was measured at the end of the loading process in tensile direction (in this case: fill) and transverse direction (in this case: warp). At the end of the hold time the creep strain ε_{creep} was measured. The results are illustrated in Figure 48. The stress and strain are each plotted against time. The initial strain in tensile direction is ε_{inst} = 10.9 % and in transverse direction ε_{inst} = -3.7 %. This yields a tensile modulus E_y = 27 / 0.109 = 248 kN/m and a Poisson's ratio ν_{xy} = 3.7 / 10.9 = 0.34. Both match very well the results presented for this material in Table 4 and Table 5.

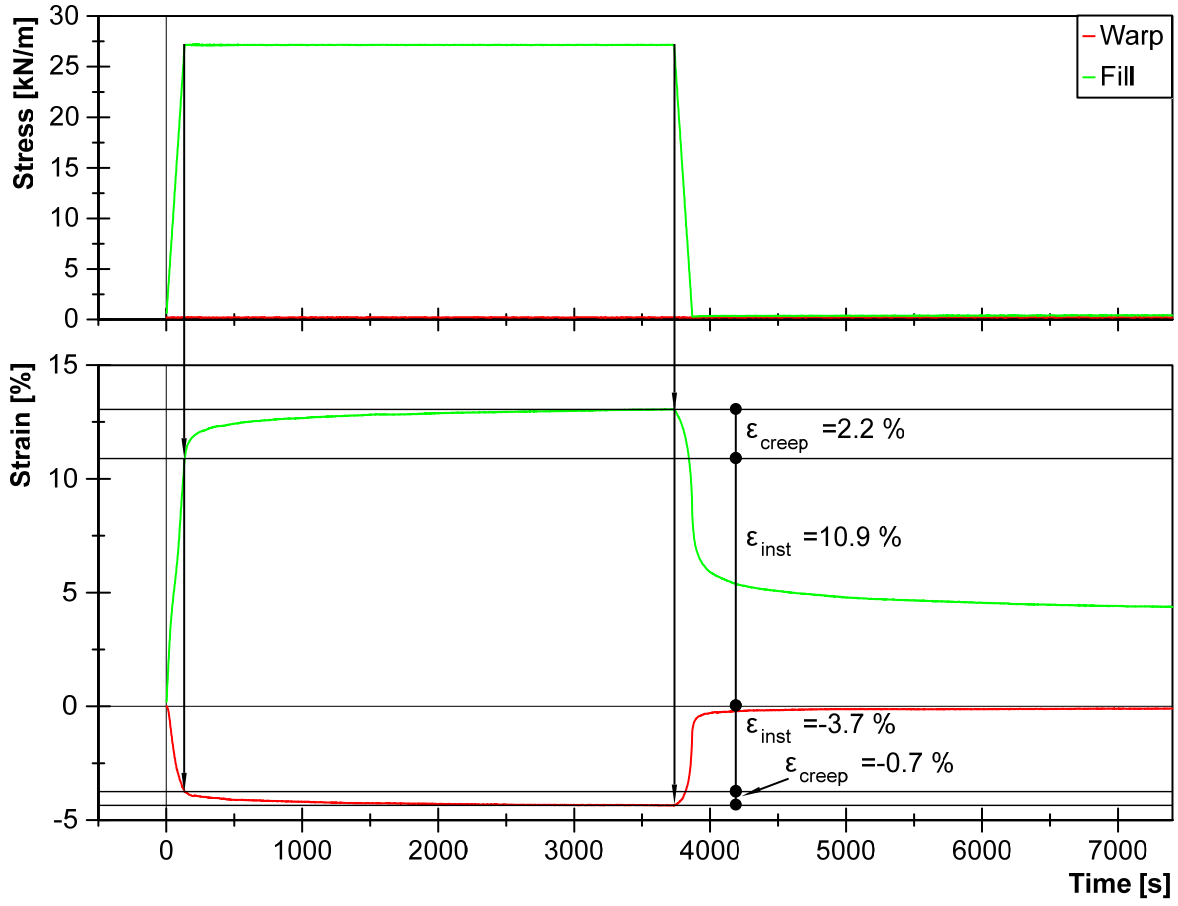

Figure 48 Creep strain in tensile and transverse direction under a load duration of 60 minutes

At the end of the hold time, additional creep strain of ε_{creep} = 2.2 % occurs in tensile direction and ε_{creep} = -0.7 % in transverse direction. This means a final strain in tensile direction of ε_{fin} = 13.1 % and in transverse direction of ε_{fin} = -4.4 %. A tensile-creep modulus E_{creep} can be determined according to [DIN EN ISO 899-1:2003] as $E_{y,creep}$ = 27 / 0.131 = 206 kN/m. Furthermore, a Poisson's ratio for the long-term load

of ν_{xy} = (3.7+0.7) / (10.9+2.2) = 0.34 is discovered. Finally, this demonstrates that the Poisson's ratio does not change while the tensile modulus decreases under long-term loads.

For warp stressing, the initial strain in warp was measured as ε_{inst} = 5.1 % and in transverse direction as ε_{inst} = -0.22 %. This results in a tensile modulus of E_x = 525 kN/m and a Poisson's ratio of ν_{yx} = 0.04. At the end of the hold time, a tensile-creep modulus of $E_{x,creep}$ = 383 kN/m but the same magnitude for the Poisson's ratio ν_{yx} result from ε_{fin} = 7.1 % in loading direction and ε_{fin} = 0.3 % in transverse direction.

The main conclusion is that Poisson's ratio does not change for long-term loading. With this knowledge and considering the findings of *Reinhardt* that creep in tensile direction was of the same order of magnitude for uniaxial and biaxial stressing, see Chapter 3.5.3.2, it can be concluded that biaxial creep tests can be omitted when design elastic constants are to be approximated for a long-term load situation. Instead, only the tensile modulus can be varied using a creep coefficient. Following [DIN EN 1995-1-1:2010], a creep coefficient k_{def} can be defined as $k_{def} = \varepsilon_{creep} / \varepsilon_{inst}$. For the present tests this gives k_{def} = 2.2 / 10.9 = 0.20 for fill and k_{def} = 1.9 / 5.1= 0.37 for warp. With the given definition of k_{def}, the final strain results in $\varepsilon_{fin} = \varepsilon_{inst} \cdot (1+k_{def})$. Equally, the tensile modulus can be modified to the tensile-creep modulus: $E_{creep} = E / (1+k_{def})$.

The creep coefficients for warp and fill may be determined according to [DIN EN ISO 899-1:2003] in uniaxial tensile creep tests. As the only long-term load in Europe is snow, it would be reasonable to combine the creep test with a temperature of T ≤ 0°C. In these tests the load is held constant until the creep process has completely finished. This procedure covers a snow load that could last for months. The test matrix should consider that the highest creep coefficients possibly may not result from the highest stress levels, see Chapter 3.5.2.3. For this reason it is recommended that the creep tests are conducted on an anticipated stress level resulting from the snow load for a specific structure.

6.2.5 Tests with alternation of warp and fill stressing

Under cyclic loading in an unaltered stress ratio, the hysteresis loops move to higher strain but the movement decays after several load cycles. After the last load in a test protocol and a subsequent sufficient recovery time, irreversible strain remains in the fabric, see Chapter 3.5.2.2. Figure 49 illustrates this mechanism by means of warp stress-strain loops under five cycles of uniaxial warp stressing. The irreversible strain at the end of the measurement is marked with a dot. However, this has already been demonstrated in the previous chapters. In a membrane structure this strain state is coupled with a certain prestress level. The higher the irreversible strain, the lower the prestress level.

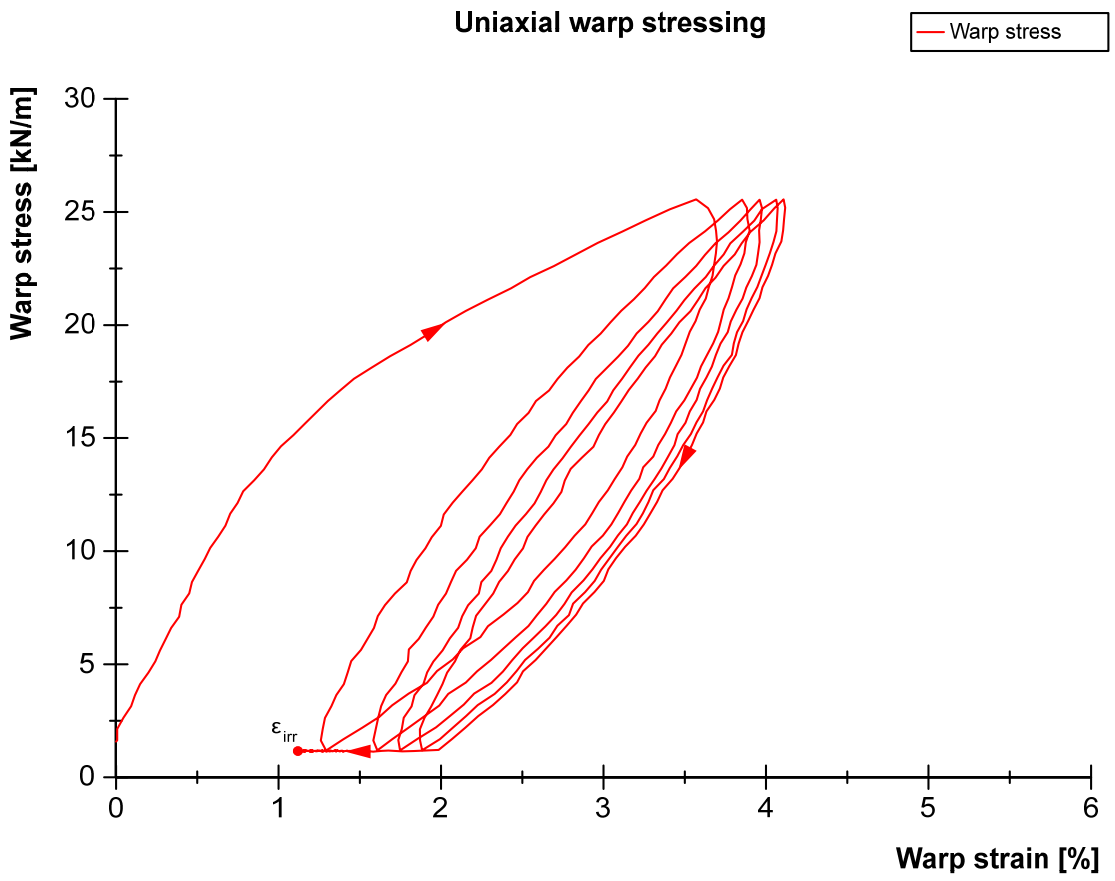

Figure 49 Irreversible strain after cyclic loading and a subsequent recovery time

The question to be discussed here concerns what happens if the main stress direction changes as is to be expected for anticlastic structures. To examine this, a test is performed in which a number of cycles of uniaxial stressing in one main fabric direction is followed by uniaxial stressing in the transverse direction. This test protocol is realised by again conducting the uniaxial tests on the biaxial test rig, see previous chapters for details.

The test protocol according to *Blum, Bögner and Némoz* [BBN04] is applied for this purpose. This is similar to the previous uniaxial tests. The only difference is a certain prestress level as a basis from which the uniaxial stressing begins. In the present context, five cycles of warp stressing are followed by five cycles of fill stressing. The single sets of load cycles are separated by a recovery time of 30 minutes and also framed by two additional 30-minute recovery times. This complete sequence is referred to here as one “load block”. In fact, this test was primarily performed to validate the biaxial test and evaluation procedure proposed in [BBN04]. The validation is described in detail in Chapter 7. In relation to the present object of investigation, it is important to note that the complete test protocol proposed in [BBN04], i. e. one load block, was repeated five times, see Figure 50.

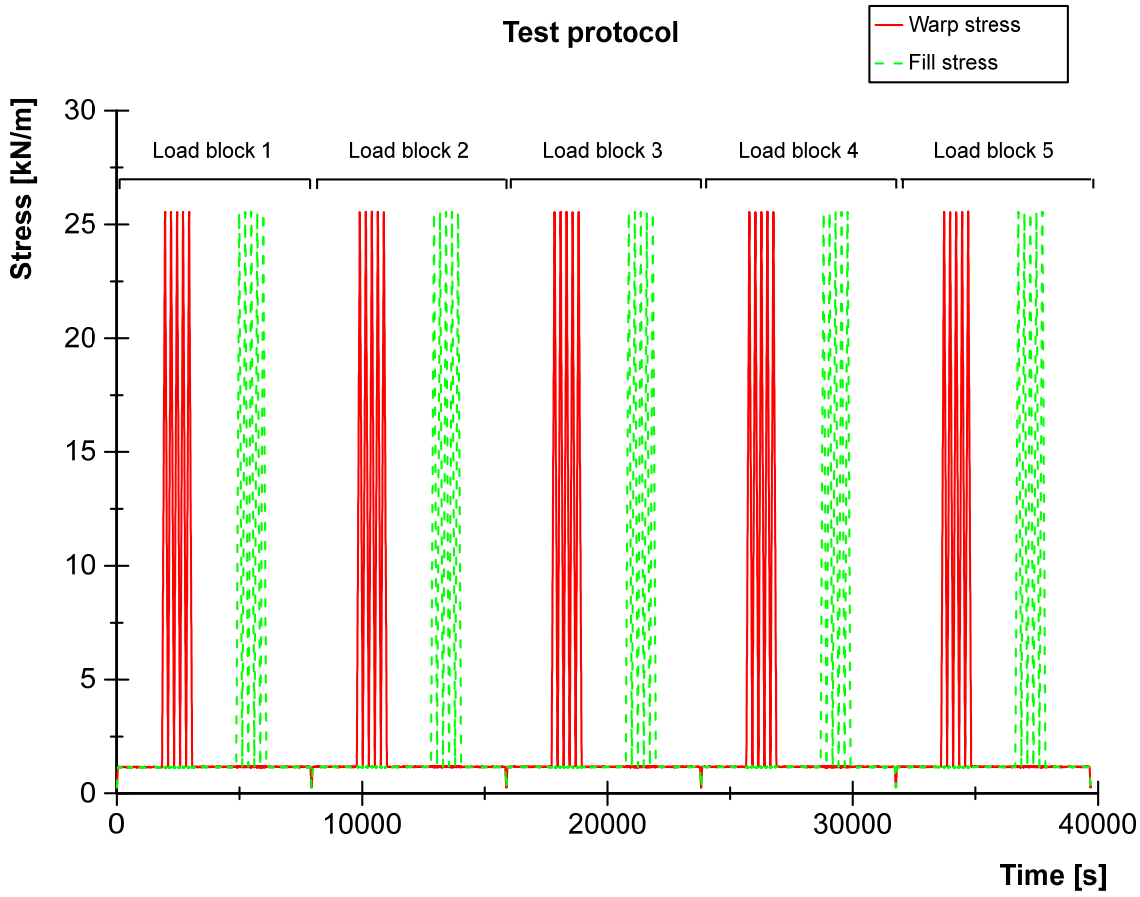

Figure 50 Test protocol for investigation into the impact of load direction alternation

The test data shown in the following is of PES-PVC type III from material producer 1. As usual, the maximum test stress was ¼ of the data sheet tensile strength of the fabric direction with the lower strength. The prestress level is p = 1 kN/m. However, the prestress level can be neglected for the purposes of the present examination.

Figure 51 illustrates that irreversible strain at the end of the warp stressing sequence including the 30-minute recovery time decreases considerably as a result of the following fill stressing. This can be seen from the starting point of the warp stress-strain path in load block two. It means that the strain that seemed to be irreversible is actually rather a temporary residual strain, which is conditional and only lasts until the condition of transverse stressing occurs. When transverse stressing – or rather a change in the stress ratio in general – occurs, a certain amount of strain reset is observed.

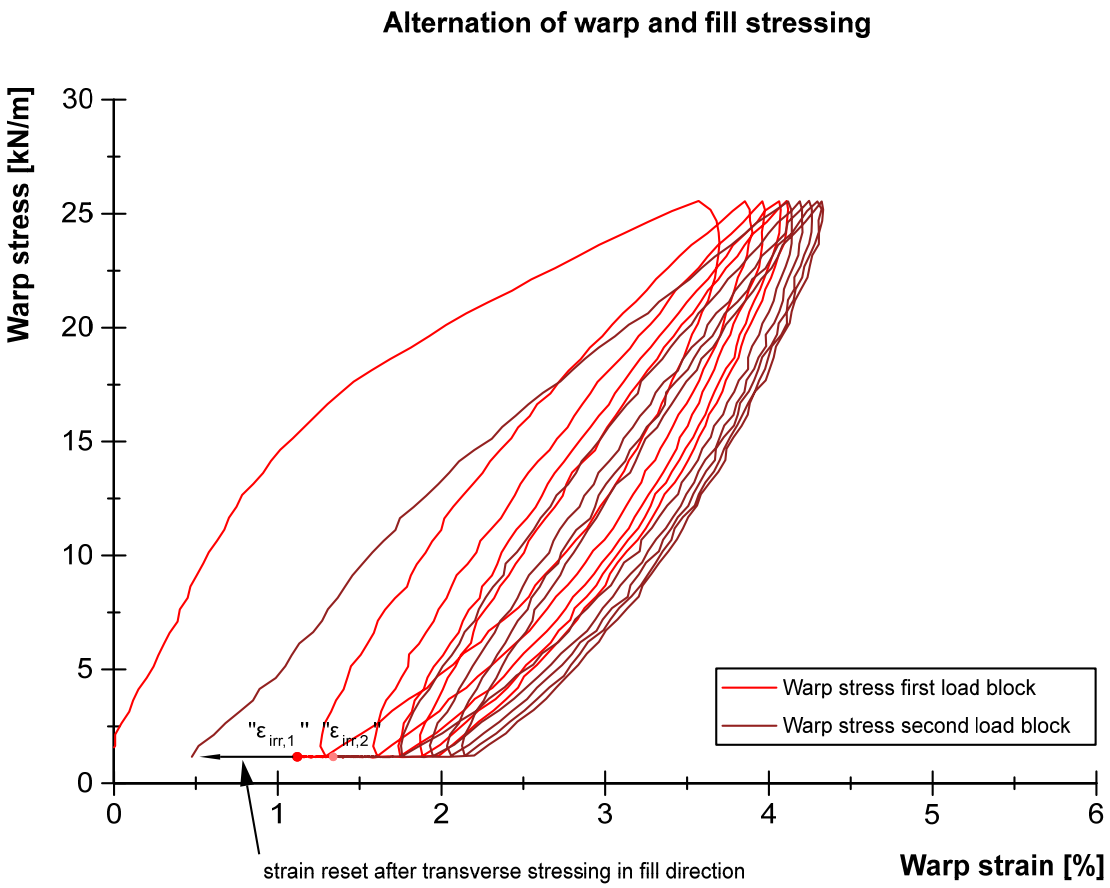

Figure 51 Reduction of “irreversible” strain due to an alternation of warp and fill stressing

In order to show the results for all load blocks clearly, Figure 52 shows for every load block only the loading paths of load cycle 1 and the unloading paths of load cycle 5. The illustration demonstrates how the behaviour stabilises with the third load block. In this condition the fabric switches between two states of temporary residual strain: one after warp stressing and one after fill stressing. Each time the stressing direction changes between warp and fill, the fabric reverts to its previous state, back and forth.

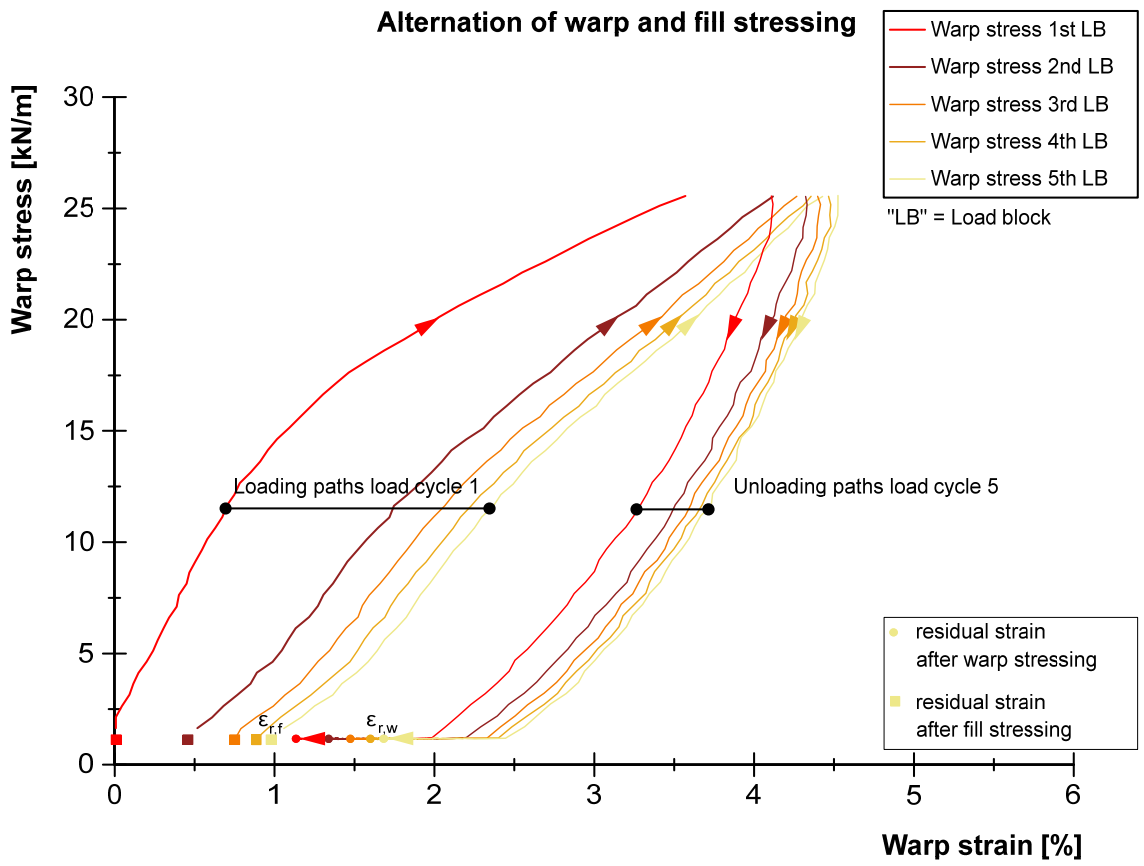

Figure 52 Switch between two states of residual strain

The following mechanism is a possible explanation of the observed behaviour: during stressing in one direction, e. g. warp direction, the crimp in the stressed yarns decreases, whereas the crimp in the perpendicular yarns increases. Where stressing is in perpendicular direction, this process is reversed: the warp yarn crimp increases again while the fill yarn crimp decreases. Assuming a bidirectional “back and forth” with the same magnitude of stresses in every load cycle, this mechanism can be expected to be a closed circiut. This is illustrated in Figure 53: after stressing in one direction, the yarn configuration is reset by stressing with the same magnitude in perpendicular direction. The only exception is the very first loading of a virgin fabric, which eliminates the constructional stretch.

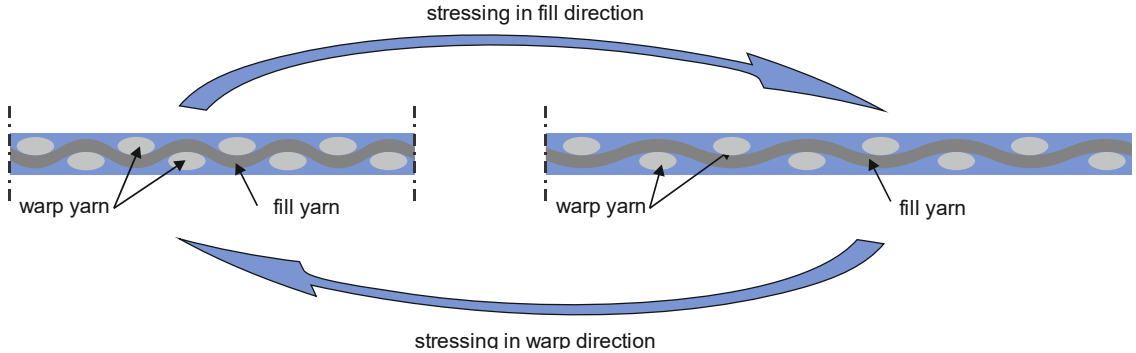

Figure 53 Reset of the yarn configuration

As the behaviour studied for warp stress-strain paths can be presumed to be the same for the fill stress-strain paths, the observed behaviour can be generalised as presented in Figure 54. It illustrates in general the closed stress-strain circuit and the two boundary residual strain states when the load direction in the principal fabric directions changes back and forth. As long as repeated loading does not change direction, the narrow stress-strain hysteresis is passed through. Every time the load direction changes, the residual strain is reset and under a subsequent load in the original direction the less steep loading path is passed through. Figure 54 also shows that the residual strain after full stressing in transverse direction is the actual amount of irreversible strain.

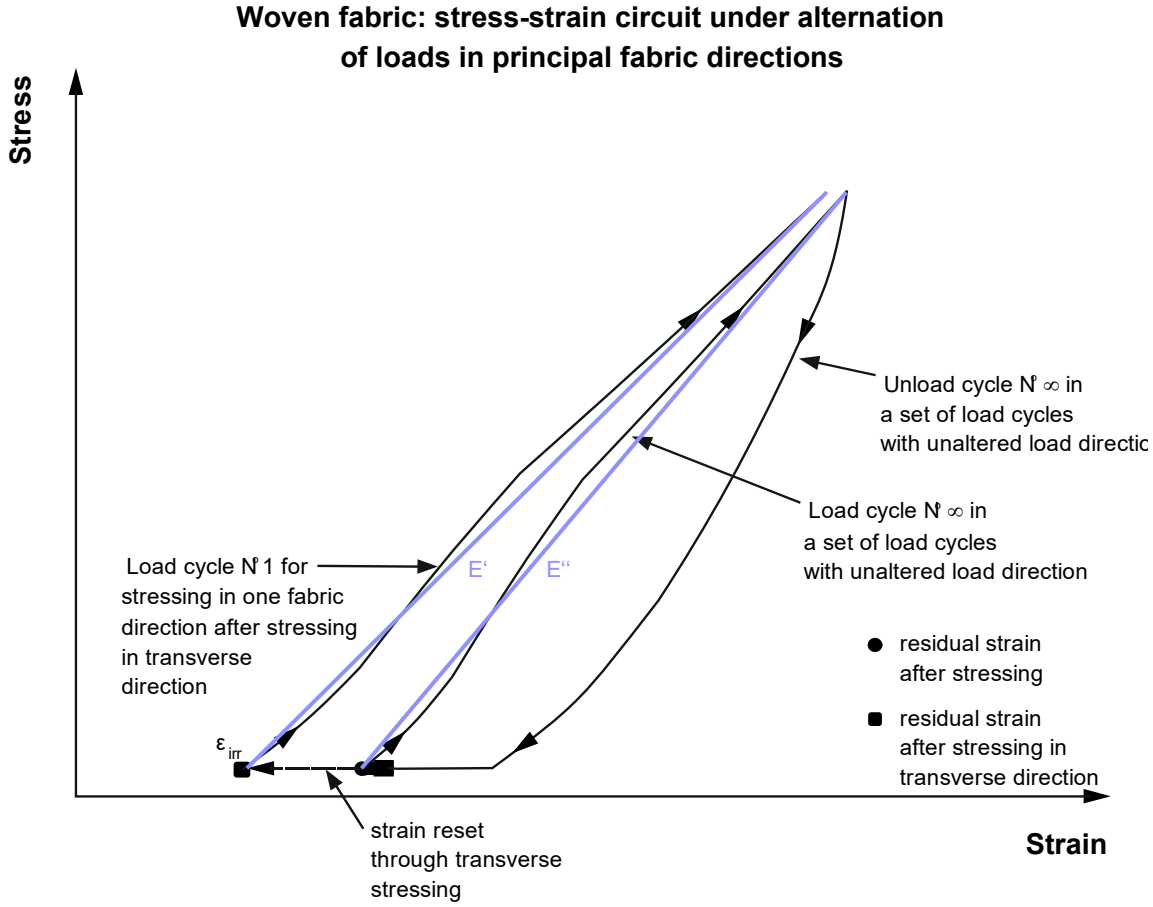

Figure 54 Stress-strain circuit including two boundary residual strain states after unloading woven fabric with alternation of loads in principal fabric directions

An alternation of load directions is typical for anticlastic structures. Apart from the stiffness of a virgin fabric, two relevant stiffness states occur for anticlastic structures. They are correlated to the illustrated boundary residual strain states: one stiffness state for unaltered load direction, marked E'', and one stiffness state directly after an alternation of the load direction, marked E'. Directly after an alternation of the load direction, the stiffness is lower: E' < E''.

This state is simultaneously associated with less residual strain at the beginning of the load path. In a membrane structure with geometrical fixed boundaries, this means

a higher prestress level. By contrast, the higher stiffness after repeated loading without alternation of the load direction is combined with a lower prestress level. This raises the question of how far these effects balance each other out. This will be investigated in the following chapters by means of experimental tests simulating a prestressed membrane structure with an orthogonal external load. If they largely balance each other out – which could be expected because of the existence of a fixed pair of max. membrane stress and correlated strain values (max $\sigma \mid \varepsilon$) – it would not matter which state is simulated for the static verification. It does indicate, however, that stiffness and prestress level cannot be treated separately from one another.

As the prestress level in a fabric structure is closely linked to the strain state of the fabric, this also means that the prestress in an anticlastic structure cannot have one constant level. With a change of direction in the external loads, the direction of the main stressing also changes. The changing yarn configuration as a result is accompanied by changing residual strains – or temporary residual strains, to be more precise. If the temporary residual strains vary between two limit values, the same must be true for the prestress level: it must vary between two limit values depending on the current yarn configuration.

After a woven textile has settled under uniaxial maximum stress in one of the main directions, the highest thinkable impact to the crimp can be induced by a uniaxial maximum stress in the transverse direction. Yarns with maximum crimp are forced to straighten and straightened yarns are subject to maximum crimp. All other stress ratios between the limiting uniaxial ones can be expected to have less impact on crimp condition.

Moreover, the test results show similar stress-strain paths for every load block and also similar pairs of maximum stress and correlated strain values (max $\sigma \mid \varepsilon$). This confirms that the “previous load history memory effect” is erased at the latest after five load cycles of one and the same stress ratio, see also the findings of *Galliot & Luchsinger* presented in Chapter 3.5.4. The stable state of the fabric is achieved, which is independent of the previous load history.

6.3 Orthogonally loaded membrane strip tests

6.3.1 General

Among other impacts, stress and deflection of a membrane structure in a certain loading situation evolve from the interaction of material stiffness and prestress level. In relation to coated architectural fabrics, varying stiffness properties and varying prestress levels associated with varying residual strains for different load cycles leave a degree of uncertainty as to the load cycle in which the maximum stress and deflection occur. This knowledge is crucial for safe design. The question of which load cycle is suitable for modelling in the structural analysis for safe design must be

addressed in order to (a) calculate the maximum stress and (b) calculate the maximum deflection.

Simulation of an orthogonally loaded prestressed fabric in an experimental test makes it possible to study the development of stress, prestress and deflection over the load cycles. For this purpose, a uniaxial membrane strip test was designed and performed, see Figure 55. In simple terms, a strip of fabric is prestressed and fixed at the longitudinal ends and subsequently loaded with an orthogonal line load q in the middle.

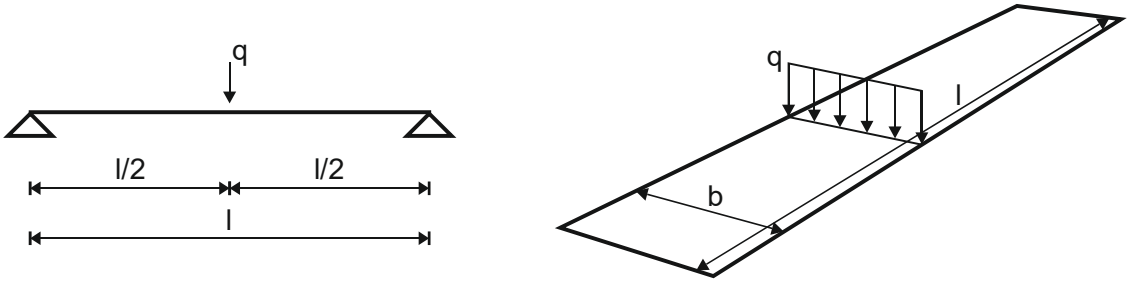

Figure 55 Structural system and isometric view of the orthogonally loaded membrane strip test

In detail, a membrane strip with a width of b = 0.10 m and a length of approximately l = 0.60 m between two clamps is installed in a horizontal picture frame. The actual length depends on the compensation value. The clamps glide on the test frame. Behind the clamp on one end of the strip is a turnbuckle for applying prestress. Behind the clamp on the opposite end is a load cell. The experimental setup simulates a membrane component with uniaxial load-bearing behaviour. It is illustrated in Figure 56. The horizontal picture frame is placed under the crossbeam of the 50 kN Zwick/Roell testing machine at the Essen Laboratory for Lightweight Structures (ELLF), see also Figure 28. A plunger is attached to the crossbeam via the machine clamp, making it possible to apply a defined line load orthogonally to the membrane plane. The testing machine is equipped with a 2 kN load cell between the machine clamp and the plunger.

In this force-controlled test, the orthogonal line load is regulated via the testing machine load cell. The line load is calibrated such that the membrane stress can be expected to be approximately ¼ of the minimum data sheet's tensile strength f_t of the tested material. It thus approximately simulates the full design load presuming a stress factor of four. The deflection is measured as the crossbeam travel of the testing machine and the horizontal portion of the membrane stress is measured with the external load cell behind one of the clamps. Strips are attached to reduce friction between the gliding clamp and the picture frame. Friction can be presumed to have no significant influence on the stress measurement.

The "orthogonally loaded membrane strip" tests were conducted with PES-PVC type III from material producer 2. Tests were performed with warp yarns in longitudinal

strip direction as well as with fill yarns in longitudinal strip direction. Tests with and without recovery times were also undertaken.

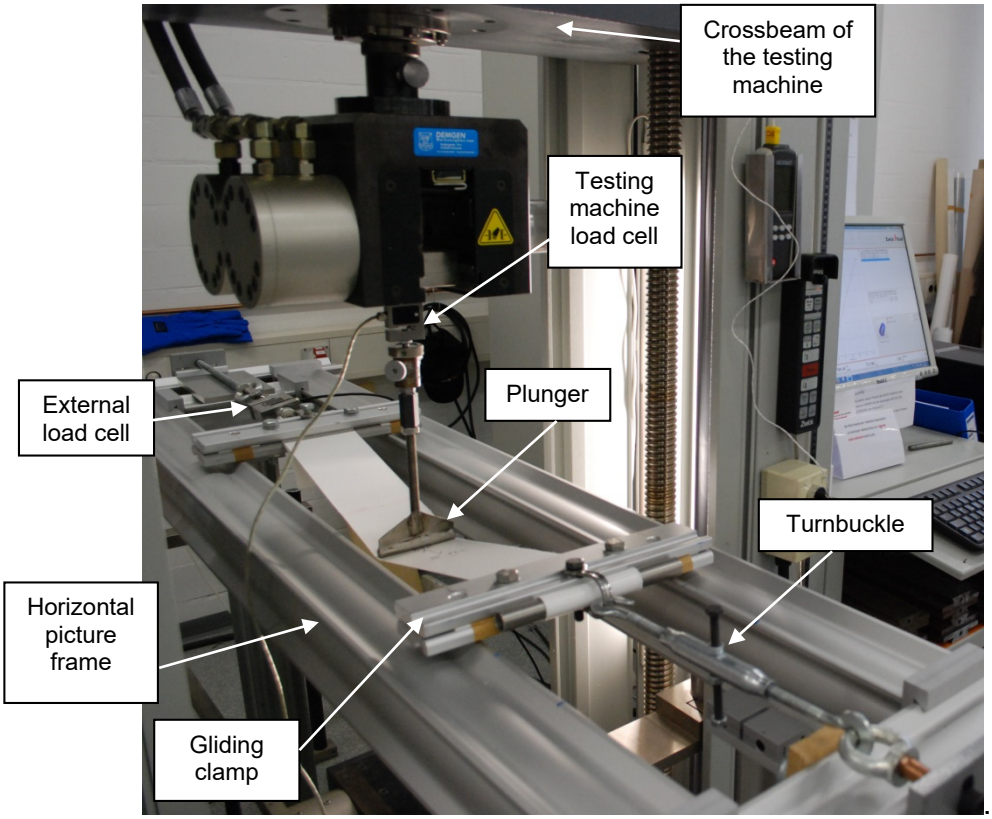

Figure 56 Experimental setup for the “Orthogonal loaded membrane strip” test, shown with a maximum deflected test specimen during a test

After the membrane strip was loosely installed with a clearance of exactly l = 0.60 m between the two gliding clamps, prestress was introduced via the turnbuckle. In preparation for these tests, compensation values were determined on the basis of the uniaxial tests described in the previous chapter. 2.0% was selected for the warp direction and 5.7% for the fill direction. Introducing this stretch to the test specimens gave them a final length between the clamps of l = 0.612 m for the specimens in warp direction and l = 0.634 m for the specimens in fill direction. These compensation values correspond to an initial prestress in warp direction of p_i = 18.3 kN/m and in fill direction of p_i = 13.7 kN/m, given as mean values of both tests. Immediately after the application of the initial prestress, a hold time of 30 minutes was included to enable relaxation. The prestressing procedure and subsequent relaxation are referred to as “phase I” of the test, see Figure 58. At the end of the relaxation phase, the prestress is 13.7 kN/m for the tests in warp direction and 9.5 kN/m for the tests in fill direction, again given as mean values here. Subsequently, five cycles of orthogonal load are applied by the plunger via the testing machine in “phase II”. The plunger is removed completely from the test specimen immediately after the fifth unload cycle. From that point on, the progression of the membrane stress in the test specimen freed from any external manipulation is measured over 30 minutes. This is “phase III” of the test:

revertive creep causes the test specimen to lose its “residual” deflection and it recovers to a plane. Prestress recovers simultaneously and tends to an asymptote.

The compensation values were calculated so as to ensure a certain predefined nominal prestress level after five cycles at full load, i. e. a load that produces a membrane stress of ¼ of the tensile strength as mentioned above. This required high initial prestress, reflected by the measured values given above. Where actual mechanically prestressed membrane structures are concerned, it could be difficult to introduce prestress of such magnitude during installation, depending on the specific structure. If this is the case, it is up to the design engineer to take appropriate measures. Envisaging a lower nominal prestress level or a retensioning system which allows the membrane to be restressed after significant loads have occurred are two possibilities. Another – depending on the location and the expected loads over the planned lifetime – is to ensure the nominal prestress level for fewer load cycles or a lower load magnitude. For instance, the characteristic wind load in [EN 1991-1-4] is defined as the load magnitude that is exceeded in the statistical average only once in 50 years. With a typical lifetime of a fabric structure of approximately 25 years, the statistical probability of such a high wind load occurring is 50%. In this light, consideration of five load cycles of such magnitude appears to be unnecessary. This way or another, design and compensation must together ensure a sufficient prestress level even at the end of the lifetime.

Although it is known to have no major impact, the load rate was chosen equal to the uniaxial tensile tests. The maximum value of the external orthogonal load was 12 kN/m, while the minimum at 0.10 kN/m is quasi equal to zero. The maximum load was determined so that a corresponding membrane stress approaching the possible design strength of $0.25 \cdot \min f_{k,23}$ could be expected for the warp strips.

6.3.2 Tests with recovery times between single load cycles

Analogous to the uniaxial tensile tests presented in Chapter 6.2.2, a recovery time of 60 minutes was scheduled after the load cycles in phase II. Figure 57 shows the load history together with the measured results for the vertical deflection f_z in the middle of the membrane warp strip. Deflection stabilises at f_z = 79 mm, which is marked by the dashed line. The membrane stress was calculated from the measured horizontal supporting force and the deflection using trigonometric relations. The stress development for the warp strip over all phases of the test is shown in Figure 58. The maximum warp stress settles at approximately σ_w = 25.1 kN/m in the fourth load cycle, again marked by the dashed line. Immediately after the unloading sequence of this load cycle, the prestress settles at approximately 3 kN/m, which was envisaged as the nominal prestress level here. A delayed elastic system is reached by that time, which can be idealised as an elastic system. Every time an external load is completely removed, a lasting prestress of p = 3 kN/m is restored. This happens together with regaining the associated form – a plane in this example.

The maximum stress of σ_w = 26.3 kN/m is detected in the first load cycle, whereas the maximum deflection appears in the last test load cycle. The maximum stress is 5% higher than the stress in the stable state of the material. A similar magnitude is observed for the deflection: the minimum deflection of approx. f_z = 77 mm is 3% less than the stable state deflection.

Figure 59 and Figure 60 indicate the same for the membrane strip in fill direction. The same line load magnitude of 12 kN/m was used for the fill strip. Under this load, together with the chosen compensation, the membrane deflection settles at approx. f_z = 93 mm and the stress at σ_f = 22.3 kN/m. The findings essentially confirm those of the tests in warp direction. The prestress falls step by step from the initial prestress immediately after installation of p_i = 13.7 kN/m to p = 9.7 kN/m after 30 minutes' relaxation and to a stable level of approx. p = 1.8 kN/m after the fourth loading. This is lower than the envisaged lasting prestress level of 3 kN/m, i. e. the chosen compensation value is revealed to still be too low.

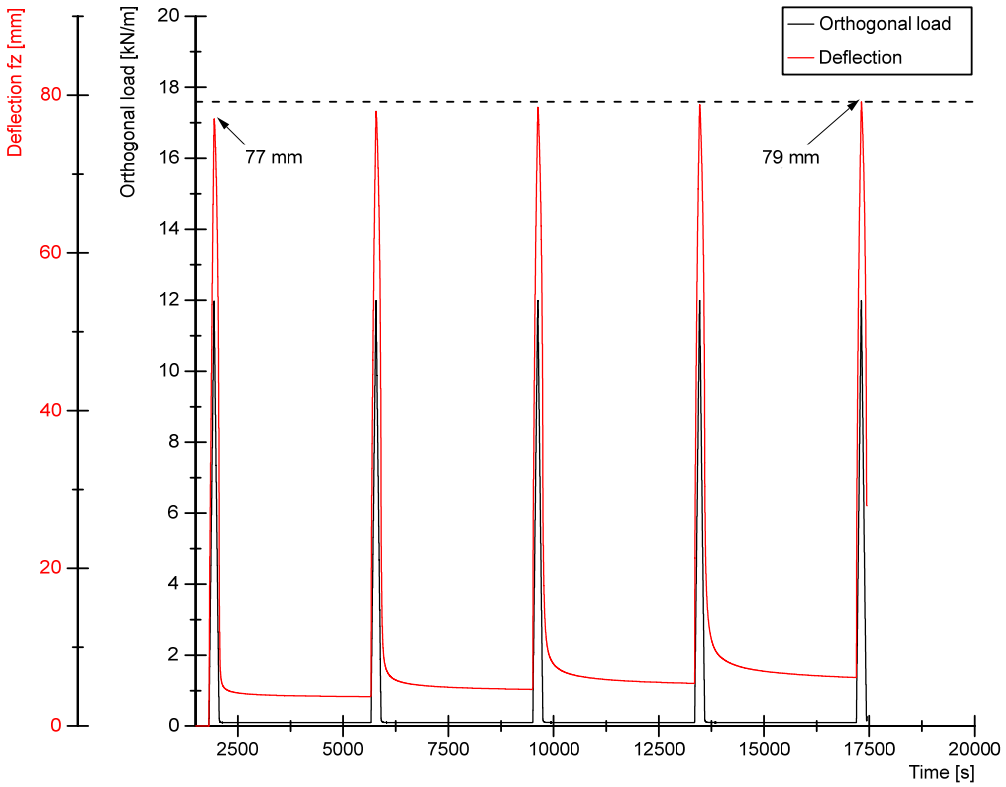

Figure 57 Orthogonal load sequence during phase II and measured deflection f_z for the membrane strip in warp direction

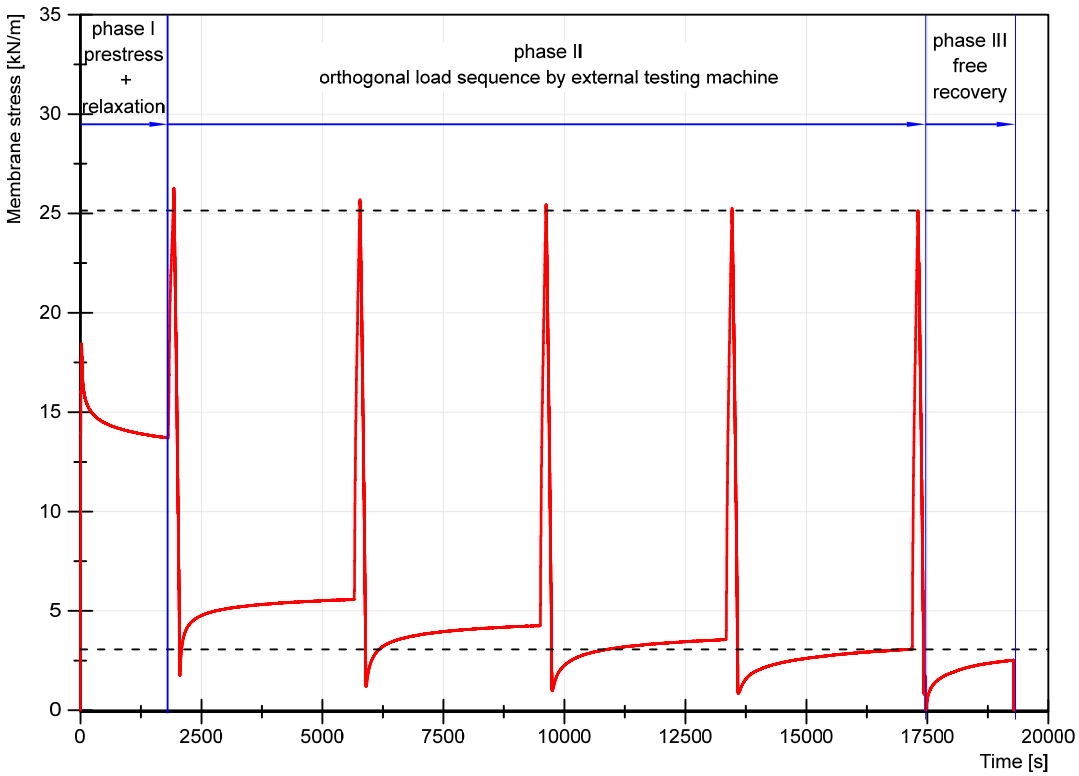

Figure 58 Membrane stress during all three phases of the orthogonally loaded strip test in warp direction

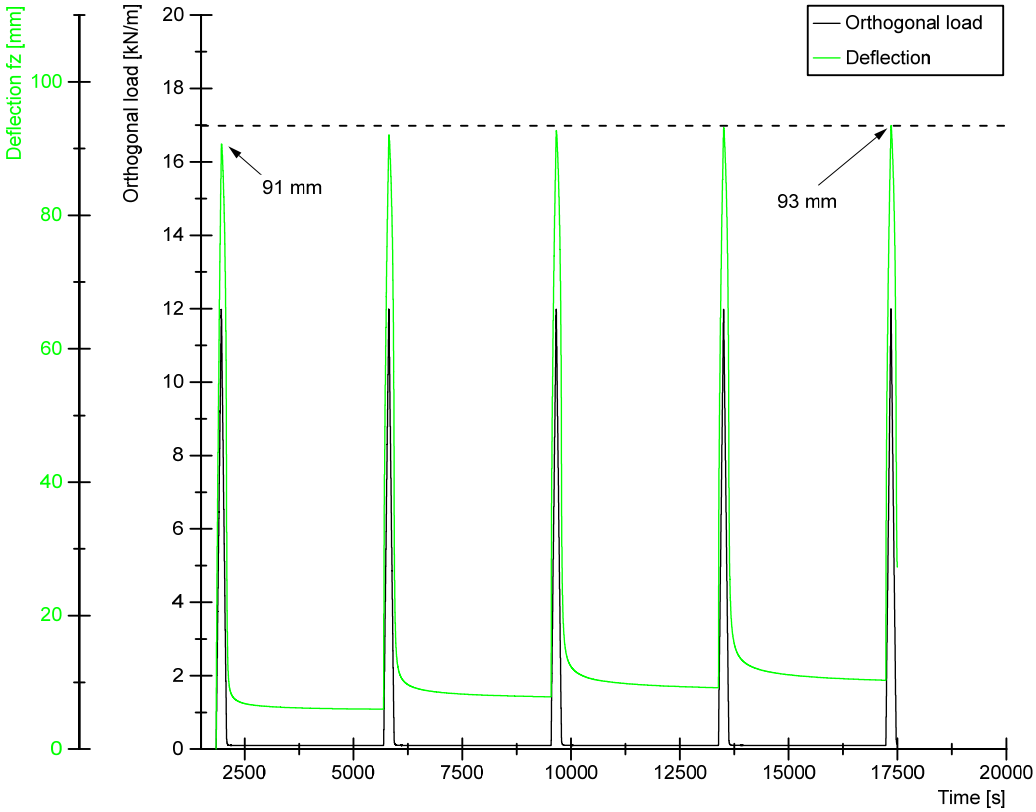

Figure 59 Orthogonal load sequence during phase II and measured deflection f_z for the membrane strip in fill direction

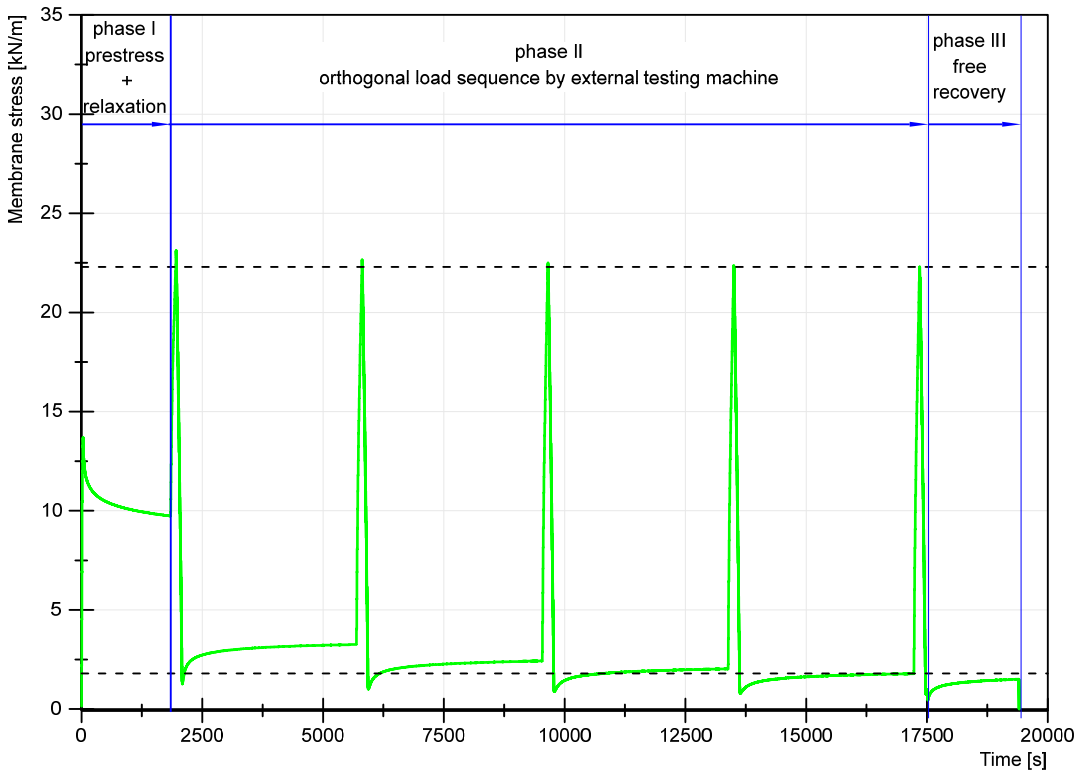

Figure 60 Membrane stress during all three phases of the orthogonally loaded strip test in fill direction

In order to confirm the correctness of specific stiffness parameters for the modelling of the uniaxial strip structure, a comparative finite element analysis was performed using the FE software package Sofistik [Sof14]. The FE model is illustrated in Figure 61. Membrane elements are used with a unit thickness of 1 mm. For reasons of better comparability with the experimental test, the boundaries at the ends of the strip are coupled with a single node on each end. Form-finding is executed in order to introduce prestress to the numeric model. The line load of 12 kN/m is orthogonally applied to the membrane elements in the middle of the strip. A third-order nonlinear analysis is conducted. Appropriate tensile moduli E for the single load cycles are derived from the uniaxial tensile tests described in Chapter 6.2.2. Applying the unit thickness in the model makes it possible to use the determined tensile moduli directly without conversion.

The results of the FE simulation align very well with the test results, as demonstrated in Table 6. Overall, the calculated stresses are slightly lower than the experimental results, while the deflections show almost the same values. Only the fill strip differs significantly for the 5th load cycle, since the calculated deflection is 7% higher than the experimental result and the stresses exhibit a difference of 14%. For the other results the difference between experiment and numerical simulation is no more than 8%.

The results essentially show that the structural analysis can be based on every load cycle as long as the prestress value associated with that specific load cycle and the

appropriate stiffness parameter – which depends for a nonlinear stress-strain path on the stress interval between prestress and expected maximum stress – are used as input. Based on the findings described above, it can be stated that correct analysis results can be obtained from modelling with the nominal prestress and an advanced load cycle in which this prestress value can be seen as enduring and using the stiffness parameters corresponding to this load cycle.

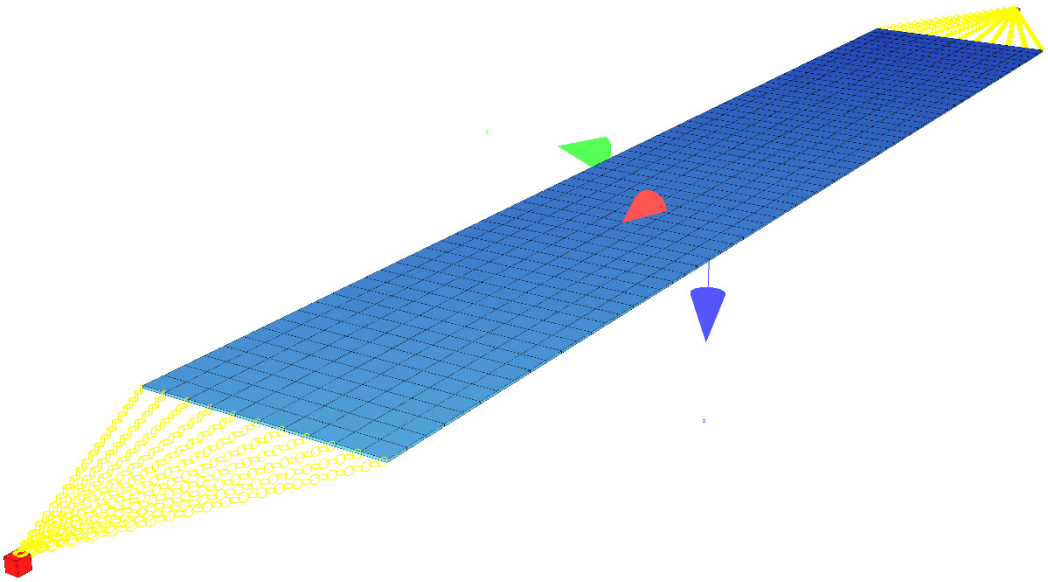

Figure 61 Finite element model of the orthogonally loaded membrane strip

Table 6 Comparison of experimental results of tests including recovery times with finite element analysis

Parameter/Load cycle number		1st load cycle	5th load cycle
Membrane strip in warp direction, l = 612 mm			
FE input	p [kN/m]	13.7	3.0
	E [kN/m]	354*	683**
FE results	max f_z [mm]	76	77
	σ_w [kN/m]	24.4	24.2
Experimental results	max f_z [mm]	77	79
	σ_w [kN/m]	26.3	25.1
Membrane strip in fill direction, l = 634 mm			
FE input	p [kN/m]	9.7	1.8
	E [kN/m]	290***	371****
FE results	max f_z [mm]	91	100
	σ_f [kN/m]	21.3	19.5
Experimental results	max f_z [mm]	91	93
	σ_f [kN/m]	23.1	22.3

* determined as secant between 13.7 kN/m and 26.3 kN/m
** determined as secant between 3.0 kN/m and 25.1 kN/m
*** determined as secant between 9.7 kN/m and 23.1 kN/m
**** determined as secant between 1.8 kN/m and 22.3 kN/m

6.3.3 Tests without recovery times between single load cycles

Analogous to the uniaxial tensile tests presented in Chapter 6.2.3, recovery is omitted in phase II. Otherwise the same load history was applied as in the previous chapter.

It appears that many measured results are the same as in the previously described tests with recovery times. For the warp strip, the initial deflection is $f_z = 77$ mm, whereas in the stable state it is $f_z = 80$ mm, see Figure 62. The initial membrane stress is measured as $\sigma_w = 26.0$ kN/m and settles at $\sigma_w = 25.0$ kN/m after five load cycles, see Figure 63.

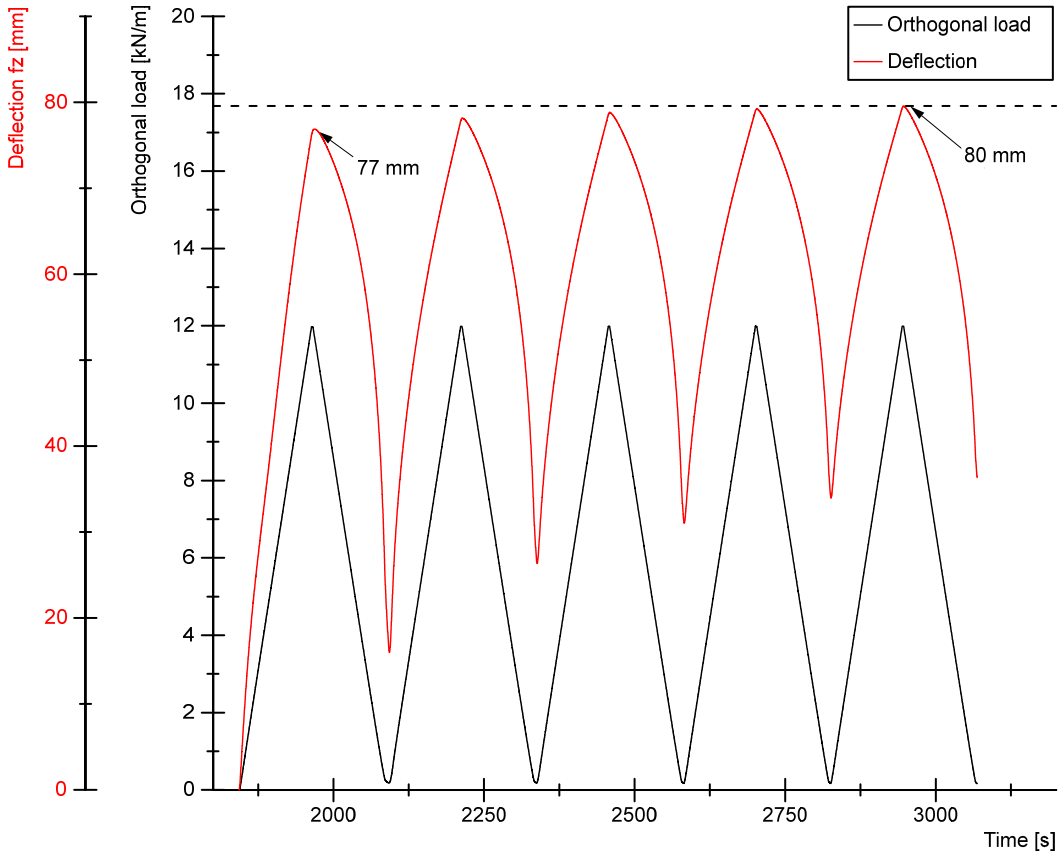

Figure 62 Orthogonal load sequence during phase II and measured deflection f_z for the membrane strip in warp direction

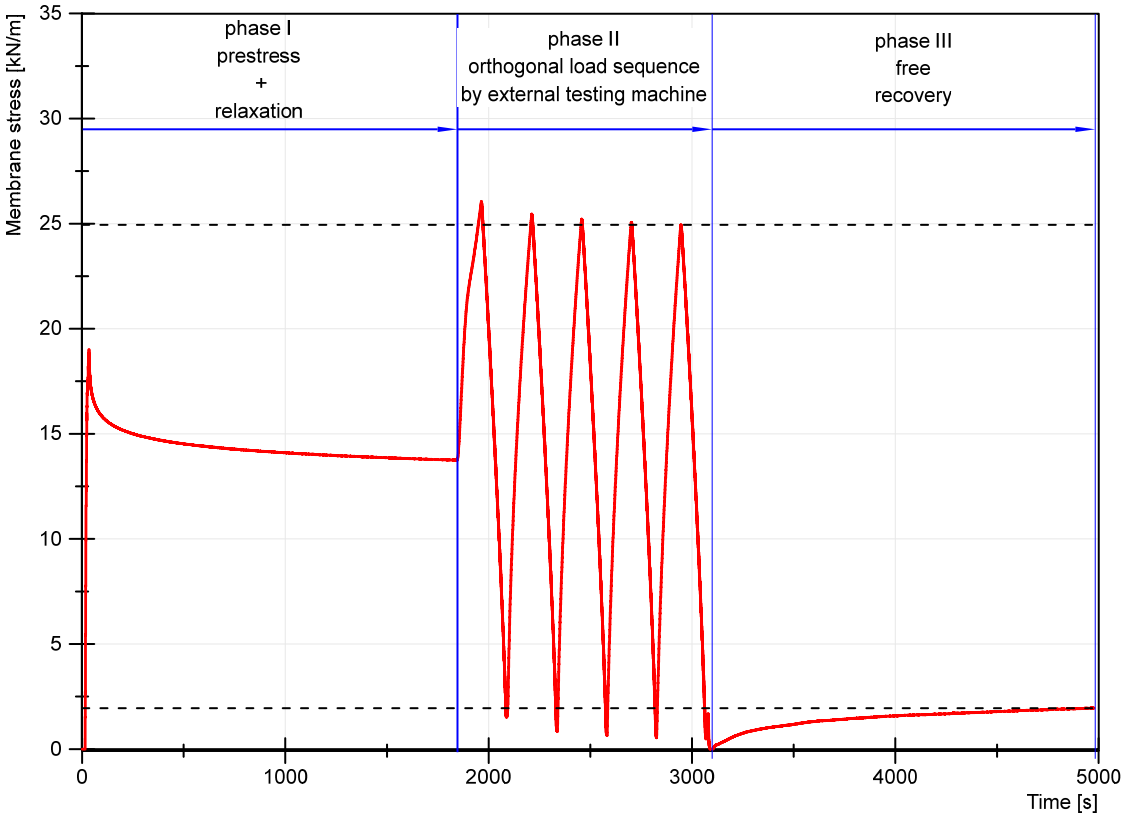

Figure 63 Membrane stress during the orthogonally loaded strip test in warp direction

A deviation from the previous tests is observed for the prestress. Although all conditions other than the recovery times are the same, and the same magnitude of prestress was measured at the beginning of the test and after relaxation, after five uninterrupted load cycles it settles at p = 2.0 kN/m at the end of the 30 minutes' free recovery in phase III and at p = 2.5 kN/m at the end of phase III when recovery times were considered. The omission of recovery times seems to reduce or at least slow the revertive creep process during free recovery.

For the fill strip the same magnitude of deflection and stress are recorded compared to the tests with recovery times: f_z = 93 mm and σ_f = 23.0 kN/m for initial loading and f_z = 96 mm and σ_f = 22.1 kN/m for the fifth load cycle, see Figure 64 and Figure 65. At p = 1.4 kN/m at the end of free recovery, the prestress is also of the same magnitude as for the test with recovery times, where it was p = 1.5 kN/m.

Overall, it can be stated for the experimental membrane strip structure that omitting recovery times has no impact on the stresses and deflections.

Table 7 provides a comparison of the experimental results with FE analysis results. The same numerical model was used as in the previous chapter. As the difference between both investigations – considering or omitting the recovery times – affects only the load cycles after the first, it is no surprise that the same quantities were found for the first load cycle. For the fifth load cycle a maximum stress difference of 8% and a maximum deflection difference of 9% for fill and 15% for warp is observed. Including also the findings of Table 6, it can be concluded that the numerical results can differ from the experimental results by approximately +-8%, with individual exceptions of up to 15%. No regularity is detected regarding the direction of the derivation, i. e. whether the simulation results in higher or lower values than the experimental measurement. It appears to be rather random. Moreover, the magnitude of difference is independent of which load cycle number is simulated.

It must be noted that for the numerical simulation of the tests without recovery times, higher tensile moduli had to be employed for the simulation of the fifth load cycle than for the simulation of the tests with recovery times, compare Table 7 and Table 6. This approach conforms with the findings in Chapters 6.2.2 and 6.2.3, which showed that omitting recovery times leads to a stiffer stress-strain response. The higher relative stiffness goes hand in hand with a lower prestress level. Combining both conditions in the numerical analysis leads to correct results.

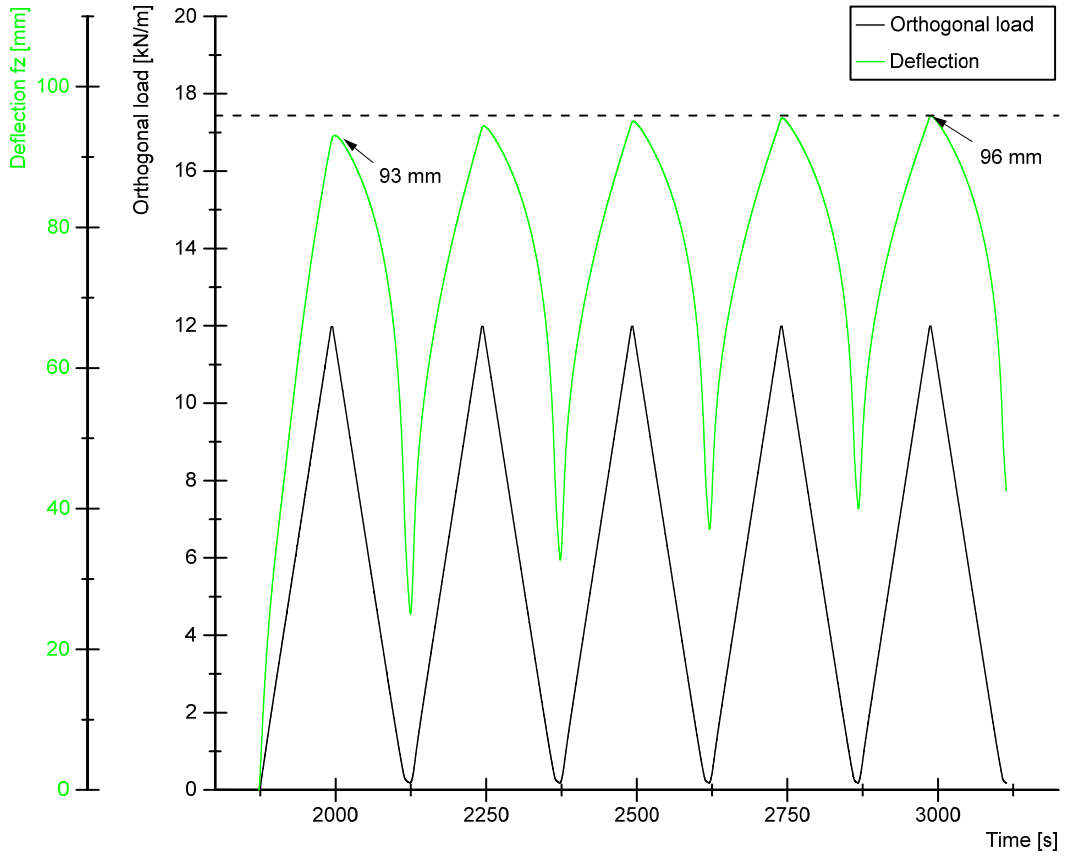

Figure 64 Orthogonal load sequence during phase II and measured deflection f_z for the membrane strip in fill direction

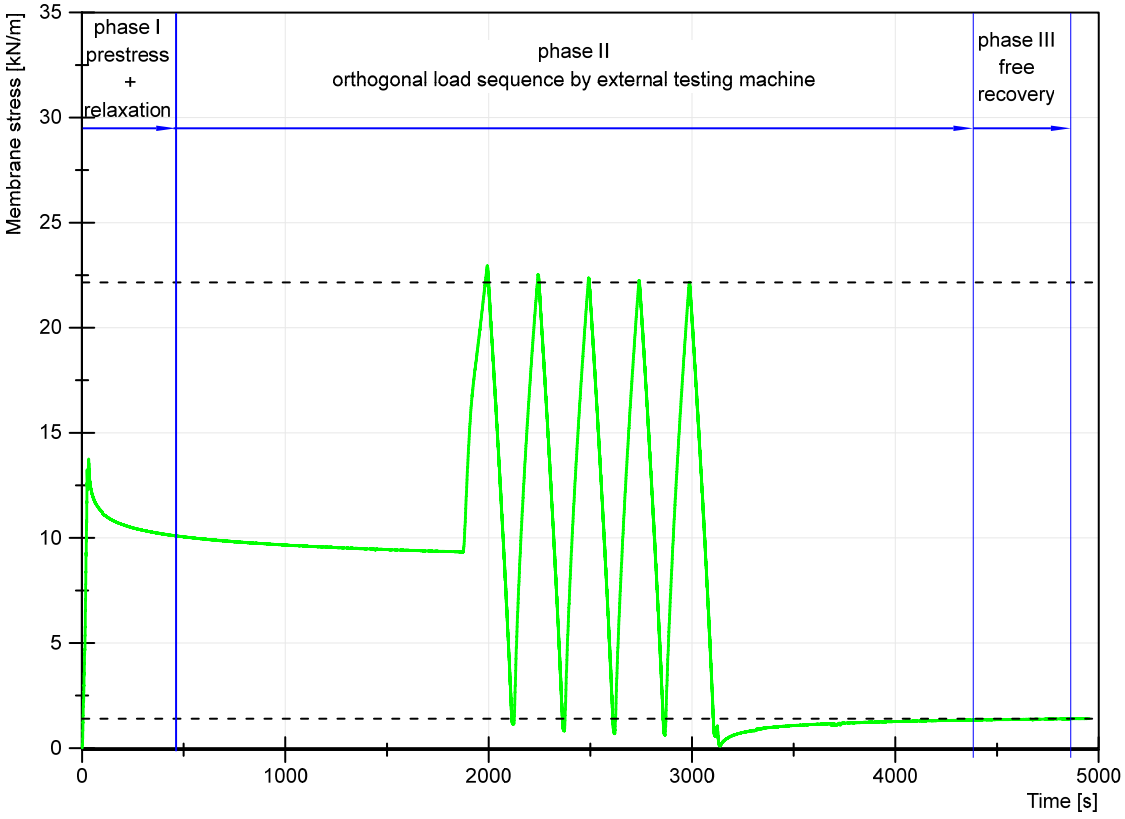

Figure 65 Membrane stress during the orthogonally loaded strip test in fill direction

Table 7 Comparison of experimental results of tests without recovery times with finite element analysis

Parameter/Load cycle number		1st load cycle	5th load cycle
Membrane strip in warp direction, l = 612 mm			
FE input	p [kN/m]	13.7	0.5
	E [kN/m]	362*	1056**
FE results	max f_z [mm]	76	69
	σ_w [kN/m]	24.6	27.1
Experimental results	max f_z [mm]	77	80
	σ_w [kN/m]	26.0	25.0
Membrane strip in fill direction, l = 634 mm			
FE input	p [kN/m]	9.3	0.6
	E [kN/m]	294***	572****
FE results	max f_z [mm]	91	88
	σ_f [kN/m]	21.1	22.1
Experimental results	max f_z [mm]	93	96
	σ_f [kN/m]	23.0	22.1

* determined as secant between 13.7 kN/m and 26.0 kN/m
** determined as secant between 0.5 kN/m and 25.0 kN/m
*** determined as secant between 9.3 kN/m and 23.0 kN/m
**** determined as secant between 0.6 kN/m and 22.1 kN/m

6.4 Conclusions

Experimental investigations were performed on the entire range of the most used coated woven fabrics in textile architecture: traditionally and biaxially prestressed PVC-coated polyester fabrics as well as PTFE-coated glass fibre fabrics. All typical material classes ranging overall from type II to type V were considered. Numerous uniaxial tensile tests with and without recovery times as well as hold times at maximum test stress level were conducted on the biaxial test rig in order to measure not only the tensile modulus but also the Poisson's ratio. Furthermore, a prestressed membrane strip test with an orthogonal load was designed and realised. This test simulates an *in situ* membrane structure, albeit only in one principal direction. The development of membrane stress, deflection and prestress level was studied in this test.

The uniaxial tensile tests clearly showed that a stable state of the fabric exists with a fixed strain corresponding to a defined stress level. The stable state can be assumed with sufficient accuracy to have been reached after five load cycles in one and the

same stress ratio for all investigated materials. The relative stiffness increases from the initial load cycle to the stable state load cycle. This effect originates in significantly varying starting strain at the beginning of a load cycle. Often, the change in relative stiffness decays significantly for load cycle numbers greater than three. This confirms results published by *Reinhardt*, see Chapter 3.3.2. Basically, many principal characteristics described by *Reinhardt* for a mesh fabric, see Chapters 3.3.2 and 3.3.3, are confirmed for common coated fabrics in general through the tests conducted.

Both tensile moduli and Poisson's ratios vary with the evaluated stress interval. However, this behaviour appears to be stronger in the first load cycles where the stress-strain paths show a higher degree of nonlinearity.

Glass-PTFE fabrics proved to generally show greater transverse strain than PES-PVC fabrics, largely independently of the producer or specific production measures. This confirms published test data, see e. g. [Me95], [GB08], [BGJ12], where all tested glass-PTFE materials from different producers show considerably higher Poisson's ratios than the tested PES-PVC materials almost throughout. One reason might be the higher yarn crimp as explained in Chapter 3.2.3. The Poisson's ratio for PES-PVC is normally of moderate magnitude up to $\nu = 0.5$, but it can be much greater at up to $\nu = 1.15$ in individual cases, particularly for high strength materials type IV and V. The maximum measured Poisson's ratio for glass-PTFE was $\nu = 2.39$. Poisson's ratio increases with increasing load cycle number.

When glass-PTFE is directly compared to PES-PVC of similar tensile strength, it is shown to be stiffer over the full working stress range, taken here to be the range between zero stress and ¼ of the tensile strength. However, it shows identical or even less stiffness for major stress ranges up to approximately 85% of the working stress range, particularly under the initial load. The reason for this effect is that PES-PVC exhibits a softening behaviour in the upper band of working stress during loading, whereas glass-PTFE exhibits a stiffening behaviour.

From tests with long-term loads it followed that long-term loading like snow can be modelled by means of uniaxial creep coefficients. They can be determined independently in warp and fill according to EN ISO 899-1 and subsequently applied to the tensile moduli in both directions. The derivation of creep coefficients k_{def} as according to Eurocode 5 was proposed. The tensile moduli can be modified for long-term loading with the creep coefficients.

Tests with an alternation of the principal loading direction revealed that woven fabric switches between two boundary strain states within a closed circuit of strain. This mechanism is due to a reset of the yarn configuration each time the load direction changes. As anticlastic structures are characterised by an alternation of the load direction, it follows that they cannot have one constant level of residual strain and thus no constant prestress level. In fact, the prestress level is expected to change

every time the direction of the external loads changes. Two boundary stiffness states are linked to this mechanism.

In civil engineering, the occurrence of the maximum design load is usually not accompanied by the occurrence of a second or further load cycle of the same order of magnitude immediately before or after. This is particularly true for fabric structures which are normally only loaded by snow and wind. There is always enough time for fabric recovery between two peak loads of significant magnitude. Bearing this in mind, the uniaxial tensile tests were conducted with and without recovery times in order to detect differences in the stress-strain behaviour. It was observed that omitting recovery times has no influence on the pair of corresponding values ($\max \sigma \mid \varepsilon$), particularly not in the stable state of the fabric. But as revertive creep is suppressed, the relative stiffness and Poisson's ratio are artificially increased. Artificially high elastic constants are correlated to a high residual strain and correspondingly to a low prestress level in a membrane structure.

The important interrelation between prestress level and stiffness parameters corresponding to various load cycles was also clearly indicated by the results of tests with prestressed and orthogonally loaded PES-PVC fabric strips. Low initial fabric stiffness and high initial prestress level balance each other out. The same applies for the higher stable-state stiffness and the corresponding lower prestress level. Overall, membrane stress and deflection are of similar magnitude for every load cycle, whereby the highest stress tends to be found in the initial load cycle and the highest deflection in the stable state of the fabric after five load cycles.

Accompanying numerical simulations of the strip tests demonstrated that structural analysis can essentially be based on every load cycle as long as corresponding stiffness parameters and prestress level are used as input data. Stiffness parameters and prestress must be seen in context and not detached from each other.

At first glance, two boundary structural states are available for reasonable modelling: (1) initial loading after installation with high initial prestress and low stiffness; or (2) the stable state of the structure, corresponding to the stable state of the fabric with nominal prestress and high stiffness. At second glance, it becomes apparent that membrane structure analysis is always based on the form-found geometry. This in turn corresponds to the nominal prestress level. From this interrelation it follows that stiffness parameters of the stable state of the fabric should be used.

Stiffness parameters determined from a test protocol that omits recovery times – and thus are artificially high – would have to be combined with a prestress level lower than the nominal one.

Hence, in order to enable the use of the nominal prestress in the structural analysis, an inter-coordinated biaxial test protocol should include a recovery time at least prior to the load sequence to be evaluated. This helps to prevent artificially high elastic

constants, which in combination with the “high” nominal prestress level would lead to distorted modelling of the stiffness of the structure. This distorted modelling would be safe-sided in terms of membrane stress but unsafe in terms of deflections.

Basing the structural analysis on the enduring nominal prestress level has a further advantage: in the corresponding stable state of the fabric, the material behaviour can be handled as elastic and the stress-strain paths have often lost much of their nonlinearity. In this state, application of elastic constants is suitable. It can therefore be recommended to derive elastic constants not from the initial load cycle but from a later load cycle in which the stiffness properties and the prestress level have settled.

The fact that the maximum stress occurs on account of the first occurrence of the design load is not problematic. This is because a fabric structure has “hidden safety” at the beginning of the lifetime due to strength reduction factors which are incorporated in the design strength to account for reductions in physical strength over a long period of time and under long-term loads and environmental impacts, see [SaP15].

7 Analysis of established evaluation procedures for elastic constants

7.1 General

Elastic constants gained from uniaxial experimental tests are not sufficient to model other stress ratios than the uniaxial, for instance a warp:fill stress ratio of 1:1. The stiffness parameters of woven fabrics basically depend on the applied stress ratio. This shall be demonstrated by means of an example: for a glass-PTFE fabric type II, elastic constants are determined in a “quasi stable state” during the third load cycle by conducting a uniaxial test without recovery times in warp and fill direction, as demonstrated in Chapter 6.2.3. The resulting set of elastic constants is subsequently used to model a stress ratio of 1:1, also measured in a biaxial test without recovery times in the third load cycle. The set of elastic constants from uniaxial testing is given in Table 8. Figure 66 shows the measured stress-strain paths from 1:1 testing and compares them with the calculated straight stress-strain lines that result when the uniaxial elastic constants are inserted in eq. (4.35). The illustration proves that the measured paths do not fit at all. The very large Poisson’s ratios in particular are responsible for much smaller calculated strain values, as a result of which the calculated stress-strain lines rotate anticlockwise about the origin of co-ordinates, far away from their corresponding measured paths.

Furthermore, uniaxially determined elastic constants usually do not observe the mechanical constraints discussed in detail in Chapter 4, for instance the reciprocal relationship eq. (4.9) or the magnitude of the Poisson’s ratios eq. (4.39). This is also the case for the example values given in Table 8. Overall, uniaxially determined elastic constants might be appropriate for detecting principles of material behaviour or comparing materials, but they prove definitely insufficient for design purposes.

Table 8 Elastic constants for a glass-PTFE fabric type II gained from separate uniaxial tensile tests in warp and fill direction

Third loading			
Uniaxial warp stressing		**Uniaxial fill stressing**	
E_x [kN/m]	**ν_{yx} [-]**	**E_y [kN/m]**	**ν_{xy} [-]**
2166	1.90	1143	2.28

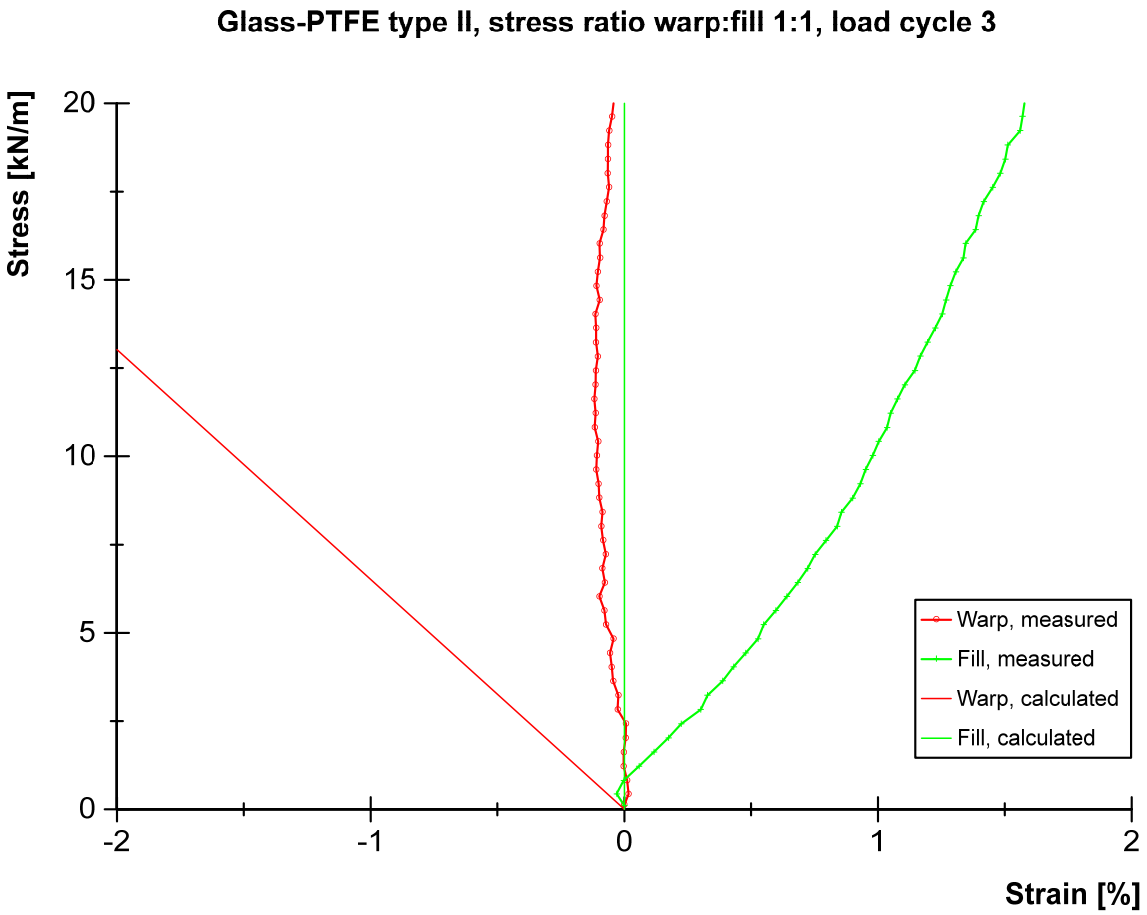

Figure 66 Comparison of measured stress-strain paths of a stress ratio 1:1, load cycle 3, with calculated stress-strain lines resulting from elastic constants gained from uniaxial tests

It is against this background that worldwide research and design aim to approximate elastic constants for specific biaxial stress ratios. There is an enormous variety of proposals put forward for biaxial testing and the correlated determination of elastic constants – although only linear approximations of the stress-strain paths are considered in the present work. Various biaxial test and evaluation procedures have been developed around the world in the last four decades. Several have been published, others are confidential in-house procedures in design offices. Only a few have the character of a standardised procedure.

An overview of the variety of work concerning biaxial testing and the determination of stiffness parameters is provided here, before four procedures are analysed in depth in the following chapters.

The interest in biaxial testing of fabrics for use in architectural membrane structures emerged in the late nineteen sixties and early seventies, see e. g. [Fr67], [Ja70], [Sk71], [Lo71], [BLL73], [Re75], [Me78]. Initially, the investigations primarily related to air-supported structures but later more and more to mechanically prestressed surface structures. The latter increasingly came to replace cable-based structures in which the membrane was only the building envelope instead of the structural element.

In their early work *Rehm & Münsch* [RM79] as well as later *Münsch & Reinhardt* [MR95] state that the Poisson's ratios determined from uniaxial tests with a measurement of the transverse strains do not apply for biaxial stress states. They determine elastic constants from the four measured paths of warp:fill stress ratio 1:1 combined with either 2:1 or 5:1. A new test specimen is used for every stress ratio. Only short-term loading is considered. Evaluation is already linked to the constitutive model described in Chapter 4, i. e. two tensile moduli and two Poisson's ratios are determined and the reciprocal relationship eq. (4.9) is satisfied. The elastic constants are determined for the best possible approximation of secants between zero stress and maximum test stress. The first and the 20th load cycles were evaluated. No prestress is considered, either in the load profile or in the evaluation stress range. The authors give a stress ratio range of $5 \geq \sigma_K/\sigma_S \geq 0.7$ in which the presented elastic constants produce a good approximation to the measured stress-strain paths. Differences between measured and calculated strain were reported to be up to 0.2% strain. Apparently, the originally investigated "air hall fabric" [RM79] was supposed only to apply to pneumatic structures. The given scope of validity poses no significant limitation for such structures.

Minami and Motobayashi [MM84] follow a similar approach in terms of the biaxial test procedure. They also use a new test specimen for every stress ratio they examine. Experimental investigations are based on five stress ratios: 1:1, 2:1, 1:2 and the uniaxial stress ratios 1:0 and 0:1. Up to three load cycles are conducted. The determination of elastic constants is also linked to the orthotropic linear-elastic constitutive model. In contrast to *Rehm & Münsch*, they attempt to approximate secants between zero stress and 10 % of the tensile strength – although the maximum test stress varies from 15 % to 32 % of the tensile strength. They use the Least Squares Method, minimising the stress error to determine one "best fit" set of constants for one set of stress-strain paths from the five stress ratios: one set for the first load and one set for the third. Their work later strongly influenced the evaluation procedures of the Japanese standard MSAJ/M-02-1995 and the biaxial test procedures upon which the evaluation procedure of the US standard ASCE-SEI 55-10 is based.

In this context it must be mentioned that using a new test specimen and performing only one load cycle would involve a large amount of constructional stretch in the strain measurement. The measured stress-strain paths are not those which characterise the stiffness behaviour of the material in the prestressed structure. Such elastic constants underestimate the actual material stiffness. As stated in Chapter 6, it is more effective to determine elastic constants for the stable state of the fabric and use these values combined with the nominal prestress in the structural analysis.

Other publications mainly address the biaxial test procedure without defining how to evaluate the recorded test data. A summarised analysis of three different biaxial test

protocols can be found in [GL11]: the test protocol of the Japanese test standard MSAJ/M-02-1995 [Me95], a test protocol proposed by *Bridgens et al.* [BGB04] and one used at the Eidgenössische Materialprüfanstalt (EMPA), Switzerland. The biaxial test protocol of the Japanese standard is discussed in depth in the following chapter. The test protocol presented by *Bridgens et al.* consists of three sections intended to simulate an *in situ* fabric. First, prestress with a magnitude of typical nominal prestress is applied for 17 hours. Second, several conditioning cycles are implemented with high stress and different stress ratios. The aim of both procedures is to remove initial creep and put the fabric in the same condition as after exposure to a load. Subsequently, “radial” stress paths are applied with maximum stress of up to 25 % of the tensile strength. “Radial” stresses refers to different warp and fill stress paths starting from the warp and fill prestress level “in all directions”. This procedure includes typical stress ratios such as 1:1, 2:1 etc. Furthermore, it also includes negative stress increments such as may occur in anticlastic structures in the supporting direction. This procedure covers the possible structural behaviour of all structural forms. A disadvantage is that each stress increment ratio is only scheduled once. Even though the test takes an impractically long time, approximately 24 hours, mainly due to the very long initial prestress hold time. Overall, it consists of some very expedient principles such as considering prestress and applying “radial” stress paths.

The biaxial test protocol used at EMPA is an extension and variation of that presented in the TensiNet European Design Guide for Tensile Surface Structures [BBN04], which is also discussed in depth in the following chapters. The originally proposed stress ratios are varied slightly, and additional stress ratios are investigated. This test protocol is also based on a certain prestress level, a feature very well-suited to prestressed membrane structures.

A direct comparison of the three analysed test protocols in [GL11] reveals considerable differences regarding the recorded stress-strain paths. In order to cover the full possible range of response, *Galliot & Luchsinger* propose a biaxial procedure that aims to give a response domain including the upper and lower limits of the material stiffness. That also means the upper and lower limits for the stiffness parameters for one and the same design situation. This appears to be dispensable provided that a decisive condition is defined in the scope of the static verification, see Chapter 6: the application of nominal prestress, combined with the stable state of the fabric, which in turn simply requires repetition of loads during the test.

Galliot & Luchsinger [GL09] additionally introduce a constitutive model with a stress ratio-dependency of the tensile moduli. Their proposal includes Poisson’s ratios but does not mention how this value should be determined. They propose testing quite a high number of stress ratios (11 in the published example) in order to enable a smooth adjustment of the tensile moduli. Details regarding the performance of biaxial

tests can be taken from the EMPA test protocol in [GL11]. Finally, this constitutive model results in a simple non-linear constitutive model that is nevertheless based on tensile moduli and Poisson's ratios. Such an extension of the linear-elastic constitutive model is capable of modelling all different stress ratios that can possibly occur over a membrane surface.

Ambroziak & Kłosowski [AK14a], [AK14b] establish a step-by-step multilinear approximation of measured stress-strain paths using the tensile modulus but disregarding Poisson's ratio. Investigations are made for initial loading [AK14b] and cyclic loading [AK14a]. It is important to note here that disregarding Poisson's ratio makes it impossible to describe transverse strain in cases where it is negative. In order to utilise step-by-step tensile moduli for specific strain intervals, a user-subroutine in the FEM software is required. In contrast to many other authors, *Ambroziak & Kłosowski* load the specimens until rupture and evaluate the entire stress-strain paths. This is not necessary when the stiffness parameter evaluation is related to satic verification.

Four published procedures that aim to determine design elastic constants for architectural fabrics for use in the constitutive equations presented in Chapter 4 are analysed in detail in the following chapters. These four combine a specified test protocol with a defined evaluation procedure:

- the Japanese standard MSAJ/M-02-1995 [Me95], abbreviated to the "MSAJ standard" hereafter,
- the TensiNet European Design Guide for Tensile Surface Structures [BBN04], abbreviated to the "TensiNet Design Guide" hereafter,
- the French Guideline "Recommandations pour la conception, la confection et la mise en oeuvre des ouvrages permanents de couverture textile" [So09], abbreviated to the "French Recommendations" hereafter, and
- the US-American design standard ASCE-SEI 55-10 [Am10],

sorted chronologically by the date of publication of the latest version. The analysis and discussion of the biaxial test and evaluation procedures according to MSAJ/M-02-1995 and the TensiNet Design Guide were previously published in [USS11], [US13], [USS15a] and [USS15b], amongst others, which are reproduced in part here. Laboratory experience shows that MSAJ biaxial tests are the most in demand today. For this reason and because of the fact that it is a precisely standardised method which allows for objective material comparisons, special attention is paid to this method in the scope of this work.

7.2 Determination of elastic constants according to MSAJ/M-02-1995

7.2.1 General

The Japanese standard MSAJ/M-02-1995 “Testing method for elastic constants of membrane materials” is published by the Membrane Structures Association of Japan (MSAJ). It consists of the test standard itself and an inherent elaborate commentary. The standard part provides precise definitions for the biaxial test procedure, the specimen shape and preparation, testing conditions etc. The detailed provisions enable reproducible tests independently of the executing laboratory and could thus serve as an appropriate basis for objective inter-laboratory material comparisons. Three different membrane materials are provided for: PTFE-coated glass fibre fabrics, PVC-coated glass fibre fabrics and PVC-coated “synthetic fibre” fabrics, strictly speaking all with plain weave and thickness $t \leq 0.5$ mm. Apparently, the term “synthetic fibres” here means organic (polymeric) fibres to distinguish them from glass fibres, which are actually anorganic synthetics.

7.2.2 Biaxial test protocol

"The MSAJ standard defines a balanced test protocol, which covers all stress ratios (warp:fill) that can appear in membrane structures independent of their form. The full test set consists of five characteristic stress ratios (warp:fill) that are processed as follows: 1:1, 2:1 and 1:2, followed by 1:0 and 0:1, see Figure 67. The symmetrical biaxial stress ratio 1:1 is characteristic of quadratic plane membranes under external loads; the uniaxial stress ratios 1:0 and 0:1 are characteristic of anticlastic structures under snow and wind suction loads. Stress ratios 2:1 and 1:2 are characteristic of synclastic structures, such as air-supported domes, cushions or inflatable beams, as well as rectangular structures with little or no curvature.

For biaxial stress ratios 2:1 and 1:2 and uniaxial stress ratios 1:0 and 0:1, only one load cycle is specified. Between these stress ratios, three 1:1 load cycles are scheduled.

The maximum test load is specified as ¼ of the nominal 'tensile strength' f_t, complying with a commonly used global stress factor of four. Normally, the tensile strengths in the warp and fill directions differ from each other. However, in this case, the MSAJ standard commentary recommends only one maximum stress level for biaxial tests; this load is ¼ of the lower strength $f_{t,min}$." [USS15a]

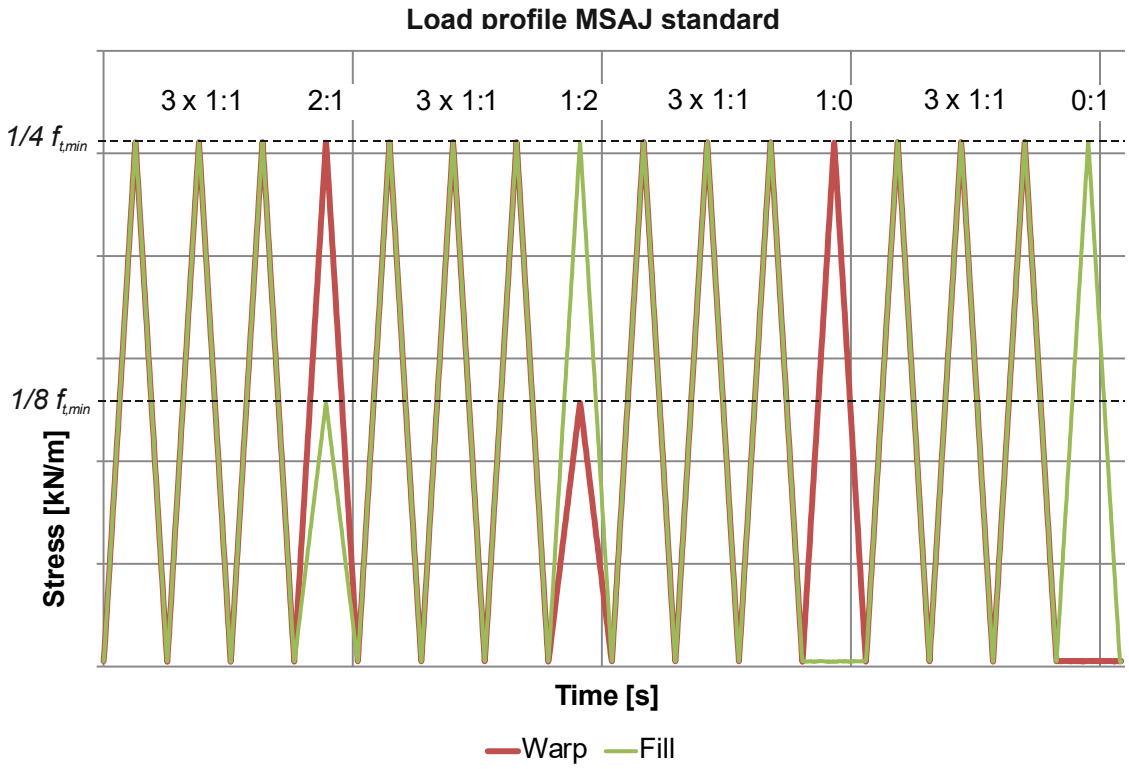

Figure 67 Load profile for biaxial tests according to MSAJ/M-02-1995 showing the five stress ratios 1:1, 2:1, 1:2, 1:0 and 0:1 [USS15a]

The stress-strain behaviour is basically dependent on the previous load history. The three initial 1:1 stress ratio cycles as well as all intermediate 1:1 stress ratio cycles condition the material before a 'new' stress ratio is imposed. The aim of this measure is to avoid the requirement for a new test specimen for each stress ratio. In fact, however, repetition cycles for the four stress ratios 2:1, 1:2, 1:0 and 0:1 would have the same effect, see Chapter 6.

7.2.3 Evaluation procedures

Based on the results of a MSAJ biaxial test, ten stress-strain paths can be extracted, see Figure 68. These paths are the warp and fill paths for the five stress ratios. With regard to the paths of the stress ratio 1:1, those of the third load cycle at the beginning of the test are extracted for the present work. "The MSAJ commentary recommends that the loading paths be extracted between the defined minimum stress level and the maximum stress level. The minimum stress level is fixed depending on the test material: 1 kN/m for 'synthetic' fibre fabrics (meaning organic, see above) and 2 kN/m for glass fibre fabrics.

The MSAJ standard commentary provides elaborate descriptions of the evaluation procedures, including examples. Because it is a commentary, it is more of a recommendation than a directive.

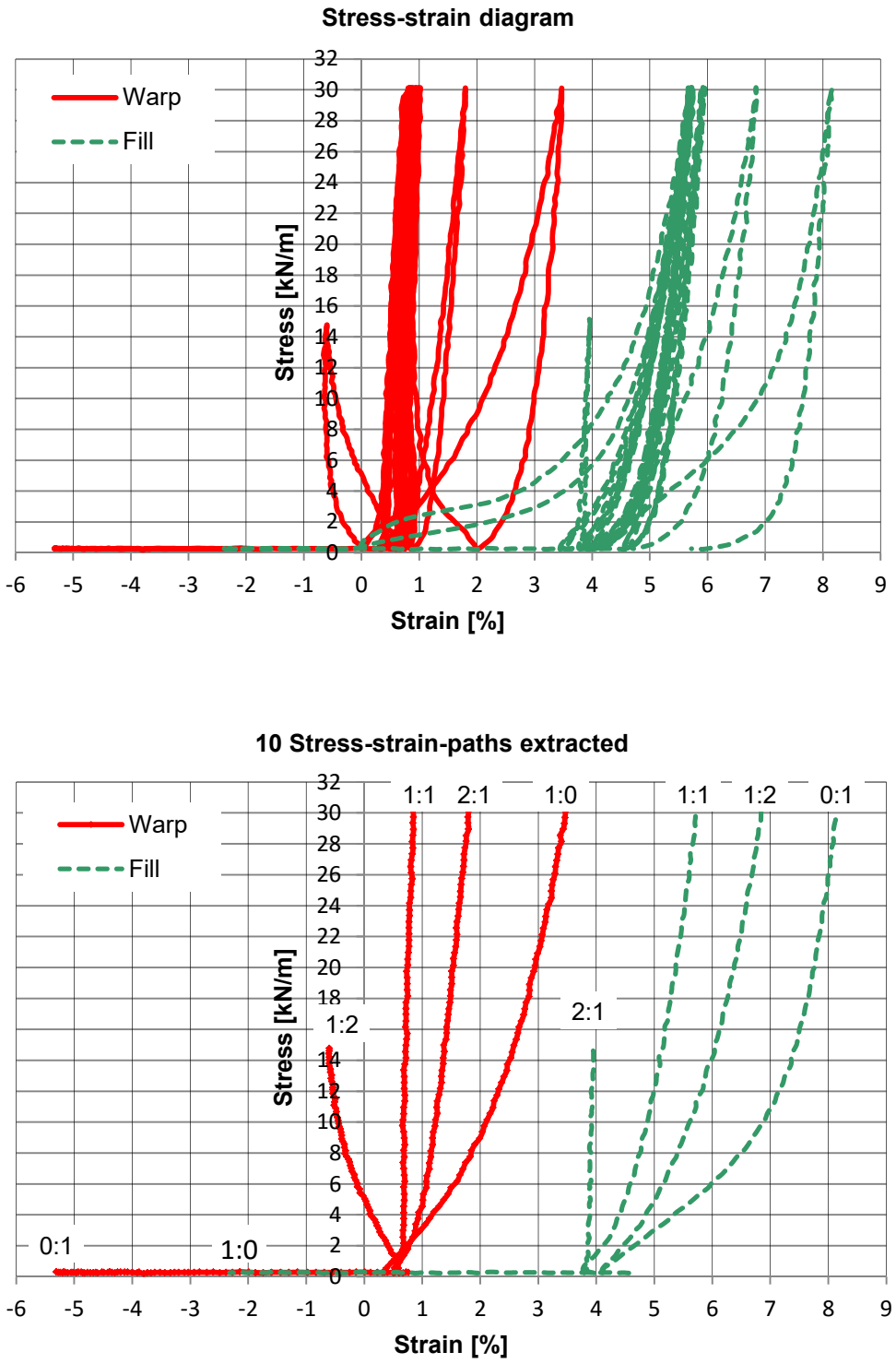

Figure 68 Stress-strain diagram as a result of a MSAJ biaxial test on a glass-PTFE material (top), ten stress-strain paths (warp/fill at five stress ratios), as extracted from the stress-strain diagram (below) [USS15b]

The goal of all the proposed evaluation procedures is to determine one single 'best fit' set of elastic constants. Three different evaluation procedures are proposed for a full linear evaluation:

- the Least Squares Method, which minimises the strain errors,

- the Least Squares Method, which minimises the stress errors, and,
- the minimax method, which minimises the maximum error.” [USS15a]

Note that for all procedures the MSAJ commentary recommends evaluating not only a specific part of the stress-strain paths, e. g. a stress level defined by the design engineer, but the complete test data. Furthermore, a multilinear approximation is defined as a fourth method.

“One noteworthy feature of the MSAJ evaluation process is that not all measured stress-strain paths are evaluated. Only eight out of ten possible paths are considered; the zero stress paths, fill direction at 1:0 and warp direction at 0:1, are omitted. The MSAJ commentary states two reasons for excluding the zero stress paths: first, an accurate strain measurement is difficult to achieve for the low stress range, and second, the test results are difficult to repeat in the low stress range [Me95].” [USS15a] Quite the contrary, laboratory experience has shown repeatability with high precision. Very low deviations of the zero stress paths are reported for PES-PVC in [USS15a] and for glass-PTFE by *Schmidt* [Sc12]. “The test results showed a high repeatability that was independent of the stress range. From that point of view, zero stress paths should not be generally excluded from an evaluation. Instead, the decision to consider them or not should be made on a case-by-case basis” [USS15a], see explanations in Chapter 7.2.5.

In the context of the MSAJ determination of elastic constants the term "fictitious elastic constants" has been introduced: “The sets of elastic constants have to be treated as ‘fictitious’ elastic constants because firstly, they shall estimate the non-linear load-deformation behaviour of the material and secondly, they shall envelop all load combinations in warp and fill direction.” [USS11]

“The determination of the fictitious elastic constants from the stress-strain-paths has to be performed stepwise in a double step correlation analysis. In the first step each curved loading path has to be substituted by a straight line. In the second step the slopes of the straight lines obtained in the first step have to be modified in such a way that they satisfy the equations of the assumed linear elastic plane stress behaviour and describe all experimental loading paths for all five stress ratios optimally by just one set of four fictitious constants. The commentary of the MSAJ-Standard recommends to use eight of the ten measured loading paths omitting the two zero stress paths, although, four paths would be sufficient to determine a set of four fictitious elastic constants.” [USS11]

From the different evaluation methods mentioned above only the Least Squares Method (LSM) is considered here. “The scope is to minimise the sum of squares of errors in a certain subject interval [a, b] between a continuous function f(x) and an approximation equation y(x):

$$S = \int_a^b \left[f(x) - y(x)\right]^2 dx \rightarrow \min. \tag{7.1}$$

The errors can either be defined as the vertical differences (stress errors S_σ) or the horizontal differences (strain errors S_ε). For the determination of the elastic constants this means that either the stress term or the strain term can be minimised: $S_\sigma \rightarrow$ min or $S_\varepsilon \rightarrow$ min. For clarification see Figure 69 (a) and (b), each showing three exemplary errors – stress and strain, respectively – between an experimental stress-strain path and an arbitrary line. The commentary of MSAJ/M-02-1995 recommends the application of various methods to determine the elastic constants and to use the most satisfactory combination of constants. It has not to be noted here, that this procedure does not fit with a ‘standardised procedure’ and will lead to variable values depending on the chosen procedure of the user, too.

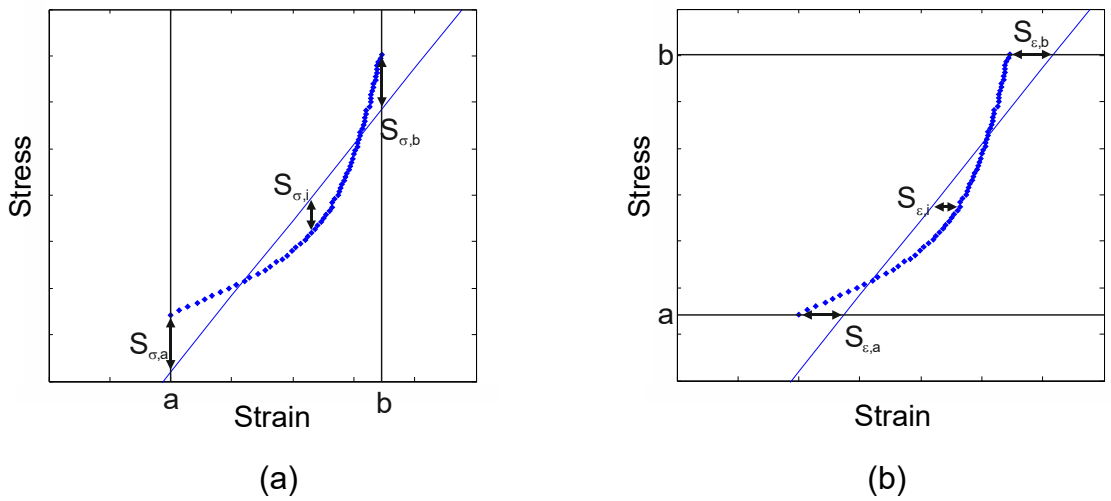

Figure 69 (a) Vertical errors calculated in order to minimise the stress term, (b) horizontal errors calculated in order to minimise the strain term [USS11]

In the design process for a membrane structure, the residual strains are taken into account in the process of compensation. This means that the membrane material is shortened by the value of the residual strains before installation. Usually, the residual strains are not included in the static calculation of a membrane structure. Therefore, it is reasonable to remove the residual strains from the test data for the determination of the elastic constants.” [USS11] This is done according to MSAJ/M-02-1995 by extracting the loading paths between the defined minimum stress level mentioned above and the maximum stress level.

7.2.4 Programmed routine for the determination of elastic constants

“For the determination of the fictitious elastic constants from test data a correlation analysis routine was programmed by using the commercial software MATLAB [ML14]. The basis of the routine is the calculation of regression lines using the Least Squares Method as proposed in the commentary of MSAJ/M-02-1995. A regression line in a stress-strain-diagram follows the linear equation (7.2), in which σ is the

stress, m is the slope, ε is the strain and b is the intersection point of the regression line with the stress-axis at zero strain:

$$\sigma = m \cdot \varepsilon + b. \tag{7.2}$$

In a first step, the routine evaluates the regression lines for all experimental stress-strain paths. Herewith, ten regression lines and their values for m and b are determined so that each of the ten stress-strain paths is fitted optimally. A regression line for an arbitrary experimental stress-strain path is shown in Figure 70. It is the nature of a regression line to reflect the slope of the path in a good manner. Usually, the regression line has another intersection point b with the stress-axis at zero strain than the test data path itself. To describe the stiffness of a linear-elastic material in a stress-strain-diagram the intersection point of the regression line is not important but the slope. To provide the typical illustration of a linear stress-strain behaviour, the intersection point of the regression line may be switched into the intersection point of the test data path for the plots, see Figure 70.

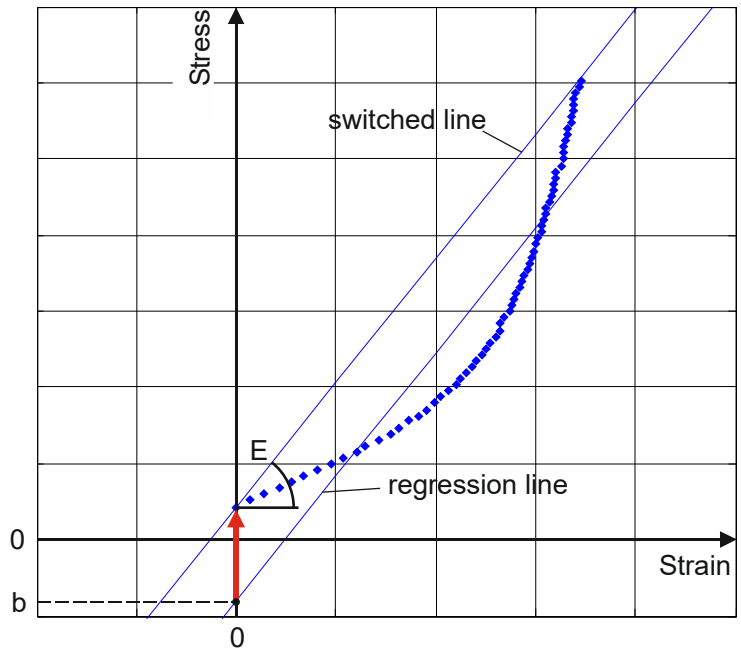

Figure 70 Regression and switched lines for a test data path [USS11]

In order to set up fictitious straight stress-strain-lines the programmed routine generates in a second step all possible combinations of the four fictitious elastic constants within limit values and increments established by the user. The increments may be quite rough in a first step of the analysis. They can be set to smaller values in an adjacent fine analysis, which will be conducted in the periphery of the best fit result of the rough analysis. In case that the reciprocal relationship, see eq. (4.9), is applied, only those combinations are taken into account that satisfy this constraint within arbitrary limits. In the investigations for this work the limits are set to

$$\frac{\nu_{yx}}{\nu_{xy}} - 0.005 < \frac{E_x}{E_y} < \frac{\nu_{yx}}{\nu_{xy}} + 0.005, \tag{7.3}$$

which seems to be precise enough.

In a third step, the strain values of the fictitious stress-strain lines are calculated for one arbitrary stress level at each stress ratio according to equation (4.37) inserting the generated constants. Knowing the strain values enables the evaluation of the slope of the fictitious stress-strain lines. Each fictitious stress-strain line j is related to the stress-strain path j of the test data. The slopes of the fictitious stress-strain lines j are calculated with equation (7.4) at the various stress ratios using arbitrary values for σ_x and σ_y. The only constraint is that the ratios of σ_x and σ_y satisfy the respective stress ratio.

$$m_j = \frac{\sigma_j}{\varepsilon_j} \tag{7.4}$$

For the further procedure the intersection point of each stress-strain line at the stress-axis at zero strain is set to the respective value b of the related regression line. This ensures that those stress-strain lines with a slope that approaches the slope of the respective regression lines lead to the ‘least squares’. In order to calculate the strain values for a fictitious stress-strain line j for each existent test data point i of the related stress-strain path j, equation (7.2) has to be transformed into equation (7.5)

$$\varepsilon_j = \frac{\sigma_j - b_j}{m_j}. \tag{7.5}$$

Finally, the sum of squared strain errors over all n test data points and m stress-strain paths considered in a determination of constants can be calculated using the following equation

$$S_\varepsilon = \sum_{j=1}^{m}\sum_{i=1}^{n}\left(\varepsilon_i - \bar{\varepsilon}_i\right)^2, \tag{7.5}$$

in which ε_i is the result of equation (7.5) and $\bar{\varepsilon}_i$ is the value of the related test data point, respectively. The value S_ε is the sum of all squared horizontal differences explained in Figure 69 (b). The optimum set of constants in the meaning of the commentary of MSAJ/M-02-1995 is the one combination of elastic constants with the minimum value S_ε.

The programmed routine was validated with the exemplary test data presented in the commentary of MSAJ/M-02-1995. Hereby, very similar results were achieved by using the Least Squares Method minimising the strain term compared to the presented ones in the commentary of MSAJ/M-02-1995.” [USS11]

Figure 71 shows an example of the development of the correlation measure S_ε during an initial rough correlation analysis of all combinations of elastic constants which are possible for the specified user defined range and increments. Test data evaluation for a glass-PTFE fabric type III is illustrated, including eight measured stress-strain paths ("original MSAJ"). It demonstrates that it is possible to locate the global minimum of S_ε within a cloud of correlation measures plotted against the combination number. Examining only the lower envelope of the cloud (see red curve) shows that the correlation measure S_ε initially decreases strongly; subsequently the decrease decays and the correlation measure S_ε tends towards the global minimum; afterwards it increases again.

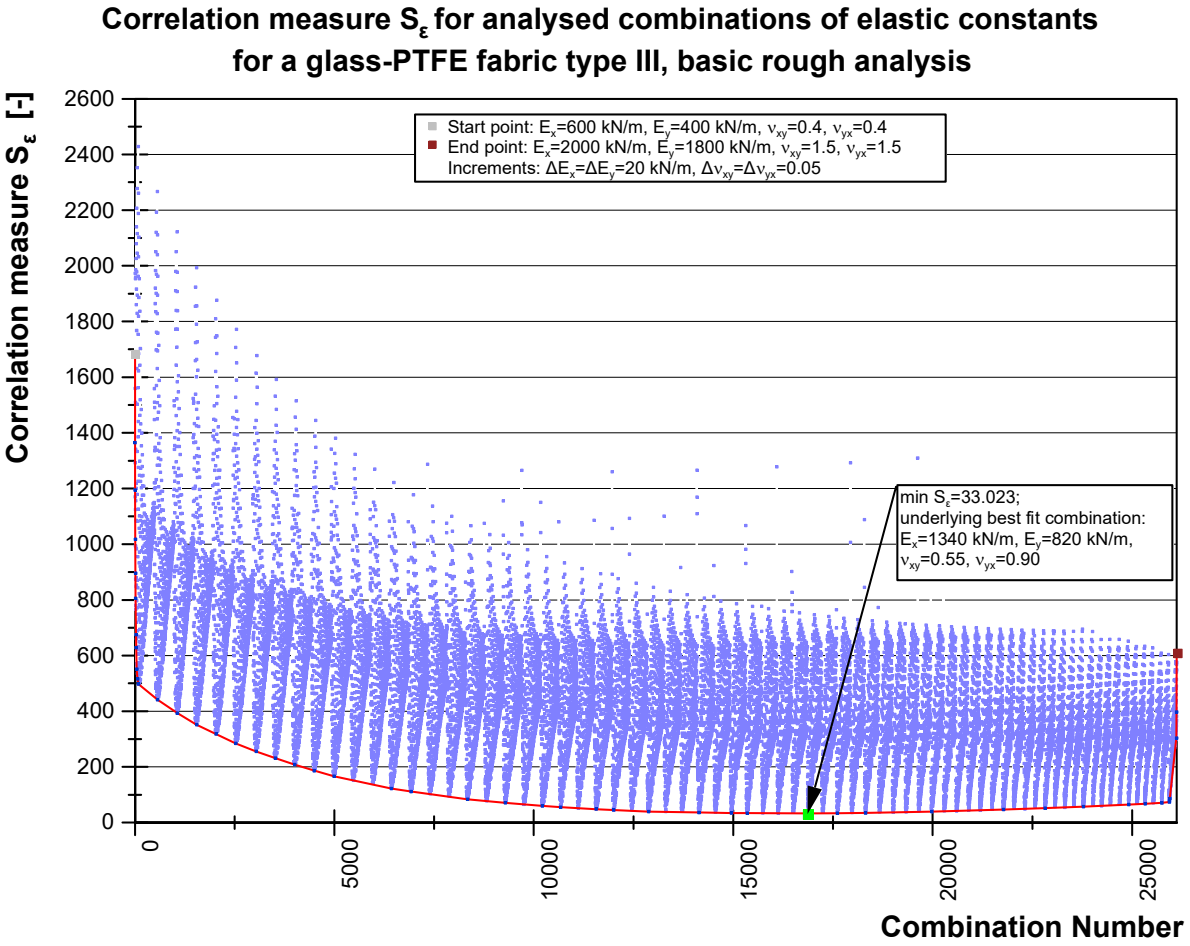

Figure 71 Development of the correlation measure plotted against the combination number

7.2.5 Example evaluation of test data

An example determination of fictitious elastic constants was conducted using a glass-PTFE fabric type III with a nominal tensile strength according to the producer's data sheet of 140/120 kN/m in warp/fill. The maximum test stress was thus derived as 120/4 = 30 kN/m. Working according to the original MSAJ evaluation, only eight recorded stress-strain paths were evaluated, omitting the zero stress paths at 1:0 and 0:1. The Least Squares Method minimising the strain term was used by means

of the programmed correlation analysis routine presented above. Figure 72 displays the resulting set of fictitious elastic constants as well as the correlation of the corresponding straight stress-strain lines to the measured stress-strain paths. Note that “the strains are plotted against the ‘major stress’, which is meant to be the larger one at each stress ratio. This form of plotting was chosen to avoid meaningless horizontal lines for the zero stress paths”. [USS11]

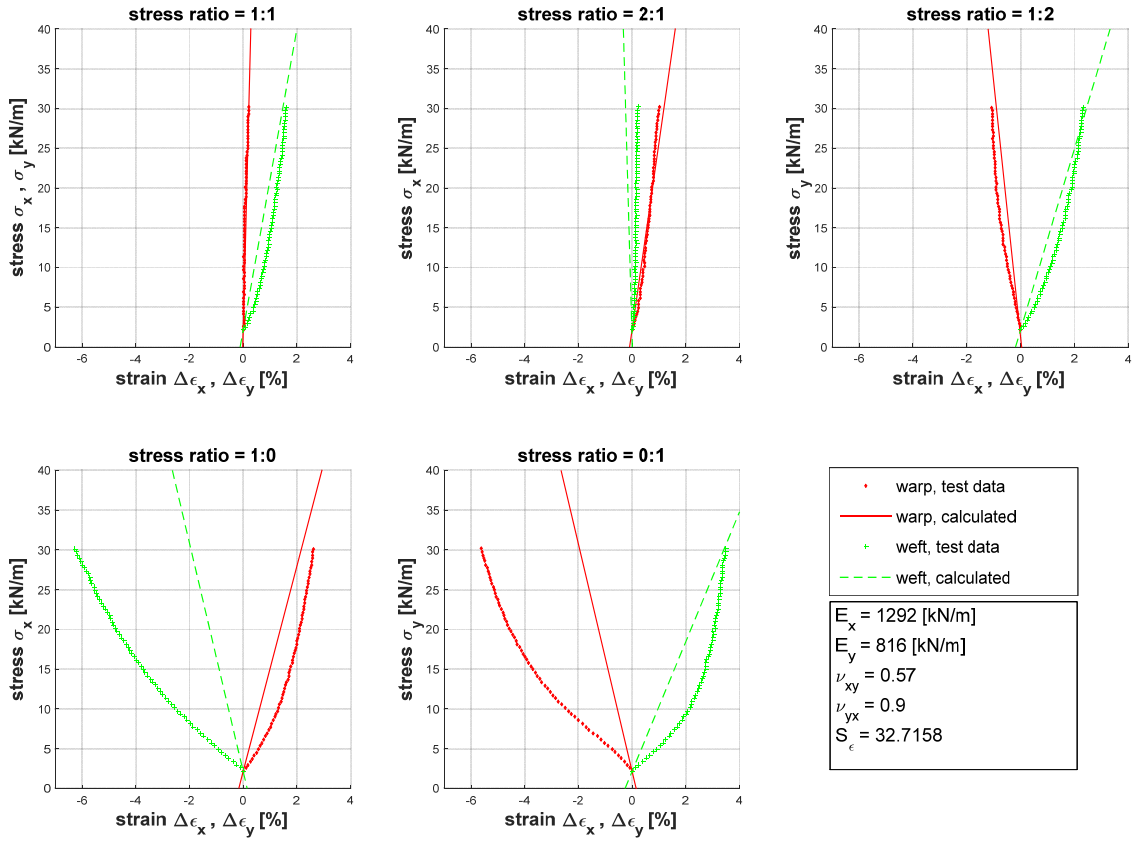

Figure 72 Comparison of measured stress-strain paths with calculated stress-strain lines corresponding to elastic constants resulting from test data of a glass-PTFE fabric type III according to MSAJ; evaluated according to original MSAJ specifications including 8 stress-strain paths

The assessment of the fit quality – apart from the procedure described in Chapter 7.2.4 – is not simple because an ad hoc understandable definition of the “ideal” straight line is missing. Intuitively one valuates the fit quality by comparing the strain at the tip of a measured stress-strain path to the respective calculated strain. That means to compare the resulting straight line to the secant in the stress interval 0-max σ. This method is used here for the discussion of the fit quality.

Concentrating on the maximum stress level at σ = 30 kN/m, most straight stress-strain lines fit their measured stress-strain paths quite well, see Figure 72. A poor fit is apparent for fill at stress ratio 2:1: while the measured strain is positive (elongation), the calculated strain is negative (contraction). An extremely bad fit is shown for the zero stress paths at 1:0 and 0:1. A maximum error of over 4 % strain occurs at σ = 30 kN/m! This is not surprising since they were omitted from the

evaluation. For the other stress-strain paths the fit quality is acceptable with a maximum error at σ = 30 kN/m of ca. 0.5 % strain.

The poor fit of the zero stress paths prompted *Bridgens & Gosling* [BG10] to open a discussion on possible modifications of the MSAJ evaluation procedure. Arguing reasonably that the zero stress paths contain relevant mechanical information regarding the load bearing behaviour of anticlastic structures, they investigated the effect of taking them into account. The result of this modification is illustrated in Figure 73. “It may be concluded by plausibility from this illustration that, in order to achieve an improved matching of the two calculated zero stress lines with their experimental counterparts, smaller theoretical values for ε_y at 1:0 and ε_x at 0:1 would be necessary. This would imply smaller values for the tensile moduli and higher values for the Poisson’s ratios. …The two calculated zero stress lines fit indeed somewhat better with their experimental counterparts, but for the ‘price’ of greater disagreement for all other calculated stress-strain lines.” [USS11] Compared to the original MSAJ determination, the worst error for the zero stress paths decreases to 2.5 % strain at maximum stress level, but for the other stress-strain paths it increases to 1.7 % strain. This is an unsatisfactory result.

Particularly for glass-PTFE fabrics that exhibit large transverse strain, it appears that the mechanical restriction eq (4.39) can often not be satisfied. This also applies to the given example, see Figure 73: the product of Poisson’s ratios is $\nu_{xy} \cdot \nu_{yx} = 0.83 \cdot 1.24 = 1.03 > 1$ and hence it is an unfeasible set for structural analysis. Overall, the evaluation of all ten stress-strain paths is not a practicable option, particularly not for glass-PTFE fabrics.

In order to enhance the fit, further modifications were first discussed in [USS11]. The principle of these modifications is to only evaluate a necessary number of stress-strain paths. For the determination of four elastic constants, four stress-strain paths are required (disregarding that only three of them are independent of each other). The selection of four out of the ten possible paths is based on the structural form (anticlastic or synclastic/plane) and – for anticlastic structures – on the load case. These modifications have been defined “to simulate reasonable decisions of rationally thinking structural design engineers with regard to their specific membrane structure. For a synclastic structure with almost identical membrane stresses in warp and fill direction under design loading, the determination might reasonably be conducted using the stress ratio 1:1, combined with either 2:1 or 1:2 (at least four stress-strain paths are needed for the determination of the unknowns). For an anticlastic structure with predominant warp stressing under the critical design load case, the stress ratios 2:1 and 1:0 might be reasonable, and for the opposite type of stressing the stress ratios 1:2 and 0:1.” [USS11] Results for these determination options are documented in Figure 74 to Figure 77. The determination options for synclastic structures lead to a good fit (maximum error at σ = 30 kN/m of 0.26 %

strain), whereas the determination options for anticlastic structures lead to an acceptable fit for the uniaxial stress ratios (maximum error at σ = 30 kN/m of ca. 0.6 % strain) and a slightly poorer fit in the biaxial stress ratios, see warp direction in 2:1 (Figure 76, error ca. 0.8 % strain) and fill direction in 1:2 (Figure 77, error ca. 1.0 % strain). Qualitatively the same can be observed for PES-PVC fabrics, as the example of a PES-PVC fabric type III in [USS15a] shows.

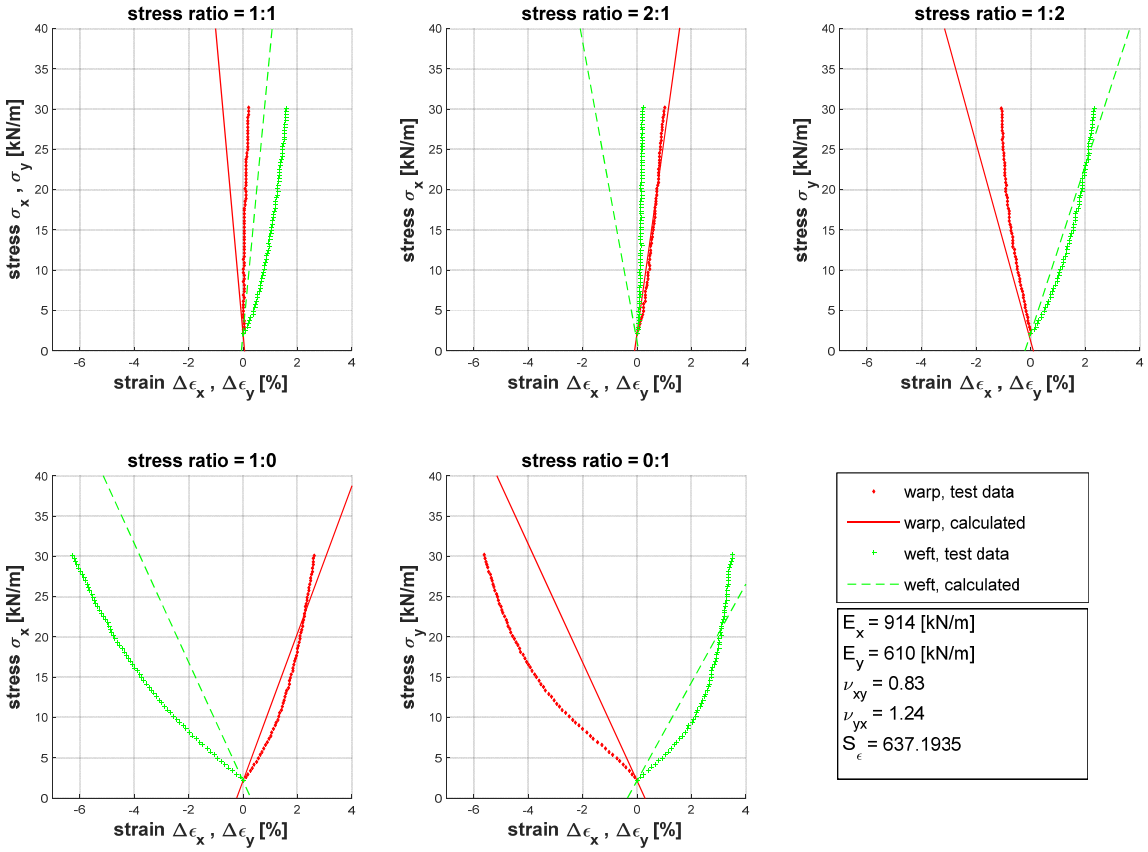

Figure 73 Comparison of measured stress-strain paths with calculated stress-strain lines corresponding to elastic constants resulting from test data of a glass-PTFE fabric type III according to MSAJ; evaluation includes all 10 stress-strain paths

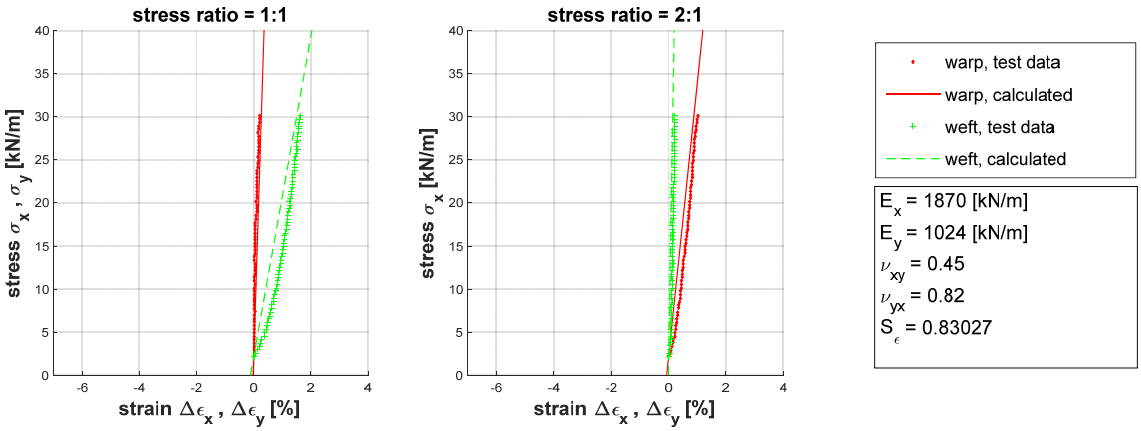

Figure 74 Comparison of measured stress-strain paths with calculated stress-strain lines corresponding to elastic constants resulting from test data of a glass-PTFE fabric type III according to MSAJ; evaluation includes 4 paths of stress ratios 1:1 and 2:1

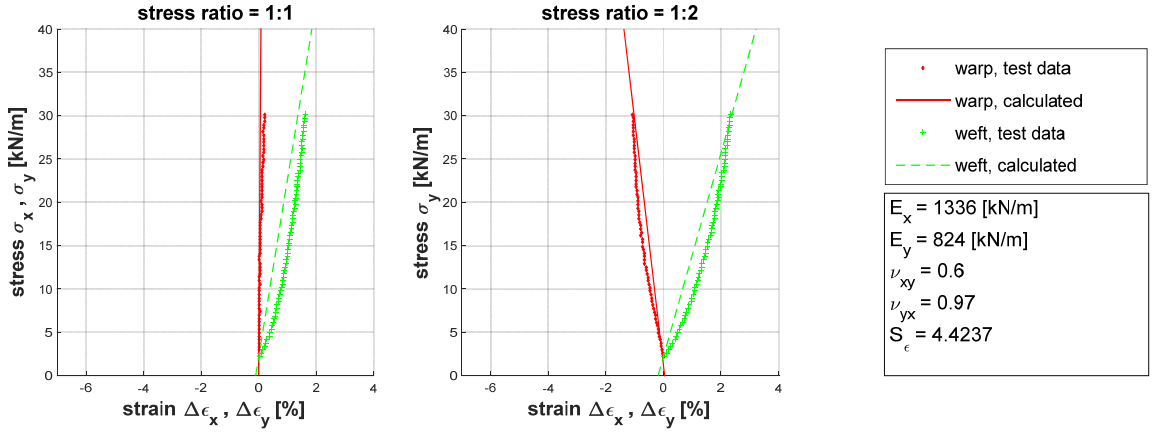

Figure 75 Comparison of measured stress-strain paths with calculated stress-strain lines corresponding to elastic constants resulting from test data of a glass-PTFE fabric type III according to MSAJ; evaluation includes 4 paths of stress ratios 1:1 and 1:2

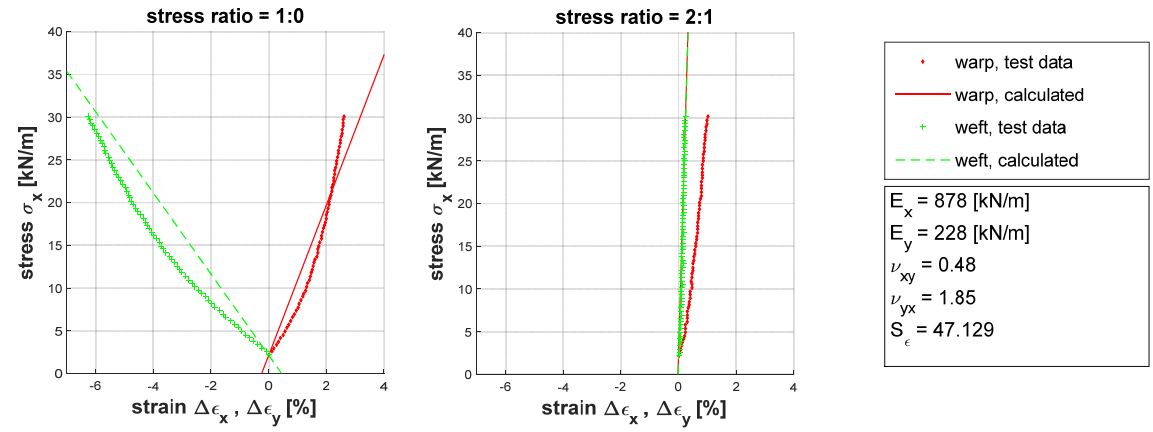

Figure 76 Comparison of measured stress-strain paths with calculated stress-strain lines corresponding to elastic constants resulting from test data of a glass-PTFE fabric type III according to MSAJ; evaluation includes 4 paths of stress ratios 1:0 and 2:1

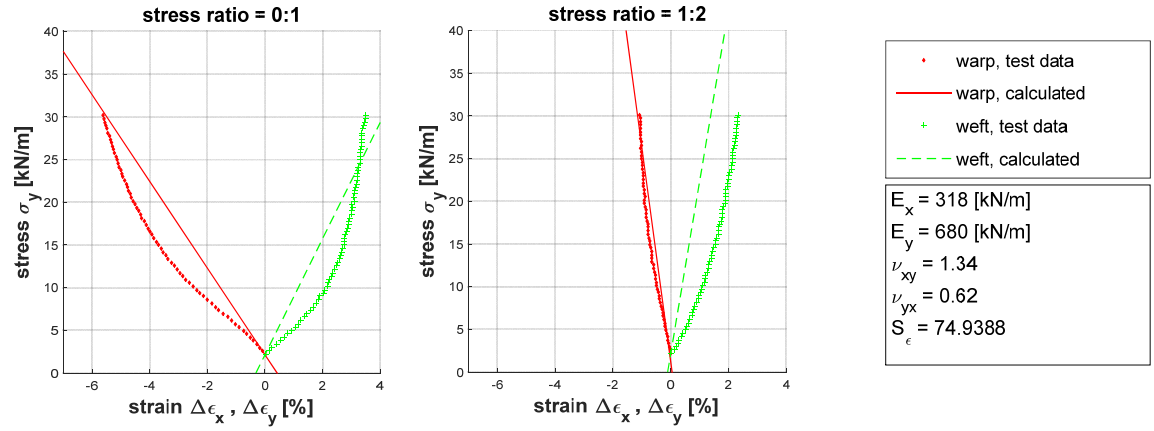

Figure 77 Comparison of measured stress-strain paths with calculated stress-strain lines corresponding to elastic constants resulting from test data of a glass-PTFE fabric type III according to MSAJ; evaluation includes 4 paths of stress ratios 0:1 and 1:2

The determination options are summarised in Table 9 and the numerical results of all discussed determination options are summarised in Table 10.

Table 9 Determination options for MSAJ tests

Determination option (DO)	
1	Original MSAJ determination: 8 stress-strain paths evaluated (zero stress paths omitted) [Me95]
2	MSAJ modified: all ten stress-strain paths evaluated [BG10]
3	Particular DO for plane structures, synclastic structures and anticlastic structures with low curvature and predominant warp stressing: MSAJ stress ratios 1:1, 2:1, 4 stress-strain paths [USS11]
4	Particular DO for plane structures, synclastic structures and anticlastic structures with low curvature and predominant fill stressing: MSAJ stress ratios 1:1, 1:2, 4 stress-strain paths [USS11]
5	Particular DO for anticlastic structures, load case with warp stressing: MSAJ stress ratios 1:0, 2:1, 4 stress-strain paths [USS11]
6	Particular DO for anticlastic structures, load case with fill stressing: MSAJ stress ratios 0:1, 1:2, 4 stress-strain paths [USS11]

Table 10 Fictitious elastic constants from one MSAJ biaxial test on a glass-PTFE fabric type III obtained using different determination options

Determination option (DO)		**Tensile modulus [kN/m]**		**Poisson's ratio [-]**		$\nu_{xy} \cdot \nu_{yx}$ **[-]**	**Note**
		E_x	E_y	ν_{xy}	ν_{yx}		
1	All stress ratios – 8 stress-strain paths	1292	816	0.57	0.90	0.51 < 1 ✓	MSAJ original
2	All stress-ratios – 10 stress-strain paths	914	610	0.83	1.24	1.03 > 1 ↯	MSAJ modified
3	Two stress ratios: 1:1 / 2:1 – 4 stress-strain paths	1870	1024	0.45	0.82	0.37 < 1 ✓	practical approach (synclastic)
4	Two stress ratios: 1:1 / 1:2 – 4 stress-strain paths	1336	824	0.60	0.97	0.58 < 1 ✓	practical approach (synclastic)
5	Two stress ratios: 1:0 / 2:1 – 4 stress-strain paths	878	228	0.48	1.85	0.89 < 1 ✓	practical approach (anticlastic)
6	Two stress ratios: 0:1 / 1:2 – 4 stress-strain paths	318	680	1.34	0.62	0.83 < 1 ✓	practical approach (anticlastic)

For all investigated PES-PVC fabrics, ranging from type II to type V from four different material producers, as well as all investigated glass-PTFE fabrics from type II to IV, numerous sets of fictitious elastic constants determined each on the basis of a MSAJ biaxial test are compiled in Annex B. A comparison of the PES-PVC constants of the different material producers shows that they are quite similar – except for the material with the biaxially prestressed coating system. With growing tensile strength properties, the tensile moduli also increase. The stiffness is dependent rather on the material class than on the material producer. These observations become explicable when considering that the evaluation covers the "full" working stress range up to ¼ of the tensile strength and that several load cycles preceded those that were evaluated. In this situation, the stress-strain behaviour of the base materials – which have similar yarn size and yarn density to fabrics with similar tensile strength properties, see Annex A – clearly has a major impact on the stress-strain behaviour of the coated woven fabric. Thus differences in weaving and coating – as long as basically the same technology is used, i. e. traditional or biaxially prestressed coating, for instance – are less pronounced than in the low stress ranges and the first load cycles. Here, in fact, there were considerable differences in constructional stretch between material producers which is not expressed by elastic constants.

"It can be summarised, that the values of fictitious elastic constants evaluated from one and the same biaxial MSAJ-test depend extremely on the underlying determination option – even if, as performed in the present investigations, only one numerical correlation method is applied (here: the Least Squares Method minimising the strain term), and if the calculated lines are optimised only for one stress range (here: between minimum and maximum experimental test stress)." [USS11]

One single set of fictitious elastic constants is not able to model all possibly occurring stress-strain paths. In the example application to a glass-PTFE fabric type III, the original MSAJ elastic constants fitted single paths well, particularly in the 1:1 and 1:2 stress ratios. But some paths, particularly the fill paths in stress ratio 2:1 as well as the zero stress paths, proved to be a poor fit. Evaluating all ten stress-strain paths is not a solution. This determination option leads to a poor fit for most stress-strain paths. The investigations provide evidence that only selective evaluation of the measured stress-strain data results in a convincing fit for the selected paths. Reasonable selection must therefore be performed according to the requirements of an investigated structure, primarily based on the distinction between synclastic/plane and anticlastic forms and the direction of the main stress in the fabric for anticlastic forms.

7.2.6 Discussion and conclusions

In principle, it makes sense to state a set of stress ratios that covers all possible and typical stress ratios appearing in architectural membrane structures and to determine

one set of elastic constants to cover the material response for all these stress ratios. Unfortunately, however, the application proves that this approach is impossible for fabrics. Neither evaluation of all ten stress-strain paths nor omitting the zero stress paths produces an acceptable fit for all stress-strain paths, particularly for the zero stress paths themselves. This is because the different stress ratios primarily require different magnitudes of Poisson's ratios – magnitudes that are mutually exclusive. Proof that this is the case is provided in [UKS13]: the uniaxial stress ratios require large Poisson's ratios for a good fit ($\nu > 1$), whereas the other stress ratios require small ones (e. g. $\nu < 0.5$). Because particularly the uniaxial stress ratios show a poor fit based on the MSAJ procedure, reasonable application of "fictitious MSAJ-elastic constants" is limited to synclastic membrane structures.

With regard to the experimental test results gained in Chapter 6, the weakest features of the MSAJ biaxial test protocol revealed to be the absence of load cycling in the stress ratios 2:1, 1:2, 1:0 and 0:1 and the absence of recovery times. Conducting only one load cycle is not in concordance with the usual approach in membrane structure analysis based on nominal prestress. The softening effect of omitting further load cycles and the stiffening effect of disregarding recovery times may balance each other out, but this appears rather to be a coincidence than an intentional course of action. Three load cycles for the stress ratio 1:1 appear to be acceptable since for most fabrics and load situations this number is sufficient to reach a stable state of the fabric. Moreover, disregarding a certain prestress level in the load profile – a main feature of tensile structures – is considered a shortcoming, although considering minimum stress levels during the evaluation helps to compensate this omission to a certain degree.

Example evaluations proved that the objective of having only one single set of fictitious elastic constants by means of which all types of structures under all types of loading can be treated is highly disputable. This could easily be rectified with reasonable user-defined selection of stress-strain paths for the evaluation. The example application of such different determination options demonstrated that the elastic constants react quite sensitively.

Nonetheless, due its precise definitions regarding the biaxial test protocol and the elaborate specifications regarding the evaluation of the test data, the MSAJ standard provides a very suitable tool for material comparisons on an objective basis. Concerning the use of the resulting elastic constants as input data for the structural design, however, the design engineer is recommended to act with caution, carefully select a reasonable determination option and examine thoroughly the results of the structural analysis.

7.3 Determination of elastic constants according to the European Design Guide for Tensile Surface Structures

7.3.1 General

In 2004, the European Design Guide for Tensile Surface Structures [FM04] was published by the TensiNet Association, referred to as the TensiNet Design Guide hereafter. This guide does not claim to be or resemble a standard but is rather a "state-of-the-art report being a first step in that direction" [FM04]. In this context, *Blum, Bögner and Némoz* [BBN04] proposed a biaxial test and evaluation procedure completely different from the previously published procedure established in the Japanese standard. An example application of these load profiles and variations thereof are presented together with measured strain for a glass-PTFE fabric in Appendix A4 [BBG04] of the TensiNet Design Guide. Unfortunately, the determination of elastic constants from the measured test data is not demonstrated.

7.3.2 Biaxial test protocol

"The TensiNet Design Guide test protocol consists of a constant pre-stress simulation, followed by cycles of superimposed warp loading and, after additional holding time at the pre-stress level, more cycles of fill loading. A third hold time is scheduled at the end of the test." [USS15a] This loading history, as shown in Figure 78, disregards the structural behaviour of synclastic structures, but it appears to offer a good simulation of anticlastic structures. The warp:fill stress ratio is not constant during one load cycle – as it is in the MSAJ test protocol – but changes continuously during loading and unloading.

Here, the emphasis is placed on the responsibility of the design engineer with regard to the defnition of stress levels in the test. The load profile in Figure 78 is given as an example. Test stresses and prestress level are expected to be defined by the design engineer according to the needs of the specific verification. However, some numerical recommendations are provided. The maximum test stress is adjusted to the working stress. Assuming a stress factor of five, the working stress is understood to be 1/5 of the minimum nominal tensile strength in warp and fill. Additionally, it is argued that the full working stress occurs in the membrane only very rarely, if at all. For the biaxial test it is proposed to set the stress to 80 % of the working stress. The prestress level is recommended as between 1/10 and max. 1/5 of the working stress. In terms of tensile strength, this yields 1/50 up to 1/25 of the tensile strength, which are practicable magnitudes.

The prestress levels in warp and fill can also differ from each other. Moreover, it is even recommended for general application of the procedure to repeat it with different warp:fill prestress ratios of 1:1, 2:1 and 1:2. The example application presented in Appendix A4 of the TensiNet Design Guide suggests applying the various stress ratios not only to the prestress but also to the working stress. However, the "stress

ratio" here is understood completely differently than usual: it is used as the ratio of maximum warp stress during the warp load cycles to maximum fill stress during the fill load cycles, thus a ratio of independent stresses. According to this definition, the prestress ratio or "stress ratio" respectively, as illustrated in Figure 78, is 1:1, since prestress and maximum test stress in warp and fill are equal. Finally, this thought leads to three different load profiles (or even five if "stress ratios" of 1:5 and 5:1 are additionally considered as in Appendix A4). Presumably this is intended to cover anticlastic structures with quite different magnitudes of curvature in both principal directions. Unfortunately, the underlying idea is not described in any further detail. Furthermore, it remains unclear how to evaluate the test data of these different load profiles: is the intention to determine one set of elastic constants for every investigated load profile/"stress ratio"?

Lastly, it should be mentioned that no load rate or time durations for the hold times at prestress level are defined.

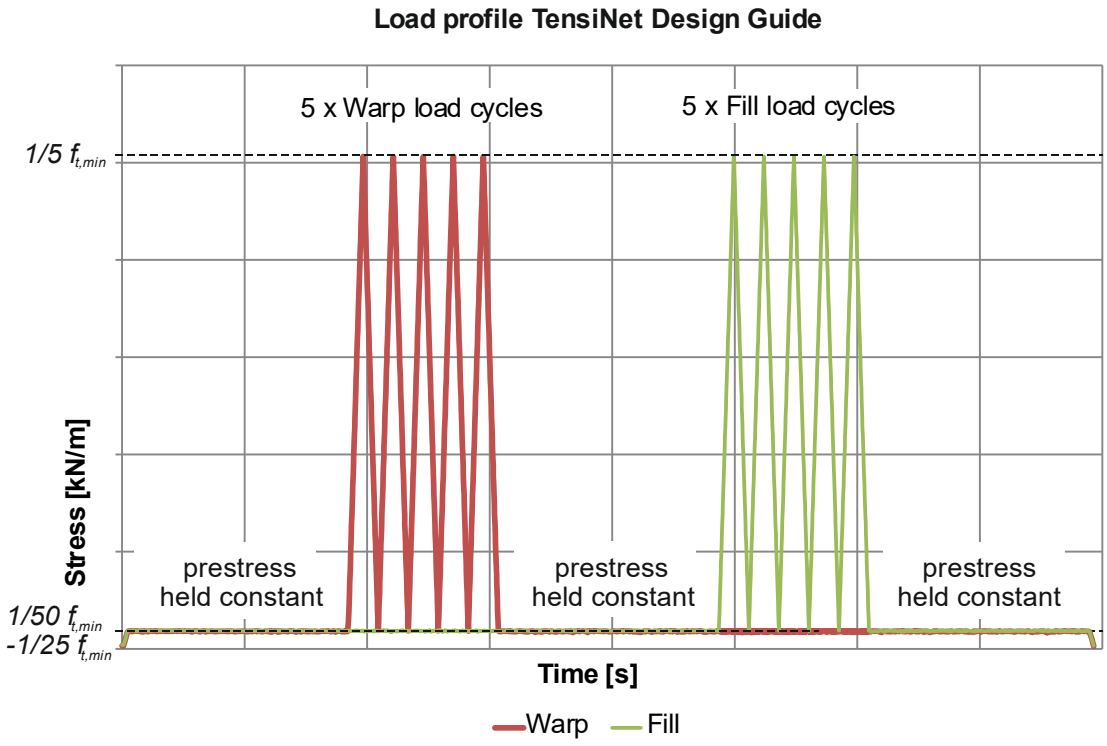

Figure 78 Load profile for biaxial tests according to the TensiNet Design Guide, including non-binding numerical recommendations for the stress levels

7.3.3 Evaluation procedure

"The TensiNet Design Guide procedure is based on four stress-strain paths: two paths from one of the warp loading cycles, and two paths from the same fill loading cycle. The strain differences $\Delta\varepsilon$ are extracted from the test results for the full stress differences $\Delta\sigma$. With four stress-strain paths, four equations can be solved, enabling the determination of four independent elastic constants. These constants describe

secants between the pre-stress and the maximum stresses. To achieve a symmetric stiffness matrix using only three independent elastic constants, an approximation solution must be applied. Suggestions of how to perform that approximation are not given in the TensiNet Design Guide. One possible solution might be to average the ratios on both sides of eq. (4.9), and this averaging procedure is used for the evaluations in this work." [USS15a]

The objective of the TensiNet Design Guide procedure is apparently to determine one single set of elastic constants for short-term loading.

The authors use the direct stiffness formulation in terms of tensors, given in Chapter 4 with engineering constants, see eq. (4.40).

7.3.4 Example evaluation of test data

Biaxial tensile tests according to the TensiNet Design Guide procedure were performed with three different classes of PES-PVC fabrics (types II, III and IV) from two material producers and one glass-PTFE fabric type III.

In all biaxial tests performed in connection with this work according to the TensiNet Design Guide procedure, only the "stress ratio" 1:1 was applied, i. e. maximum warp stress and maximum fill stress are equal. Furthermore, the test stress levels were adjusted to those of the Japanese standard. This was done in order to enable a direct comparison of the resulting sets of elastic constants. This means that the maximum test stress level was chosen to be ¼ of the minimum nominal tensile strength and the prestress level for polyester fabrics was chosen to be p = 1 kN/m and for glass fibre fabrics p = 2 kN/m, based on the evaluation recommendations of the MSAJ standard commentary.

Elastic constants were determined using the fifth load cycles each for warp and fill stressing. The results for the different PES-PVC fabrics are given in Table 11 to Table 13 and for the glass-PTFE fabric in Table 14. In all cases, the elastic constants are given in terms of the inverse stiffness formulation, see eq. (4.37).

Table 11 Sets of elastic constants obtained in the TensiNet Design Guide tests for test specimens with a PES-PVC material type II

Material producer	Tensile modulus [kN/m]		Poisson's ratio [-]		$\nu_{xy} \cdot \nu_{yx}$ [-]
	E_x	E_y	ν_{xy}	ν_{yx}	
1	804	596	0.39	0.53	0.21 < 1
3	743	569	0.35	0.45	0.16 < 1

Table 12 Sets of elastic constants obtained in the TensiNet Design Guide tests for test specimens with a PES-PVC material type III

Material producer	Tensile modulus [kN/m]		Poisson's ratio [-]		$\nu_{xy} \cdot \nu_{yx}$ [-]
	E_x	E_y	ν_{xy}	ν_{yx}	
1	1016	728	0.43	0.60	0.26 < 1
3	1025	648	0.46	0.73	0.33 < 1

Table 13 Sets of elastic constants obtained in the TensiNet Design Guide tests for test specimens with a PES-PVC material type IV

Material producer	Tensile modulus [kN/m]		Poisson's ratio [-]		$\nu_{xy} \cdot \nu_{yx}$ [-]
	E_x	E_y	ν_{xy}	ν_{yx}	
1	1300	850	0.45	0.70	0.32 < 1
3	1328	865	0.62	0.95	0.58 < 1

The correlation between measured and calculated stress-strain paths typical for PES-PVC fabric type III from material producer 1 is illustrated in Figure 79. In this example, "the stress-strain paths of the leading stresses were perfectly modelled, whereas for the transverse directions, the trend was met, although with a maximum strain difference of 0.8% strain at the maximum stress level." [USS15a] Although the Poisson's ratios are considerably higher throughout than those resulting from the MSAJ procedure, they are small enough for the product of the Poisson's ratios to be clearly smaller than one in all cases, see Table 11 to Table 13. All sets thus represent feasible sets of design elastic constants.

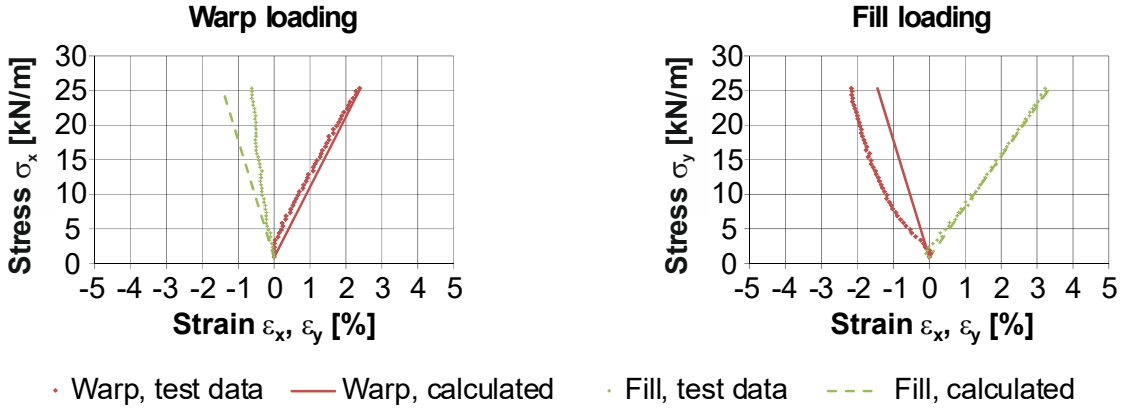

Figure 79 Correlation between measured and calculated stress-strain paths for the TensiNet Design Guide test, typical for PES-PVC fabric type III from material producer 1

The first biaxial test on the glass-PTFE fabric was conducted using the above mentioned numerical specifications. "The determination results reveal much bigger elastic constants than those obtained by the MSAJ procedure, for the tensile stiffness

as well as for the Poisson's ratios. The latter ones give a product $\nu_{xy} \cdot \nu_{yx} > 1$, which means, that this set of constants is unfeasible for a structural analysis, see explanations above." [USS15b] Assuming that the Poisson's ratios decrease if the stress range is narrowed, a second test was conducted with a stress range between p = 3 kN/m and maximum stress of 13 kN/m. These values are the supposed prestress level and the anticipated maximum stress level of the investigated four point sail in Chapter 7.6. From the results in Table 14 it can be seen that all values of the elastic constants decrease compared to the first test procedure. However, the product of the Poisson's ratios still clearly exceeds 1.0. The results demonstrate that no feasible elastic constants could be evaluated for the investigated glass-PTFE fabric type III, neither for a general case nor for a specific structure and stress range. Considering the findings in Chapter 6 that glass-PTFE exhibits much higher transverse strain and Poisson's ratios than PES-PVC fabrics, it can be predicted that the TensiNet Design Guide procedure leads to unfeasible sets of elastic constants for glass-PTFE fabrics in general.

Table 14 Sets of elastic constants obtained by two differently performed TensiNet Design Guide tests for test specimens with a glass-PTFE material type III

Test N°	Tensile modulus [kN/m]		Poisson's ratio [-]		$\nu_{xy} \cdot \nu_{yx}$ [-]
	E_x	E_y	ν_{xy}	ν_{yx}	
1	2460	1340	1.32	2.42	3.19 >> 1
2	1660	660	0.78	1.98	1.54 > 1

7.3.5 Discussion and conclusions

The TensiNet Design Guide procedure consists of several expedient features. The consideration of a prestress level in the test is appreciated since prestress is essentially crucial for tensile structures. A good feature for design practice is the open frame with basically sound non-binding numerical recommendations regarding the stress levels. Only the recommendation to set the maximum test stress equal to 80 % of the working stress, because the working stress might only occur rarely, does not seem reasonable. The circumstance that the working stress for many membrane structures only occurs rarely if at all is most probably true. Nevertheless, the design of the structure must ensure that the structural analysis is correct for the worst case scenario. For this reason, it appears to be more reasonable to adjust the biaxial test procedure to the full possible working stress in the general case (unless the design engineer adjusts it to the anticipated characteristic stress in the critical design load case).

In the light of the experimental results described in Chapter 6, the fivefold repetition of load cycles appears to be a safe approach. It ensures that the stable state of the fabric will be reached for the investigated stress ratio. The derived elastic constants

could thus be used combined with the nominal prestress level in the structural analysis.

Time durations for the hold times are not provided. A default setting would have been beneficial. Assuming a sufficient duration is foreseen in the tests, the proposed load profile would include recovery times on prestress level. This would avoid the effect of artificial stiffening as described in Chapter 6.

The proposal is not a standardised procedure. Too few specifications are provided for that to be the case. Thus a comparison of different materials on an objective basis is not possible. However, this was not the aim of the proposed procedure. The objective was to serve practical application; accordingly, most specifications are left to the design engineer.

The most critical characteristics are (1) that the procedure is limited to anticlastic structures due to the specified load profile and (2) that it leads for glass-PTFE fabrics to sets of elastic constants that are far beyond feasibility. Hence practical application is limited to anticlastic structures made of PES-PVC fabrics. For these the procedure delivers elastic constants with acceptable correlation to the measured test data.

7.4 Determination of elastic constants according to the French Recommendations

7.4.1 General

The “Recommandations pour la conception, la confection et la mise en oeuvre des ouvrages permanents de couverture textile” [So09] is a design guide for prestressed permanent membrane structures first published in 1997 in the "Annales de l’ITBTP" by the Institut Technique du Bâtiment et des Travaux Publics. The version discussed here is an updated version from the year 2007. It is referred to as the “French Recommendations” hereafter. Basically, this document is a guideline for the design and verification of prestressed membrane structures made from PES-PVC and glass-PTFE fabrics. Biaxial testing and the determination of elastic constants for design purposes is considered in a short annex to the guideline.

7.4.2 Biaxial test protocol

First a prestress load profile is implemented. Five load cycles are to be conducted with a warp:fill stress ratio of 1:1 between a minimum defined stress of 0.25 kN/m and a maximum stress of 5 % of the fill nominal tensile strength $f_{t,fill}$. Subsequently, ten further load cycles under “working stress” are conducted, five of which are performed with different maximum stresses. This working stress test sequence is recommended to be performed in a test series of three tests with three different stress ratios: 1:1, 2:1 and 1:2, i. e. three test specimens are required. The working stress test sequence with a stress ratio of 2:1 is presented as an example in Figure 80. During the first five load cycles, the maximum test stress is specified as 10 % of

the warp nominal tensile strength $f_{t,warp}$; in the subsequent five load cycles it is 25 % of $f_{t,warp}$. The actual prestress of an investigated structure is disregarded during these ten working stress load cycles; the minimum stress is a fixed value of 0.25 kN/m.

A constant stress rate is required for the initial prestress cycles as well as the working stress cycles, but no definition is given.

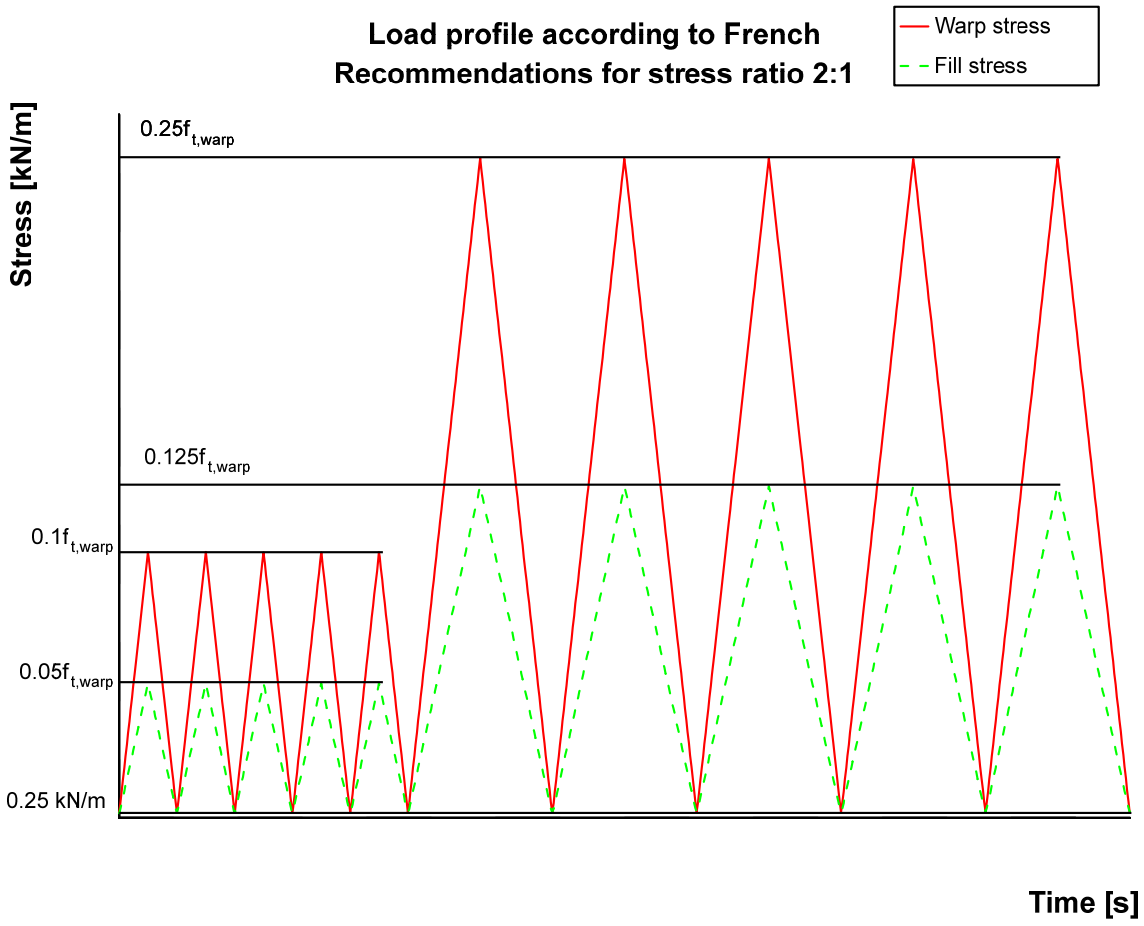

Figure 80 Two series of five load cycles (in this example in the stress ratio 2:1) that are to be performed subsequently to five prestress load cycles in stress ratio 1:1

7.4.3 Evaluation procedure

The goal is to determine one set of two tensile moduli. The warp tensile modulus is determined from the test with stress ratio 2:1 and the fill tensile modulus from the test with stress ratio 1:2. Remarkably, the test with stress ratio 1:1 is not used further in conjunction with the described evaluation. The tensile moduli are defined as the gradient of the secant between the end point of unloading in the first load cycle and the end point of loading in the fifth load cycle, both in the second series of five load cycles. This is illustrated in Figure 81. E_x and E_y are determined independently from each other such as to fit only the ratio of stress difference to strain difference in the respective biaxial test. The connection of points of different load cycles delivers a kind of “global stiffness”, compare the definition in Chapter 6.2.2.

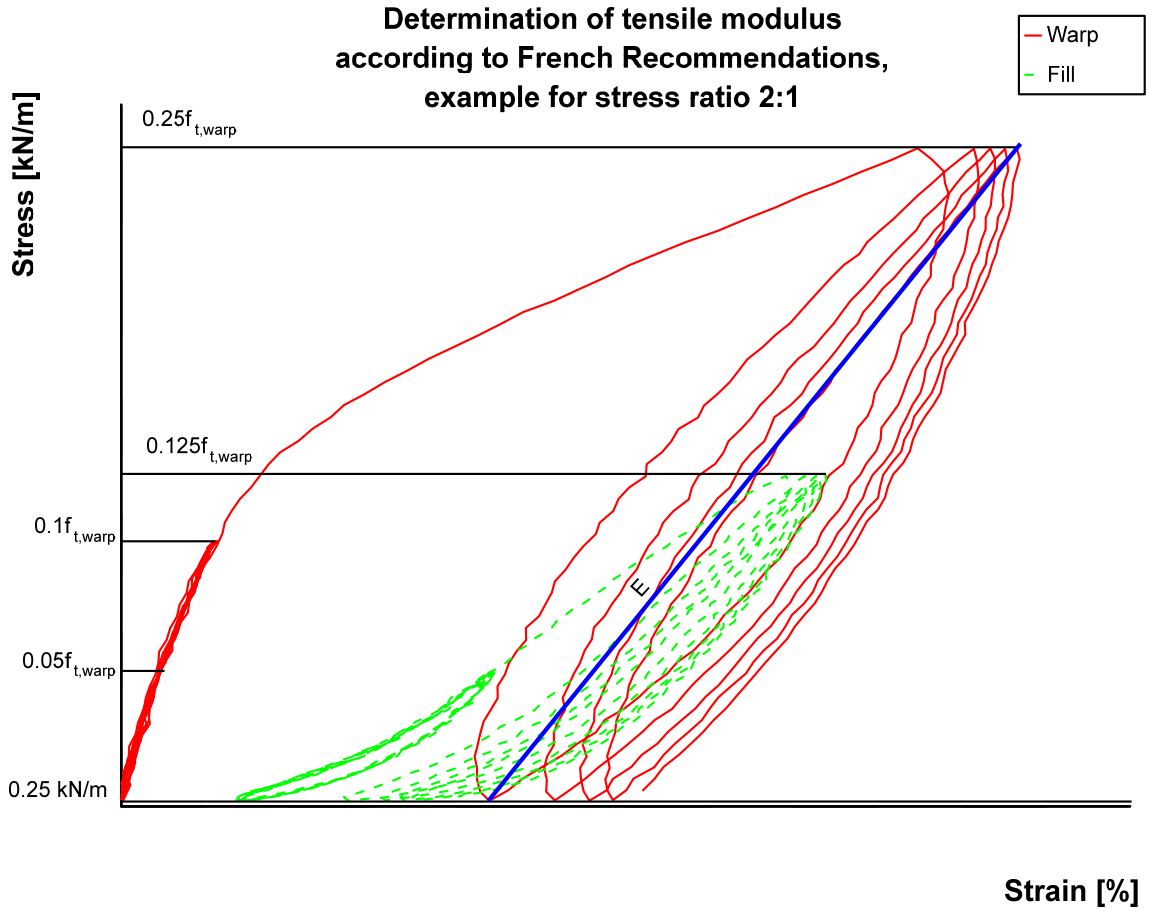

Figure 81 Measured stress-strain data for the test with stress ratio 2:1, determination of the warp tensile modulus as secant between the end point of unloading in the first load cycle and the end point of loading in the fifth load cycle, both in the second series of five load cycles

The determination of Poisson's ratios is not described. However, the guideline recommends "in the absence of an accurate measurement of the Poisson's ratio" using the following values: $\nu_{xy} = 0.3$, $\nu_{yx} = 0.5$. These numerical recommendations are given completely independently of the fabric. This seems questionable considering the very high Poisson's ratios measured particularly for glass-PTFE fabric, see Chapter 6. If the orthotropy ratio of the determined tensile moduli E_y/E_x were not the same as ν_{xy}/ν_{yx} randomly, compare eq. (4.9), it would not be possible to apply both Poisson's ratios anyway. Because of this and the absence of a proposal for the determination of the Poisson's ratio, presumably only one fixed Poisson's ratio is applied in engineering practice and the second is determined automatically via the reciprocal relationship eq. (4.9) by the analysis software. This procedure does not reflect the very high orthotropy ratios some woven fabrics may exhibit.

As the tensile moduli are determined independently from each other and are combined subsequently with fixed Poisson's ratios, the question arises as to how this set of patchwork constants behaves when inserted in the constitutive model eq. (4.37). The intended fit of the independently established secants is lost with this procedure. This is illustrated in terms of an example application hereafter.

7.4.4 Example evaluation of test data

An example application was performed conducting one biaxial test on a traditionally coated PES-PVC fabric type III from material producer 2. Simplified, stress ratios 2:1 and 1:2 were combined in one biaxial test. Figure 82 illustrates the complete load profile. The determination of tensile moduli is illustrated in Figure 83.

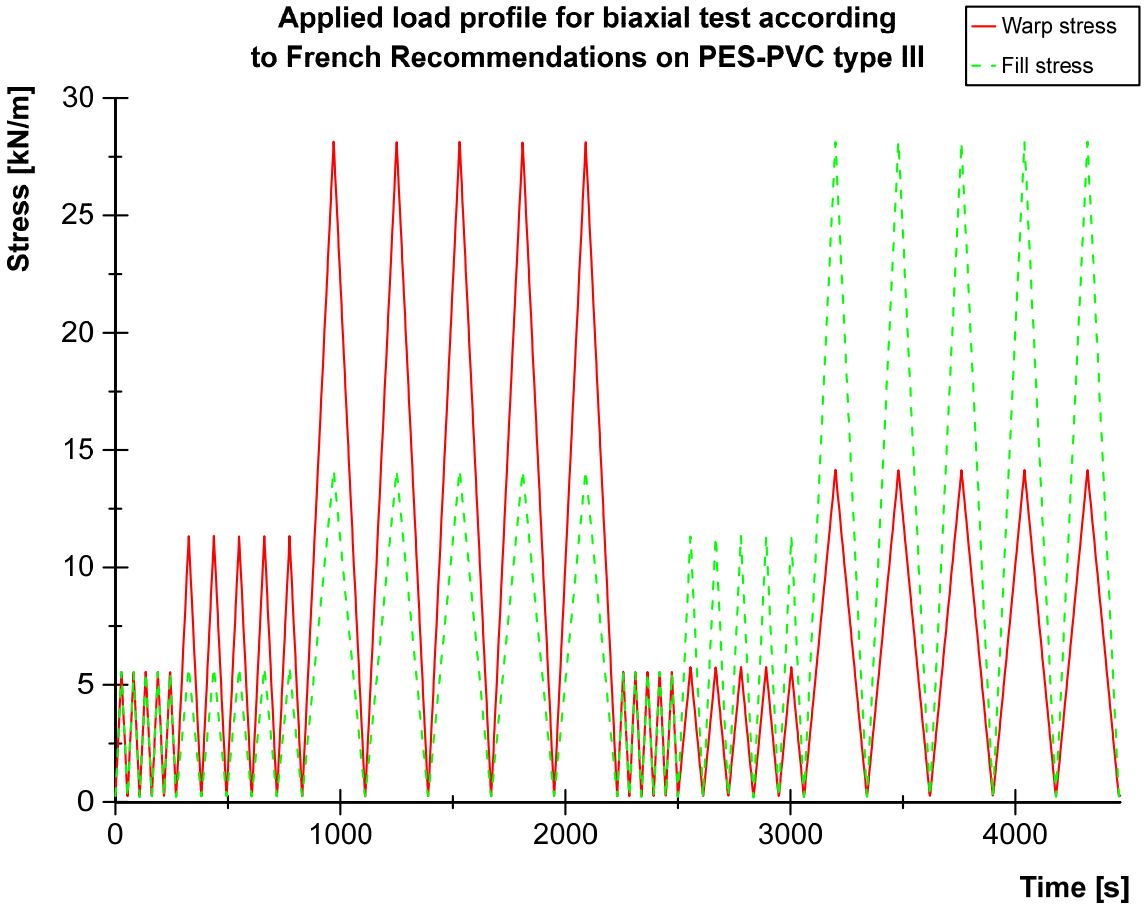

Figure 82 Complete load profile for the example application of the French Recommendations with a traditionally coated PES-PVC fabric type III

The problem which arises subsequently is that the strain increments upon which the determination of the tensile moduli was based will change when the elastic constants are inserted in the constitutive eq. (4.37). This happens as a result of subtracting the transverse strain term. Control over the fit quality is lost as a result. For this reason, it is recommended to always evaluate tensile moduli and Poisson's ratios together.

This conclusion can be clarified by means of the above mentioned example. The major stress increment $\Delta\sigma = 28\text{-}0.25 = 27.75$ kN/m combined with the determined tensile moduli and the predefined Poisson's ratio $\nu_{xy} = 0.30$ (yielding $\nu_{yx} = 0.30 \cdot 888/522 = 0.51$) leads to strain increments for stress ratio 2:1 of

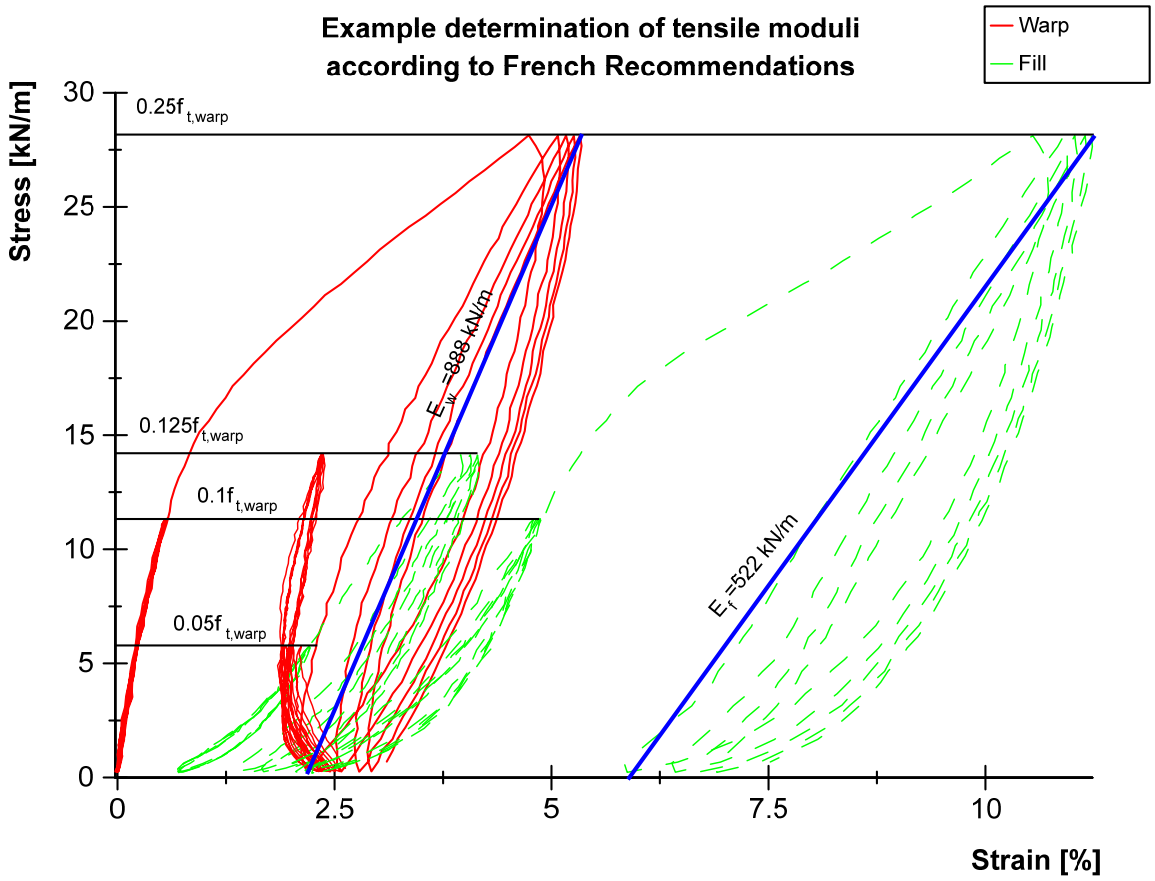

Figure 83 Determination of tensile moduli for the example application of the French Recommendations with a traditionally coated PES-PVC fabric type III

$$\Delta\varepsilon_x = \frac{1}{E_x}\Delta\sigma_x - \frac{\nu_{xy}}{E_y}\Delta\sigma_y = \frac{27.75}{888} - \frac{0.30 \cdot 13.875}{522} = 0.0233\ [-],$$
$$\Delta\varepsilon_y = -\frac{\nu_{yx}}{E_x}\Delta\sigma_x + \frac{1}{E_y}\Delta\sigma_y = -\frac{0.51 \cdot 27.75}{888} + \frac{13.875}{522} = 0.0106\ [-] \quad (7.6)$$

and for the stress ratio 1:2 of

$$\Delta\varepsilon_x = \frac{1}{E_x}\Delta\sigma_x - \frac{\nu_{xy}}{E_y}\Delta\sigma_y = \frac{13.875}{888} - \frac{0.30 \cdot 27.75}{522} = 0.0003\ [-],$$
$$\Delta\varepsilon_y = -\frac{\nu_{yx}}{E_x}\Delta\sigma_x + \frac{1}{E_y}\Delta\sigma_y = -\frac{0.51 \cdot 13.875}{888} + \frac{27.75}{522} = 0.0452\ [-]. \quad (7.7)$$

Adding these data to the stress-strain diagram leads to Figure 84 for stress ratio 2:1 and Figure 85 for stress ratio 1:2. Only the last four decisive load cycles are plotted in each diagram. The warp path in stress ratio 2:1 as well as the fill path in stress ratio 1:2 show considerable deviation from their original target specifications. The transverse strain fits very poorly in stress ratio 2:1, while it “accidentally” fits well in stress ratio 1:2.

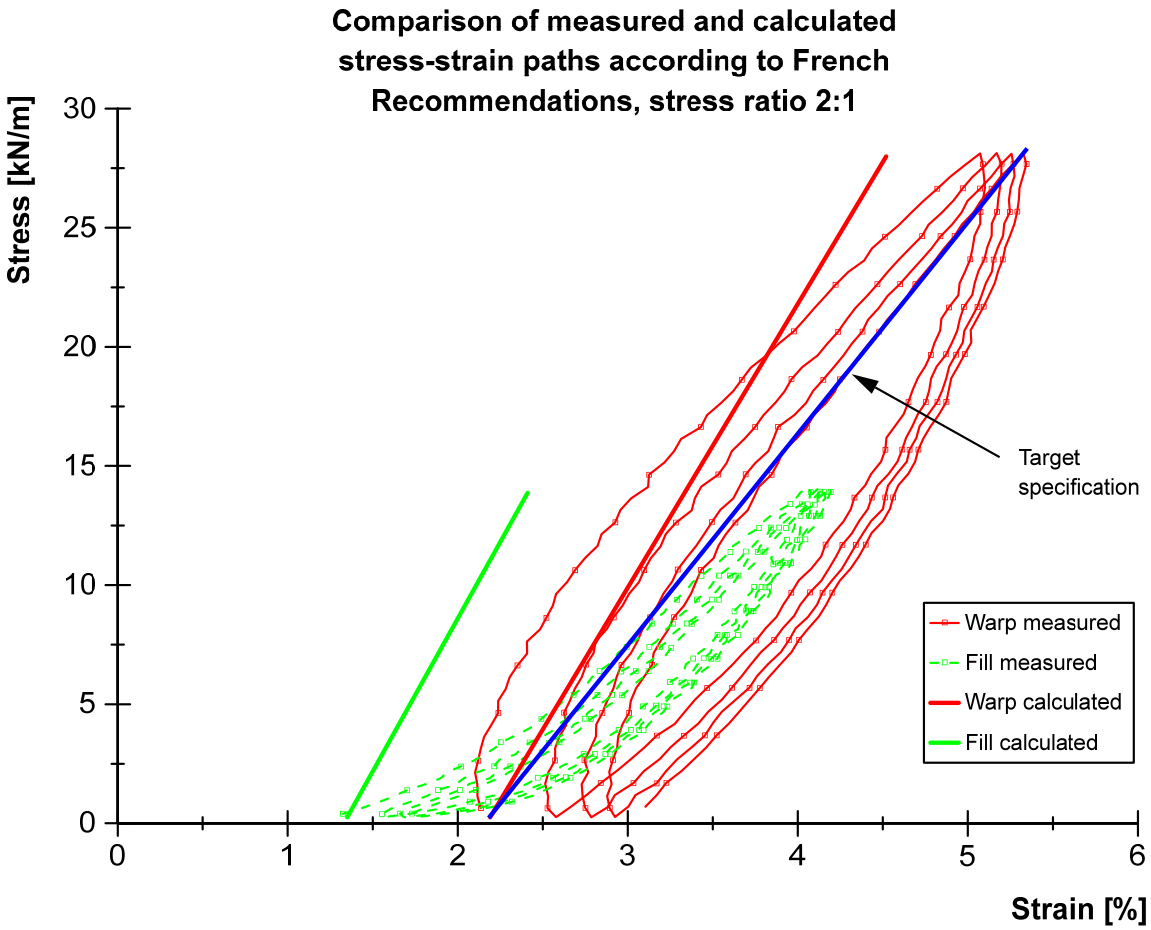

Figure 84 Comparison of measured and calculated stress-strain paths for the example application of the French Recommendations with a traditionally coated PES-PVC fabric type III, stress ratio 2:1

7.4.5 Discussion and conclusions

The French Recommendations propose three tests with different stress ratios: 1:1, 2:1 and 1:2. Three independent tests would be unnecessary in the light of the findings of Chapter 6. The number of five load cycles would alone be sufficient to reach a stable state of the fabric. Thus, the three different stress ratios could subsequently be conducted with one test specimen. Furthermore, it is suggested that after five load cycles the impact of the initial prestress load cycling is insignificantly low. This also applies to the first five working stress load cycles at a lower stress level. Both could be omitted. Furthermore, considering the results of Chapter 6, recovery times are not included as is a certain prestress level in the “working stress” load cycles. Only the strain increment between prestress and the working stress level is actually of interest in the scope of structural design.

The determination of elastic constants is limited to the determination of fictitious tensile moduli. They are derived from the stress ratios 2:1 and 1:2. The aim is to obtain one set of elastic constants which is able to cover all possible stress ratios between 2:1 and 1:2. Due to these stress ratios the procedure is rather limited to synclastic structures.

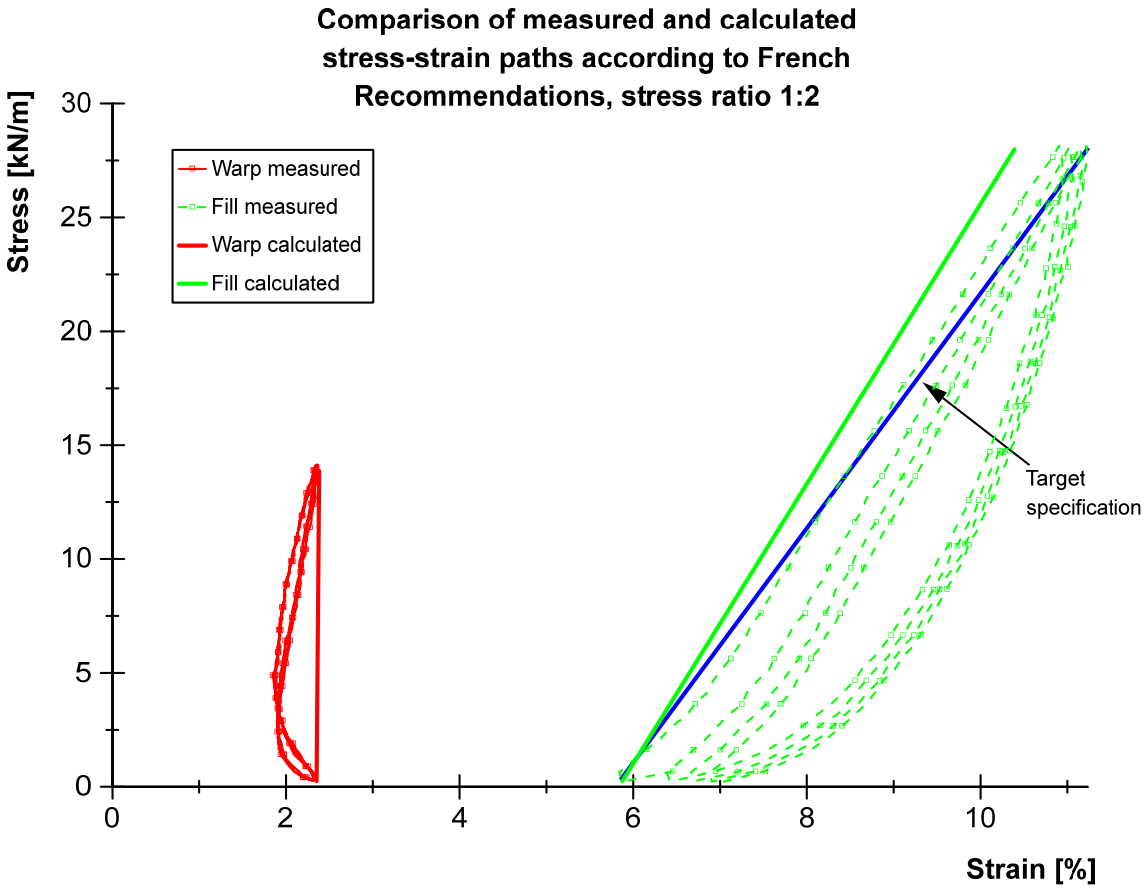

Figure 85 Comparison of measured and calculated stress-strain paths for the example application of the French Recommendations with a traditionally coated PES-PVC fabric type III, stress ratio 1:2

Employing a kind of “global stiffness” leads to comparably “soft” tensile moduli. This means a safe-sided approach with regard to the deflections of the investigated fabric structures, but it is unsafe with regard to the membrane stress. The complete set of elastic constants is “artificially composed” from the experimentally determined fictitious tensile moduli and predefined numerical recommendations for the Poisson’s ratios. This procedure appears unable to ensure a suitable fit of decisive stress-strain paths, particularly not for high transverse strain glass-PTFE fabrics. Tensile moduli and Poisson’s ratios must be determined in one step in order to ensure a good fit when they interact in the constitutive equations.

However, the number of load cycles appears to be well chosen, as does the recommended stress levels during the biaxial tests. The derived elastic constants should nevertheless be applied with caution by the design engineer.

7.5 Determination of elastic constants according to ASCE/SEI 55-10

7.5.1 General

The US standard ASCE/SEI 55-10 "Tensile Membrane Structures" [Am10] is primarily a valuable code for design and construction practice. A detailed

commentary is also an inherent part of the document. It includes all tensile membrane structures which exceed a defined size, temporary and permanent, but it explicitly excludes air-supported and air-inflated structures. The standard does not limit the application to any membrane material, i. e. it applies for all fabrics and foils as well.

The determination of elastic constants is dealt with in an appendix. The proposed evaluation method is based on fixed stress ratios. Published test data for PES-PVC and glass-PTFE is obtained in the manner of *Minami and Motobayashi* [MM84]. They use the same five stress ratios as the later established Japanese standard MSAJ/M-02-1995, but they do not combine them in one biaxial test. Instead, they use a new test specimen for every stress ratio (and they even use differently shaped test specimens for the uniaxial stress ratios). The evaluation procedure is explained by means of these test data. Hence, resulting elastic constants can in no way be compared to MSAJ elastic constants. Nonetheless, the standard also refers to MSAJ/M-02-1995 for further testing techniques.

The chapters on physical testing and physical properties provide further provisions and requirements. A distinction is made between differently determined sets of elastic constants. On the one hand, the material manufacturer shall provide elastic constants. These general elastic constants shall be based on the stress ratios 1:1, 2:1 and 1:2 “as a minimum”. The biaxial tests shall be based on a fixed stress range of 0.175 kN/m to 30 % of the strip tensile strength. The evaluation procedure stated in the appendix and discussed in the following is proposed as one procedure to derive the required elastic constants. On the other hand, contrary to this general material characterisation, there is a requirement for individual test and evaluation in which biaxial test stresses are to be selected “to simulate the design stresses predicted by analysis”. In general, the distinction between the two approaches, a general and a practical one, is beneficial from an engineering point of view. Both support the design engineer: With the former method a new material can be compared with a known material on an objective basis while with the latter proper constants for specific design situations are determined.

7.5.2 Evaluation procedure

Unless initial loading test data is used, each measured stress-strain path during loading aimed to be evaluated is cut out from the complete test data record between zero stress and the maximum test stress. Subsequently the paths are normalised, i. e. the start point is moved to zero strain.

The second step is linearisation of the test data for each measured (and normalised) stress-strain path. This is performed completely independently of the other stress-strain paths. The linearisation is recommended to be conducted with mathematical software using the Least Squares Method. Resulting straight lines displayed in the standard for the example of a glass-PTFE fabric with stiffening stress-strain

behaviour meet their measured counterparts far below the maximum test stress. It can be anticipated as a basis for further evaluation that these lines lead to a comparably “soft” behaviour of the model which may produce a good fit at half of the test stress level.

In the example test data, uniaxial stress ratios 1:0 and 0:1 are included (at least the test data for the stressed direction). However, these test data are removed on the grounds that “they are not biaxial behaviour and they give erroneous values”. This means that the evaluation is based on six straight lines to arrive at the four unknown elastic constants. It must be mentioned that omitting uniaxial test data reduces the feasibility of the procedure to synclastic structures. In specific cases of anticlastic structures with low curvature and/or fabrics with high transverse strain for which the typical uniaxial load-bearing behaviour is not as pronounced, this procedure might also be applicable. However, this has to be decided by the design engineer from case to case.

Following the description of the procedure, stress and associated strain values for the six straight lines are inserted in the constitutive equations. ASCE-SEI 55-10 uses the direct stiffness formulation of the constitutive model as stated in eq. (4.40), but additionally equations are provided from which to obtain tensile moduli and Poisson’s ratios according to the inverse stiffness formulation. The information from only two straight lines can be inserted in the two single constitutive equations. Thus this procedure must be repeated three times if all six recommended straight lines are made use of. Meanwhile, three equations are needed to determine the three unknown independent elastic constants. Theoretically, twenty (!) possibilities arise for selecting three equations from six. Consequently, twenty sets of elastic constants occur, one for each possible set of three equations. The standard recommends to “average” the results to obtain one single set of elastic constants. However, an example application using the glass-PTFE test data published in the standard reveals that some combinations result in elastic constants that do not satisfy the mechanical restrictions, e. g. lead to negative tensile moduli. How such outcomes should be handled in detail is not proposed.

One example set of resulting elastic constants is presented in the American standard. This applies to a glass-PTFE fabric with warp tensile strength of 144 kN/m and fill tensile strength of 128 kN/m. These values are very similar to those of the glass-PTFE fabric type III investigated in this work, given as 142.9 kN/m/120.3 kN/m warp/fill, see Table 3, but the strain presented in the ASCE standard is significantly greater. This is obviously because a new test specimen was used for every stress ratio, see explanations above, and for that reason a large amount of constructional stretch is included. The elastic constants provided are E_x = 634 kN/m, E_y = 213 kN/m, ν_{xy} = 0.29 and ν_{yx} = 0.87. Unfortunately, a graphical comparison of measured and calculated stress-strain paths is not presented in the standard. In order to verify the

quality of the fit, the published test data were roughly compared to the straight stress-strain lines corresponding to the given set of elastic constants. This is illustrated in Figure 86. Partly, a very poor fit at maximum test stress level is observed for the stress ratios that were the foundation of the evaluation. The maximum error is ca. 6 % strain (!), see fill direction at 1:2 stress ratio. Presumably, this results from the flat-angled straight lines upon which all evaluation is based in the American standard. From these lines, it can be suggested that the aim was not to achieve a good fit at maximum test stress level. Unfortunately, this is not precisely defined. However, the fit appears to be of acceptable quality only up to a major stress level of approximately 10 kN/m.

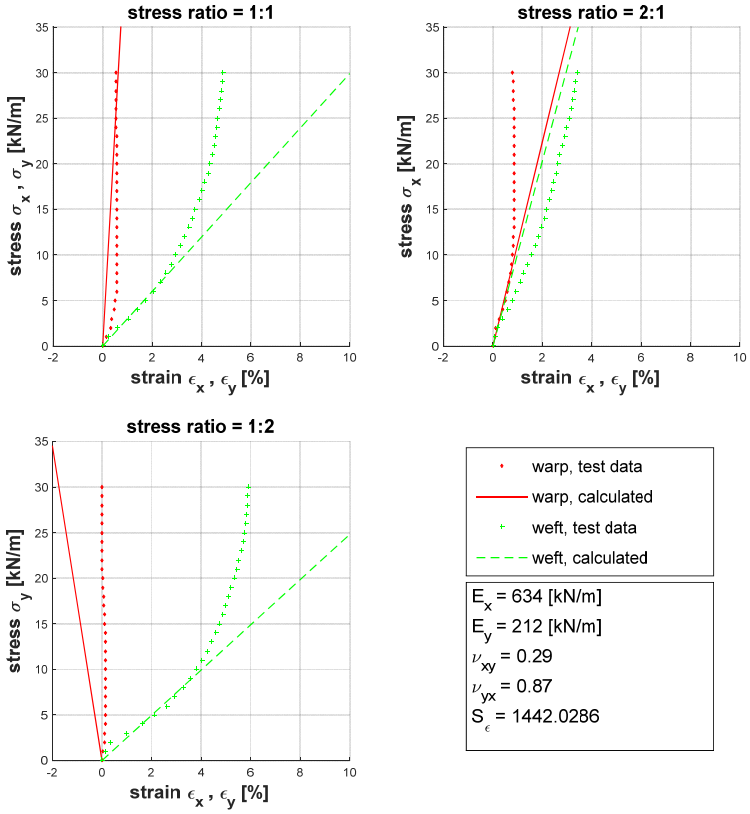

Figure 86 Test data for glass-PTFE fabric as published in the ASCE standard compared to straight stress-strain lines corresponding to the stated set of ASCE elastic constants

7.5.3 Discussion and conclusions

The US standard ASCE-SEI 55-10 provides an evaluation procedure for biaxial tests with three fixed stress ratios of 1:1, 2:1 and 1:2. In which test context these stress ratios should be performed is not precisely defined. Two different methods are mentioned: the method used by *Minami and Motobayashi* to use a new test specimen for every load ratio and the method of the MSAJ/M-02-1995, which includes these and other stress ratios in a complete load profile to be conducted on a single test specimen.

The described evaluation procedure aims to determine one single set of elastic constants that is able to model the stress-strain response in the stress ratios 1:1, 2:1 and 1:2. As a result, it is in principle rather limited to synclastic structures, which contradicts the exclusion of air-supported and air-inflated structures from the standard. The proposed procedure is based on the independent linearisation of the six stress-strain paths considered and inserting the pairs of values of stress and associated strain corresponding to these straight lines into the constitutive equations. This leads to six equations.

The precise process for the determination of the three independent elastic constants remains unclear to the user. Twenty theoretical possible combinations exist when determining three independent constants from six equations. Consequently, twenty different sets of elastic constants result from this procedure. Finally, the results should be averaged. How single values that do not observe the mechanical restrictions should be handled or how the reciprocal relationship is ensured during this step is not described. The procedure therefore seems to be rather impractical.

Moreover, the evaluation procedure itself is confusing and unpredictable. On which stress level a good fit with the measured stress-strain data will be realised is not foreseeable. The unpredictability is intensified further with the averaging of numerous sets of elastic constants. The example elastic constants presented in the standard for a glass-PTFE fabric have been validated with the published stress-strain paths. This comparison provided evidence of a poor fit of the behaviour of the underlying material. Overall, the proposed evaluation procedure does not prove to be suitable for determining design elastic constants. For use as a standardised, general material characterisation, a precisely defined biaxial test procedure would be required.

Furthermore, using a new test specimen for every stress ratio and conducting only one load cycle for which elastic constants are determined is not advisable when aiming to achieve elastic constants for design purposes, see explanations in Chapter 7.1.

Disregarding prestress during the evaluation (and already in the biaxial test protocol) is likewise not useful in connection with prestressed fabric structures.

7.6 Spectrum of structural analysis results under different evaluation procedures for elastic constants

Individual publications emphasise the tremendous impact the uncertainty of design elastic constants can have on analysis results [Ba02], [BB12]. In the following, the impact of different sets of elastic constants that were determined on the basis of a MSAJ biaxial test is analysed. The results of the analysis were first published in a series of three journal papers [US13], [USS15a], [USS15b], which are reproduced in part here. The investigations presented there cover two different anticlastic structures, a barrel vault and a four-point sail, and different materials, one glass-

PTFE fabric type III and PES-PVC fabrics type II, III and IV from two material producers. In the scope of this work the results for the four-point sail spanned with the glass-PTFE fabric are illustrated because it emphasises the huge impact particularly of high Poisson's ratios. The glass-PTFE fabric, however, excludes the TensiNet Design Guide procedure. For this reason, only sets of elastic constants evaluated from a MSAJ biaxial test are considered, making use of different determination options given in Table 9.

"A 10x10 m square hypar with two high points and two low points is exemplarily examined (a saddle shaped example is given by the authors in [US13]). The edges are fixed. The prestress is chosen to be isotropic with p = 3.0 kN/m in the main anisotropic fabric directions. The shear modulus is supposed to be G = 50 kN/m. The structural analysis is conducted with the finite element software package SOFiSTiK 2014 [Sof14] applying a third order analysis. The structure is vertical loaded downwards with q = 0.60 kN/m^2.

Three different curvatures are analysed, with h = 0 m (plane structure), h = 2 m and h = 4 m, see Figure 87, Figure 88 and Figure 89. The warp direction runs between the high points, so that for the curved variations of the structure the warp direction expands for a downward load while the weft direction contracts. Preliminary FE analyses show stress ratios of approximately 4:1 and greater in the centre of the structure for the load q. Thus, the four measured stress-strain paths of the MSAJ load ratios 1:0 and 2:1 are picked out to determine the elastic constants for DO 5 in Table 9. The plane variation of the structure is characterised by stress ratios between 1:1 and 2:1. Corresponding to that, elastic constants for DO 3 are determined based on the four stress-strain paths of these two stress ratios.

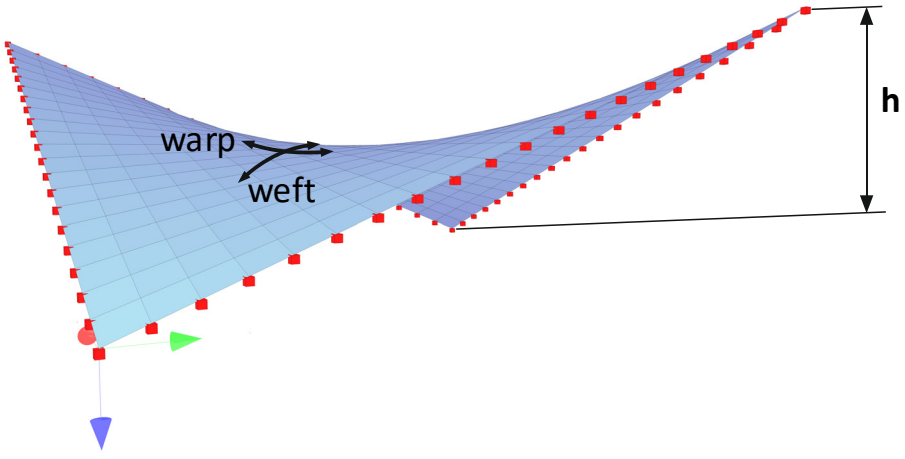

Figure 87 Simple hypar with 2 low points and 2 high points and fixed edges for the example analyses [USS15b]

Figure 88 shows the resulting membrane warp stress σ_w as the result of the structural analyses for the three sets of elastic constants of DO 1 to DO 3 (DO 3 is replaced by DO 5 for the curved structures, respectively)." [USS15b] Due to the circumstance that DO 2 in Table 10 is an unfeasible set of constants because the product of the

Poisson's ratios exceeds 1.0, the constants are replaced by numbers given by *Bridgens and Gosling* [BG10]: E_x = 752 kN/m, E_y = 611 kN/m, ν_{xy} = 0.88 and ν_{yx} = 1.08. For this set of elastic constants, the product of the Poisson's ratios is 0.95 and thus just within the limit. These values are obtained from the same material, albeit from another batch.

"In fact, the analyses have not only been conducted for these fixed sets of elastic constants but were combined with sensitivity analyses of the Poisson's ratio: while the tensile stiffnesses E_x and E_y of DO 1 to DO 3 and DO 5 have been hold constant the Poisson's ratio ν_{xy} has been varied during the analyses. In this way the huge impact of a high Poisson's ratio can be illustrated in warp stress (σ_w)-Poisson's ratio (ν_{xy})-diagrams as done in Figure 88. The stress resulting for the one Poisson's ratio ν_{xy} associated with a respective set of elastic constants from DO 1 to DO 3 and DO 5 is marked on the curves in the diagrams. Thus the stress values linked to the fixed sets of elastic constants of Table 10 can easily be observed. The stress σ_w is always extracted from the middle of the membrane, although the maximum stress occurs sometimes at other locations.

In the plane structure, the set of constants of DO 1 results in σ_w = 12.3 kN/m while DO 2 results with σ_w = 22.5 kN/m in an over 80% greater stress value, although the tensile moduli are considerable smaller. The reason can immediately be identified in the σ_w -ν_{xy} -diagram as the influence of the high value of Poisson's ratio ν_{xy}. In the curved structures with h = 2.0 m and h = 4.0 m the set of elastic constants from DO 2 results in 60%-75% greater stresses compared to the results from DO 1. The results of DO 3 (plane structure) and DO 5 (curved structures) lay in between.

On the one hand, it can be seen from the curves closing ranks that with increasing curvature of the structure the influence of the material stiffness parameters decrease. But on the other hand, the concrete sets of elastic constants demonstrate their enormous importance, especially the high magnitudes of Poisson's ratios. This emphasises the role of Poisson's ratio as part of a whole set of elastic constants. A comparison or assessment only of the tensile moduli – as done sometimes – is not sufficient.

Figure 89 shows the influence of the spectrum of fictitious elastic constants on the deflection results. The images represent a section through one of the diagonal symmetry axes of the structures in order to allow for a clear differentiation between the reference geometry (represented by the net) and the deformed geometry (represented by the grey shaded surface). In the plane structure max f_z varies between 20 cm (DO 2) and 39 cm (DO 1 and 3), which is a variation of almost factor 2. For the curved structures, the deflections decrease considerably as expected. But the results also show a variation of 60%-70%. That means, that the deflections may possibly be underestimated by a factor of up to 2, which can lead to damages of the membrane in case of hitting the primary structure.

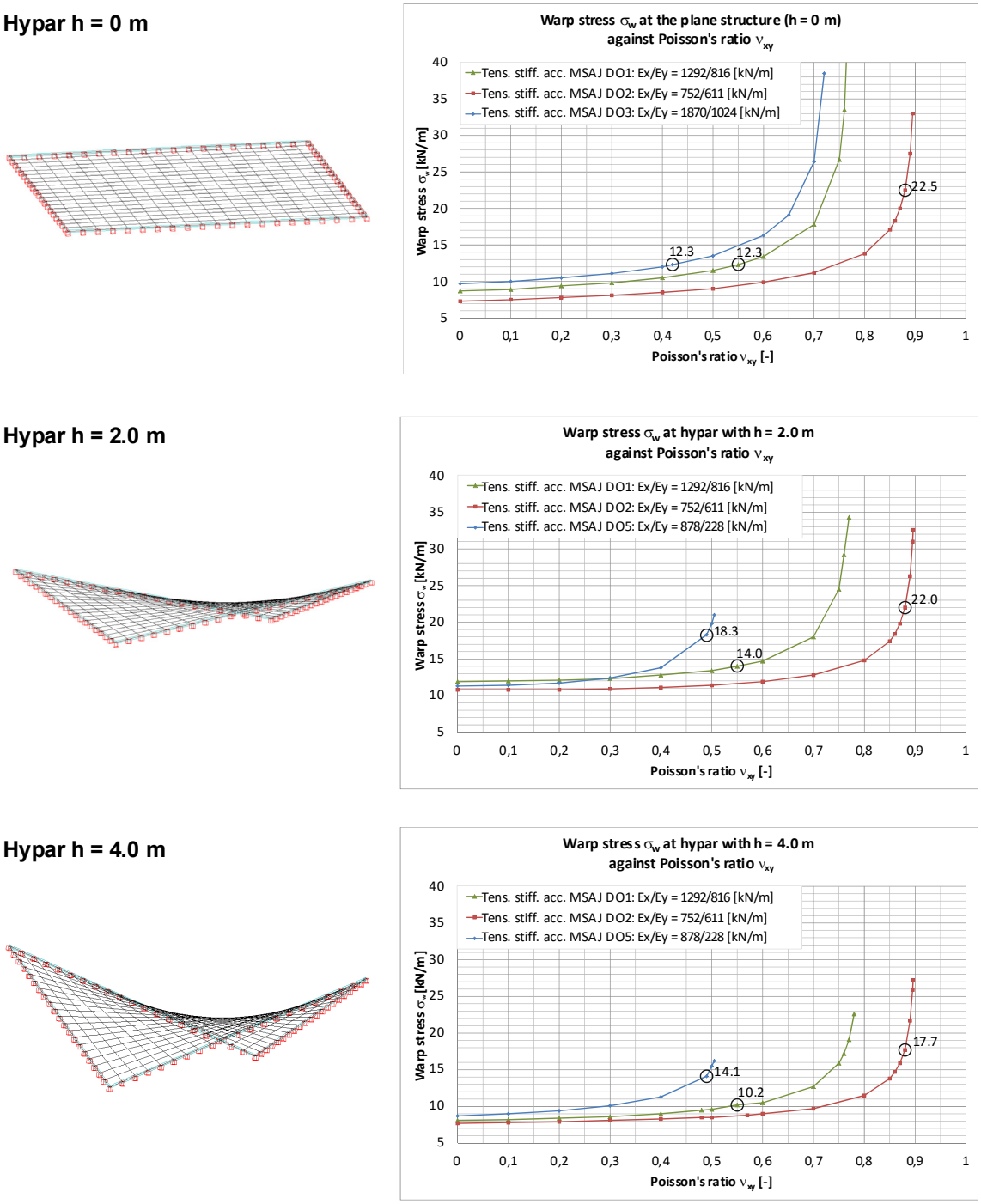

Figure 88 Warp stress σ_w in the middle of hypar structures with three different curvatures obtained with three different sets of elastic constants from Table 10 [USS15b]

This exemplary structural analysis demonstrates the immense range of stress and deflection results due to a great variety of fictitious elastic constants that could be used by design engineers for one and the same material product. None of the underlying determination options is validated by static load tests on curved structural components, which means that the real stresses and deflections are left unknown to the engineer.” [USS15b]

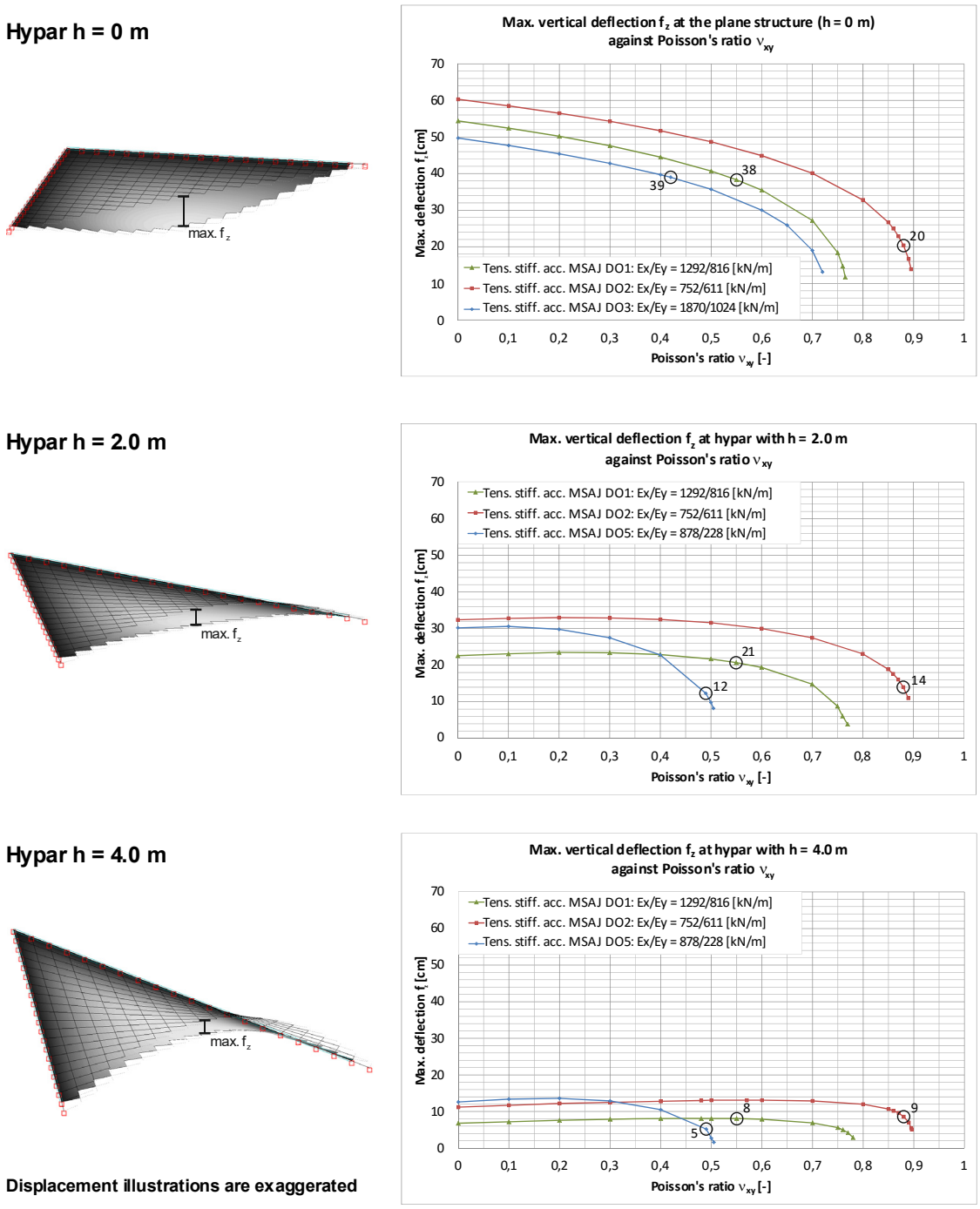

Figure 89 Maximum deflection f_z at the centre of hypar structures with three different curvatures obtained with three different sets of elastic constants from Table 10 [USS15b]

The stresses and deflections under determination option 2, which considers all ten MSAJ stress-strain paths for evaluation, appears to be out of the ordinary, particularly with regard to the plane structure, see e. g. Figure 88. This impression becomes even stronger for the barrel vault structure investigated in [US13], where the DO 2 results clearly stand out from all other stresses, independently of the curvature. This alone is not evidence of inaccuracy. However, remembering the considerable mismatch of most of the ten stress-strain paths leads to the suggestion that the results obtained with this set of elastic constants are not reliable. Furthermore, it operates in the boundary area of the mechanical restrictions in terms

of Poisson's ratio. The high product $\nu_{xy} \cdot \nu_{yx}$ approaching the limit of 1.0 apparently leads to artificially high and therefore unreliable membrane stress.

However, even if the results from this determination option are disregarded, the stresses still exhibit great variation of up to approximately 40%, see the marked stresses under DO 1 and DO 5 for the curved structures in Figure 88. For DO 1 and DO 5, a similar case applies as just mentioned for DO 2: only a partly good fit is achieved between measured and calculated stress-strain paths. Additionally, DO 5 also exhibits a quite high product of Poisson's ratios. This means that at least for the curved versions of the structure – the main concern of these arguments – the unlimited reliability of the FE results is questionable.

7.7 Conclusions

Evidence has been provided that elastic constants obtained from uniaxial tensile tests are unsuitable as elastic constants for design purposes. In fact, biaxial test procedures together with complementary evaluation procedures are required. Only both components together can ensure proper determination of stiffness parameters.

Four procedures have been found worldwide that combine both test and evaluation procedures: the Japanese test standard MSAJ/M-02-1995, the TensiNet Design Guide, the French Recommendations and the US-American design standard ASCE-SEI 55-10. They have been critically analysed and discussed. The approaches in terms of biaxial test protocols and evaluation procedures are very different and can hardly be compared directly.

Most biaxial test methods vary the stress while keeping the stress ratio constant: MSAJ/M-02-1995 (and accordingly ASCE-SEI 55-10) and the French Recommendations. Only the TensiNet Design Guide procedure keeps the stress constant in one main fabric direction while processing the stress in the transverse direction.

The handling of prestress and recovery times in the biaxial test protocol is very different. The Japanese standard disregards prestress (but subsequently considers it in the evaluation procedure) and the French Recommendations use it as an initial conditioning of the fabric but disregard it in the main test section which delivers the stress-strain paths to be evaluated. Only the TensiNet Design Guide provides for a continuous prestress level during the test. Recovery times are also only considered by the TensiNet Design Guide procedure.

The number of five load cycles is sufficient in the French Recommendations and the TensiNet Design Guide procedure. Only one load cycle as defined in the MSAJ test protocol is insufficient considering that the evaluated elastic constants are to be applied combined with the nominal prestress as is the usual procedure in membrane structure analysis.

None of the procedures provides high precision elastic constants in all design situations. In some circumstances the modelling ability was acceptable, such as for MSAJ with synclastic structures and for TensiNet Design Guide with anticlastic structures combined with PES-PVC fabrics. In other cases the modelling ability has proved to be rather poor.

While MSAJ, French Recommendations and ASCE are rather limited to synclastic structures, the TensiNet Design Guide procedure is limited to anticlastic structures. Furthermore, the TensiNet Design Guide procedure is clearly limited to PES-PVC fabrics. Completely unfeasible elastic constants are obtained from it for glass-PTFE fabrics.

None of the procedures is validated with static load tests on spatially curved membrane components.

An example application of differently determined sets of elastic constants for one and the same material to a simple hypar structure with different magnitudes of curvature revealed a large amount of variation for stresses and deflections. This reflects the uncertainty the design engineer has been left with to date. The identified deficits of state-of-the-art procedures emphasise the urgent need for further development.

8 Refined biaxial test and evaluation procedures

8.1 General

The goal of the present work is to develop principles for biaxial test protocols and correlated evaluation strategies rather than finalised procedures. The aim of the methods to be developed is to determine suitable sets of elastic constants as input stiffness parameters in the structural design, termed design elastic constants hereafter. The term suitable design elastic constants is understood in this context as elastic constants that lead to a clearly safe design which is as economical as possible. Safe design means

- not to underestimate the membrane stress in the ultimate limit state and
- not to underestimate the membrane deflection in the serviceability limit state,

whereas economical design means

- not to overestimate the membrane stress in the ultimate limit state and
- not to overestimate the membrane deflection in the serviceability limit state.

Any approach should satisfy these restraints as well as possible. The above listed contrasting demands can be approached with design elastic constants that are specifically determined for the structure to be verified – and in the case of anticlastic structures additionally for a specific load case to be verified.

Design elastic constants are supposed to model the stress-strain behaviour in the working stress range of a membrane structure, i. e. for the stress increments $\Delta\sigma$ between the prestress level and max σ under an external load. The objective of the biaxial test protocols developed for this purpose is to simulate as realistically possible stress increments in a specific structure for the decisive load cases. This includes simulating the prestress situation as proposed e. g. by [BBN04]. Thus, it is the stress increment $\Delta\sigma$ that is of importance rather than the stress level max σ and – presuming x and y are the main structural directions – it is consequently rather the stress increment ratio $\Delta\sigma_x/\Delta\sigma_y$ than the stress ratios σ_x/σ_y as traditionally used, see e. g. [RM79], [Me95].

It was demonstrated in Chapter 6 that coated woven fabrics behave in a fairly linear and elastic manner when they reach a stable state for a specific stress ratio. In the stable state the yarn crimp of both warp and fill has firmly adjusted to the applied stress ratio. The analysis of the biaxial procedure of [BBN04] in Chapter 7 proved that this is also true for load cycles with no fixed stress ratio.

Within the frame of the static verification of a fabric structure, only the states of maximum stress and maximum deflection are of interest. The objective must be to approximate a set of elastic constants that optimally fit the secants of the decisive stress-strain paths in the working stress range. A secant provides an exact prediction

of the strain increment for a given stress increment, see Figure 90 for a general illustration. Differences between the secant and a not perfectly linear stress-strain path on stress levels other than the decisive maximum stress level max σ have no relevance. Furthermore, it is not of interest whether a structure will ever really experience the maximum stress level that results from the static verification. The only objective is to ensure safety in the event of loads as supplied by the respective standards such as [EN 1991-1-4]. Thus, elastic constants determination must be orientated towards the maximum stress level of the static verification.

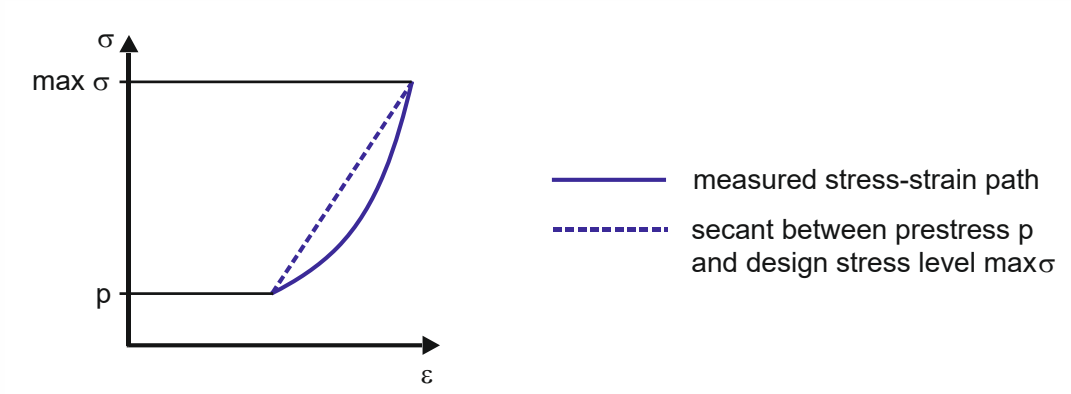

Figure 90 Secant as exact prediction of the strain increment for a predefined stress increment

Strictly speaking, the above statements are only valid for the particular location in the membrane surface which is exposed to the maximum stress, termed the characteristic location within this work. All other locations exhibit different stress levels and might also exhibit different stress ratios or stress increment ratios, see Figure 11 for an example map of stress increments and stress ratios. Depending on the specific structure, the extent of regions which do not match with the stress increments and the stress increment ratio of the characteristic location can be small or large. However, it is presumed that the stress-strain relations at the characteristic location are the important ones to model in order to achieve a suitable approximation of the overall stiffness behaviour of the membrane. If this is doubted for a specific structure it is recommended to model those areas of the membrane with significantly different stiffness behaviour with separate material models, each associated with a particular and appropriate set of elastic constants.

Anticlastic and synclastic or plane structures exhibit very different structural behaviour with different stress developments under external load. Consequently, determination procedures are developed separately for anticlastic and synclastic/plane structures, see Figure 91.

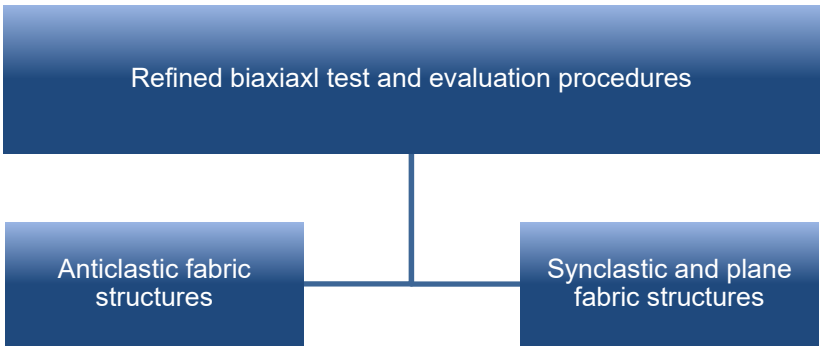

Figure 91 Development of separate biaxial test and evaluation procedures for anticlastic and synclastic/plane fabric structures

In Chapter 6 it was stated that the occurrence of the nominal prestress is closely linked to the stable state of the fabric in which this prestress value can be seen as enduring. When the nominal prestress is used in the form-found structural model – as is common practice in membrane structure analysis – the application of stiffness parameters of the stable state of the fabric is the only correct way to achieve consistent analysis results. Figure 92 illustrates this principle. In actual fact, the membrane stress can be expected to be slightly higher during the first load cycles than in the stable state. This was clearly demonstrated in the orthogonally loaded strip tests, see Chapter 6.3. But the slightly higher initial membrane stress is covered by long-term strength reduction factors which in practical terms mean an additional safety margin in the beginning of the structure. Thus a safe and simultaneously economical verification of the architectural fabric is ensured. The deflections also settle at a steady level in the stable state and hence can be well predicted.

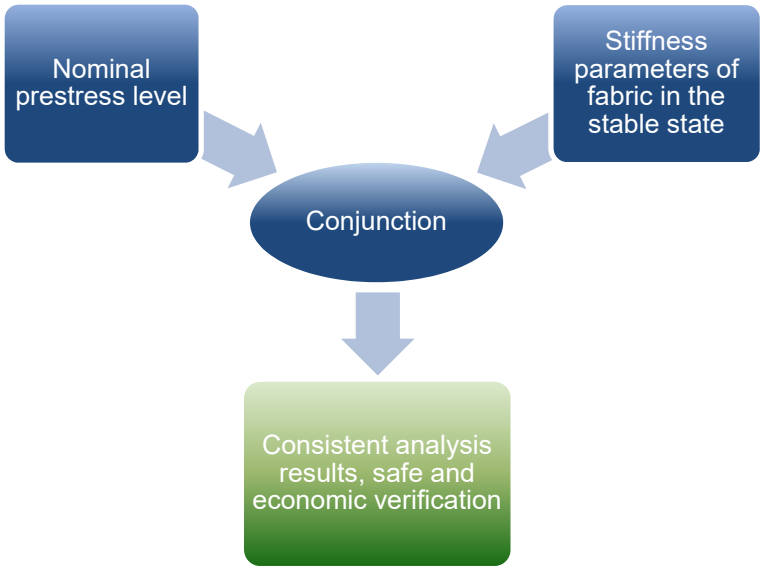

Figure 92 Interaction of prestress level and state of the fabric that vary over the load cycle number

Another reason to model the stable state instead of the stress-strain response due to initial loading is simply that the strain is smaller for this case and – most significantly – small enough to satisfy the definition of “small strain” according to the theory of

elasticity, see Chapter 4.4. In the initial state, the strain to be modelled could be approximately twice the size, see Chapter 6.2.2.

For the present work, it is presumed in general that the compensation planning is conducted in such a way that the nominal prestress is reached when the fabric has reached its stable state. This means that an enduring state of the structure is achieved and the structural behaviour can reasonably be simplified as elastic – keeping in mind that it is actually still viscoelastic.

For design purposes, biaxial test and evaluation procedures must be adaptable to individual structural requirements. For this reason, the developed procedures are first and foremost composed as a conceptual framework. The design engineer is expected to define the input parameters. However, numerical recommendations are presented to enable a useful approach in the event that no specifications are provided.

The new procedures make it possible to suitably model the crucial parts of the stress-strain paths and thus lead to an improvement of the precision of structural analysis compared to the established methods discussed in Chapter 7.

8.2 Cable analogy

The tensile deformation of spiral strands and full locked cables – both of which are used with membrane structures – is characterised by non-elastic and elastic deformation. The non-elastic part of the deformation is very pronounced during the first loading of the virgin cable. The residual strain after unloading is called the “constructional stretch”. During the first load cycles, the individual wires of the cables align themselves. The more this process draws to a close the more the force-elongation behaviour stabilises. Eventually it becomes reproducible and predictable. This behaviour resembles very much that of twisted yarns and woven fabrics.

In order to determine the stiffness of a steel cable, several load cycles are applied to eliminate the constructional stretch. This leads to a stable tensile modulus. Eurocode 3 Part 1-11 is the code for the design of steel tension components [EN1993-1-11:2010]. In order to determine a stable tensile modulus this code demands an appropriate number of load cycles in general and recommends five load cycles as a minimum. Indeed, depending on the type of cable, it may take 10 to 30 load cycles to eliminate the constructional stretch [Pe13]. The tensile modulus E_Q for non-permanent loads, i. e. for the working stress range between permanent loads G+P and non-permanent loads Q, is determined as a secant modulus fitting the stress-strain path in a stress interval between σ_{inf} and σ_{sup}, calculated with the loads F_{inf} and F_{sup} and the metal cross-section area. The minimum and maximum loads F_{inf} and F_{sup} are defined as the smallest and largest cable force resulting from characteristic permanent and non-permanent loads. This procedure is illustrated in Figure 93 based on a stress-strain diagram presented in [Pe00].

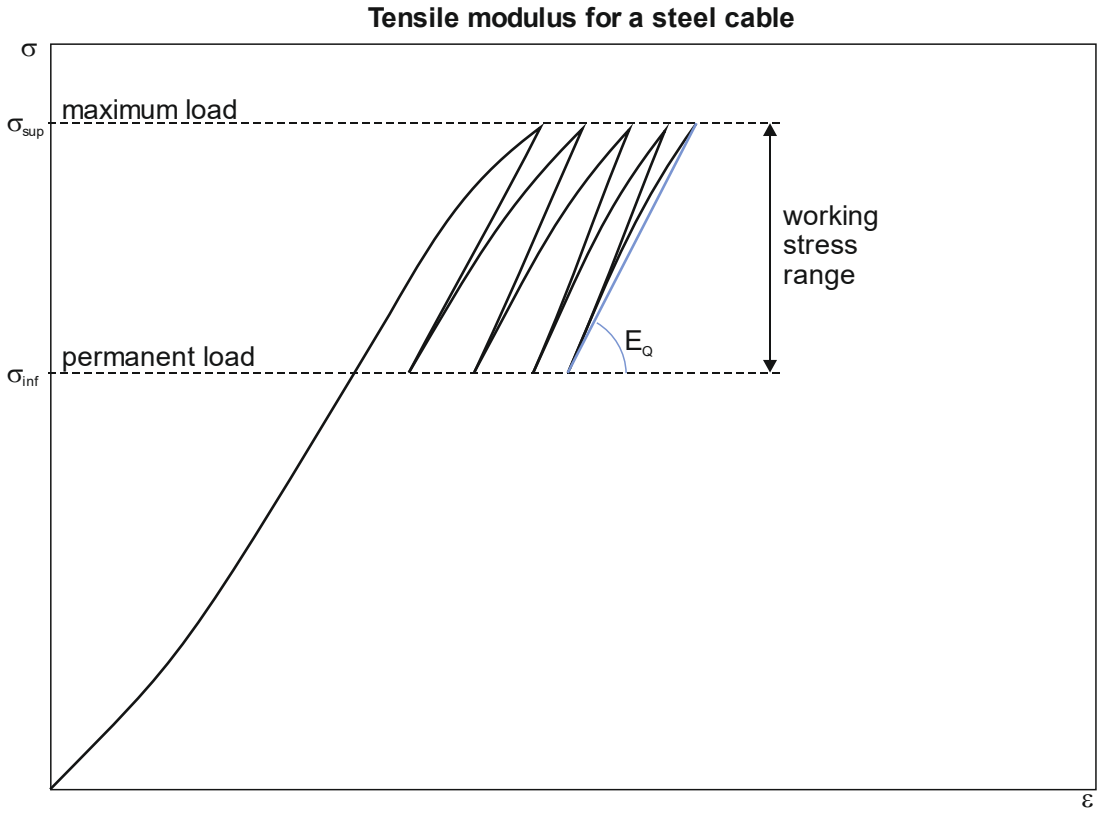

Figure 93 Secant tensile modulus E_Q for non-permanent loads that fits the stress-strain path of a steel cable in the fifth load cycle (schematic)

Cables are often custom-designed and manufactured. In spite of this, EN 1993-1-11 provides approximate values for the tensile modulus for different types of cables.

One difference to fabrics is that cables are often prestretched before installation. This means that the initial prestress level immediately after installation is not (significantly) higher than the nominal prestress level and the cable is (almost) in its stable state straight after installation. This is frequently not the case for structural fabrics. Nonetheless, the static verification for fabric structures must reasonably also be performed for the stable state, see descriptions above.

8.3 Anticlastic fabric structures

8.3.1 General

In anticlastic structures, different stress increment ratios apply for different external loading directions. The analyses of established determination procedures for elastic constants revealed that one single set of elastic constants does not fit several stress ratios with appropriate accuracy. Based on [USS11], it is established as a principle in this work to determine one set of elastic constants for each load or load combination in each of both main loading directions. The term “main loading directions” means for a horizontal or quasi horizontal roof structure downward loading on the one hand and upward loading on the other hand. These are typically snow or wind pressure on the one hand and wind suction on the other hand. In principle, the viscoelastic material response to long-term loads like snow can be simulated with an appropriate

viscoelastic material model in conjunction with linear-elastic parameters or, more simply, considered by means of an especially determined set of elastic constants. The biaxial test protocol proposed here only considers short-term loads. Long-term loads can be considered by applying creep coefficients k_{def} to the tensile moduli in warp and fill as proposed in Chapter 6.2.4.

Each of the two loading directions is linked to a specific stress increment ratio warp:fill in the characteristic location of the membrane surface, see Chapter 2.5. Consequently, this means that two sets of design elastic constants are usually required for the short-term wind loads: one for wind pressure and one for wind suction. This also requires a structural model for each loading situation, which is a disadvantage from a practical point of view. However, it makes it possible to model measured stress-strain paths much more accurately than with the existing approaches and it works for all common architectural fabrics at the same time. This is shown hereafter.

Negative strain increments can occur in anticlastic structures in the supporting direction. Consequently, Poisson's ratio should be considered in the set of design elastic constants to enable the modelling of negative strain increments [UKS13].

The refined biaxial test and evaluation procedure presented here distinguishes between the simulation of two load cases or correlated stress increment ratios respectively: one with warp stressing and one with fill stressing, assuming that warp and fill align with the main structural directions.

For each load case, one set of three independent design elastic constants must be determined, understanding that the application of the reciprocal relationship eq. (4.9) is required as a mechanical restriction. It thus follows that for each load case at least three stress-strain paths have to be provided for evaluation. To achieve this, two limiting stress increment ratios are simulated in the biaxial test. This provides four $\Delta\sigma$-$\Delta\varepsilon$ paths, one for warp and one for fill in each of the two stress increment ratios. The aim here is to optimally fit these four $\Delta\sigma$-$\Delta\varepsilon$ paths with the three independent design elastic constants. This can only be achieved with an approximation solution.

Linked to the nominal prestress level, design elastic constants are determined in the stable state of the fabric, see Chapter 6.3. The stable state is achieved to a sufficient extent in the fifth load cycle, see Chapter 6.2. For this reason, every stress increment ratio is scheduled five times. Moreover, it was shown in Chapter 6.2.5 that the stress-strain paths are largely independent of the previous load history when the stable state is reached. For that reason, the order of the single stress increment ratios in the test protocol does not matter.

It should be mentioned that in anticlastic structures a single nominal prestress level does not exist, not even in the stable state of the fabric. As a result of crimp interchange, the prestress level can be expected to exhibit certain "seesaw" changes

every time the loading direction on the structure changes, see Chapter 6.2.5. Nonetheless, for the definition of a biaxial test protocol it is considered that a stable nominal prestress level can be ensured by the compensation planning.

It is expected that all stress increment ratios between the limiting ones can be modelled with similar accuracy as for the two limiting stress increment ratios upon which the determination of the elastic constants is based. This means that the determined sets of elastic constants are expected to be appropriate for a certain field of the membrane surface and not only for the characteristic location. The better the limiting stress increment ratios can be narrowed down, the better all stress ratios inbetween can be expected to be modelled.

The stress ratio near corners usually approaches 1:1 also in anticlastic structures. This might not be modelled accurately with the determined sets of elastic constants. However, lower accuracy material modelling in locally limited corner regions is not expected to have a significant adverse influence on the overall stress and deflection results.

8.3.2 Biaxial tensile test protocol

8.3.2.1 Principles

For an anticlastic structure it can be presumed in the event of an external load that it is the carrying direction of the structure which is mainly activated, i. e. a considerable positive stress increment $\Delta\sigma_c = \max \sigma_c - p_c > 0$ starting from the nominal prestress level in the carrying direction p_c. This behaviour resembles very much that of the “one-dimensional” cables. The biaxial test protocol aims to simulate exactly this working stress range.

The simulation in the supporting direction aims to narrow the *in situ* stress development of the investigated fabric structure. The stress increment in the supporting direction $\Delta\sigma_s$, starting from the prestress level in the supporting direction p_s, can be covered with lower and upper expectable limits. It depends on the transverse strain properties of the fabric material on the one hand and on the strain ratio, which in turn depends on the ratio of curvature in the main structural directions, on the other, see Chapter 2.4. Thus, it cannot be given definitely prior to the structural analysis (and hence prior to the evaluation of the elastic constants), but lower and upper limits of the stress level in the supporting direction under external loads can be anticipated.

Given a material with no transverse strain, the stress in the supporting direction σ_s will diminish compared to the prestress level p_s due to the strain reduction in the supporting direction, see Figure 11. For an idealised structural design, σ_s equals zero precisely in the state of maximum stress in the carrying direction $\max \sigma_c$. This denotes a stress increment of $\Delta\sigma_s = -p_s$ and can be taken as the lower limit of the stress in the supporting direction. For a material with a certain amount of transverse

strain, the stress level σ_s can be supposed to be higher. In a first step, it may be assumed that no stress increment occurs, i. e. $\sigma_s = p_s$ and $\Delta\sigma_s = 0$. The distinction between these two limit cases implies two stress increment ratios in the biaxial test protocol: stress increment ratio 1 (abbreviated: SIR1) provides an anticipated upper limit of the stress in the supporting direction σ_s and stress increment ratio 2 (abbreviated: SIR2) provides the idealised lower limit.

These subsequently implemented two stress increment ratios can be recognised in Figure 94. The first begins after a hold time t_1 at prestress level. The testing of each stress increment ratio comprises five single load cycles. Four load cycles are scheduled for conditioning of the fabric to the applied stress increment ratio, and the fifth – the "solitaire" – is intended to deliver the stress-strain paths to be evaluated. To avoid artificial stiffening of the material, a recovery time t_2 is scheduled before the fifth load cycle, see Chapter 6.2.3; however, it is only scheduled before the fifth load cycle to shorten the biaxial test duration.

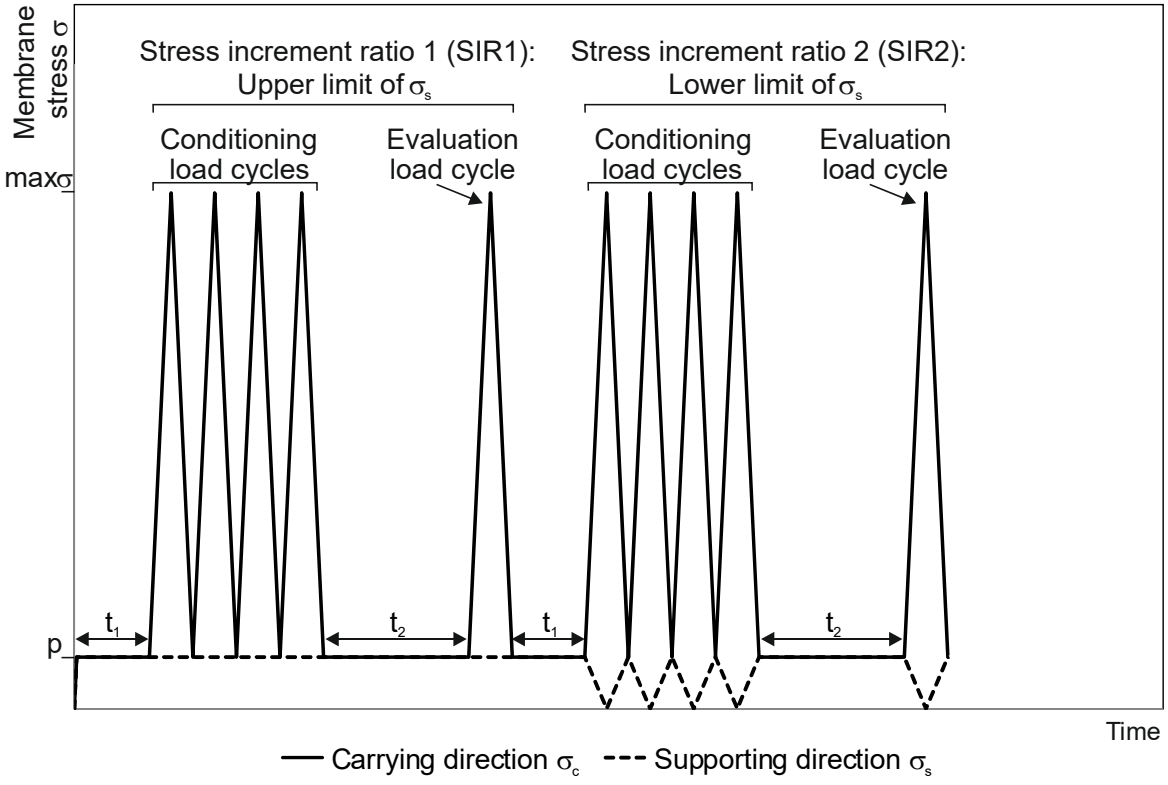

Figure 94 General biaxial test protocol for the determination of design elastic constants for anticlastic fabric structures

More precise limit levels for the supporting direction could be given by the design engineer or could be investigated by means of strain-controlled biaxial tests. In the event that an increase in stress in the supporting direction is expected due to high transverse strain of the material and/or small magnitude of curvature, see Chapter 2.4, the upper limit can be extended to a certain positive stress increment $\Delta\sigma_s > 0$.

Because a change of the external load direction leads in an anticlastic structure to a switch between carrying and supporting direction, the load history presented in

Figure 94 must be repeated for the second fabric main direction. The consequence is the complete load history illustrated in Figure 95. In the first test sequence the warp is considered the carrying direction, in the second sequence the fill. However, the order of warp and fill stressing could also be switched because the conditioning makes the stress-strain behaviour in the single test sequences sufficiently independent of the previous load history.

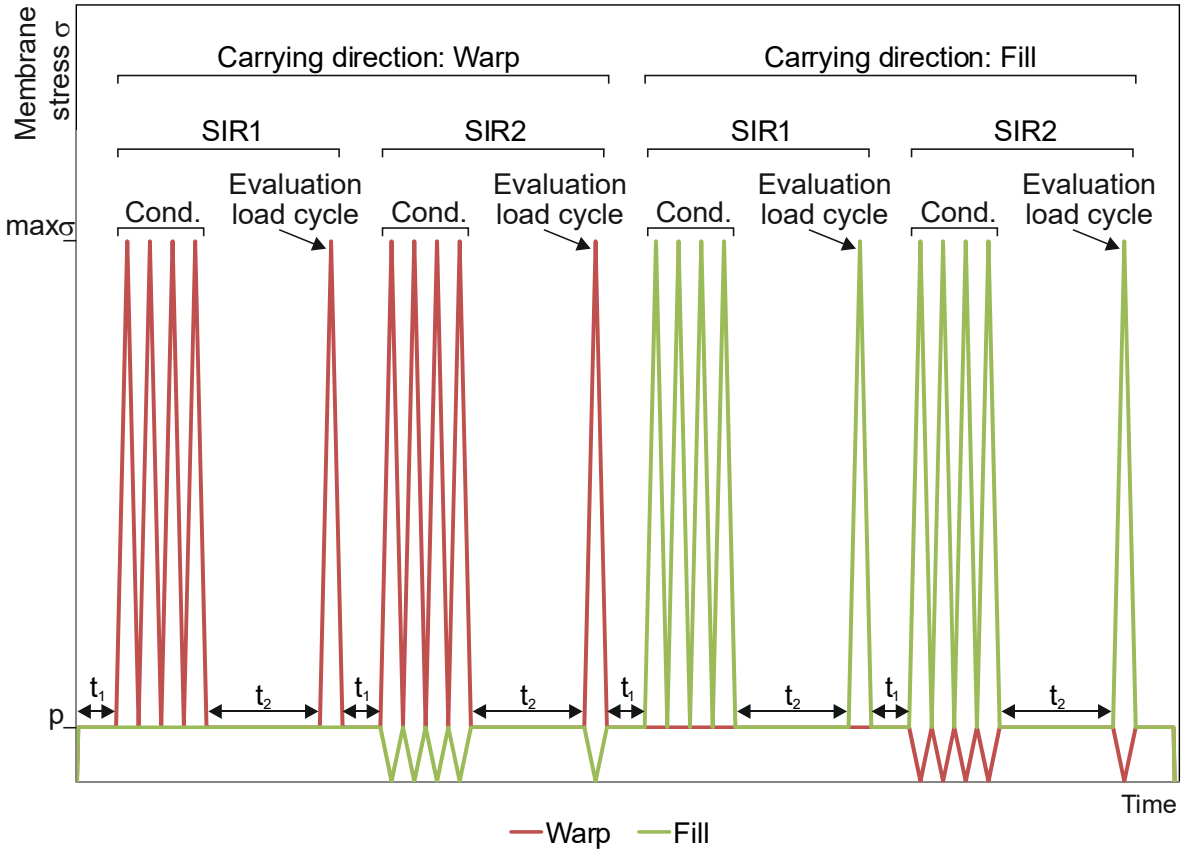

Figure 95 General biaxial test protocol for the determination of design elastic constants for anticlastic fabric structures, subsequently considering both fabric main directions as the carrying direction

The biaxial test procedure only considers short-term loading. However, in anticlastic structures, snow as a long-term load lasting for days to months is very likely to occur all across Europe. Snow as a load in gravitation direction either stresses the warp as the carrying direction or the fill. Long-term loads generate creep in the fabric, leading to an increase in deflection and curvature and correspondingly to a decrease in stress in the structure. This must be considered in the static verification to avoid unsafe deflection results. As found in Chapter 6.2.4, creep is linked to a decreased tensile modulus, while Poisson's ratio is not affected. In order to avoid biaxial long-term testing, it can be recommended to modify the biaxially determined "short-term" tensile moduli to tensile-creep moduli, using the creep coefficient k_{def}. The creep coefficient may be determined independently of the biaxial test in uniaxial creep tests separately in warp and fill according to [DIN EN ISO 899-1:2003]. Creep coefficients that were determined at room temperature can be applied safe-sided for the

deflection analysis, since it is well known that polymers experience greater creep at higher temperatures. The creep coefficient of the fabric direction that counts as the carrying direction for the long-term load should be used for modification. Note that the tensile moduli in both main fabric directions must be modified with the same creep coefficient in order to further satisfy the reciprocal relationship eq. (4.9). An example application is demonstrated in Chapter 8.3.4.

Strictly speaking, the creep coefficients must be applied to elastic constants that were determined from a biaxial test at low temperature T ≤ 0°C. This would consider the generally higher stiffness of architectural fabrics at low temperature compared to room temperature. The higher stiffness at low temperature and the reduced stiffness due to creep may possibly cancel each other out. This should be examined for the fabric to be investigated.

8.3.2.2 Numerical recommendations

The biaxial test protocol is open for adjustment by the design engineer. If not specified by the design engineer, however, the following numerical recommendations for stress levels and the duration of hold and recovery times are provided as a useful guide.

For economically favourable full utilisation of the material, the maximum stress in the carrying direction σ_c should meet or at least approach the design tensile strength. No uniform European code for the verification of fabric structures exists today. Adjusting the principles of [EN 1990:2002] to the requirements of membrane structures, the design tensile strength f_d is determined as $f_d = f_{k,23} / (\gamma_M \cdot k_{tot})$, where $f_{k,23}$ is the characteristic tensile strength (5% fractile) at room temperature T = 23 °C, γ_M is the safety factor on the resistance side and k_{tot} reflects the totality of several strength reduction factors that consider the physical reality of deterioration of synthetic and mostly organic membrane materials [SaP15]. Moreover, the safety factor on the action side γ_F could be considered in the present context regardless of whether it is actually applied on the action or resistance side. The product ($\gamma_F \cdot \gamma_M \cdot k_{tot}$) is also known as the stress factor.

A stress factor level of four is a usual magnitude; sometimes it is a little lower and sometimes higher depending on the code used and the specific design situation, see e. g. [PWB13], [Go13b], [USS14]. Applying this value, no more than 25 % of the characteristic tensile strength $f_{k,23}$ can be used for the static verification. Consequently, the maximum test stress in the carrying direction σ_c can be presumed to be 25 % of $f_{k,23}$. For reasons of simplicity, the tensile strength of the fabric direction with the lower tensile strength can be used with no major economic loss.

The prestress levels in the main structural directions as well as the duration of the hold times t_1 and t_2 can also be specified according to the project. If not otherwise specified, an isotropic prestress of 2.0 % of the mean tensile strength $f_{m,23}$ of the

fabric direction with the lower tensile strength can be recommended as a useful approach. It should be noted that (1) the prestress level is defined by the design engineer in order to fulfil structural and architectural requirements, primarily dependent on the magnitude of curvature, and (2) in general a material with higher magnitude of creep and relaxation should be subjected to higher prestress in order to prevent the fabric from going slack. Nonetheless, the recommendation for the prestress level reflects a quite usual magnitude, consistent with typical recommendations between 1.3 % and 2.5 % [FM04]. It can be taken as an initial guide, independently of the material.

If no measured tensile strength values are known to the user, the manufacturer's data – which reflect mean values – can be taken as an appropriate basis for defining the prestress and maximum test stress level.

The hold time t_1 at prestress level is a contribution to eliminate creep. However, as it is scheduled before the conditioning load cycles and, furthermore, the stress level is rather low, this hold time is not expected to have a significant influence on the stress-strain path of the solitary evaluation load cycle. Hence a short duration can be chosen. This hold time is rather good for structuring the test protocol since it highlights the prestress level.

The recovery time t_2 is of greater importance. The objective is to prevent artificial stiffening of the material as described in Chapter 6.2.3. The duration should be chosen such that revertive creep can (largely) finish in that time. In general, this depends on the material. However, tests with 60-minute recovery times showed that the revertive creep process was widely finished during this time span for all tested materials, see Chapter 6.2.2.

PES-PVC and glass-PTFE fabrics exhibit a moderate rate-dependency, see Chapter 3.5.2.1. A typical loading rate in force-controlled biaxial tests is 0.2 (kN/m)/s. In case different stress increments are scheduled in both fabric directions, as is the case in Figure 94, this rate is usually applied at the higher gradient.

8.3.3 Evaluation procedure

Regions which exhibit high stress in the carrying direction usually account for a relatively extensive area of the membrane surface under a decisive load or load combination, see Figure 11 for an example. Moreover, the high stress areas are also usually those which exhibit the largest deflections. It can be deduced from these circumstances that it is crucially important for accurate simulation to ensure good curve-fitting for the measured stress-strain paths particularly on a certain high stress level or interval.

Assuming the partial factor of the action side γ_F is applied on the resistance side by means of a stress factor, see explanations in the previous chapter and also the open discussion on this topic within the standardisation work [SaP15], the evaluation

stress level seems likely to be equated to the level of the maximum characteristic stress max σ_k. This is meant to be the decisive (maximum) stress – without partial factors – for the verification of the load-bearing capacity of the structural fabric according to [EN 1990:2002]. It appears at the characteristic location of the membrane, see Chapter 2.5. How good or bad the measured data are modelled e. g. on stress levels near the prestress can be presumed to have no noteworthy influence on the accuracy of the structural analysis. Consequently, the evaluation stress level σ_e is equated to the maximum characteristic stress max σ_k (and is intended to usually equal the maximum test stress max σ) and only the error on the evaluation stress level σ_e is evaluated, see Figure 96. Since the stress level for the evaluation is predefined, only the strain error can be calculated:

$$E_{\varepsilon,e} = \left|\varepsilon_m - \varepsilon_c\right| \tag{8.1}$$

where $E_{\varepsilon,e}$ is the strain error at evaluation stress level, ε_m is the measured strain on the evaluation stress level and ε_c is the calculated strain on the evaluation stress level.

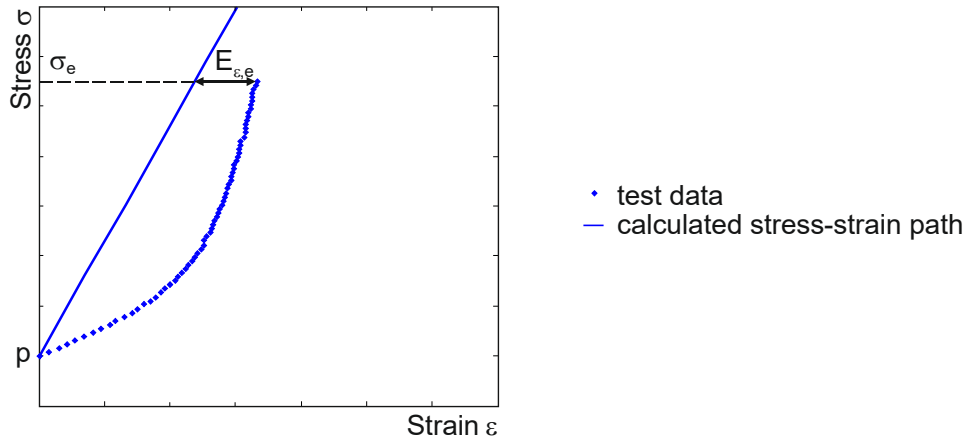

Figure 96 Strain error on the evaluation stress level

The maximum characteristic stress max σ_k must be anticipated by the design engineer. Bearing in mind the lightweight structures principle of full cross-section utilisation, the design strength level can alternatively be taken for the evaluation: $\sigma_e = f_{k,23} / (\gamma_F \cdot \gamma_M \cdot k_{tot})$, see the previous chapter. Either way, since the stress-strain behaviour of fabrics is fairly linear in the stable state of the material, the difference is not expected to be crucial. However, on the chosen evaluation stress level σ_e, the strain error between a measured strain and a calculated strain due to a specific set of elastic constants inserted in eq. (4.35) can be computed. Note that the strain and the stress in eq. (4.35) must actually be substituted by strain and stress increments between the prestress level and the chosen evaluation stress level. Finally, four errors $E_{\varepsilon,e,i}$ result, one for each measured stress-strain path in the two stress increment ratios. This is illustrated in Figure 97. To make the transverse strain paths

clearly visible, all strain is plotted against the major stress of a stress increment ratio, see Chapter 6.

The aim is to optimally match with the stress-strain relation on evaluation stress level for all four measured stress-stain paths. In order to avoid an exceptional poor fit of one of the four, the “minimax” method lends itself to application. “Minimax” means to minimise the maximum error: max $\{E_{\varepsilon,e,1}, E_{\varepsilon,e,2}, E_{\varepsilon,e,3}, E_{\varepsilon,e,4}\} \rightarrow$ min. Of course that increases the error for the other three paths, but this procedure ensures that the errors are distributed on all four paths and that none is fitted unduly poorly. Finally, this leads to a set of elastic constants that fits all four stress-strain paths with an – somewhat averaged – acceptable error magnitude.

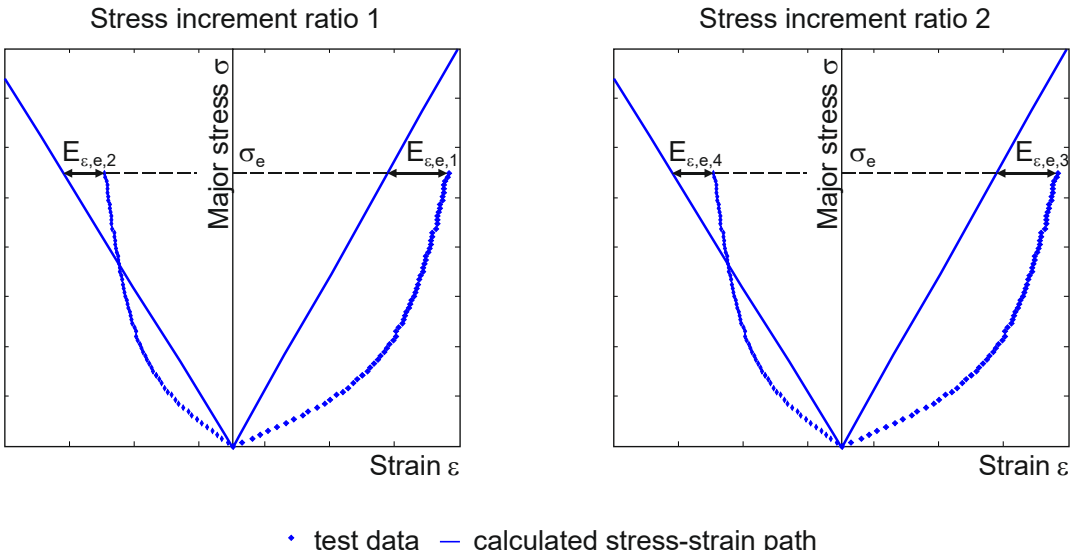

Figure 97 One strain error per stress-strain path

For the determination of the design elastic constants from biaxial test data according to the procedure in Chapter 8.3.2.1, a numerical correlation analysis routine was programmed using the commercial software MATLAB [ML14]. In order to set up straight stress-strain lines, the programmed routine generates all possible combinations of the three independent elastic constants within limit values and increments established by the user. The fourth constant is calculated via the reciprocal relationship eq. (4.9). Strain values are calculated at the evaluation stress level for each path according to eq. (4.35) inserting the generated constants. The difference between the calculated strain ε_c and the measured strain ε_m is computed for each of the four paths and the maximum error of the four is stored. Finally, when all possible combinations of elastic constants are evaluated, the set of elastic constants associated with the minimum of the stored maximum errors is picked. This set is assessed as the optimal set of design elastic constants.

A special case evaluation possibility appears when choosing $\Delta\sigma_s = 0$ for one of the limits (lower or upper) in the biaxial test protocol. This enables an easy approach to the elastic constants “by hand” through consecutive determination. For instance, if

warp is the carrying direction, i. e. $\Delta\sigma_c = \Delta\sigma_w = \Delta\sigma_x$, fill is the supporting direction, i. e. $\Delta\sigma_s = \Delta\sigma_f = \Delta\sigma_y = 0$ in stress increment ratio 1. The stress and strain increments of stress increment ratio 1 enable the tensile modulus E_x and the Poisson's ratio ν_{yx} to be determined:

$$\Delta\varepsilon_x = \frac{\Delta\sigma_x}{E_x} - \underbrace{\nu_{xy}\frac{\Delta\sigma_y}{E_y}}_{=0} \quad \Rightarrow \quad E_x = \frac{\Delta\sigma_x}{\Delta\varepsilon_x}, \tag{8.2}$$

$$\Delta\varepsilon_y = \underbrace{\frac{\Delta\sigma_y}{E_y}}_{=0} - \nu_{yx}\frac{\Delta\sigma_x}{E_x} \quad \Rightarrow \quad \nu_{yx} = -\frac{\Delta\varepsilon_y E_x}{\Delta\sigma_x}. \tag{8.3}$$

Knowing E_x and ν_{yx}, the tensile modulus E_y can be determined subsequently with the stress and strain increments of stress increment ratio 2 where $\Delta\sigma_s = \Delta\sigma_f = \Delta\sigma_y \neq 0$:

$$\Delta\varepsilon_y = \frac{\Delta\sigma_y}{E_y} - \nu_{yx}\frac{\Delta\sigma_x}{E_x} \quad \Rightarrow \quad E_y = \frac{\Delta\sigma_y}{\Delta\varepsilon_y + \nu_{yx}\dfrac{\Delta\sigma_x}{E_x}}. \tag{8.4}$$

Poisson's ratio ν_{xy} can finally be derived from the reciprocal relationship eq. (4.9), which ensures the symmetry of the compliance matrix:

$$\nu_{xy} = \nu_{yx} \cdot \frac{E_y}{E_x}. \tag{8.5}$$

Accordingly, for the evaluation of the stress-strain paths where fill is the carrying direction, the procedure begins with the determination of E_y and ν_{xy}, followed by E_x and ν_{yx}.

This procedure optimally fits three paths: the x- and y-paths in stress increment ratio 1 and the y-path in stress increment ratio 2. To what extent the x-path in stress increment ratio 2 is fitted depends on how much the material behaviour matches the restraint of the reciprocal relationship. Generally speaking, a considerable error may occur. However, experience shows that in many cases this approach leads to quite suitable results for the elastic constants which do not differ very much from the results of the minimax method.

8.3.4 Example application

Example application is done with plane cruciform test specimens with in-plane loading in the yarn parallel cruciform arms using the biaxial test rig in the Essen Laboratory for Lightweight Structures (ELLF) at the University of Duisburg-Essen. For the example tests and evaluations, one fabric from all three groups investigated is chosen: one PES-PVC fabric with traditional coating, one PES-PVC fabric with biaxially prestressed coating and one glass-PTFE fabric. In order to prove the feasibility of the developed procedure for all common architectural fabrics, those fabrics from each material group are picked out that exhibit the largest Poisson's

ratios according to Table 4. This is done because the investigations in Chapter 7 showed that this characteristic frequently leads to infeasible sets of elastic constants.

For all three biaxial tests the upper limit of $\Delta\sigma_s$ was chosen equal to zero and the lower limit $\Delta\sigma_s$ = -p. The numerical recommendations given in the previous chapter were applied: an isotropic prestress level of 2.0 % of the mean tensile strength $f_{m,23}$ measured according to [DIN EN ISO 1421:1998-08] was selected and rounded to an integer; the maximum test stress level max σ_c was set to 25 % of the characteristic tensile strength $f_{k,23}$ and rounded to an integer. The concrete values are summarised in Table 15. The hold time t_1 was always fixed to five minutes, the recovery time t_2 to 60 minutes. The stress-time plot for the glass-PTFE fabric is given as an example in Figure 98.

Table 15 Test stress levels for the investigated materials

Material group	**Material**	**Measured tensile strength [kN/m]**				**Derived test stress levels [kN/m]**	
		$f_{m,23}$		**$f_{k,23}$**		**p = 0.02·min $f_{m,23}$, rounded**	**max σ = 0.25·min $f_{k,23}$, rounded**
		Warp	**Fill**	**Warp**	**Fill**		
PES-PVC traditionally coated	Prod. 2, type V	208.7	188.8	198.4	176.4	4.0	44.0
PES-PVC biaxially prestressed coated	Prod. 4, type IV	169.1	144.2	164.3	135.8	3.0	34.0
Glass-PTFE	Prod. 5, type II	117.2	122.8	113.3	116.5	2.0	28.0

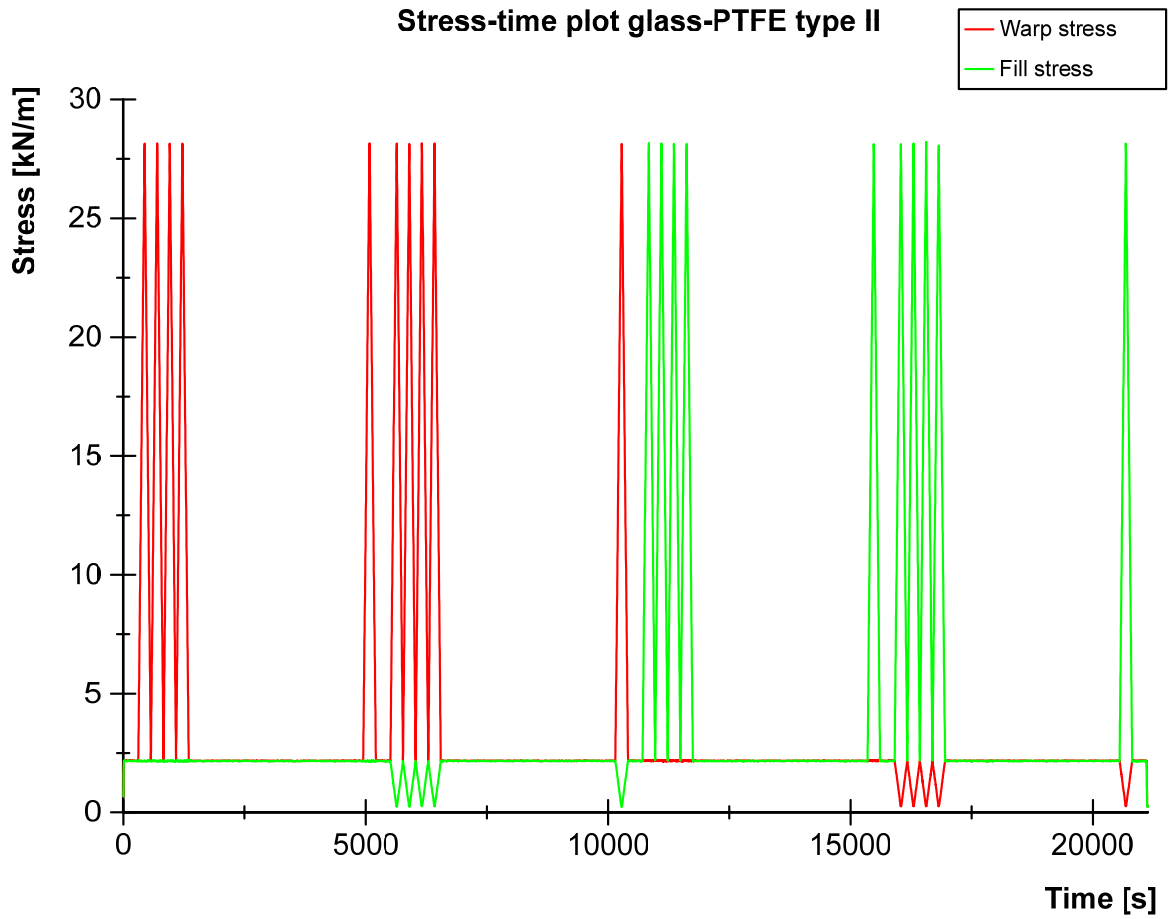

Figure 98 Example stress-time plot for the biaxial test on the glass-PTFE fabric type II

The four solitary stress-strain paths were evaluated using the programmed correlation analysis routine described in the previous chapter, employing the minimax method minimising the strain error max $E_{\varepsilon,e}$ at the user defined evaluation stress level σ_e. For the evaluation with this numerical routine, steps for the tensile moduli of ΔE = 5 kN/m and for the Poisson's ratio of $\Delta\nu$ = 0.01 were chosen. The resulting sets of design elastic constants and the associated straight stress-strain lines, as well as the correlation between them and the measured solitaire stress-strain paths, are presented separately for warp as the carrying direction and fill as the carrying direction in Figure 99, Figure 100 and Figure 101. The evaluation stress level σ_e is marked in each diagram with a horizontal dot-and-dashed line. As throughout this work, the strain is always plotted against the major stress of a stress increment ratio to make the transverse strain paths of the uniaxial stress increment ratios visible as curved paths instead of horizontal lines.

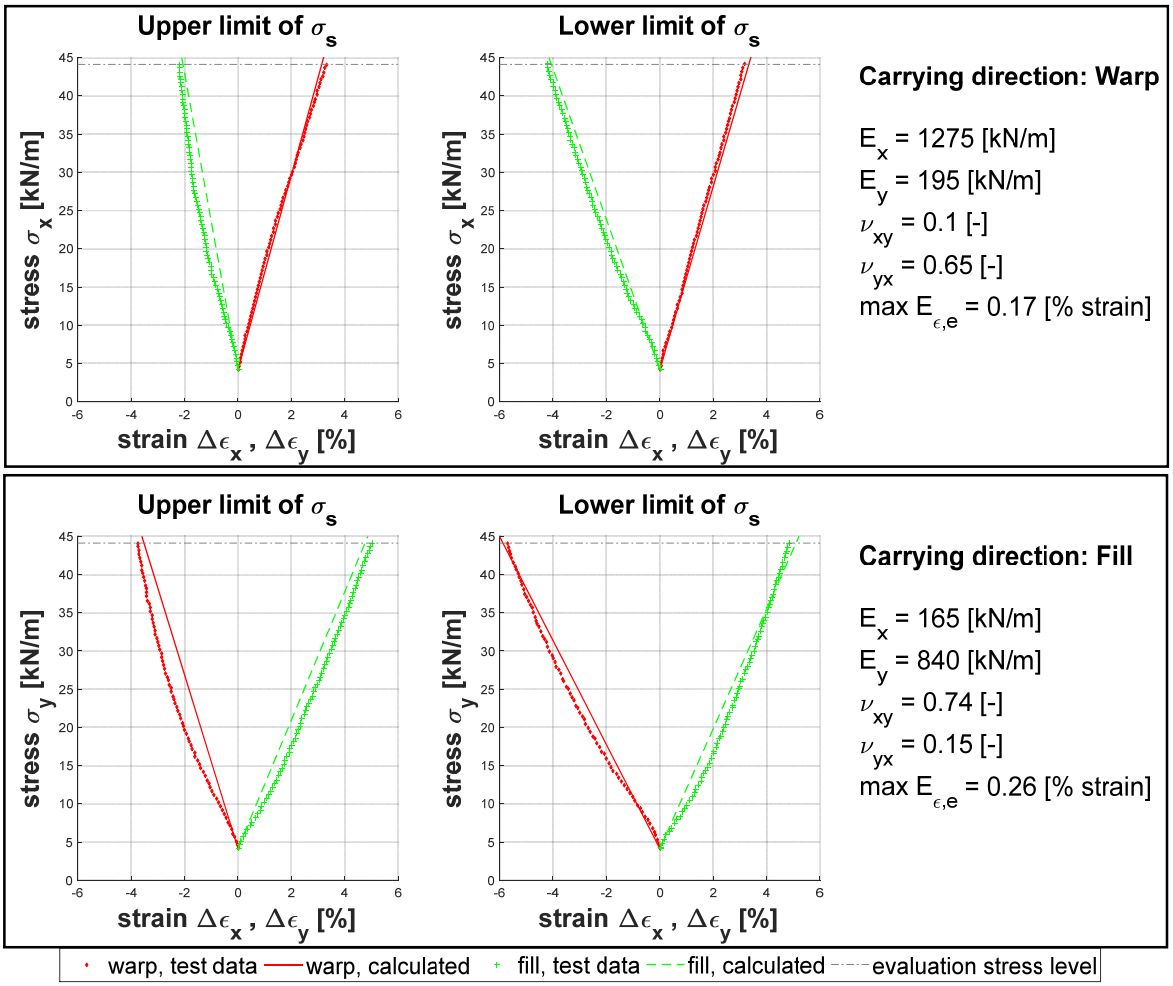

Figure 99 Comparison of measured stress-strain paths of traditionally coated PES-PVC fabric type V and calculated stress-strain paths resulting from the presented sets of elastic constants

For all investigated materials the calculated stress-strain paths fit the measured ones very well, particularly at the evaluation stress level σ_e. Overall, the maximum strain error at level σ_e is not greater than max $E_{\varepsilon,e}$ = 0.26% strain, which occurs for the traditionally coated PES-PVC fabric type V. This is a good approximation. The smallest deviation is min $E_{\varepsilon,e}$ = 0.02% strain, reached for the glass-PTFE fabric when warp is the carrying direction. The corresponding set of elastic constants represents an optimal fit. All measured stress-strain paths are fairly linear. The only exception appears for the paths for fill stressing of the glass-PTFE fabric, see Figure 101.

The results for the PES-PVC fabric with biaxially prestressed coating system are displayed in Figure 100. They illustrate that the property of approximately equal tensile moduli plays no role for modelling the behaviour in an anticlastic structure. The very large orthotropy ratio of the resulting set of design elastic constants enables large Poisson's ratios, e. g. ν_{yx} = 0.78 during warp stressing. This can be used for modelling the large transverse strain typical of woven fabric.

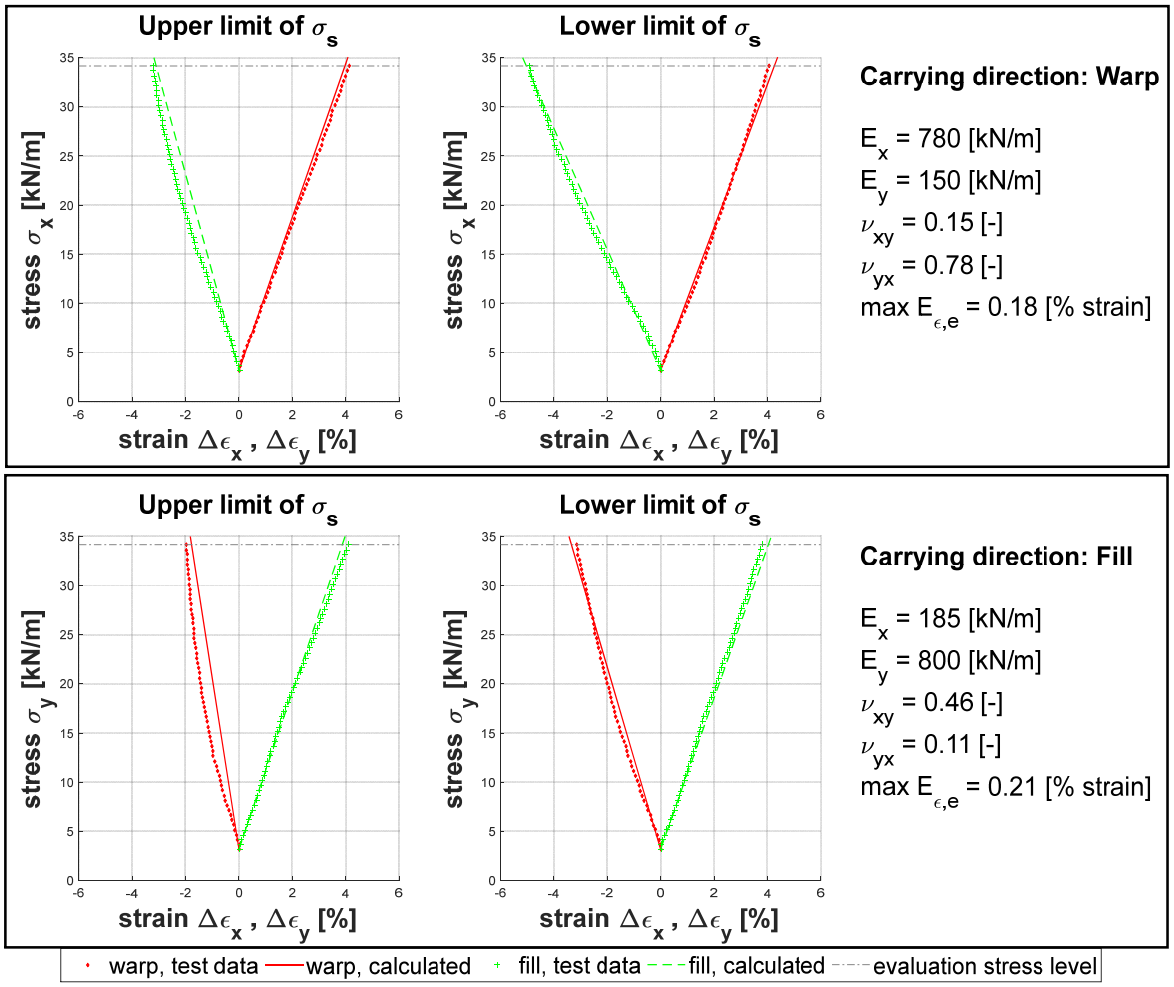

Figure 100 Comparison of measured stress-strain paths of PES-PVC fabric type IV with biaxially prestressed coating system and calculated stress-strain paths resulting from the presented sets of elastic constants

This becomes particularly clear for the glass-PTFE fabric: when warp is the carrying direction, the large orthotropy ratio E_x/E_y permits the large Poisson's ratio ν_{yx} = 1.98, much greater than one, without contravening the mechanical restrictions. This set of elastic constants is thus able to model the large contraction transverse to the carrying direction. This applies analogously when fill is the carrying direction. This fact proves quite clearly that linear elastic constitutive law is a suitable approach for modelling woven fabric provided that warp and fill stressing are handled separately.

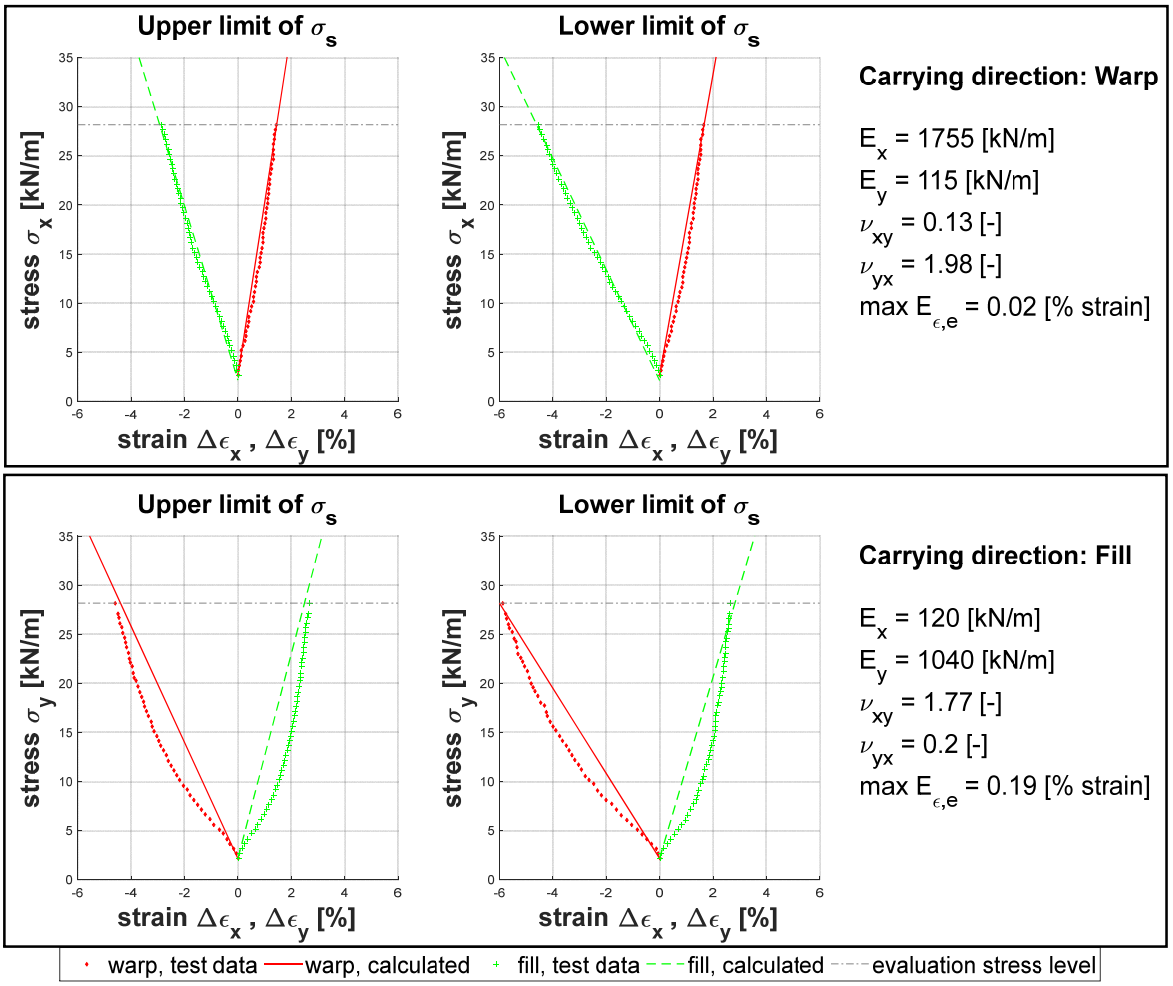

Figure 101 Comparison of measured stress-strain paths of glass-PTFE fabric type II and calculated stress-strain paths resulting from the presented sets of elastic constants

Table 16 summarises the resulting sets of design elastic constants and demonstrates that the mechanical restriction eq. (4.37) is satisfied for every set. The maximum value is $\nu_{xy} \cdot \nu_{yx} = 0.35 << 1$. This allows reliable analysis results. The given sets of elastic constants are indeed intended for design purposes, but note that to maintain accuracy they are valid only for the underlying boundary conditions such as the predefined stress levels given in Table 15, durations for t_1 and t_2 of 5 min. and 60 min., and for short-term loading approximately at room temperature. The last condition explicitly includes maximum wind loads which typically occur at approximately T = 15°C in central Europe. As the “investigated structure” was not further specified, the evaluation stress level was always chosen generally as $\sigma_e = \max \sigma = 0.25 \cdot f_{k,23}$.

The evidence suggests that the developed procedure also works well for fabrics with less transverse strain properties. Hence it promises to function for all common architectural fabrics.

Table 16 Design elastic constants of the investigated materials for the test stress levels given in Table 15 and t_1 = 5 min. and t_2 = 60 min.

Carrying direction	Tensile modulus [kN/m]		Poisson's ratio [-]		$\nu_{xy} \cdot \nu_{yx}$
	E_x	E_y	ν_{xy}	ν_{yx}	
PES-PVC traditionally coated type V					
Warp	1275	195	0.10	0.65	0.07 < 1
Fill	165	840	0.74	0.15	0.11 < 1
PES-PVC biaxially prestressed coated type IV					
Warp	780	150	0.15	0.78	0.12 < 1
Fill	185	800	0.46	0.11	0.05 < 1
Glass-PTFE type II					
Warp	1755	115	0.13	1.98	0.26 < 1
Fill	120	1040	1.77	0.20	0.35 < 1

Up to now, the design elastic constants have only considered short-term loads since the biaxial test protocol disregarded long-term loading. Simplified, long-term loading can be regarded as applying the independently determined creep coefficients k_{def} to the tensile moduli. As an example, it is assumed that the investigated traditionally coated PES-PVC type V is used in an anticlastic membrane structure where the fill is the carrying direction for snow. It was shown in Chapter 6.2.4 that creep can be considered more simply by modifying the tensile modulus in the stressed direction to a tensile-creep modulus: $E_{creep} = E / (1+k_{def})$. For this example, a creep coefficient in fill direction with a magnitude of $k_{def} = 0.20$ is assumed. Thus, the fill tensile modulus E_y = 840 kN/m determined above can be modified to $E_{y,creep} = 840 / (1+0.20) = 700$ kN/m. If the corresponding tensile modulus in warp is also modified to $E_{x,creep} = 160 / (1+0.20) = 133$ kN/m, the reciprocal relationship eq. (4.9) is still satisfied: $\nu_{xy} / E_{y,creep} = 0.74 / 700 = 0.0011 = 0.14 / 133 = \nu_{yx} / E_{x,creep}$. This again produces a feasible set of design elastic constants.

Since $\Delta\sigma_s = 0$ in the test protocol presented in Figure 98, the measured stress-strain paths could alternatively be evaluated "by hand" as explained in Chapter 8.3.3. This must result in every case in three optimally fitted stress-strain paths, while the fourth obtains a certain strain error larger than that obtained by using the somewhat "averaging" minimax method. The resulting sets of elastic constants and the strain error of the fourth stress-strain path are summarised in Table 17. The sets of elastic constants consecutively determined "by hand" show no significant differences to those determined with the minimax method, see Table 16. This applies particularly for the glass-PTFE fabric type II while warp is the carrying direction. The reason is

that the material fully satisfies the reciprocal relationship for this stress state. However, the same can be stated with an acceptable level of accuracy for all other cases where this constraint is approximately satisfied. This can also be observed from the strain errors which are not much greater than those achieved with the minimax method. The “by hand” evaluation therefore appears to be a suitable evaluation tool for all common architectural fabrics.

Table 17 “By hand” evaluated design elastic constants of the investigated materials for the test stress levels given in Table 15 and t_1 = 5 min. and t_2 = 60 min.

Carrying direction	Tensile modulus [kN/m]		Poisson’s ratio [-]		$\nu_{xy} \cdot \nu_{yx}$	Strain error at the fourth path $E_{\varepsilon,e,4}$ [% strain]
	E_x	E_y	ν_{xy}	ν_{yx}		
PES-PVC traditionally coated type V						
Warp	1208	193	0.11	0.67	0.03 < 1	0.36
Fill	199	796	0.75	0.19	0.14 < 1	0.55
PES-PVC biaxially prestressed coated type IV						
Warp	750	171	0.18	0.78	0.14 < 1	0.35
Fill	252	759	0.49	0.16	0.08 < 1	0.46
Glass-PTFE type II						
Warp	1781	112	0.13	2.00	0.26 < 1	0.01
Fill	148	967	1.70	0.26	0.44 < 1	0.38

Lastly, an example application of a resulting set of elastic constants to a specific anticlastic structure is demonstrated. A glass-PTFE fabric type III is chosen for this example in order to be comparable to the FE results of the hypar structure in Chapter 7.6. A biaxial test was conducted according to the principles and numerical recommendations in the previous chapters. The numerical recommendations were employed in order to obtain an initial set of elastic constants for a preliminary structural analysis, based on the measured tensile strength values given in Table 3: prestress level p = 2.0 kN/m, max σ = 28.0 kN/m (both rounded to an integer), t_1 = 5 minutes and t_2 = 60 minutes. Evaluation of the measured stress-strain data yields two sets of elastic constants. They are presented in Figure 102. As previously for the glass-PTFE fabric type II, the resulting set of elastic constants for warp as the carrying direction leads to a perfect fit with a maximum strain error of only $E_{\varepsilon,e}$ = 0.04 % strain. It is important to remember that these sets of elastic constants correspond to the nominal prestress level in a structure.

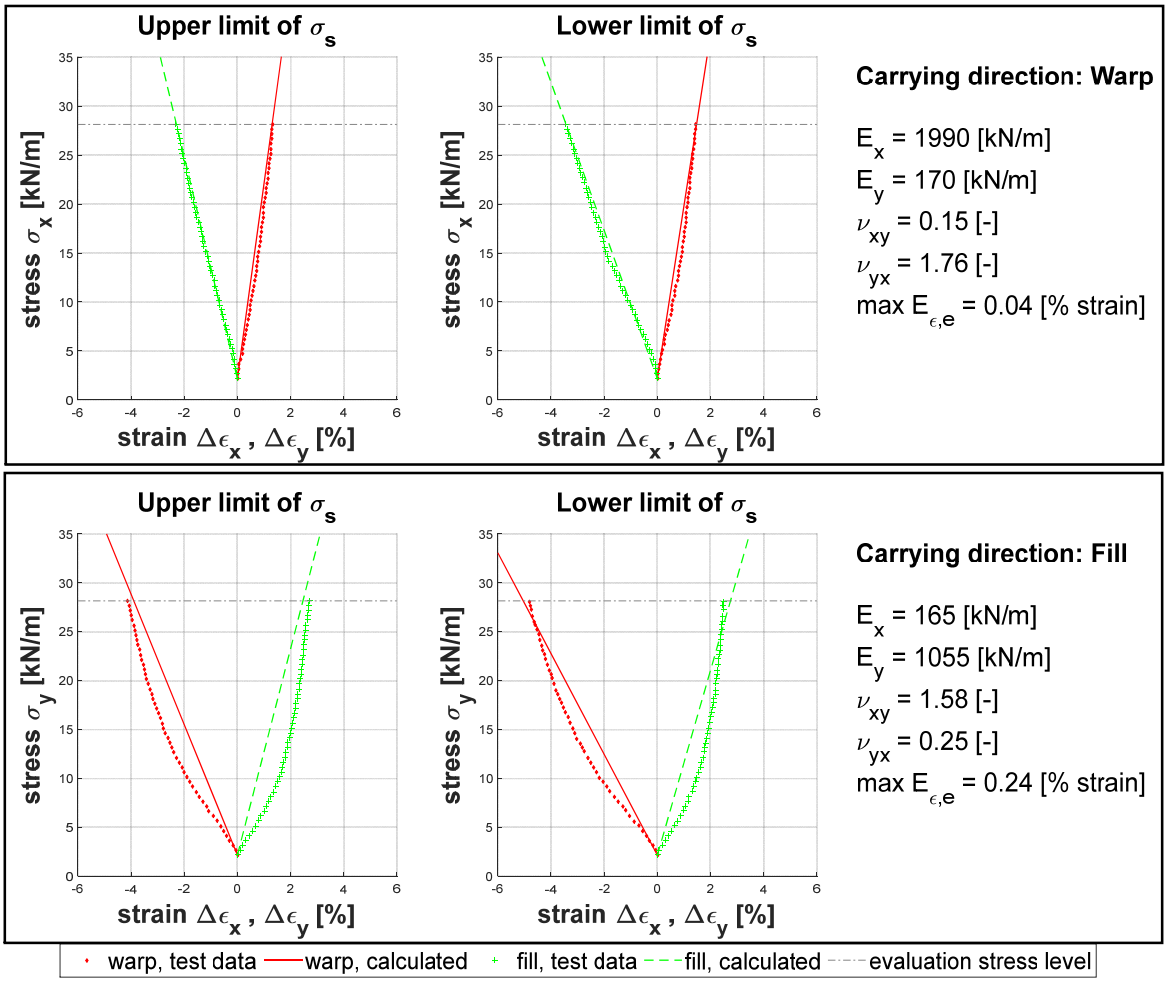

Figure 102 Comparison of measured stress-strain paths of glass-PTFE fabric type III and calculated stress-strain paths resulting from the presented sets of elastic constants

The hypar structure in Chapter 7.6 is investigated again for a snow load of q = 0.60 kN/m^2. This downward gravitational load stresses the warp direction of the fabric. The first set of elastic constants for warp as the carrying direction is therefore used. Two different degrees of curvature are examined corresponding to a height difference between low and high points of h = 2 m and h = 4 m. The nominal prestress is chosen again to be $p_x = p_y = 3.0$ kN/m. Results of the geometrically nonlinear finite element analysis are illustrated in Figure 103 in terms of stresses and Figure 104 in terms of deflections. Both Figures also repeat the results from the previously investigated sets of elastic constants for easy comparison.

The stress results conform very well with those obtained with the original MSAJ set of elastic constants (DO 1, see Table 10) – despite the very different approaches. Partly this can be traced back to two effects which cancel each other out: the MSAJ procedure leads to artificial stiffening since it omits recovery times in the test protocol, while the test protocol leads to “soft” stress-strain paths because only one (initial) load cycle is performed for each stress ratio (except for the stress ratio 1:1). In fact, this explanation applies for all three previously investigated determination options (DO 1 to DO 3 in the diagrams), which all are based on the MSAJ test

protocol. This means that the good conformance is actually rather a coincidence. This becomes particularly clear when considering that the zero-stress paths are entirely mismatched by the original MSAJ evaluation procedure – paths that can be presumed to play a significant role for the investigated anticlastic structure.

Hypar h = 2.0 m

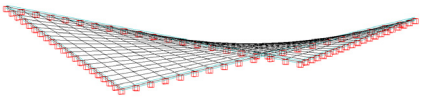

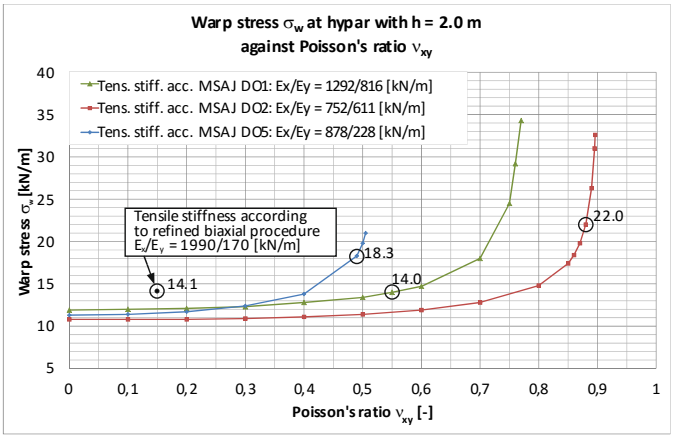

Hypar h = 4.0 m

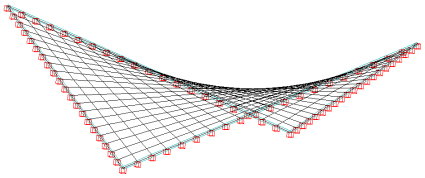

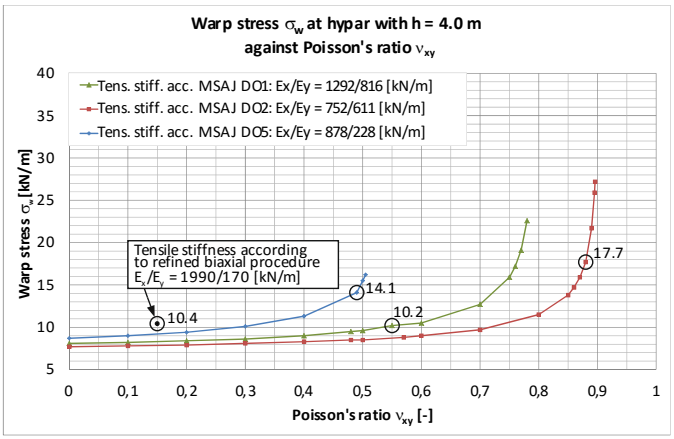

Figure 103 Warp stress σ_w at the centre of hypar structures with two different curvatures obtained for different sets of elastic constants for a glass-PTFE fabric type III (MSAJ determination options see Table 9)

The determination option with an evaluation of all ten MSAJ-stress-strain paths is still out of the ordinary, compare chapter 7.6.

Presuming that the good fit with the measured decisive stress-strain paths indicates that the FE results based on the elastic constants determined in the refined procedure are reliable, this means that the deflections are underestimated in determination option (DO) 4 by approximately 15 % to 25 %, depending on the structural curvature. Such an underestimation of deflections brings with it a probability of damage when the membrane hits the secondary structure or any other installed equipment. Simultaneously, the membrane stress is overestimated by approximately 30 %, which makes the design uneconomical.

Creep during the snow load is not considered in this example. Due to the creep process a slightly higher deflection and a slightly lower stress can be expected.

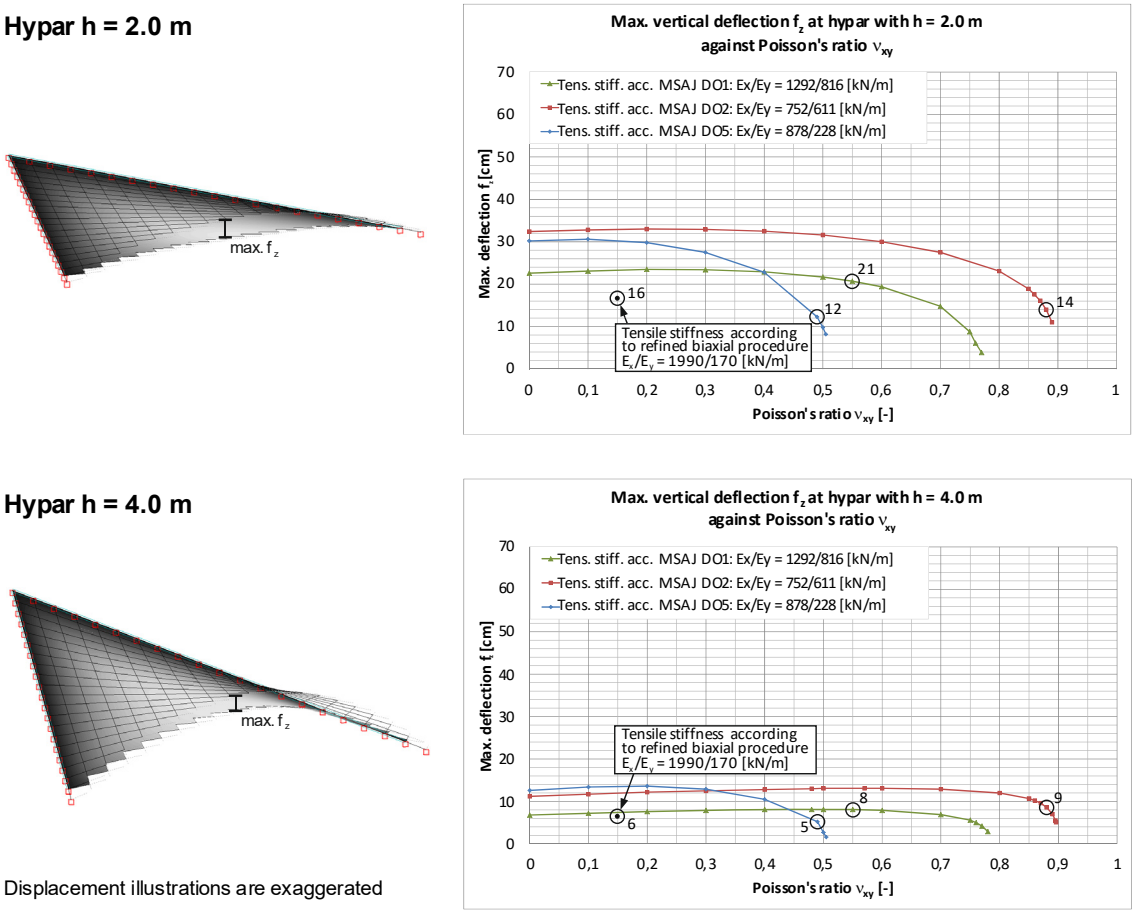

Figure 104 Maximum deflection f_z at the centre of hypar structures with two different curvatures obtained for different sets of elastic constants for a glass-PTFE fabric type III (MSAJ determination options see Table 9)

Since the measured stress-strain paths for warp as carrying direction are almost linear, see Figure 102, a repetition of the biaxial test (or only a repetition of the evaluation of the same test) with different stress levels (prestress and evaluation stress level) is unnecessary.

In contrast, for fill as carrying direction it might be worthwhile to evaluate the experimental test data once with an evaluation stress level equal to the anticipated maximum stress level of the examined structure. Due to the convex (stiffening) stress-strain response of the glass fibre fabric, lower tensile moduli can be expected for an evaluation stress level lower than the maximum test stress level chosen here at ¼ of the minor characteristic tensile strength. Considering uniform wind suction of $q = -1.0$ kN/m^2 normal to the membrane surface for the hypar structure above examined and using the lower set of elastic constants in Figure 102 for this loading situation leads to a maximum fill stress of max $\sigma_f = 16.0$ kN/m and a maximum deflection of $f_z = 17$ cm. Evaluating the stress-strain data in Figure 102 for fill as carrying direction only up to 16 kN/m leads to the following set of elastic constants: $E_x = 170$ kN/m, $E_y = 705$ kN/m, $\nu_{xy} = 1.47$ and $\nu_{yx} = 0.35$ with a maximum strain error of max $E_{\varepsilon,e} = 0.17$ % strain. Primarily, the tensile modulus in fill direction is

considerably lower than for the evaluation of the entire stress-strain data. This set of elastic constants yields a maximum fill stress of max σ_f = 15.6 kN/m, which is almost the same as the previous result, but the maximum deflection rises to f_z = 23 cm. Using the initial set of elastic constants for a preliminary analysis underestimates the deflection by approximately 25% in the investigated case. This cannot be ignored. Thus, it can be recommended to adjust the evaluation stress level to the anticipated maximum stress in any case in which the stress-strain paths are explicitly nonlinear in order to ensure most accurate results.

Experience with using the refined sets of design elastic constants in structural analyses shows that the computation time is reduced because equilibrium and convergence are reached earlier compared to sets of elastic constants according to [Me95] or [BBN04]. The analysis is also more robust.

Overall, the determined sets of design elastic constants proved to accurately model even challenging materials with large transverse strain properties. Therefore, structural analysis results based hereon appear to be a reliable approach. For the final proof, an experimental validation with spatially curved membrane components is recommended.

8.4 Synclastic and plane fabric structures

8.4.1 General

The structural behaviour of synclastic and plane structures under external loads is similar, since for plane membrane structures static equilibrium under an external load is only possible with development of a curved synclastic shape. However, a distinction must be made between mechanically and pneumatically prestressed structures. Plane structures are mechanically prestressed. They are used normally for facades or billboards and are usually avoided for roof structures because of the risk of snow and water ponds. For facades sometimes open mesh fabrics are used to minimise the area exposed to wind load. Often PES-PVC fabrics are used, particularly when the membrane is to be printed such as for billboards. Pneumatically prestressed structures related to fabrics are mainly air-supported domes, more rarely inflatable beams, and in single cases also cushions. Figure 105 illustrates some general forms and defines coordinates. Beside cylindrical domes, air-supported structures can also be constructed as hemispherical or even spherical forms, see Figure 2.

The membrane stresses to be expected depend very much on the aspect ratio, i. e. for a plane structure, for instance, on the ratio width to length.

For air-supported domes snow is not a critical load case, thus no long-term loads have to be considered. Plane structures are usually built as (almost) vertical structures to avoid snow loads and ponds resulting from snow and melting water. Thus usually no long-term loads have to be considered here either. It is only for

inflatable beams that long-term loads in general (not only snow) could be a reasonably possible load case. However, in the event that long-term loads appear as decisive loads for the static verification, they might be considered with the creep coefficient k_{def} applying the method described above for anticlastic structures.

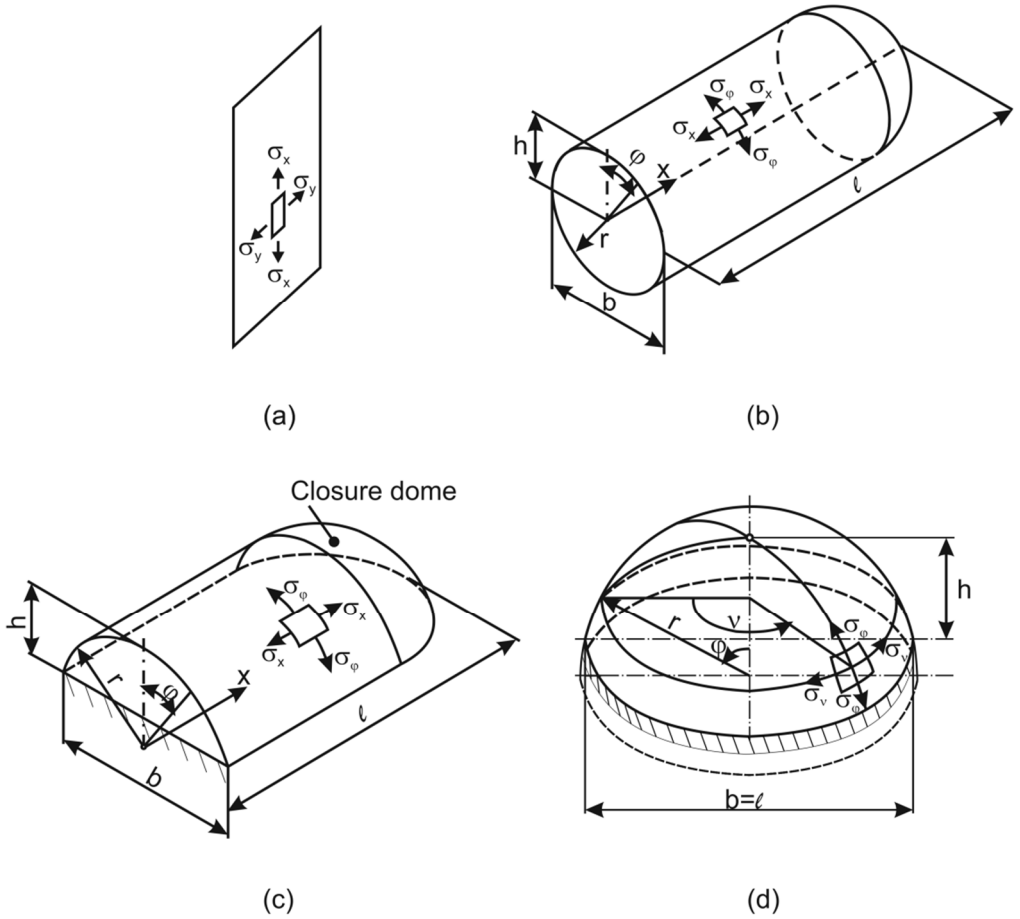

Figure 105 General forms and coordinates for plane/synclastic structures: plane structure (a), full cylindrical inflatable beam (b), air-supported dome [DIN 4134:1983] (c) and hemispherical dome [DIN 4134:1983] (d)

8.4.2 Biaxial tensile test protocol

8.4.2.1 Principles

The basic procedure is as follows:

- anticipate the stress increments in both principal structural directions and the corresponding stress increment ratio,
- encompass the estimated stress increment ratio with two boundary stress increment ratios.

Testing of two stress increment ratios in the biaxial test leads to four stress-strain paths which can be fitted in an approximation solution with the three independent elastic constants. To this extent, the procedure is similar to the one for anticlastic

structures. The principles concerning number of load cycles and hold times stated in Chapter 8.3.2.1 apply analogously.

By contrast, only one “load block” with two stress increment ratios is required. This is because in plane and synclastic structures every load case that increases the stress in one structural direction compared to the prestress level also leads to an increase of stress in the perpendicular direction. The only exceptions to this rule are (1) rectangular plane structures with such a high aspect ratio that the load-bearing behaviour is uniaxial, and (2) inflated beams, where – after inflation – only the longitudinal direction exhibits normal stress increments under external load. The distinction between “carrying direction: warp” and “carrying direction: fill” is not required here. Consequently, this means that only one set of design elastic constants is necessary. The generalised biaxial test protocol is presented in Figure 106.

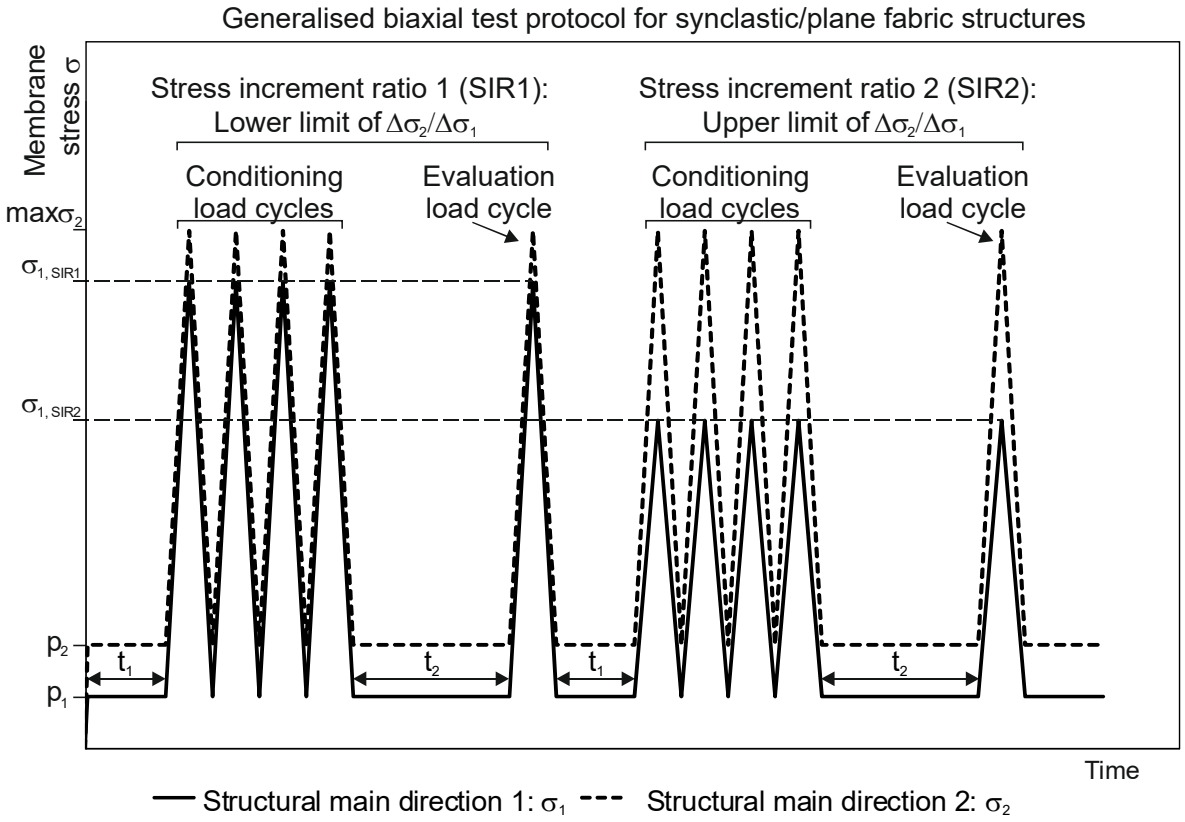

Membrane form	σ_1	σ_2
Plane rectangular	σ_x	σ_y
Cylindrical	σ_x	σ_φ
Spherical	σ_ϑ	σ_φ

Figure 106 Generalised biaxial test protocol for the determination of design elastic constants for synclastic and plane fabric structures, allocation of structural directions

After the initial hold time t_1 at prestress level, two stress increment ratios are subsequently conducted with five load cycles for each stress increment ratio. The evaluation load cycle is the solitary one after the recovery time t_2. The two stress

increment ratios are separated by another hold time t_1. The procedure presumes a uniform surface load. The test protocol for rectangular plane membranes is valid for $\ell_x > \ell_y$. The allocation of structural directions for plane, cylindrical and spherical forms to the structural directions named 1 and 2 in the generalised biaxial test protocol are given in the table within Figure 106.

With regard to cylindrical air-supported domes, it depends on the form of the closure dome and on the aspect ratios of the cylinder whether the circumferential or the longitudinal direction is subject to greater stress under wind load, see [DIN 4134:1983]. For most constellations, however, the circumferential direction is more highly stressed.

For this reason, general rectangular plane structures as well as cylindrical and hemispherical air-supported domes can be summarised well in one biaxial test protocol. Note that the presented protocol is of generalised form: σ_1 can be set as the higher stress if required. Particularly for quadratic plane membranes, higher stresses in x-direction can be expected than in y-direction, assuming that warp is aligned with the x-direction and fill with the y-direction. For a better understanding of the relative magnitude of the stress levels in Figure 106, Figure 107 presents the appearance of the biaxial test protocol particularly for plane quadratic structures. It applies analogously for those air-supported domes in which the longitudinal direction is more highly stressed than the circumferential direction.

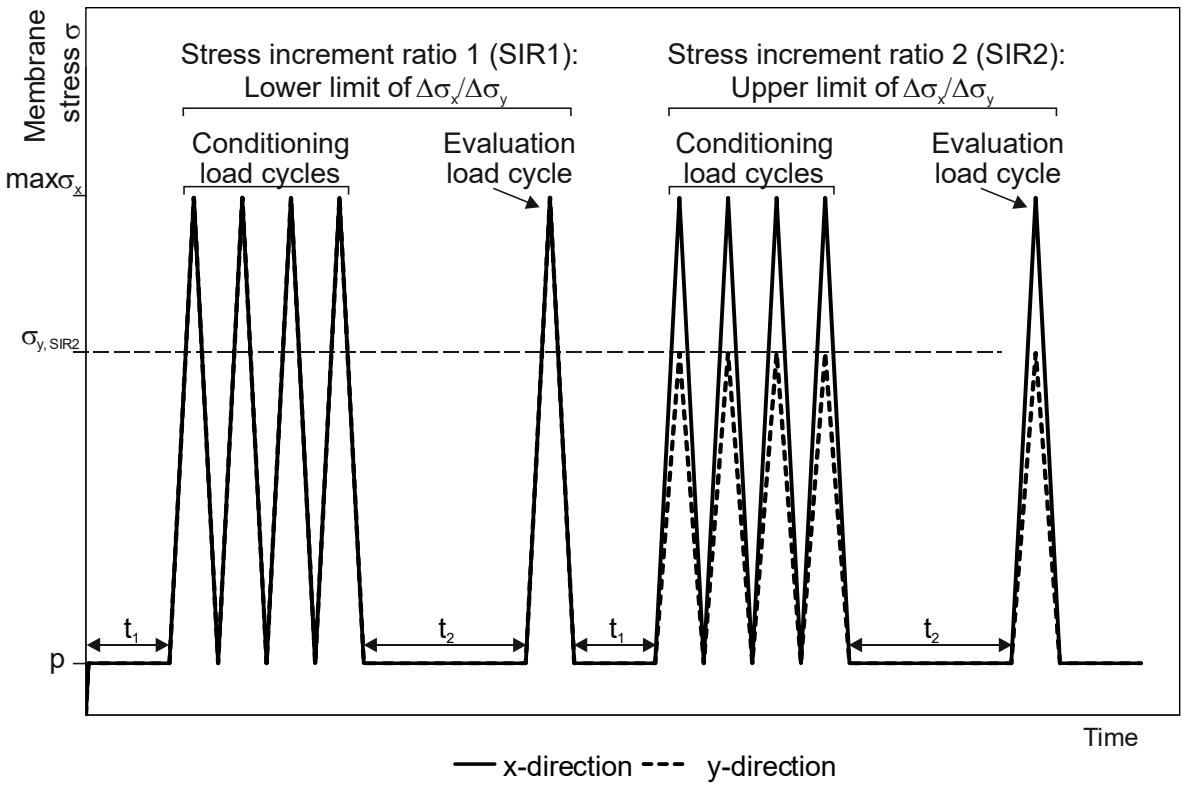

Figure 107 Appearance of the biaxial test protocol for the determination of design elastic constants for plane quadratic fabric structures with higher stress in x-direction

In special cases where the stress increment ratio will not vary much over the membrane surface and can well be predicted, it might be appropriate to test only one stress increment ratio and derive only two elastic constants (E_x, E_y) from the two stress-strain paths, omitting Poisson's ratios.

Inflated beams exhibit a particular stress development under bending, which differs significantly from that of the other structures described above. In the basic state immediately after inflation, the beam exhibits a prestress in circumferential direction that is twice as great as in longitudinal direction. Once inflated, it behaves like a regular circular hollow section under external loads. When the inflated beam exhibits a bending moment, a positive stress increment in longitudinal direction $\Delta\sigma_x > 0$ occurs at one half of the cross-section, while a negative stress increment $\Delta\sigma_x < 0$ of the same magnitude occurs on the opposite half, see Figure 108. The limit magnitude of the negative stress increment is $\min \Delta\sigma_x = -p_x$ because beyond that level the stabilising prestress is exhausted, the surface would wrinkle and the beam would fail. Because of the symmetry this means for the positive stress increment a limit of the same magnitude: $\max \Delta\sigma_x = +p_x$. Considering the general principles stated above, the biaxial test protocol can be adjusted as presented in Figure 109. Note that this procedure solely considers pure bending without any additional external normal forces in the beam and that it simulates only the behaviour at the location of the maximum bending moment. The shear stiffness is likewise not considered.

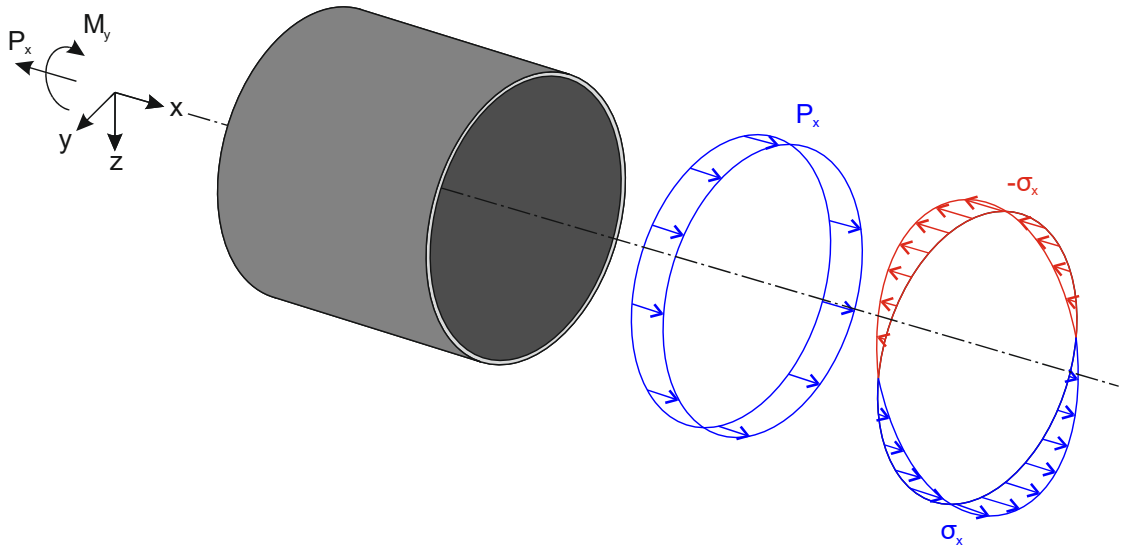

Figure 108 Stress distribution for a prestressed circular hollow section under a bending moment

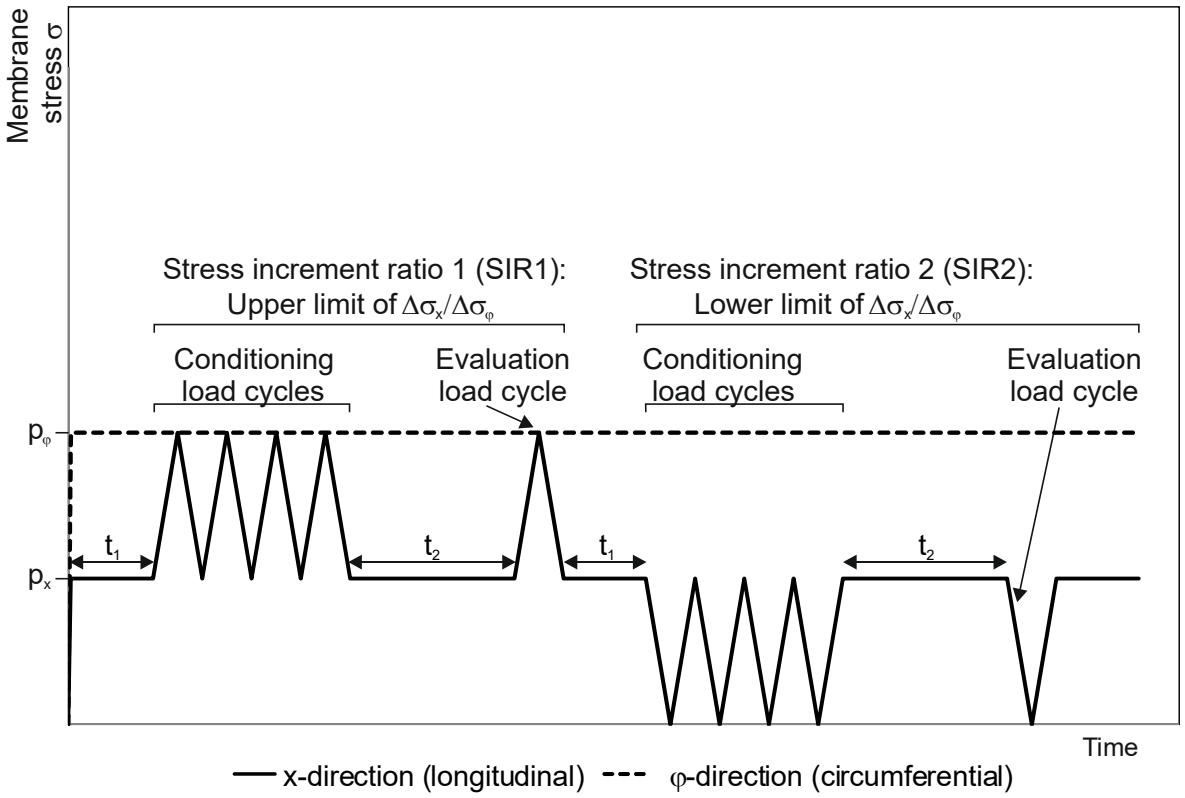

Figure 109 Appearance of the biaxial test protocol for the determination of design elastic constants for inflated beams under pure bending due to external loads

8.4.2.2 Numerical recommendations

For plane quadratic structures it is reasonable to presume an isotropic prestress. Given that the membrane would be isotropic or transversely isotropic, a stress increment ratio $\Delta\sigma_x/\Delta\sigma_y$ of one would occur under uniform surface load. Presuming the ratio of uniaxial tensile moduli $1 \leq E_x/E_y < 2$ – which covers most fabrics –, warp:fill stress increment ratios of between 1:1 and 2:1 can be expected.

For rectangular plane structures an anisotropic prestress might be favourable. Note that it is beneficial to plan the warp in the long span and the fill in short span since this reduces the number of required seams. Thus, usually a higher prestress and a higher stress increment can be expected in fill for plane rectangular membranes with an aspect ratio ℓ_x / ℓ_y of considerably greater than one. The limiting constellation is uniaxial load-bearing behaviour.

Reference values for stress increment ratios for air-supported domes can be found in [DIN 4134:1983]. They depend e. g. on whether the structure is cylindrical or hemispherical, as well as on the aspect ratios width/length and height/radius. In general, a prestress ratio of $p_x/p_\varphi = ½$ applies for any cylindrical forms (no matter if it is an air-supported dome or an inflated beam), where p_x is the prestress in longitudinal direction and p_φ the prestress in circumferential direction.

For cylindrical domes with a closure dome on a rectangular ground plot, stress increment ratios $\Delta\sigma_\varphi/\Delta\sigma_x$ for wind load can be found in [DIN 4134:1983] of between

1.0 and approximately 1.5. Adequately presuming warp in the higher stressed circumferential direction this would mean a warp:fill stress increment ratio of $1.0 < \Delta\sigma_w/\Delta\sigma_f < 1.5$. This could be transferred for the biaxial test as one lower boundary stress increment ratio of $\Delta\sigma_w/\Delta\sigma_f = 1.0$ and one upper boundary stress increment ratio of $\Delta\sigma_w/\Delta\sigma_f = 1.5$, each on top of the prestress with ratio $p_w/p_f = 2$.

As far as the magnitude of prestress is concerned, 2.0 % of the mean tensile strength $f_{m,23}$ of the fabric direction with the lower tensile strength can be recommended to be presumed in the direction under greater prestress. This is a useful approach in the event that the magnitude is not further specified. Note that in inflated beams – which are high pressure structures [SaP15] – these values could be significantly higher.

The maximum test stress can be presumed to be 25 % of $f_{k,23}$. For reasons of simplicity the tensile strength of the fabric direction with the lower tensile strength can be used with no major economic loss. More precise values may be anticipated by the design engineer.

8.4.3 Evaluation procedure

In general, the evaluation procedure presented in Chapter 8.3.3 for anticlastic structures can be applied for both synclastic and plane structures. Three independent design elastic constants can be determined from the four stress-strain paths by means of an approximation solution. Also for synclastic and plane structures it is reasonable to only evaluate the fit at a predefined evaluation stress level σ_e. If not further specified, evaluation stress level σ_e. can be assumed also as the design tensile strength, usually $0.25 \cdot f_{k,23}$. The programmed correlation analysis routine presented in Chapter 8.3.3 can also be applied for synclastic and plane structures: it generally determines three independent elastic constants that optimally fit the measured strains at evaluation stress level using the minimax method.

If simplified to test only one stress increment ratio as described above, two elastic constants can be determined from the two pairs of measured stress-strain values at evaluation stress level. Poisson's ratio can be disregarded for this constellation. The two unknown elastic constants E_x and E_y can be derived from the two single equations involved in eq. (4.35). If no negative strain increments occur, they are solely able to model the two stress-strain paths accurately.

8.4.4 Example application

The application of the proposed procedure is demonstrated for a plane quadratic fabric structure as an example. An isotropic prestress is assumed. The actual characteristic stress increment ratio of the structure under external surface load is expected to be between 1:1 and 2:1. These both are taken as the boundary stress increment ratios in the biaxial test. The maximum test stress is set to $0.25 \cdot f_{k,23}$. Again, those materials with high transverse strain properties are expected to be the most difficult ones to model. The procedure can be expected to work well for all common

architectural fabrics if it works for those with the highest transverse strain. The selection of materials for the example application and the stress levels are the same as presented in Table 15. Figure 110 illustrates an example of the stress-time diagram for the glass-PTFE fabric type II.

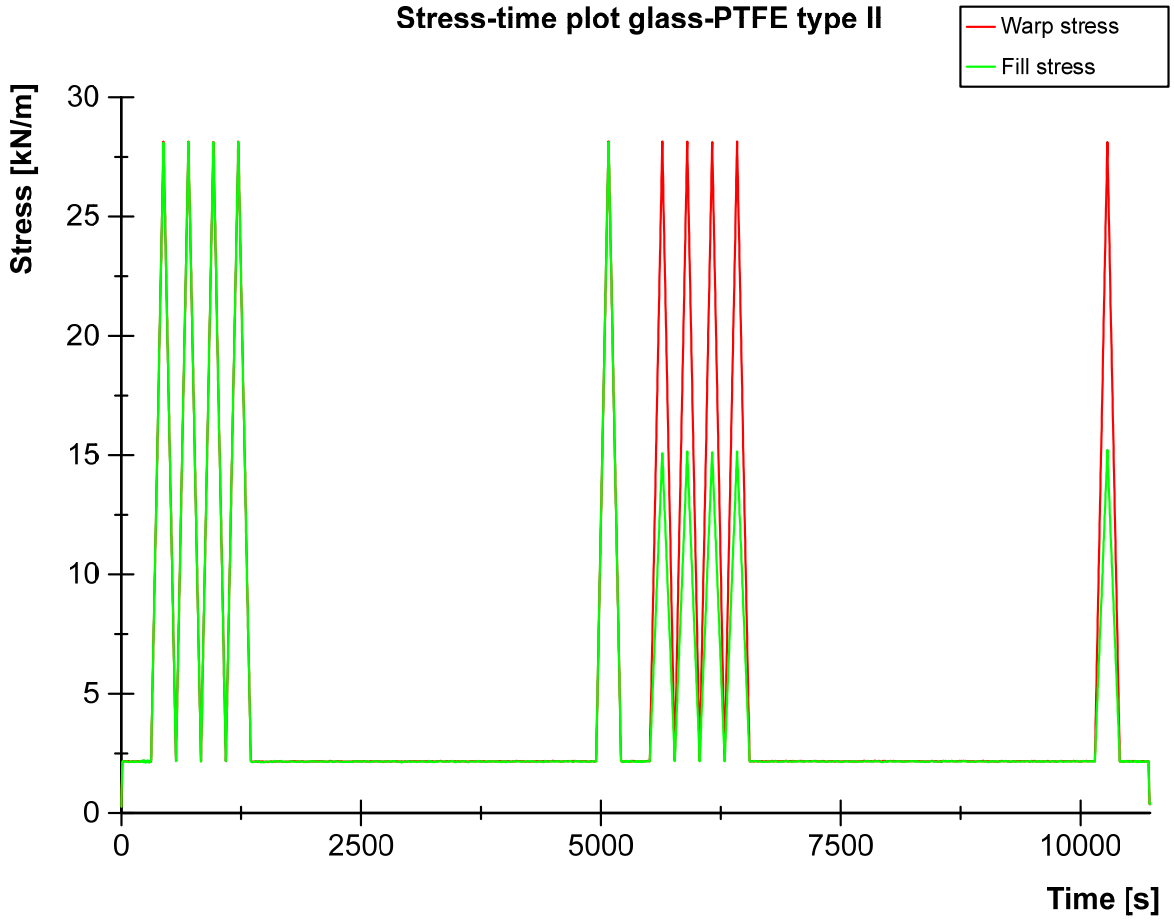

Figure 110 Example stress-time plot for the biaxial test on the glass-PTFE fabric type II

For the evaluation with the numerical Matlab routine, steps for the tensile moduli of ΔE = 5 kN/m and for the Poisson's ratio of $\Delta\nu$ = 0.01 were chosen.

The resulting sets of design elastic constants and their fit are illustrated for the three investigated materials in Figure 111, Figure 112 and Figure 113.

For all investigated materials the calculated stress-strain paths fit the measured ones very well. Overall, the maximum strain error at level σ_e is not greater than max $E_{\varepsilon,e}$ = 0.26% strain, occurring in the biaxially prestressed coated PES-PVC fabric type IV. This is a good approximation. For the glass fibre fabric a maximum strain error of max $E_{\varepsilon,e}$ = 0.01% strain could be achieved. This is an optimal fit. In terms of mechanics it means that the material behaviour fully satisfies the reciprocal relationship.

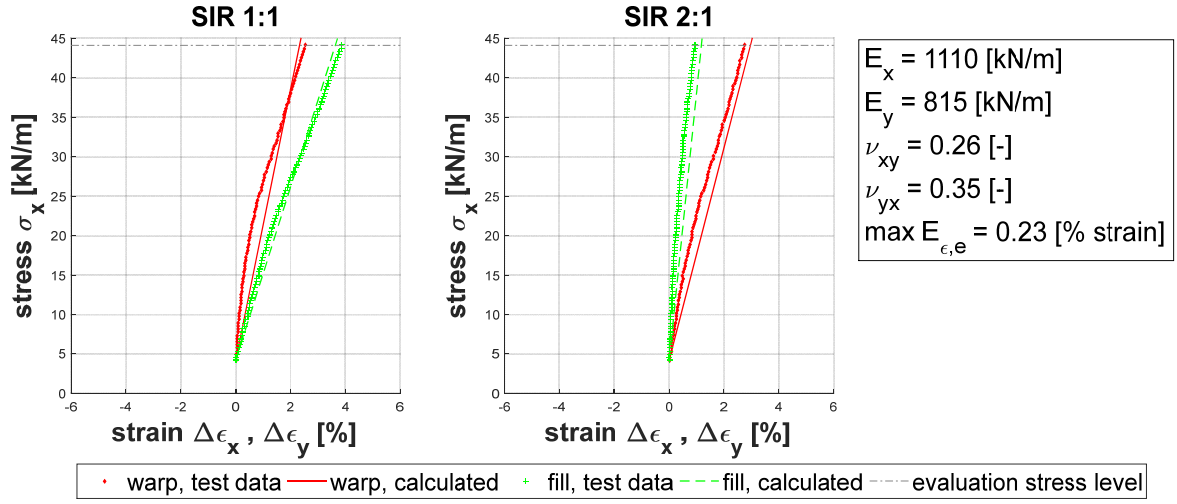

Figure 111 Comparison of measured stress-strain paths of traditionally coated PES-PVC fabric type V and calculated stress-strain paths resulting from the presented set of elastic constants

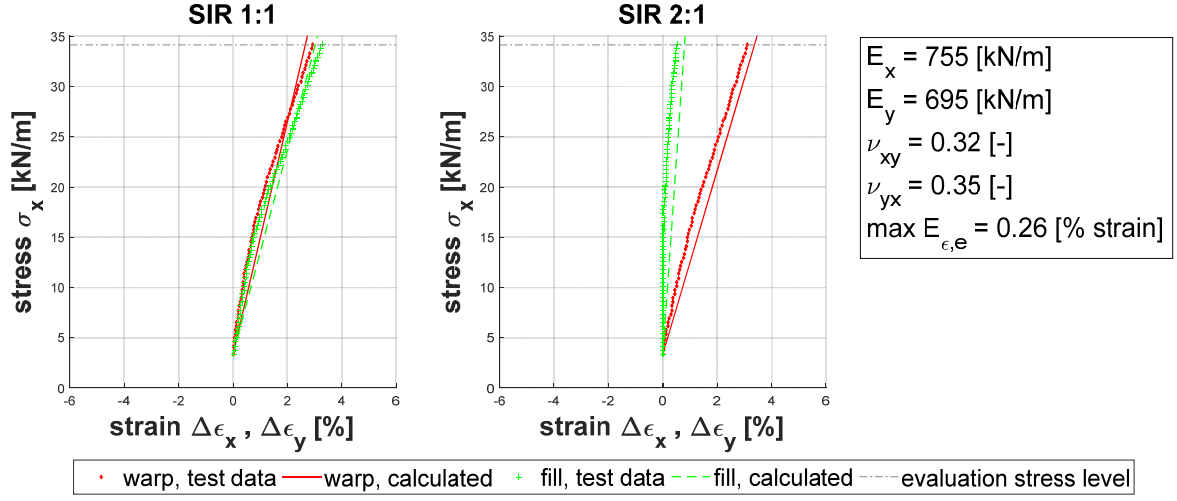

Figure 112 Comparison of measured stress-strain paths of PES-PVC fabric type IV with biaxially prestressed coating system and calculated stress-strain paths resulting from the presented set of elastic constants

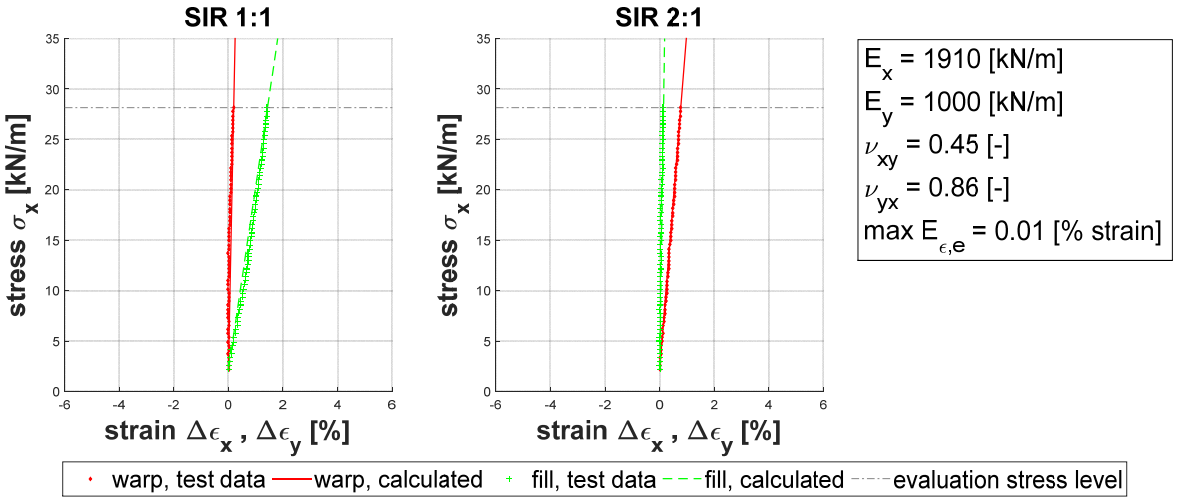

Figure 113 Comparison of measured stress-strain paths of glass-PTFE fabric type II and calculated stress-strain paths resulting from the presented set of elastic constants

The measured stress-strain paths of the glass fibre fabric are practically linear, while for the polyester fabrics a concave (i. e. softening) curvature of the paths is still clearly recognisable in the fifth load cycle. All sets of elastic constants fit the 1:1 stress increment ratios very well. The orthotropy ratio of the materials can thus be obtained directly. The biaxially prestressed polyester fabric appears to be approximately transversely isotropic. The traditionally coated polyester fabric is shown to be moderately anisotropic and the glass fibre fabric strongly anisotropic.

The application to a defined structure is demonstrated for the plane quadratic fabric structure discussed in Chapter 7.6. However, one difference exists: warp and fill are parallel to the edges. The load has again the magnitude of $q = 0.60$ kN/m^2, although it must be imagined not to be a snow load. A snow load would lead to ponding in a horizontal plane structure and have to be avoided. Thus, in this example the load could be imagined to be a wind load.

From the investigations into this structure performed within Chapter 7, it is well known that a maximum stress increment ratio of approximately 1.4:1 occurs. This ratio approaches 1:1 near the corners. The biaxial test is therefore performed with the two limiting stress increment ratios of 1:1 and 1.5:1.

As glass-PTFE type II appeared to be almost linear, the same is expected for glass-PTFE type III. For this reason, no significant difference is expected whether the prestress level is chosen at the above recommendation of 2.0 % of $f_{m,23}$ leading to $p = 2.0$ kN/m or at the predefined nominal prestress level of the example structure of $p = 3.0$ kN/m. However, in this example application, the predefined nominal prestress level is taken into account only to emphasise the adaptability of the test protocol. The same is done for the maximum stress level. With the results of Chapter 7.6, the maximum stress can be anticipated to be approximately max $\sigma = 15$ kN/m. Figure 114 documents the load history. The chosen hold times are $t_1 = 5$ minutes and $t_2 = 60$ minutes.

Evaluation of the measured stress-strain data yields one set of elastic constants, see Figure 115. As previously for the glass-PTFE fabric type II, see Figure 113, the resulting set of elastic constants shows a perfect fit with a maximum strain error of only $E_{\varepsilon,e} = 0.01$ % strain.

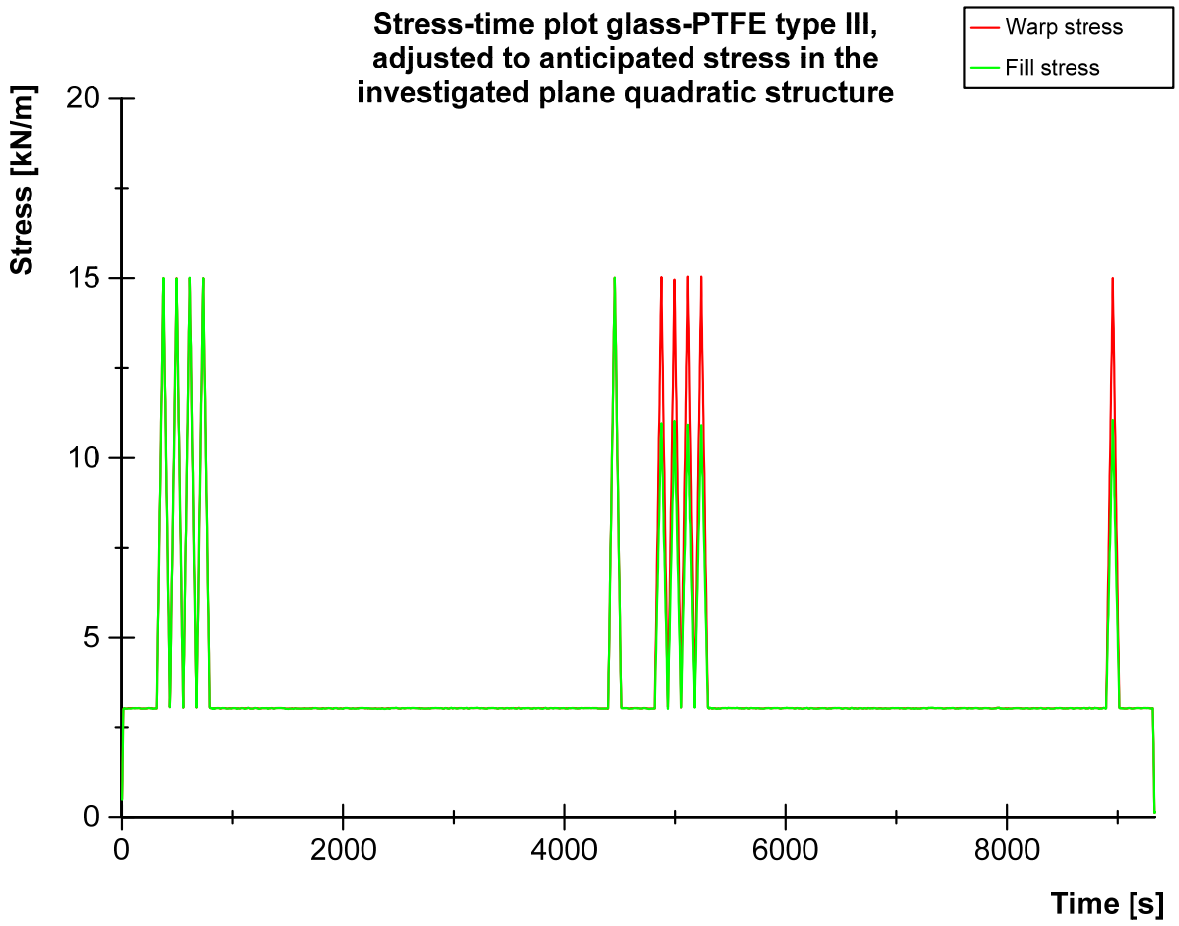

Figure 114 Stress-time plot for the biaxial test on the glass-PTFE fabric type III to determine design elastic constants for use in the investigated plane quadratic fabric structure

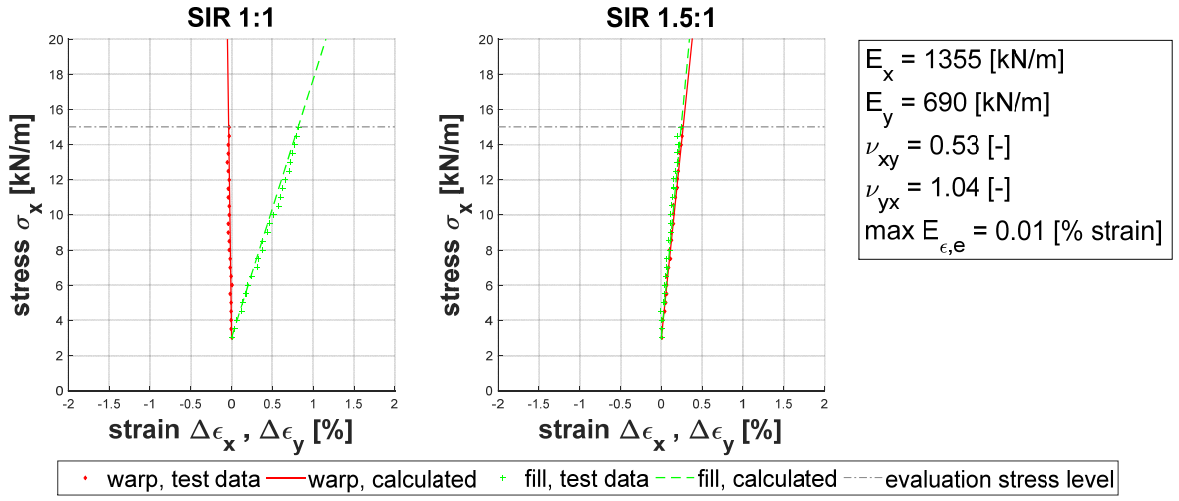

Figure 115 Comparison of measured stress-strain paths of glass-PTFE fabric type III and calculated stress-strain paths resulting from the presented set of elastic constants

Using this set of design elastic constants in the geometrically nonlinear finite element analysis leads to results as stated in Figure 116 in terms of stresses and Figure 117 in terms of deflections. Both Figures also repeat the results from the previously investigated sets of elastic constants for easy comparison.

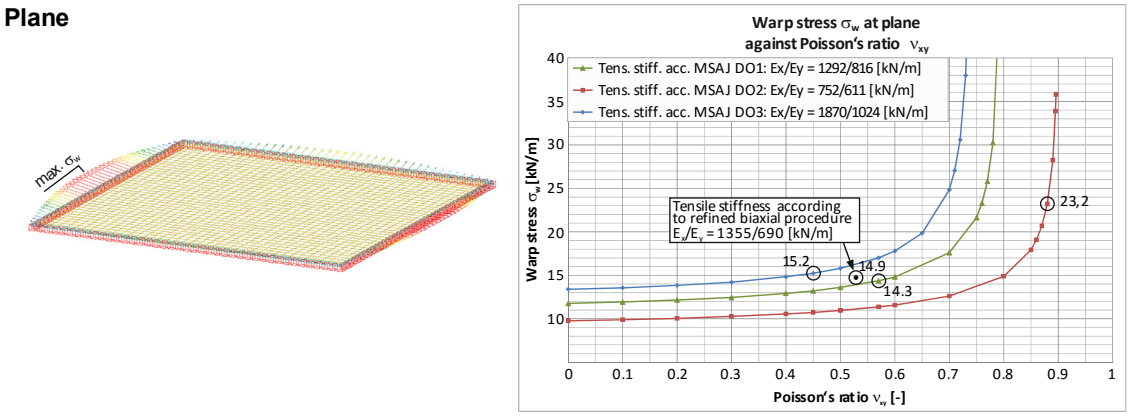

Figure 116 Warp stress σ_W at the centre of the plane structure, obtained for different sets of elastic constants for a glass-PTFE fabric type III (MSAJ determination options see Table 9)

The stress and deflection both conform very well with those based on elastic constants obtained from the original MSAJ procedure (green curve) as well as from the modification stated in [US13], which uses only the MSAJ stress-strain paths of stress ratios 1:1 and 2:1 for the evaluation (blue curve). Although at first glance similar stress ratios are used in the MSAJ test protocol and the refined and customised procedure developed here, the approaches differ considerably. The MSAJ test procedure omits recovery times and prestress level and performs only one load cycle in the 2:1 stress ratio. As already discussed in Chapter 8.3.4, it is suggested that these two opposing effects cancel each other out to a certain extent. In this light it appears rather to be a coincidence that the FE results are similar.

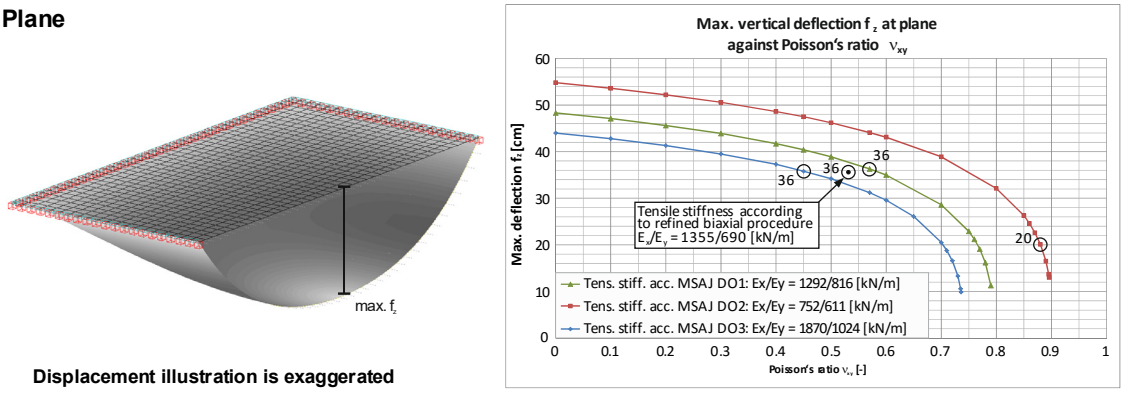

Figure 117 Maximum deflection f_z at the centre of hypar structures with two different curvatures, obtained for different sets of elastic constants for a glass-PTFE fabric type III (MSAJ determination options see Table 9)

For the set of elastic constants based on the evaluation of all ten MSAJ stress-strain paths, the same applies as already stated in Chapter 7.6. The resulting stress and deflection do not appear to be reliable.

By contrast, the design elastic constants derived from the refined biaxial test procedure can be expected to simulate the material performance in the plane structure well. Stress-strain paths are generated in the biaxial test which are very

close to the expected ones within the entire surface of the structural fabric. Furthermore, these stress-strain paths are perfectly fitted by the straight stress-strain lines corresponding to the determined set of design elastic constants. The FE results are suggested to be reliable even though a final experimental proof is not yet available. This suggestion is also based on the fact that the measured stress-strain response is quasi linear and that the material behaviour fully satisfies the mechanical restraint of the reciprocal relationship eq. (4.9).

8.5 Conclusions

Elastic constants for general material characterisation must be distinguished clearly from elastic constants for design purposes. For the general material characterisation, uniaxial tests that include the measurement of transverse strain can serve as the basis from which elastic constants can be derived. However, these are clearly inappropriate for design purposes. Design elastic constants should be tailored to specific design situations.

In this work, principles for biaxial test protocols were developed and presented separately for anticlastic and synclastic/plane structures. The fundamental principle is that the characterising stress increment ratio under a uniform load is narrowed down with two boundary stress increment ratios in the biaxial test protocol to as close to reality as possible. This method narrows the decisive stress-strain paths to tight range. Implementing the two boundary stress increment ratios leads to four measured stress-strain paths. An approximation solution can be used to determine three unknown independent elastic constants from four stress-strain paths. The minimax method and – especially for anticlastic structures – an option for determining elastic constants "by hand" were proposed as associated evaluation procedures with the aim to determine elastic constants for design purposes. Particularly the latter method enables a quick and easy evaluation by the design engineer. Both methods aim to match the calculated strain with the measured strain exclusively at a specific, user-defined evaluation stress level.

Usually, the design of membrane structures is based on the equilibrium shape corresponding to nominal prestress level. The nominal prestress level is that level predefined by the design engineer to ensure a sufficiently stiff and wrinkle-free structure over the full lifetime. It – together with the geometry of the boundaries – is the basic variable for the form-finding procedure. In order to ensure the constancy of the required prestress level, it is correlated to the stable state of the fabric. Design elastic constants must therefore be determined for this state. For this reason, five load cycles are scheduled in the biaxial test protocol. This number has previously proven to be sufficient to reach the stable state for all common architectural fabrics.

Another advantage of modelling the stable state of the fabric is that the strain increments are small enough to satisfy the definition of “small strain” according to the theory of elasticity.

Moreover, a recovery time is scheduled prior to the fifth load cycle for each stress increment ratio. The recovery time enables revertive creep in the fabric. This is a good way of simulating natural loading like wind or snow where load peaks are always separated by a certain amount of time sufficient for the major part of the revertive creep process to be completed. Omitting the material recovery would result in a stiffer material response than can actually be expected for natural loading.

The principles developed for a biaxial test protocol generally provide a fundamental framework. The procedures are open to customisation and adjustment to structural requirements. The stated principles conform to the European standardised procedure for steel cables that exhibit a structural behaviour closely related to tensile surface structures.

The objective in relation to anticlastic structures is to determine two sets of design elastic constants for short-term loads, one for warp as the carrying direction and one for fill as the carrying direction. If long-term loads like snow can occur on a structure, the creep effects can be modelled by means of a third set of elastic constants. This set can be achieved by modifying the tensile moduli of the one short-term set of elastic constants that conforms to the carrying direction under snow load – warp or fill – with a creep coefficient.

Poisson's ratios should generally be considered to make the modelling negative strain increments possible. Negative strain increments can be expected to occur frequently in the supporting direction of anticlastic structures and they can have a considerable extent. To a lesser extent they can also occur in synclastic/plane structures.

"Secant" elastic constants are determined such that the corresponding straight stress-strain lines fit the measured stress-strain paths at one single stress level: the evaluation stress level equals the maximum characteristic stress level in the structure to be verified. This procedure ensures that the stress-strain paths of the fabric at the decisive stress increment ratios are accurately modelled at the crucial stress levels. When warp is the carrying direction, the large orthotropy ratio E_x/E_y permits a very large Poisson's ratio ν_{yx}. This set of elastic constants thus makes it possible to model the very large contraction transverse to the carrying direction. This applies analogously when fill is the carrying direction. This fact is striking evidence that linear elastic constitutive law is a suitable approach for modelling woven fabric provided that warp and fill stressing are handled separately.

This principles of biaxial testing and evaluating the recorded test data can also be applied for synclastic and plane fabric structures. In this case the aim is to determine only one set of elastic constants.

The stress levels and length of the hold and recovery times are open to definition by the design engineer. General numerical recommendations were provided for the case that no detailed specifications are made.

The procedures proved to function very well for all common PES-PVC and glass-PTFE fabrics. Example sets of design elastic constants determined using the procedures proved to be a very good fit for measured stress-strain paths. The procedures – particularly that for anticlastic structures – make it possible to model even the large transverse strain that is typical of woven fabrics.

The example application in which appropriate stress increment ratios were simulated for an anticlastic as well as for a plane quadratic fabric structure provided evidence of the practical applicability of the procedures.

Consequently, structural analysis results based on these design elastic constants can be presumed to be a reliable, safe and economical design approach. However, the final experimental proof is yet to be supplied. Static load tests with spatially curved fabric components are recommended for this purpose.

9 Conclusions and outlook

General

One important and challenging task relating to the structural analysis of fabric structures is the determination of fabric stiffness parameters. Today, the complex nonlinear and viscoelastic material behaviour of architectural fabrics is simplified by applying an orthotropic linear-elastic constitutive model using “tensile modulus” and “Poisson’s ratio” as elastic constants. The goal of the present work was to push forward the understanding of the stiffness behaviour of coated woven fabrics and advance methods for determining suitable sets of elastic constants for design purposes.

Experimental investigations

Uniaxial tensile tests on all common PES-PVC and glass-PTFE fabrics were conducted for the examination of the fundamental stiffness behaviour of architectural fabrics. The uniaxial tensile tests were performed on a biaxial test rig in order to permit measurement of transverse strain and alternation between warp and fill stressing.

First and foremost, these tests clearly demonstrated that at the latest after five load cycles, a stable state of the fabric occurs for all common architectural fabrics. This state is subject to stable stress-strain hysteresis, which is independent of the previous load history.

All tests were conducted including as well as omitting recovery times. Omitting recovery times suppresses the revertive creep process after unloading. Due to this circumstance, fabrics appear stiffer when no recovery times are included in the test protocol.

A method of handling creep was derived from uniaxial tests with long-term loads. The tests revealed that there is no change in the resulting Poisson’s ratios compared to tests with short-term loads. This means that it is justified to solely modify the tensile modulus to a tensile-creep modulus. A procedure defining a creep coefficient k_{def} oriented towards EN 1995 for the verification of timber structures was proposed.

From tests with warp and fill stressing switching back and forth it was observed for anticlastic structures – which are characterised by an alternation of the stressing direction when the direction of the external load changes – that they exhibit different states of temporary residual strain. This also means that they cannot have one constant prestress level. Two boundary stiffness states are linked to this mechanism.

Static load tests with orthogonally loaded membrane strips clearly indicated the strong relation between prestress level and fabric stiffness. These two properties balance each other out to a certain extent. Basically, stress and deflection are of the same order of magnitude in every load cycle, although as a tendency the highest

stress occurs during the initial load and the highest deflection in the stable state of the fabric. The nominal prestress and the stable state stiffness of the fabric are closely linked.

Accompanying numerical simulation of the prestressed and orthogonally loaded membrane strips clearly demonstrated that every load cycle can be modelled sufficiently provided that stiffness parameters that fit the respective load cycle number and the corresponding prestress level are used as input data. Stiffness parameters and prestress level must be seen in conjunction with and not detached from each other.

As membrane structure analysis is always based on the nominal prestress level, the appropriate input stiffness parameters are those of the stable state of the fabric.

An additional advantage of modelling the stable state of the fabric is that the strain increments are small enough to satisfy the restriction of “small strain” according to the theory of elasticity. This could be ensured for the whole assortment of common PES-PVC and glass-PTFE fabrics in all typical design situations.

Development of refined biaxial test and evaluation procedures

The indepth analysis of four internationally established biaxial test and evaluation procedures demonstrated expedient features but simultaneously revealed several severe shortcomings. Based on these procedures, different sets of elastic constants were determined, some of which proved to be unfeasible as input parameters for the structural analysis because mechanical restrictions were not satisfied. The feasible sets were employed in accompanying numerical simulations. The result was a large spectrum of stresses and deflections. This revealed the great level of uncertainty in the state-of-the-art determination of elastic constants.

In order to overcome these uncertainties, principles for refined biaxial test and evaluation procedures were developed that include the findings described above. These principles provide the design engineer a tool with which to determine suitable stiffness parameters for all practical design situations in the field of fabric structure analysis. They consider anticlastic as well as synclastic or plane structures.

In general, four stress-strain paths are always generated in the biaxial tensile test to determine one set of four elastic constants. Two boundary stress increment ratios are therefore scheduled in the biaxial test procedure. These boundary stress increment ratios narrow down the anticipated stress increment ratio at the characteristic location of the membrane surface.

The stress increments always start from a predefined prestress level. For each stress increment ratio five load cycles are included. Since natural loading like wind and snow is characterised by a large amount of time between two load peaks of significant magnitude, the consideration of recovery times in the test protocol produces a good simulation. In other words, disregarding recovery times in the test

protocol leads to an artificially stiff stress-strain response that does not reflect the physical reality. In general, the procedures are open to individual adjustment by the design engineer with regard to the prestress and anticipated stress levels as well as the duration of the hold times. However, numerical recommendations were provided for the event that no specifications are available.

While for synclastic and plane structures only one set of design elastic constants is required, two sets are envisaged for anticlastic structures: one for warp as the carrying direction and one for fill as the carrying direction. For long-term loads, a further set of elastic constants may be required depending on the creep characteristics of the fabric used.

The proposed evaluation procedures determine “secant” elastic constants in such a way that the calculated strain fits the measured strain very precisely at a user-defined evaluation stress level.

The new procedures proved to work well for all common architectural fabrics. They are also able to model the large transverse strain of some architectural fabrics that showed Poisson’s ratios of up to $\nu = 2$ under biaxial stress states. At the same time, all mechanical restrictions are satisfied. Given the good correlation of the refined sets of elastic constants with measured stress-strain paths, the new procedures thereby contribute to a reliable prediction of stress and deflection in fabric structures.

In conjunction with the presented refined biaxial test and evaluation procedures, elastic constants have proved to be a suitable tool with which to approach the stiffness behaviour of coated woven fabrics within static verification. Strain errors to be expected are small compared to the amount of strain occurring.

Outlook

The anisotropic linear-elastic constitutive law nevertheless remains an approximation of the generally nonlinear and nonelastic material behaviour. Progress will be made with material models that are able to model these characteristics.

The refined biaxial test and evaluation procedures presented in this work centre on the stress increment ratio at the location of the maximum stress of a membrane structure. They do not consider the stress levels or stress increment ratios at other locations on the membrane surface. It is therefore recommended to validate the procedures with static load tests on spatially curved membrane components for which stress levels and stress increment ratios implicitly vary over the surface. Shear stiffness should then also be considered for accurate comparative numerical simulations. It is further recommended to verify whether the refined procedures developed here can reasonably be combined with the method of varying tensile moduli proposed by *Galliot & Luchsinger* to cover stress increment ratios over an entire membrane surface.

Future research should also include the impact of discontinuities such as seams in the membrane on the stiffness properties of a complete membrane panel. As mentioned above, it is recommended that the temperature dependency of the fabric stiffness combined with the creep characteristics is studied for all common architectural fabrics. A further interesting characteristic is the stiffness behaviour of aged materials.

Harmonisation work is currently underway to develop a Eurocode for tensile membrane structures and related standards. One of the envisaged related standards is being prepared by CEN/TC248 WG04 “Coated fabrics” and aims at the establishment of a biaxial test procedure for the determination of elastic constants for coated fabrics. The results achieved in this work will be discussed in WG04 for implementation in the biaxial test standard. This may lead to a more unified approach to elastic constants that also permits safe and economical prediction of stress and deflection in architectural fabric structures.

10 Bibliography

[Aba14] Abaqus. Dassault Systemes, 2014.

[AG93] Ayorinde, E. O.; Gibson, R. F.: Elastic constants of orthotropic composite materials using plate resonance frequencies, classical lamination theory and an optimized three-mode rayleigh formulation. *Composites Engineering*, Vol. 3, pp. 395–407, 1993.

[AK14a] Ambroziak, A.; Kłosowski, P.: Mechanical properties of polyvinyl chloride-coated fabric under cyclic tests. *Journal of Reinforced Plastics and Composites*, Vol. 33, pp. 225–234, 2014.

[AK14b] Ambroziak, A.; Kłosowski, P.: Mechanical properties for preliminary design of structures made from PVC coated fabric. In Construction and Building Materials, Vol. 50, pp. 74–81, 2014.

[Am10] American Society of Civil Engineers: Tensile Membrane Structures, 2010.

[Ans14] ANSYS. CADFEM, 2014.

[Ba02] Baumann, T.: Statisch-konstruktive Eigenschaften von PTFE-beschichtetem Glasgewebe. *Bauingenieur*, Vol. 77, pp. 158–166, 2002.

[Ba07] Ballhause, D.: *Diskrete Modellierung des Verformungs- und Versagensverhaltens von Gewebemembranen*. Dissertation. Institut für Statik und Dynamik der Luft- und Raumfahrtkonstruktionen; University of Stuttgart, 2007.

[BB12] Bridgens, B.; Birchall, M.: Form and function: The significance of material properties in the design of tensile fabric structures. *Engineering Structures*, Vol. 44, pp. 1–12, 2012.

[BB87] Blum, R.; Bidmon, W.: Spannungs- und Dehnungsverhalten von Bautextilien. Theorie und Experiment. SFB 64, Stuttgart, 1987.

[BBG04] Blum, R.; Bögner, H.; Gipperich, K.; Seery, S.: An example of the application of the testing procedure described in Appendix A3 on a PTFE coated glass fabric. In: Forster, B.; Mollaert, M. (Eds.): European Design Guide for Tensile Surface Structures. TensiNet Association, Brussel, pp. 323–344, 2004.

[BBN04] Blum, R.; Bögner, H.; Némoz, G.: Testing methods and standards. In: Forster, B.; Mollaert, M. (Eds.): European Design Guide for Tensile Surface Structures. TensiNet Association, Brussel, pp. 219–241, 2004.

[Be11] Beccarelli, P.; Bridgens, B. N.; Galliot, C.; Gosling, P. D.; Stimpfle, B.; Zanelli, A.: Round-robin biaxial tensile testing of architectural coated fabrics. Proceedings of the IABSE-IASS Symposium, 2011.

[Be15] Beccarelli, P.: Biaxial Testing for Fabrics and Foils. Springer International Publishing, Cham, 2015.

[BG04] Bridgens, B. N.; Gosling, P. D.: Direct stress–strain representation for coated woven fabrics. *Computers & Structures*, Vol. 82, pp. 1913–1927, 2004.

[BG10] Bridgens, B. N.; Gosling, P. D.: Interpretation of results from the MSAJ "Testing Method for Elastic Constants of Membrane Materials". Proc.

TensiNet Symposium, pp. 49–57, UACEG, Sofia, Bulgaria, 16-18 September 2010.

[BGB04] Bridgens, B. N.; Gosling, P. D.; Birchall, M. J. S.: Membrane material behaviour: concepts, practice and developments. *Structural Engineer*, Vol. 82, pp. 28–33, 2004.

[BGJ12] Bridgens, B.; Gosling, P.; Jou, G.T., Hsu, X.Y.: Inter-laboratory comparison of biaxial tests for architectural textiles. *The Journal of the Texile Institute*, Vol. 103, pp. 706–718, 2012.

[BLL73] Blum, R.; Losch, M.; Luz, E.: Determination of the Elastic Properties of a Coated Fabric. *Materialpruefung/Materials Testing*, Vol. 15, pp. 278–280, 1973.

[Bö04] Bögner, H.: *Vorgespannte Konstruktionen aus beschichteten Geweben und die Rolle des Schubverhaltens bei der Bildung von zweifach gekrümmten Flächen aus ebenen Streifen.* Dissertation, Stuttgart, 2004.

[CJS03] Cavallaro, P. V.; Johnson, M. E.; Sadegh, A. M.: Mechanics of plain-woven fabrics for inflated structures. *Composite Structures*, Vol. 61, pp. 375–393, 2003.

[CS88] Craig, P. D.; Summerscales, J.: Poissons ratios in glass fibre reinforced plastics. *Composite Structures*, Vol. 9, pp. 173–188, 1988.

[DIN EN 1049-2:1994-02] Textiles; Woven fabrics; Construction; Methods of analysis; part 2: Determination of number of threads per unit length, 1994.

[DIN EN 1995-1-1:2010] Eurocode 5: Design of timber structures - Part 1-1: General - Common rules and rules for buildings, 2010.

[DIN EN ISO 1421:1998-08] Rubber- or plastics-coated fabrics – Determination of tensile strength and elongation at break, 1998.

[DIN EN ISO 2076] Textilien - Chemiefasern - Gattungsnamen (Textiles – Man-made fibres – Generic names), 2013.

[DIN EN ISO 2286-2:2015-04] Rubber- or plastics-coated fabrics – Determination of roll characteristics - Part 2: Methods for determination of total mass per unit area, mass per unit area of coating and mass per unit area of substrate, 2015.

[DIN EN ISO 2286-3:2015-04] Rubber- or plastics-coated fabrics – Determination of roll characteristics – Part 3: Method for determination of thickness, 2015.

[DIN EN ISO 899-1:2003] Plastics - Determination of creep behaviour; Part 1: Tensile creep, 2003.

[DIN 4134:1983] Tragluftbauten: Berechnung, Ausführung und Betrieb; Air-supported structures; structural design, construction and operation, 1983.

[EN 13084-7] Free-standing chimneys – Part 7: Product specifications of cylindrical steel fabrications for use in single wall steel chimneys and steel liners, 2006.

[EN 1990:2002] Eurocode 0 – Basis of structural design, 2002.

[EN 1991-1-4] Eurocode 1: Actions on structures – Part 1-4: General actions – Wind actions, 2010.

[EN1993-1-11:2010] Eurocode 3: Design of steel structures – Part 1-11: Design of structures with tension components, 2010.

[FM04] Forster, B.; Mollaert, M. (Eds.): European Design Guide for Tensile Surface Structures. TensiNet Association, Brussel, 2004.

[Fr67] Fritzsche, E.: Strain Measurements on Industrial Fabrics for Pneumatic Structures. In: Feder, D. (Ed.): Proceedings of the 1st International Colloquium on Pneumatic Structures. University of Stuttgart, pp. 137–141, 1967.

[GB08] Gosling, P. D.; Bridgens, B. N.: Material Testing & Computational Mechanics - A New Philosophy For Architectural Fabrics. *International Journal of Space Structures*, Vol. 23, pp. 215–232, 2008.

[GB09] Göppert, K.; Balz, M.: Membrantragwerke. In: Kuhlmann, U. (Ed.): Stahlbau-Kalender 2009. Ernst & Sohn Verlag für Architektur und technische Wissenschaften GmbH & Co. KG, Berlin, Germany, pp. 707–759, 2009.

[GHW11] Gross, D.; Hauger, W.; Wriggers, P.: Technische Mechanik 4. Hydromechanik, Elemente der Höheren Mechanik, Numerische Methoden. Springer-Verlag, Berlin, Heidelberg, 2011.

[GL09] Galliot, C.; Luchsinger, R. H.: A simple model describing the non-linear biaxial tensile behaviour of PVC-coated polyester fabrics for use in finite element analysis. *Composite Structures*, Vol. 90, pp. 438–447, 2009.

[GL11] Galliot, C.; Luchsinger, R. H.: Determination of the response of coated fabrics under biaxial stress: comparison between different test procedures. In: Oñate Ibáñez de Navarra, E.; Kröplin, B.; Bletzinger, K.-U. (Eds.): International Conference on Textile Composites and Inflatable Structures V. Structural Membranes, pp. 636–647, CIMNE, Barcelona, Spain, 2011.

[Go13a] Goldsmith, N.: The material characteristics of fabrics. In Huntington, C. G. (Ed.): Tensile fabric structures. Design, analysis, and construction, Reston, Va., 2013.

[Go13b] Gosling, P. D.; Bridgens, B. N.; Albrecht, A.; Alpermann, H.; Angeleri, A.; Barnes, M.; Bartle, N.; Canobbio, R.; Dieringer, F.; Gellin, S.; Lewis, W. J.; Mageau, N.; Mahadevan, R.; Marion, J.-M.; Marsden, P.; Milligan, E.; Phang, Y. P.; Sahlin, K.; Stimpfle, B.; Suire, O.; Uhlemann, J.: Analysis and design of membrane structures: Results of a round robin exercise. *Engineering Structures*, Vol. 48, pp. 313–328, 2013.

[Gr69] Grosberg, P.: The tensile properties of woven fabrics. In Hearle, J. W. S.; Grosberg, P.; Backer, S. (Eds.): Structural Mechanics of Fibres, Yarns and Fabrics. Volume 1. Wiley-Interscience, New York, pp. 339–354, 1969.

[HM01] Hake, E.; Meskouris, K.: Statik der Flächentragwerke. Einführung mit vielen durchgerechneten Beispielen. Springer, Berlin, 2001.

[Ho79] Hosser, D.: Erläuterungen zum Bemessungskonzept für Tragluftbauten. (unpublished), Frankfurt, 1979.

[IBG13] Iliffe, C. N.; Bridgens, B. N.; Gosling, P. D.: A predictive model for the design of functional textiles. In Bletzinger, K.-U.; Kröplin, B.; Oñate Ibáñez de Navarra, E. (Eds.): International Conference on Textile Composites and

Inflatable Structures VI. STRUCTURAL MEMBRANES 2013, pp. 395–406, CIMNE, Munich, Germany, 2013.

[Ja70] Jagfeld, P.: Ein- und mehrachsige Zugversuche an der Dachfolie des Deutschen Pavillons auf der Weltausstellung 1967 in Montreal. *Melliand Textilberichte*, pp. 349–354, 1970.

[Jo75] Jones, R. M.: Mechanics of composite materials. McGraw-Hill Kogakusha, Tokyo, 1975.

[Kn10] Knippers, J.; Cremers, J.; Gabler, M.; Lienhard, J.: Atlas Kunststoffe + Membranen. Werkstoffe und Halbzeuge, Formfindung und Konstruktion. Inst. für Internat. Architektur-Dokumentation, München, 2010.

[Ko08] Koslowski, H. J.: Chemiefaser-Lexikon. Begriffe, Zahlen, Handelsnamen. Deutscher Fachverlag, Frankfurt am Main, 2008.

[Le68] Lempriere, B. M.: Poisson's ratio in orthotropic materials. *AIAA Journal*, Vol. 6, pp. 2226–2227, 1968.

[Lo71] Losch, M. H.: *Bestimmung der mechanischen Konstanten für einen zweidimensionalen, nichtlinearen, anisotropen, elastischen Stoff am Beispiel beschichteter Gewebe.* Dissertation, University of Stuttgart, 1971.

[Me78] Meffert, B*.: Mechanische Eigenschaften PVC-beschichteter Polyestergewebe.* Dissertation , RWTH Aachen, 1978.

[Me95] MSAJ/M-02-2995: Testing Method for Elastic Constants of Membrane Materials. Membrane Structures Association of Japan, 1995.

[Mi06] Minami, H.: A Multi-Step Linear Approximation Method for Nonlinear Analysis of Stress and Deformation of Coated Plain-Weave Fabric. *Journal of Textile Engineering*, Vol. 52; pp. 189–195, 2006.

[Mi81] Minte, J.: *Das mechanische Verhalten von Verbindungen beschichteter Chemiefasergewebe.* Dissertation, RWTH Aachen, 1981.

[ML14] Matlab. The MathWorks, Inc., 2014.

[MM84] Minami, H.; Motobayashi, S.: Biaxial deformation property of coated plain-weave fabrics. Proceeding of the International Symposium on Architecturakl Fabric Structures. The Design Process, Glenview, Illinois, 1984.

[MR95] Münsch, R.; Reinhardt, H.: Zur Berechnung von Membrantragwerken aus beschichteten Geweben mit Hilfe genäherter elastischer Materialparameter. *Bauingenieur*, Vol. 70, pp. 271–275, 1995.

[Pe00] Peil, U.: Bauen mit Seilen. In Kuhlmann, U. (Ed.): Stahlbau Kalender 2000. Ernst & Sohn Verlag für Architektur und technische Wissenschaften GmbH & Co. KG, Berlin, pp. 689–755, 2000.

[Pe07] Peel, L. D.: Exploration of high and negative Poisson's ratio elastomer-matrix laminates. *Physica status solidi (b)*, Vol. 244, pp. 988–1003, 2007.

[Pe13] Petersen, C.: Stahlbau. Grundlagen der Berechnung und baulichen Ausbildung von Stahlbauten. Springer Vieweg, Wiesbaden, 2013.

[PLI07] Pargana, J. B.; Lloyd-Smith, D.; Izzuddin, B. A.: Advanced material model for coated fabrics used in tensioned fabric structures. *Engineering Structures*, Vol. 29, pp. 1323–1336, 2007.

[PS10] Proff, B.; Saxe, K.: Spannende Bauwerke: Warum sich optische Messtechnik am besten zur Charakterisierung mechanischer Eigenschaften technischer Membranen eignet. *Messtec drives Automation*, 2010.

[PW92] Pestel, E.; Wittenburg, J.: Festigkeitslehre. BI-Wiss.-Verl, Mannheim, 1992.

[PWB13] Philipp, B.; Wüchner, R.; Bletzinger, K. U.: Conception and design of membrane structures considering their non-linear behavior. In Bletzinger, K.-U.; Kröplin, B.; Oñate Ibáñez de Navarra, E. (Eds.): International Conference on Textile Composites and Inflatable Structures VI. STRUCTURAL MEMBRANES 2013, pp. 114–125, CIMNE, Munich, Germany, 2013.

[Re75] Reinhardt, H.-W.: Ein- und zweiachsige Verformungs- und Festigkeitsuntersuchungen an einem beschichteten Gittergewebe. (Strength and stress-strain response of a coated fabric under one- and two-dimensional loading). Mitteilungen des SFB 64 No. 31/75, Stuttgart, 1975.

[RM79] Rehm, G.; Münsch, R.: Zum Spannungs-Dehnungs-Verhalten im Gebrauchslastbereich und zum Bruchverhalten von PVC-beschichteten Polyestergeweben. In: Brinkmann (Ed.): 2. Internationales Symposium Weitgespannte Flächentragwerke. 1. Vorberichte zum Kolloquium. Stuttgart, 1979.

[RR05] Rand, O.; Rovenski, V.: Analytical methods in anisotropic elasticity. Birkhäuser, Boston, 2005.

[SaP15] Stranghöner, N., Uhlemann, J., Bilginoglu, F., Bletzinger, K.-U., Bögner-Balz, H., Corne, E., Gibson, N., Gosling, P., Houtman, R., Llorens, J., Malinowsky, M., Marion, J.-M., Mollaert, M., Nieger, M., Novati, G., Sahnoune, F., Siemens, P., Stimpfle, B., Tanev, V., Thomas, J.-Ch.: Prospect for European Guidance for the Structural Design of Tensile Membrane Structures. Science and Policy Report (SaP-Report). Draft Version. To be published by the Joint Research Centre (JRC) of the European Commission, publication expected 2016.

[SBS11] Schröder, J.; Balzani, D.; Stranghöner, N.; Uhlemann, J.; Gruttmann, F.; Saxe, K.: Membranstrukturen mit nicht-linearem anisotropem Materialverhalten - Aspekte der Materialprüfung und der numerischen Simulation. *Bauingenieur*, Vol. 86, pp. 381–389, 2011.

[Sc12] Schmidt, H.: Steifigkeitseigenschaften textiler Membranen: Studie zur Gewährleistbarkeit durch den Hersteller - Schlussbericht August 2012. Auftraggeber: Verseidag Indutex GmbH, Krefeld. unpublished, 2012.

[Se09] Seidel, M.: Tensile surface structures. Ernst & Sohn Verlag, Berlin, 2009.

[Sk71] Skelton, J.: The biaxial stress-strain behaviour of fabrics to air-supported tents. *Journal of materials / American Society for Testing and Materials*, Vol. 6, pp. 656–682, 1971.

[SK92] Saxe, K.; Kürten, R.: Zur Temperaturabhängigkeit des Kraft-Dehnungsverhaltens PTFE-beschichteter Glasgewebe bei üblichen Verarbeitungstemperaturen. *Bauingenieur*, Vol. 67, pp. 291–296, 1992.

[So09] Société d'Edition du Bâtiment et des Travaux Publics (Ed.): Recommandations pour la conception, la confection et la mise en

oeuvre des ouvrages permanents de couverture textile. Édition 2009. SEBTP, Paris, 2009.

[Sof14] Sofistik. Manual. Sofistik AG, 2014.

[SSU14] Saxe, K.; Stranghöner, N.; Uhlemann, J.: Membranwerkstoffe: Zusammenhang zwischen Bauaufgabe und Materialauswahl. In: Stranghöner, N.; Saxe, K.; Uhlemann, J. (Eds.): 2. Essener Membranbau Symposium. 26. September 2014, Campus Essen. Shaker Verlag, Aachen, pp. 45–53, 2014.

[SU12] Stranghöner, N.; Uhlemann, J.: Möglichkeiten und Grenzen bei der Erfassung des Materialverhaltens von Gewebemembranen in der Tragwerksplanung. In Saxe, K.; Stranghöner, N. (Eds.): Essener Membranbau Symposium. 28. September 2012, Campus Essen. Shaker Verlag, Aachen, pp. 55–95, 2012.

[UKS13] Uhlemann, J.; Koenen, R.; Stranghöner, N.: The role of Poisson's ratio for the determination of elastic constants for fabrics: Proceedings of the TensiNet Symposium, Istanbul, Turkey, pp. 23–32, 2013.

[US13] Uhlemann, J.; Stranghöner, N.: Einfluss fiktiver elastischer Konstanten von textilen Gewebemembranen in der Tragwerksanalyse von Membranstrukturen. *Stahlbau*, Vol. 83, pp. 643–651, 2013.

[USS11] Uhlemann, J., Stranghöner, N., Schmidt, H., Saxe, K.: Effects on Elastic Constants of Technical Membranes Applying the Evaluation Methods of MSAJ/M-02-1995: Proceedings of the STRUCTURAL MEMBRANES, Barcelona, Spain, 2011.

[USS14] Uhlemann, J.; Saxe, K.; Stranghöner, N.: Aktuelle Sicherheitsansätze in der Bemessung von Membrankonstruktionen. In: Stranghöner, N.; Saxe, K.; Uhlemann, J. (Eds.): 2. Essener Membranbau Symposium. 26. September 2014, Campus Essen. Shaker Verlag, Aachen, pp. 55–74, 2014.

[USS15a] Uhlemann, J.; Stranghöner, N.; Saxe, K.: Stiffness Parameters for Architectural Fabrics: An Analysis of Two Determination Procedures. *Structural Engineering International*, Vol. 25, pp. 9–19, 2015.

[USS15b] Uhlemann, J.; Stranghöner, N.; Saxe, K.: Tensile structures: Investigations into the determination of elastic constants of fabrics. *Journal of the International Association for Shell and Spatial Structures*, Vol. 56, pp. 25–35, 2015.

[USS15c] Uhlemann, J.; Stranghöner, N.; Saxe, K.: Comparison of stiffness properties of common coated fabrics. *Steel Construction*, Vol. 8, 2015.

Glossary

Anticlastic
Type of doubly curved shape with a negative Gaussian curvature, for instance saddle-shaped.

Biaxial
In two orthogonal axes.

Biaxially prestressed coating system
In this coating technique for PES-PVC materials, controlled stress is applied not only to the warp yarns during coating but also to the fill yarns. This technique makes it possible to achieve rather transversely isotropic material behaviour.

Characteristic stress
Stress resulting from characteristic permanent and non-permanent loads in the meaning of EN 1990, i. e. considering a partial factor of the action side γ_F equal to one.

Characteristic tensile strength
The characteristic tensile strength is referred to as the 5%-fractile of the tensile strength according to EN 1990.

Coating
An additional layer of organic synthetic materials applied on one or both surfaces of a fabric. The primary function of the coating is to make the membrane waterproof and to protect the weave from environmental impacts such as UV rays. The second function is to make the fabric weldable.

Compensation value
The compensation value is the measure of shortening of a membrane panel such that the prestress in the membrane develops to the nominal prestress after relaxation has ceased and after several load incidents of certain magnitude have occurred.

Constructional stretch
During the first loading cycles, the individual yarns in the fabric adapt to the applied stress and stress ratio and align themselves, i. e. they lose curvature or crimp. Disproportionately high stretch is exhibited until this mechanism is complete during the loading process. This mechanism can also be observed for the single yarns, where individual filaments align themselves, and analogously also for cables, where individual wires align themselves.

Creep
Ongoing deformation under a long-term load.

Crimp interchange
Crimp interchange describes the mechanism that a change in the yarn crimp of one weave direction affects the crimp of the orthogonal yarn.

Design elastic constants
Elastic constants which can serve as input data for design purposes, in contrast to elastic constants which provide a general material characterisation unfeasible as structural analysis input data. Design elastic constants have to fit stress-strain paths correlated to a specific structure and design situation and they have to hold the mechanical restrictions of the used constitutive model.

Design strength
The design strength is referred to as the characteristic tensile strength divided by a global stress factor.

Direct stiffness formulation
Mathematical formulation of the constitutive model in which stress is calculated dependent on strain and stiffness. In the plane-stress orthotropic linear-elastic model two direct stiffness moduli in the principal directions and two interchange stiffness moduli are used as elastic constants.

Fabric
Cloth made of woven or laid yarns.

Fill yarn
The yarns in the lateral direction of a fabric web are called the fill yarns. They are also known as weft yarns.

Gaussian curvature
In a doubly curved shape, the Gaussian curvature at one point is defined as the product K of the principal curvatures k_i in the two orthogonal principal directions i at the given point: $K = k_1 \cdot k_2$, where k_i is the reciprocal of the radius of curvature R_i of an actual or approached circular segment.

Global stiffness
The global stiffness is determined from a secant connecting zero strain (“global zero”) with the maximum strain in a given load cycle.

Inverse stiffness formulation
Mathematical formulation of the constitutive model in which strain is calculated dependent on stress and compliance. In the plane-stress orthotropic linear-elastic model two tensile moduli and two Poisson’s ratio in the principal directions are used as elastic constants.

Isotropic
The material properties in all three coordinate directions are the same.

Membrane
A membrane is a structural component which resists only tensile forces. It has no bending or compressive stiffness.

Membrane stress
Stress in the membrane. For fabrics it is given in force per unit width because no precise cross-section area can be stated.

Minimax method
The minimax method is an evaluation method that aims to minimise the maximum error.

Open mesh fabric
Coated fabric with spacing between the yarns. The spacings can be closed with a transparent laminate (“laminated mesh”).

Orthotropic
Orthogonal anisotropic, i. e. material properties are unequal in all three coordinate directions.

Orthotropy ratio
The orthotropy ratio is the ratio of Young’s moduli E_x/E_y in the x,y-plane of a plane orthogonally anisotropic material.

Prestress
A basic stress level in the membrane induced during the installation. Prestress is essential for tensile membrane structures since it stiffens the membrane and prevents wrinkles, etc. The prestress level can vary over time, e. g. due to constructional stretch of the fabric, creep, revertive creep, etc.

Poisson’s ratio
The ratio of transverse strain to longitudinal strain, defined for a uniaxial stress state.

Reciprocal relationship
The reciprocal relationship states that the ratio of Poisson’s ratio in x-direction to Young’s modulus in y-direction equals the ratio of Poisson’s ratio in y-direction to Young’s modulus in x-direction. This relationship ensures the symmetry of the stiffness and compliance matrices.

Relative stiffness
The relative stiffness is determined from a secant within a specific stress interval connecting the starting strain at a specific load cycle (“relative zero”) with the maximum strain in the same load cycle.

Revertive creep
Revertive creep means the fading away of reversible strain that occurs with a delay after the load has been removed.

Stable state of a woven fabric
In the stable state of a woven fabric, the yarn crimp has adapted to the applied stress and stress ratio. This state is achieved after repetitive load cycles in one stress ratio. When the stable state is achieved, further load cycles lead to a pair of fixed values, max. membrane stress and correlated strain (max $\sigma \mid \varepsilon$). The pair of values (max $\sigma \mid \varepsilon$) in the stable state is independent of the previous load history.

Stress
see Membrane stress

Stress factor
The stress factor is a reduction factor for the tensile strength and contains both safety factors and actual strength reduction factors.

Synclastic
Type of doubly curved shape with a positive Gaussian curvature, for instance cushion-shaped.

Tensile modulus
The tensile modulus is the ratio of stress increment to strain increment of a structural component such as the composite coated fabric. It is a stiffness parameter for a homogeneous continuum and can be used for an inhomogeneous fabric if it is simplified as such. As the membrane stress is given in force per unit width, the same unit applies for the tensile modulus in the context of fabric structures.

Traditional coating
In the “traditional” coating process of PES-PVC materials, only warp yarns are stressed during the coating process, while the fill yarns are not stressed. This leads to anisotropic material behaviour in the fabric plane.

Transversely isotropic
Transversely isotropic materials have *one* isotropic plane, while the through-thickness direction obtains material properties unequal to those in the plane.

Warp yarn
The yarns in the longitudinal direction of a fabric web are called the warp yarns.

Young’s modulus
The Young’s modulus is the ratio of stress increment to strain increment for an elastic homogeneous base material, defined for a uniaxial stress state. It is given as force per unit cross-section area.

Annex A

Survey of materials investigated

Material: **PES-PVC**

Material producer: **1**

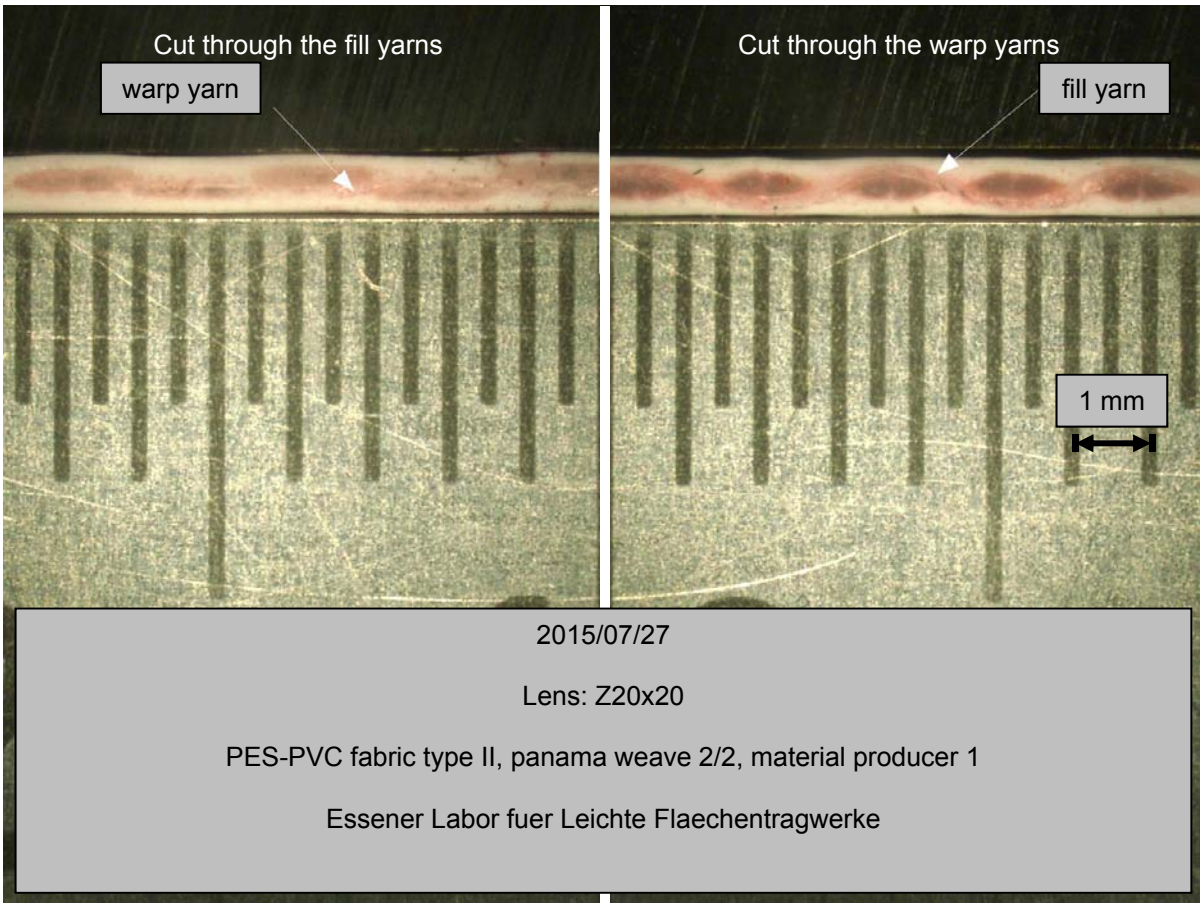

Property		Standard	Measured value	Unit
Tensile strength Warp / Fill	Mean	DIN EN ISO 1421 – strip method	95.5 / 93.3	kN/m
	5%-fractile*		89.0 / 90.0	
Type**		according to [SaP15]	II	-
Total weight		DIN EN ISO 2286-2	911	g/m^2
Thickness		DIN EN ISO 2286-3	0.75	mm
Weave		-	Panama 2/2	-
Yarn density Warp / Fill		DIN EN 1049	12.3 / 13.0	yarns/cm
Yarn size Warp / Fill		DIN EN ISO 2060	1100 / 1100***	dtex

* according to EN 1990 with a fractile factor k_n = 2.33

** according to proposed classification in [SaP15] based on the measured tensile strength

*** manufacturer information

Material: **PES-PVC**

Material producer: **1**

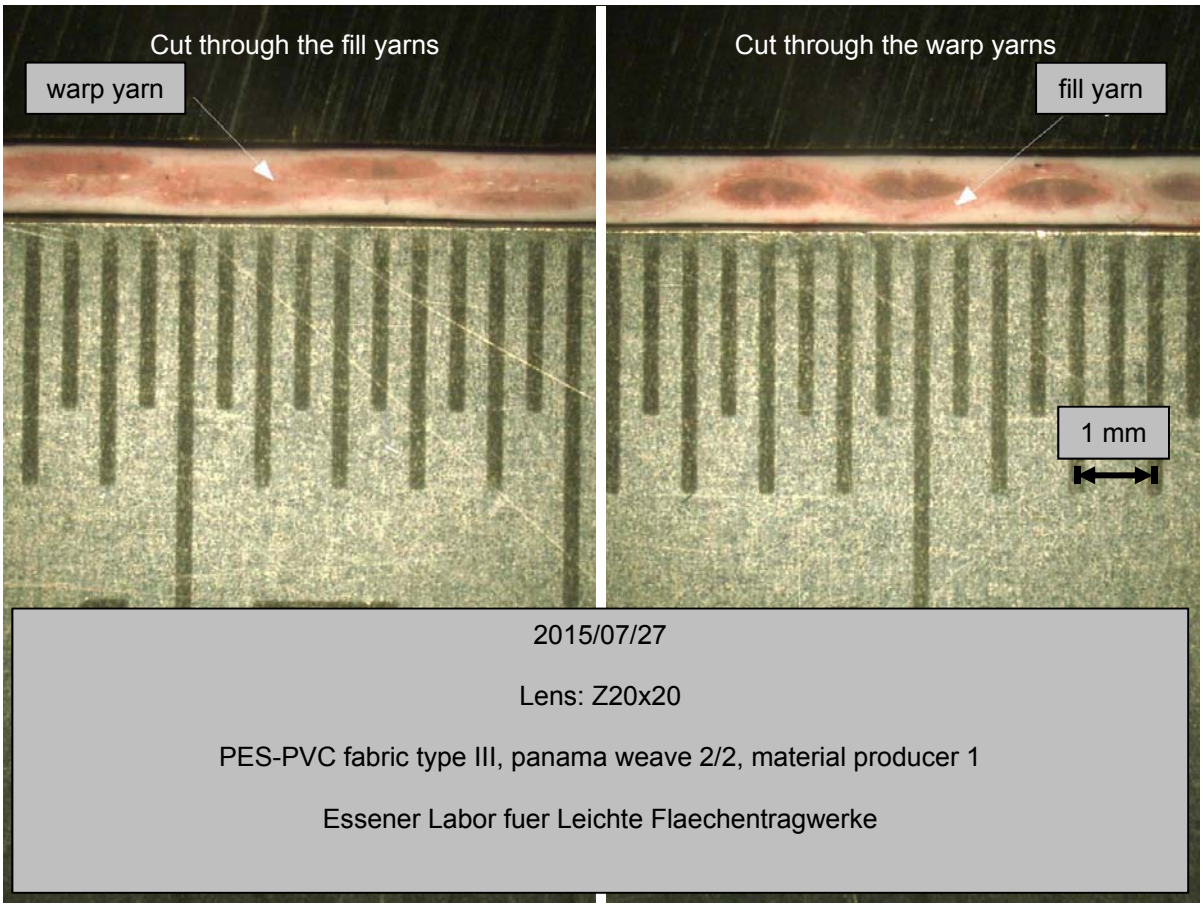

Property		Standard	Measured value	Unit
Tensile strength Warp / Fill	Mean	DIN EN ISO 1421 – strip method	127.3 / 113.6	kN/m
	5%-fractile*		124.6 / 110.4	
Type**		according to [SaP15]	III	-
Total weight		DIN EN ISO 2286-2	1036	g/m^2
Thickness		DIN EN ISO 2286-3	0.85	mm
Weave		-	Panama 2/2	-
Yarn density Warp / Fill		DIN EN 1049	10.8 / 10.4	yarns/cm
Yarn size Warp / Fill		DIN EN ISO 2060	1670 / 1670***	dtex

* according to EN 1990 with a fractile factor k_n = 2.33

** according to proposed classification in [SaP15] based on the measured tensile strength

*** manufacturer information

Material: **PES-PVC**

Material producer: **1**

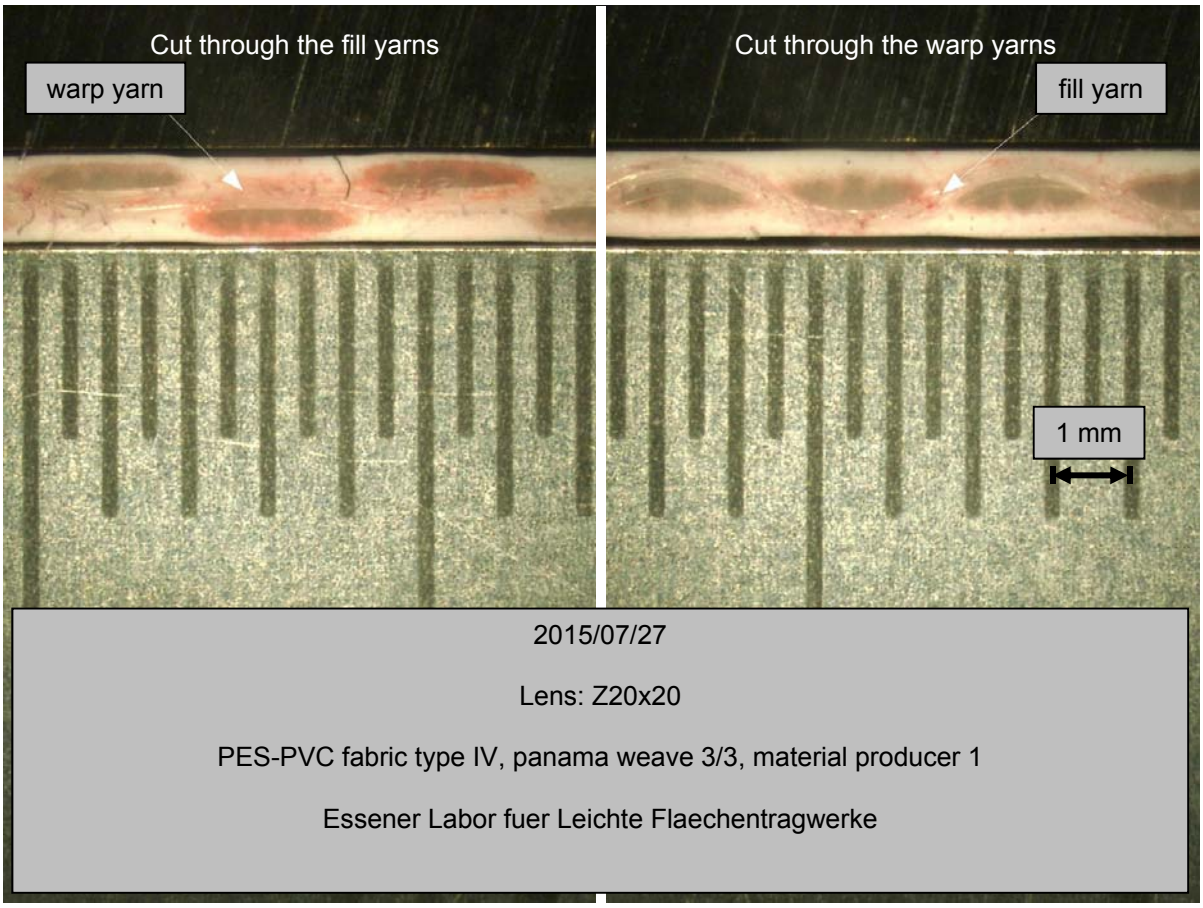

Property		Standard	Measured value	Unit
Tensile strength Warp / Fill	Mean	DIN EN ISO 1421 – strip method	167.4 / 162.0	kN/m
	5%-fractile*		164.2 / 160.1	
Type**		according to [SaP15]	IV	-
Total weight		DIN EN ISO 2286-2	1317	g/m^2
Thickness		DIN EN ISO 2286-3	1.08	mm
Weave		-	Panama 3/3	-
Yarn density Warp / Fill		DIN EN 1049	13.6 / 13.9	yarns/cm
Yarn size Warp / Fill		DIN EN ISO 2060	1670 / 1670***	dtex

* according to EN 1990 with a fractile factor k_n = 2.33

** according to proposed classification in [SaP15] based on the measured tensile strength

*** manufacturer information

Material: **PES-PVC**

Material producer: **2**

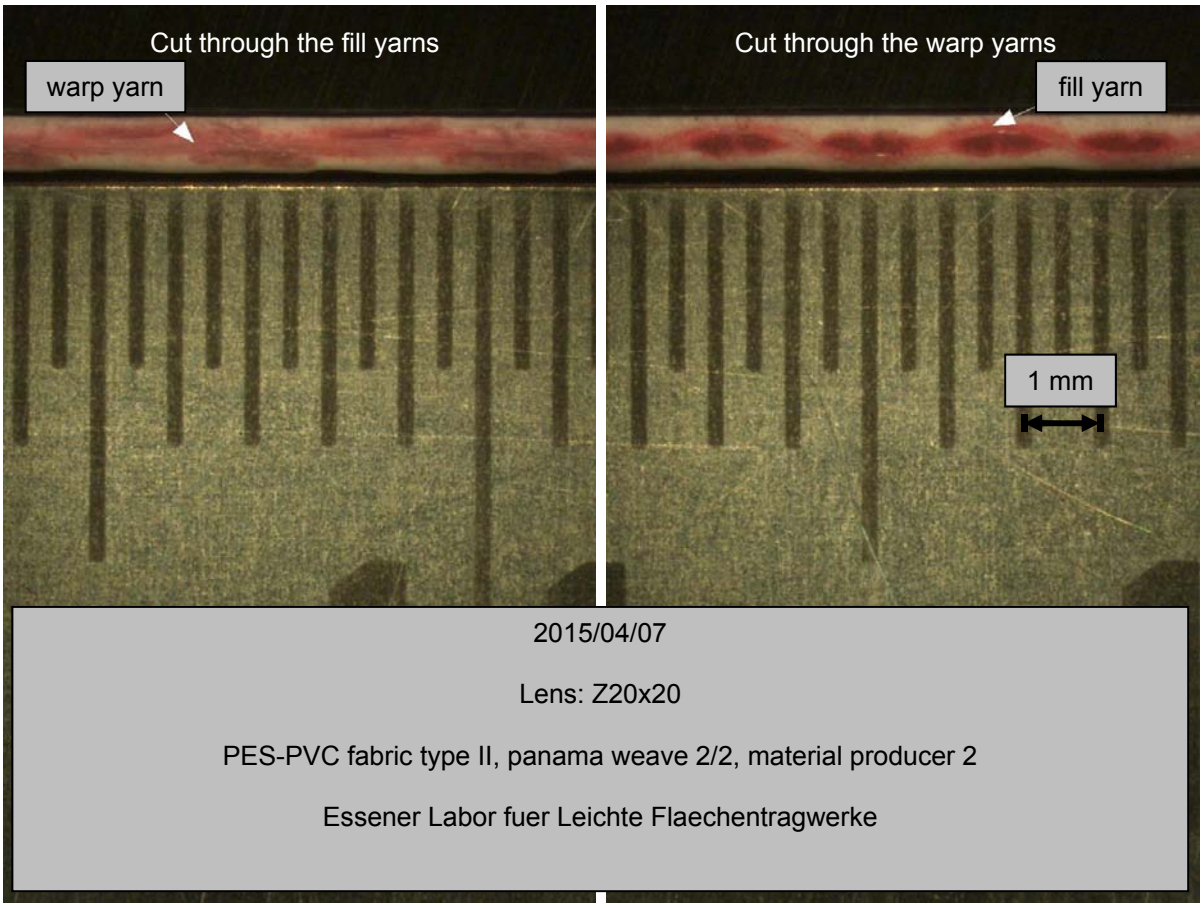

Property		Standard	Measured value	Unit
Tensile strength Warp / Fill	Mean	DIN EN ISO 1421 – strip method	91.4 / 84.1	kN/m
	5%-fractile*		89.9 / 79.9	
Type**		according to [SaP15]	II	-
Total weight		DIN EN ISO 2286-2	913	g/m^2
Thickness		DIN EN ISO 2286-3	0.76	mm
Weave		-	Panama 2/2	-
Yarn density Warp / Fill		DIN EN 1049	11.6 / 12.0	yarns/cm
Yarn size Warp / Fill		DIN EN ISO 2060	1100 /1100***	dtex

* according to EN 1990 with a fractile factor k_n = 2.33

** according to proposed classification in [SaP15] based on the measured tensile strength

*** manufacturer information

Material: **PES-PVC**

Material producer: **2**

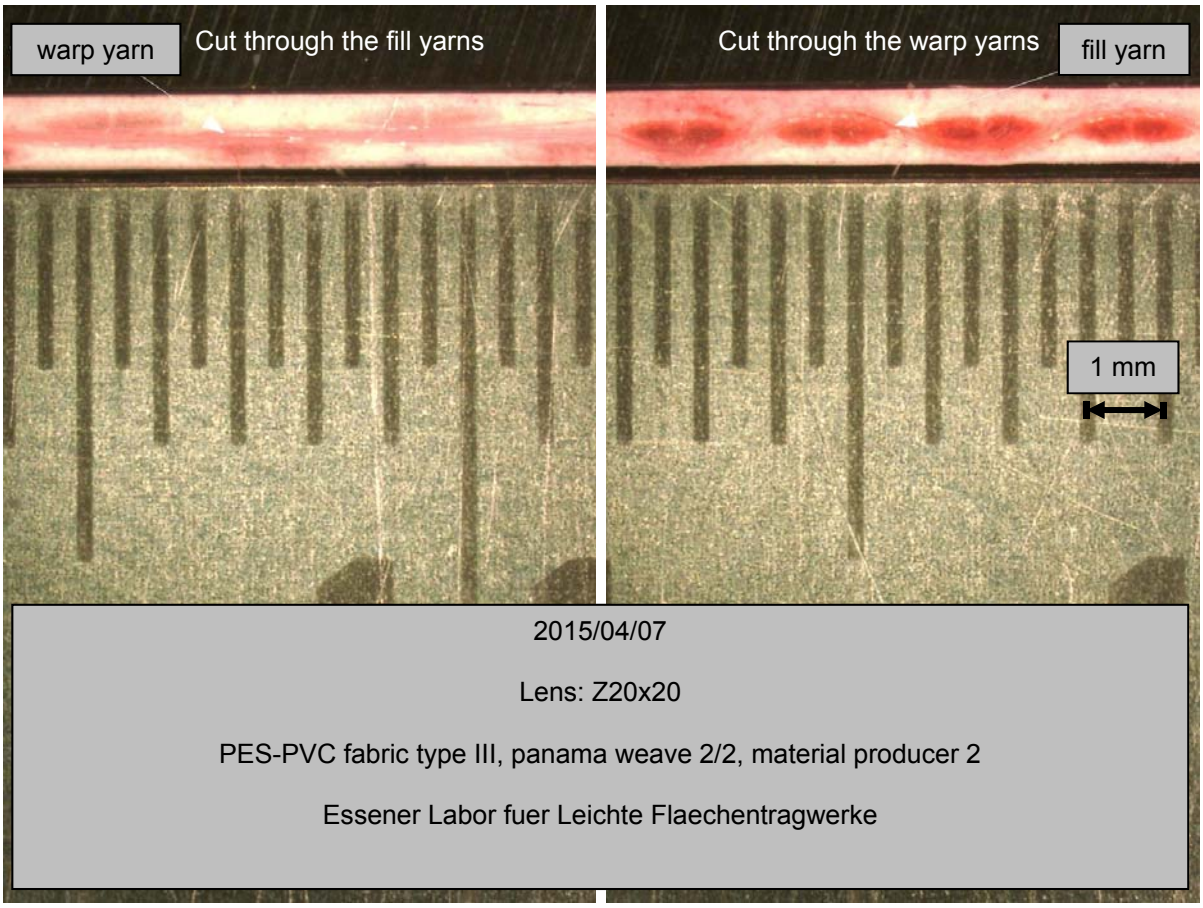

Property		Standard	Measured value	Unit
Tensile strength Warp / Fill	Mean	DIN EN ISO 1421 – strip method	118.9 / 104.1	kN/m
	5%-fractile*		113.9 / 100.4	
Type**		according to [SaP15]	III	-
Total weight		DIN EN ISO 2286-2	1266	g/m^2
Thickness		DIN EN ISO 2286-3	1.00	mm
Weave		-	Panama 2/2	-
Yarn density Warp / Fill		DIN EN 1049	10.2 / 9.8	yarns/cm
Yarn size Warp / Fill		DIN EN ISO 2060	1670 / 1670***	dtex

* according to EN 1990 with a fractile factor k_n = 2.33

** according to proposed classification in [SaP15] based on the measured tensile strength

*** manufacturer information

Material: **PES-PVC**

Material producer: **2**

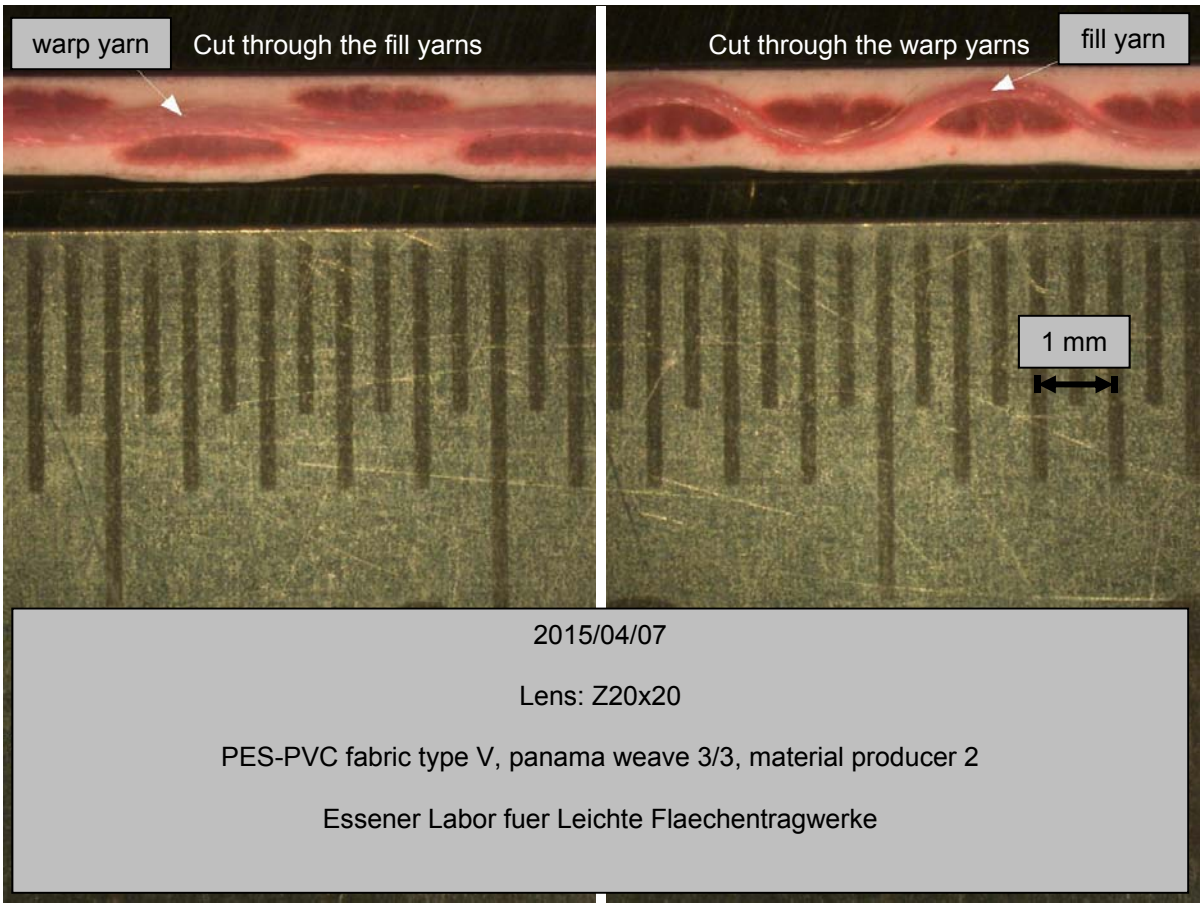

Property		Standard	Measured value	Unit
Tensile strength Warp / Fill	Mean	DIN EN ISO 1421 – strip method	208.7 / 188.8	kN/m
	5%-fractile*		198.4 / 176.4	
Type**		according to [SaP15]	V	-
Total weight		DIN EN ISO 2286-2	1594	g/m^2
Thickness		DIN EN ISO 2286-3	1.37	mm
Weave		-	Panama 3/3	-
Yarn density Warp / Fill		DIN EN 1049	13.8 / 13.5	yarns/cm
Yarn size Warp / Fill		DIN EN ISO 2060	2200 / 2200***	dtex

* according to EN 1990 with a fractile factor k_n = 2.33

** according to proposed classification in [SaP15] based on the measured tensile strength

*** manufacturer information

Material: **PES-PVC**

Material producer: **3**

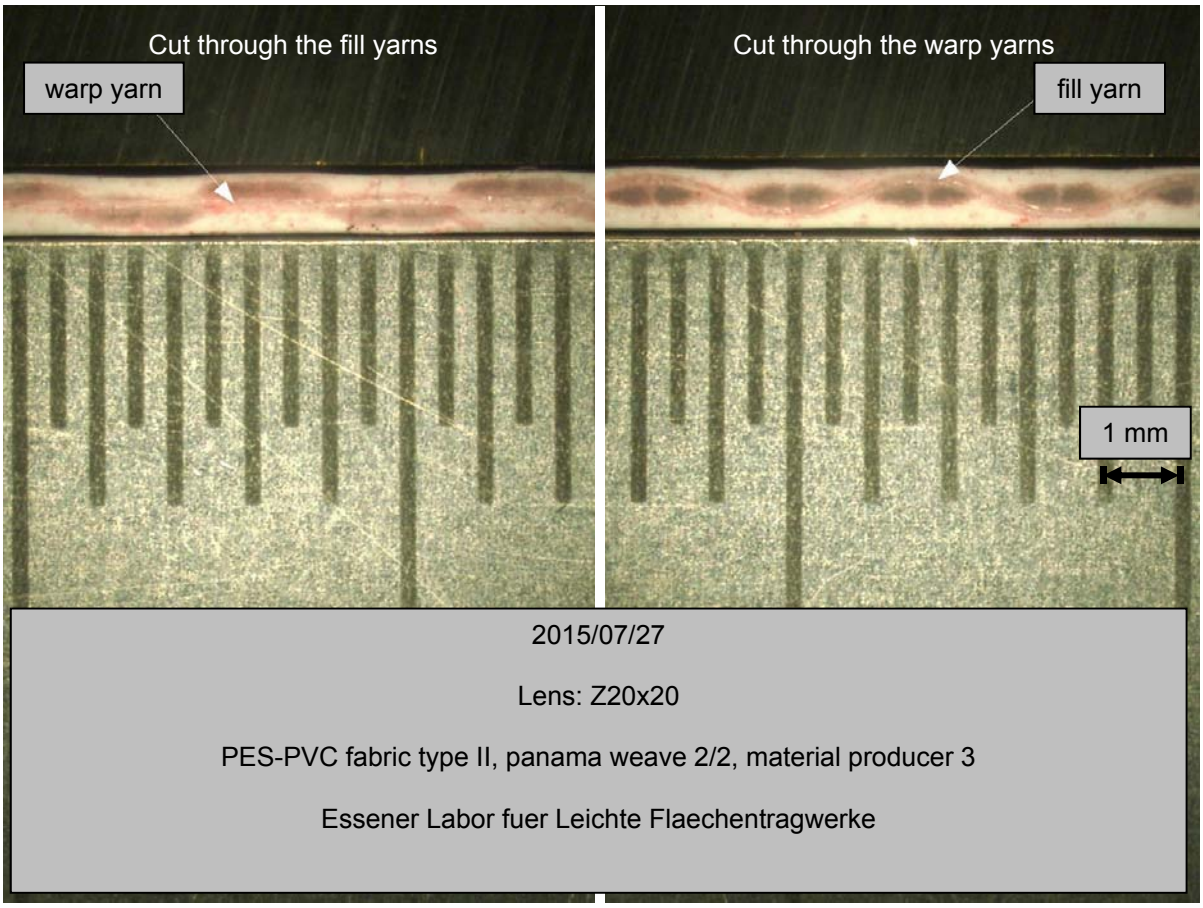

Property		Standard	Measured value	Unit
Tensile strength Warp/Fill	Mean	DIN EN ISO 1421 – strip method	87.5 / 92.6	kN/m
	5%-fractile*		80.1 / 82.0	
Type**		according to [SaP15]	II	-
Total weight		DIN EN ISO 2286-2	902	g/m^2
Thickness		DIN EN ISO 2286-3	0.77	mm
Weave		-	Panama 2/2	-
Yarn density Warp / Fill		DIN EN 1049	11.3 / 12.4	yarns/cm
Yarn size Warp / Fill		DIN EN ISO 2060	1100 / 1100***	dtex

* according to EN 1990 with a fractile factor k_n = 2.33

** according to proposed classification in [SaP15] based on the measured tensile strength

*** manufacturer information

Material: **PES-PVC**

Material producer: **3**

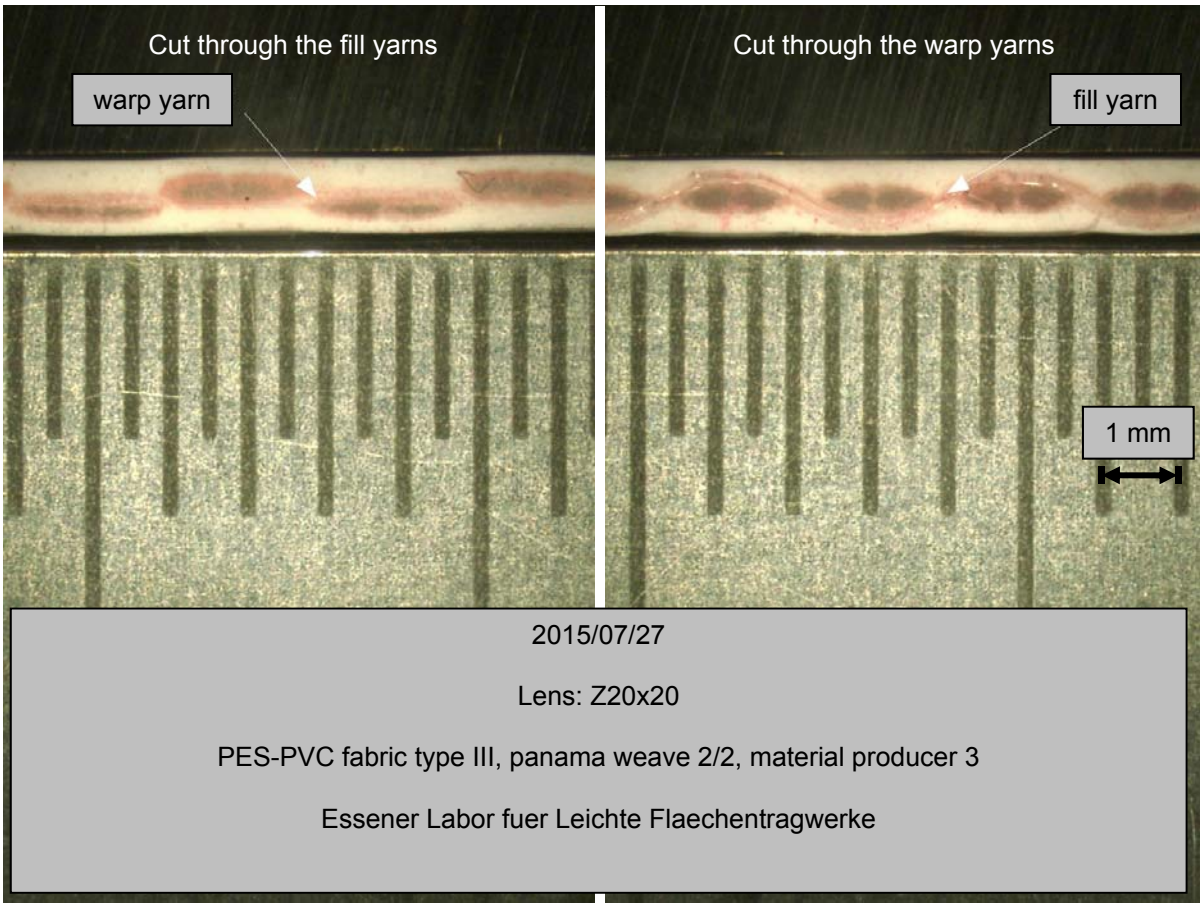

Property		Standard	Measured value	Unit
Tensile strength Warp/Fill	Mean	DIN EN ISO 1421 – strip method	129.4 / 120.2	kN/m
	5%-fractile*		126.0 / 113.7	
Type**		according to [SaP15]	III	-
Total weight		DIN EN ISO 2286-2	1078	g/m^2
Thickness		DIN EN ISO 2286-3	0.95	mm
Weave		-	Panama 2/2	-
Yarn density Warp / Fill		DIN EN 1049	10.8 / 10.5	yarns/cm
Yarn size Warp / Fill		DIN EN ISO 2060	1670 / 1670***	dtex

* according to EN 1990 with a fractile factor k_n = 2.33

** according to proposed classification in [SaP15] based on the measured tensile strength

*** manufacturer information

Material: **PES-PVC**

Material producer: **3**

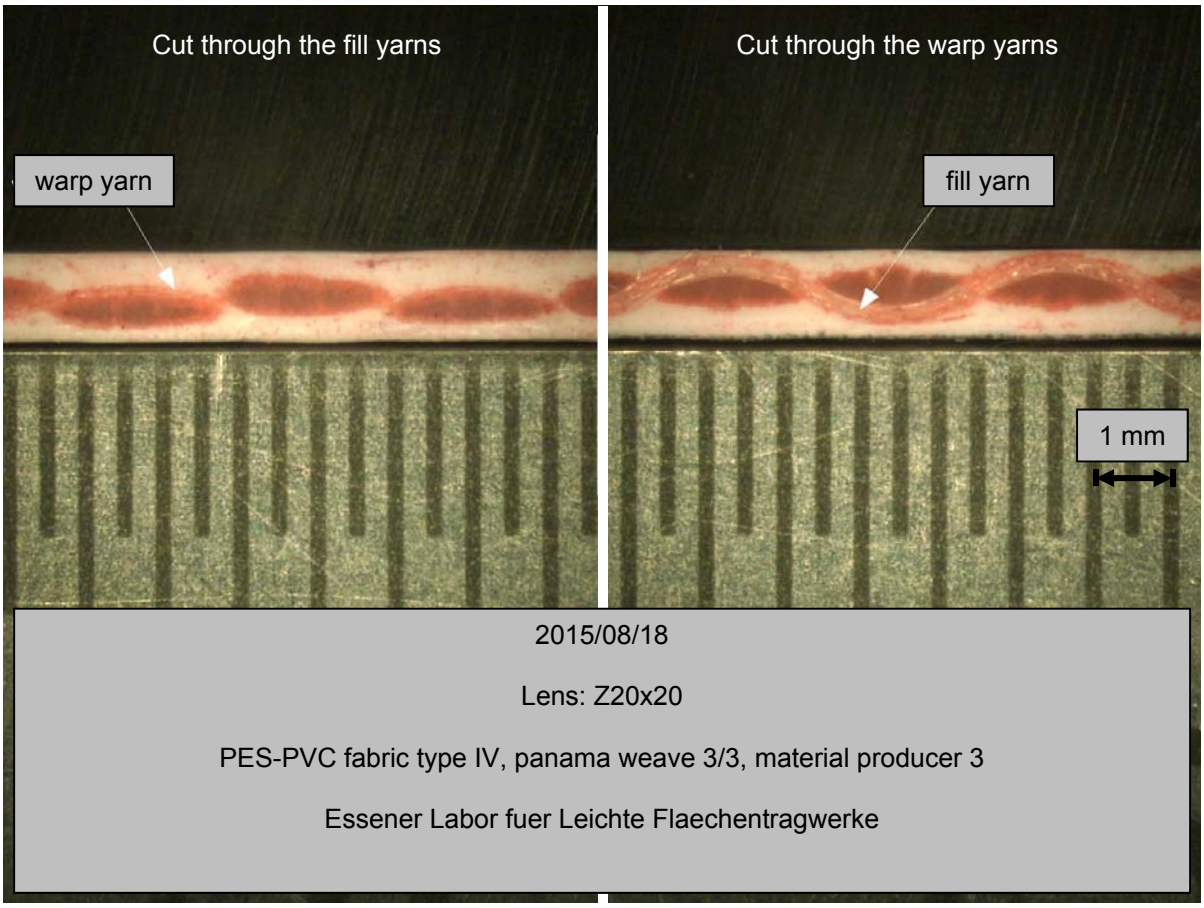

Property		Standard	Measured value	Unit
Tensile strength Warp/Fill	Mean	DIN EN ISO 1421 – strip method	167.9 / 160.6	kN/m
	5%-fractile*		161.2 / 152.7	
Type**		according to [SaP15]	IV	-
Total weight		DIN EN ISO 2286-2	1329	g/m^2
Thickness		DIN EN ISO 2286-3	1.16	mm
Weave		-	Panama 3/3	-
Yarn density Warp / Fill		DIN EN 1049	14.1 / 14.0	yarns/cm
Yarn size Warp / Fill		DIN EN ISO 2060	1670 / 1670***	dtex

* according to EN 1990 with a fractile factor k_n = 2.33

** according to proposed classification in [SaP15] based on the measured tensile strength

*** manufacturer information

Material: **PES-PVC**

Material producer: **4**

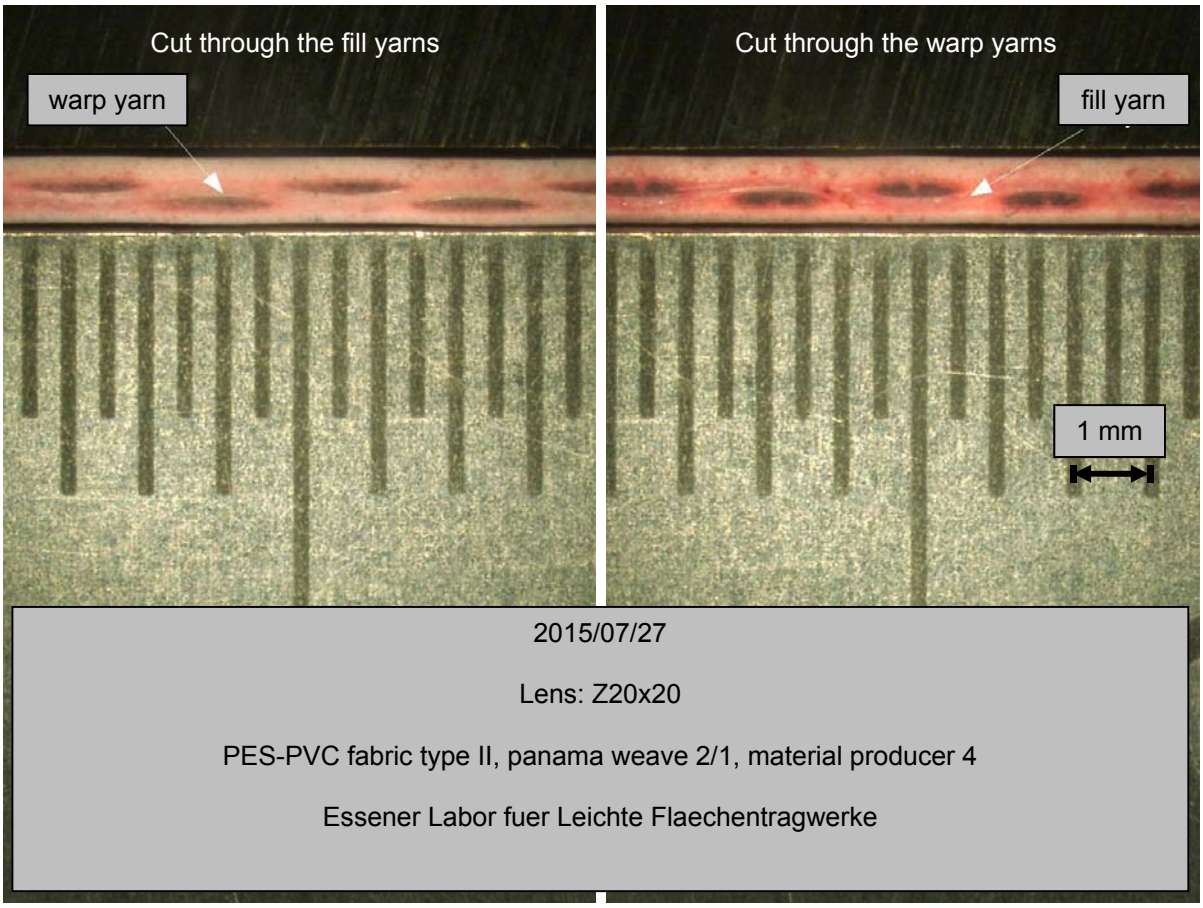

Property		Standard	Measured value	Unit
Tensile strength Warp / Fill	Mean	DIN EN ISO 1421 – strip method	87.6 / 83.8	kN/m
	5%-fractile*		82.7 / 75.0	
Type**		according to [SaP15]	II	-
Total weight		DIN EN ISO 2286-2	1051	g/m^2
Thickness		DIN EN ISO 2286-3	0.84	mm
Weave		-	Panama 2/1	-
Yarn density Warp / Fill		DIN EN 1049	11.4 / 5.8	yarns/cm
Yarn size Warp / Fill		DIN EN ISO 2060	1100 / 1100***	dtex

* according to EN 1990 with a fractile factor k_n = 2.33

** according to proposed classification in [SaP15] based on the measured tensile strength

*** manufacturer information

Material: **PES-PVC**

Material producer: **4**

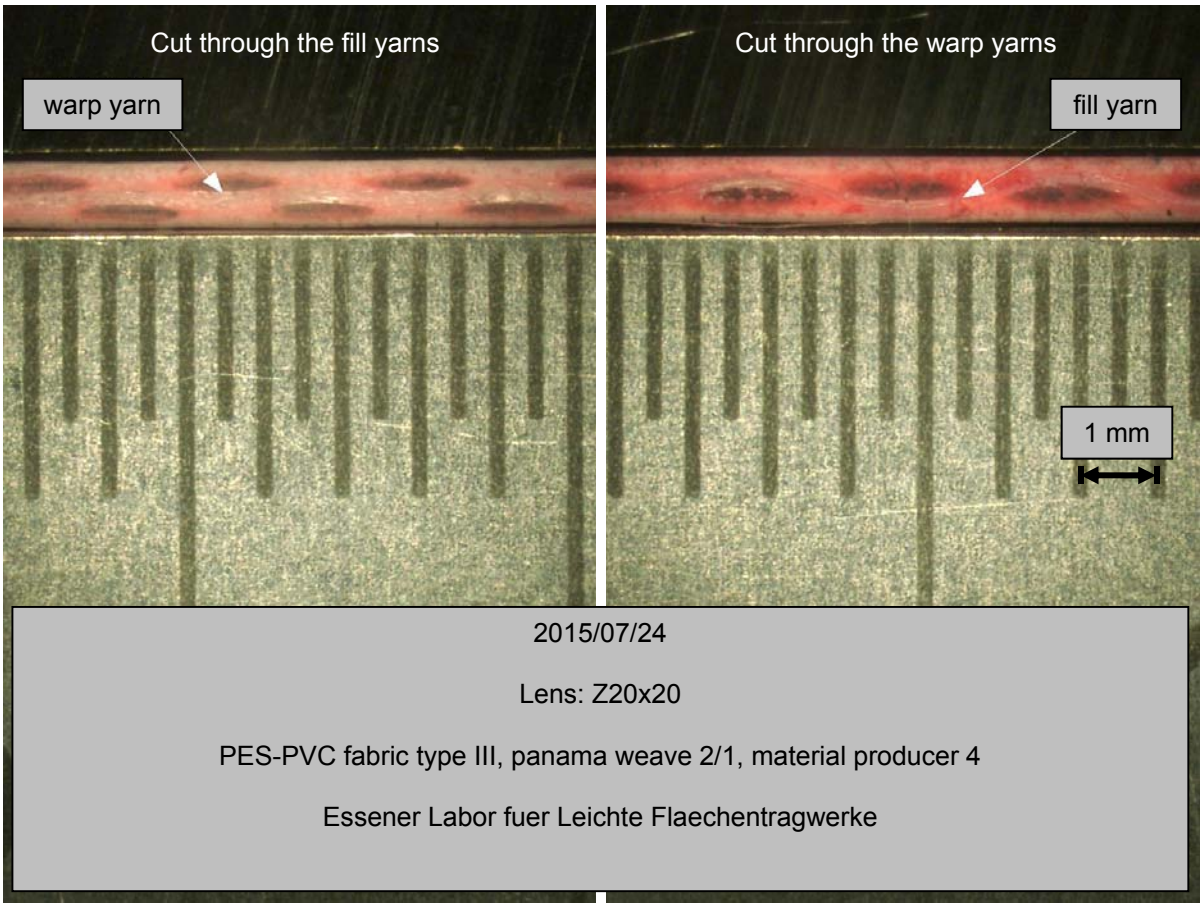

Property		Standard	Measured value	Unit
Tensile strength Warp / Fill	Mean	DIN EN ISO 1421 – strip method	116.4 / 118.2	kN/m
	5%-fractile*		110.4 / 114.9	
Type**		according to [SaP15]	III	-
Total weight		DIN EN ISO 2286-2	1053	g/m^2
Thickness		DIN EN ISO 2286-3	0.86	mm
Weave		-	Panama 2/1	-
Yarn density Warp / Fill		DIN EN 1049	9.6 / 8.0	yarns/cm
Yarn size Warp / Fill		DIN EN ISO 2060	1100 / 1670***	dtex

* according to EN 1990 with a fractile factor k_n = 2.33

** according to proposed classification in [SaP15] based on the measured tensile strength

*** manufacturer information

Material: **PES-PVC**

Material producer: **4**

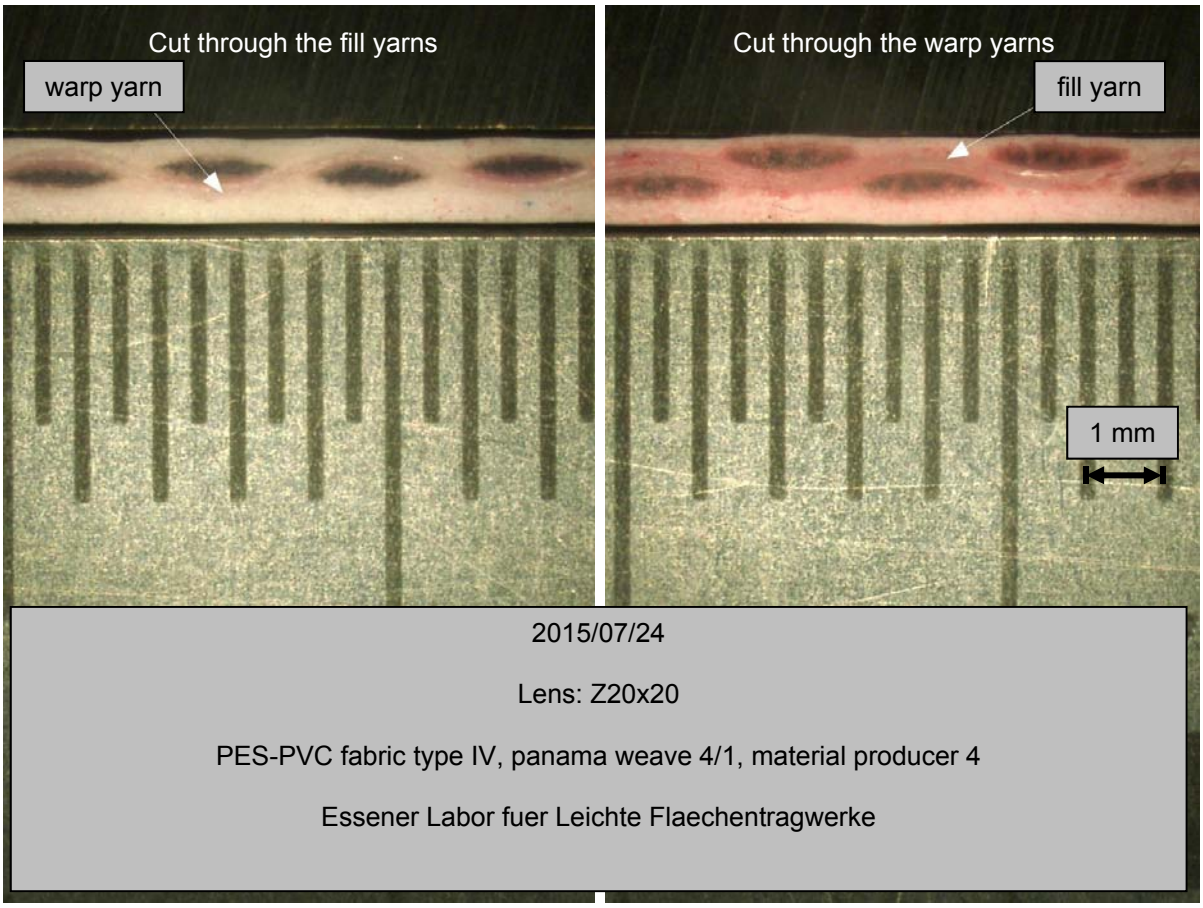

Property		Standard	Measured value	Unit
Tensile strength Warp / Fill	Mean	DIN EN ISO 1421 – strip method	169.1 / 144.2	kN/m
	5%-fractile*		164.3 / 135.8	
Type**		according to [SaP15]	IV	-
Total weight		DIN EN ISO 2286-2	1355	g/m^2
Thickness		DIN EN ISO 2286-3	1.08	mm
Weave		-	Panama 4/1	-
Yarn density Warp / Fill		DIN EN 1049	23.0 / 4.9	yarns/cm
Yarn size Warp / Fill		DIN EN ISO 2060	1100 / 2200***	dtex

* according to EN 1990 with a fractile factor k_n = 2.33

** according to proposed classification in [SaP15] based on the measured tensile strength

*** manufacturer information

Material: **Glass-PTFE**

Material producer: **5**

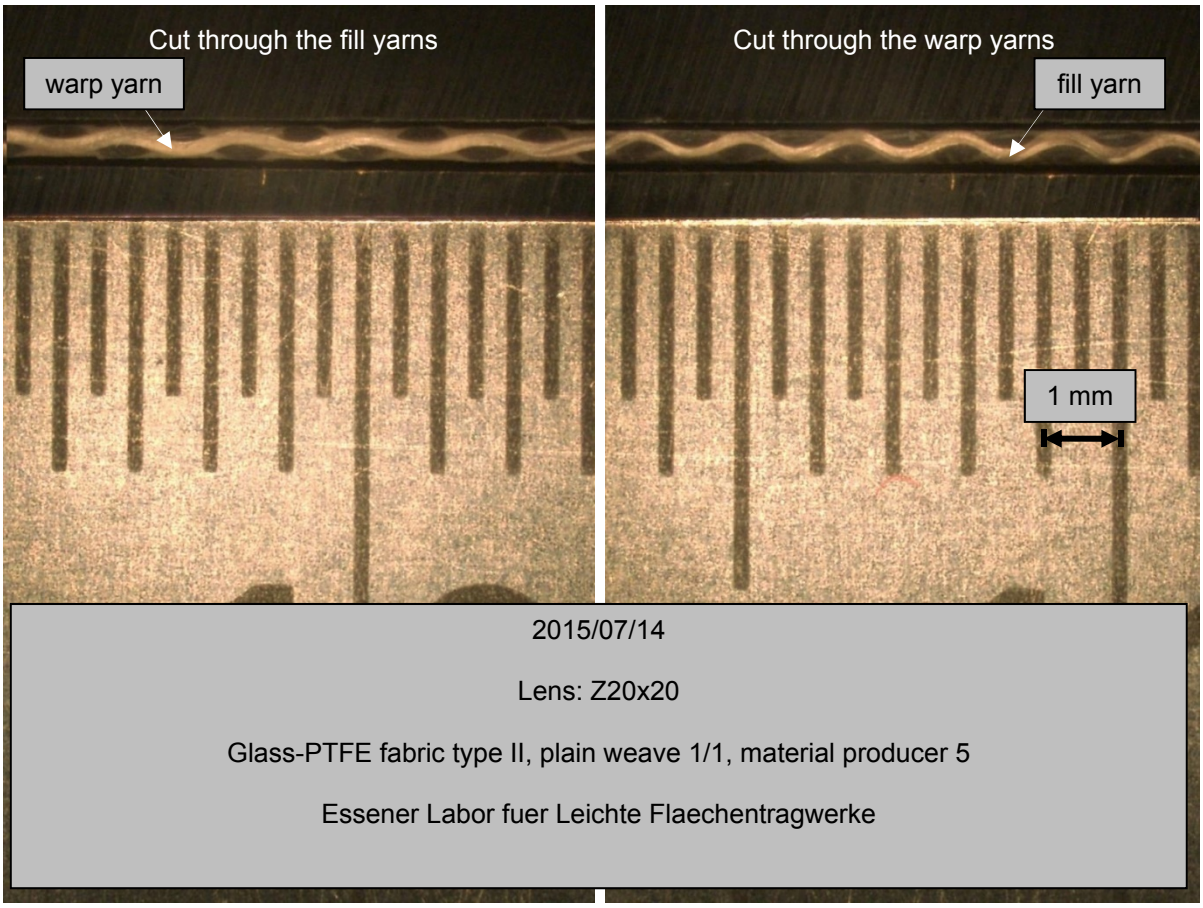

Property		Standard	Measured value	Unit
Tensile strength Warp / Fill	Mean	DIN EN ISO 1421 – strip method	117.2 / 122.8	kN/m
	5%-fractile*		113.3 / 116.5	
Type**		according to [SaP15]	II	-
Total weight		DIN EN ISO 2286-2	752	g/m^2
Thickness		DIN EN ISO 2286-3	0.46	mm
Weave		-	Plain weave 1/1	-
Yarn density Warp / Fill		DIN EN 1049	14.0 / 12.4	yarns/cm
Yarn size Warp / Fill		DIN EN ISO 2060	1360 / 1360***	dtex

* according to EN 1990 with a fractile factor k_n = 2.33

** according to proposed classification in [SaP15] based on the measured tensile strength

*** manufacturer information

Material: **Glass-PTFE**

Material producer: **5**

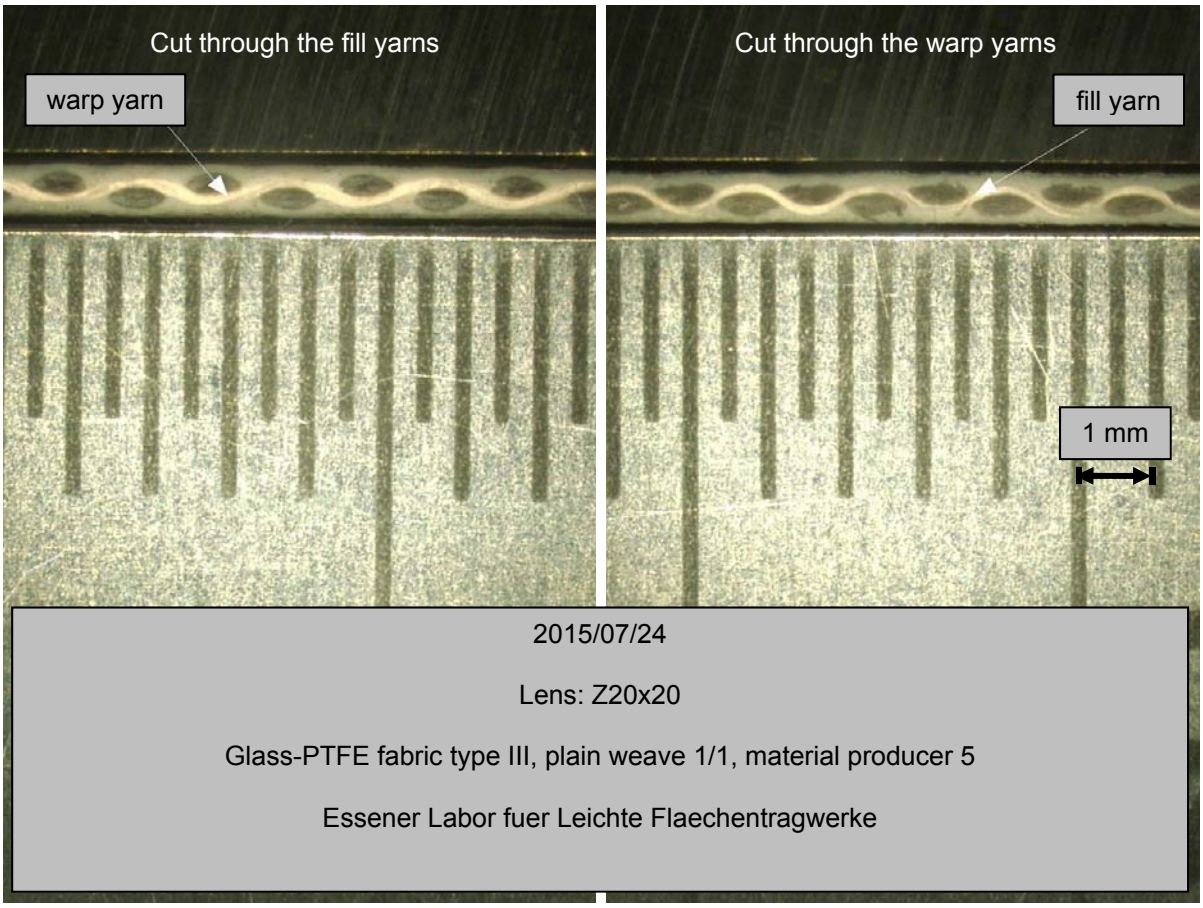

Property		Standard	Measured value	Unit
Tensile strength Warp / Fill	Mean	DIN EN ISO 1421 – strip method	142.9 / 120.3	kN/m
	5%-fractile*		129.9 / 110.2	
Type**		according to [SaP15]	III	-
Total weight		DIN EN ISO 2286-2	1195	g/m^2
Thickness		DIN EN ISO 2286-3	0.72	mm
Weave		-	Plain weave 1/1	-
Yarn density Warp / Fill		DIN EN 1049	12.2 / 10.1	yarns/cm
Yarn size Warp / Fill		DIN EN ISO 2060	2040 / 2040***	dtex

* according to EN 1990 with a fractile factor k_n = 2.33

** according to proposed classification in [SaP15] based on the measured tensile strength

*** manufacturer information

Material: **Glass-PTFE**

Material producer: **5**

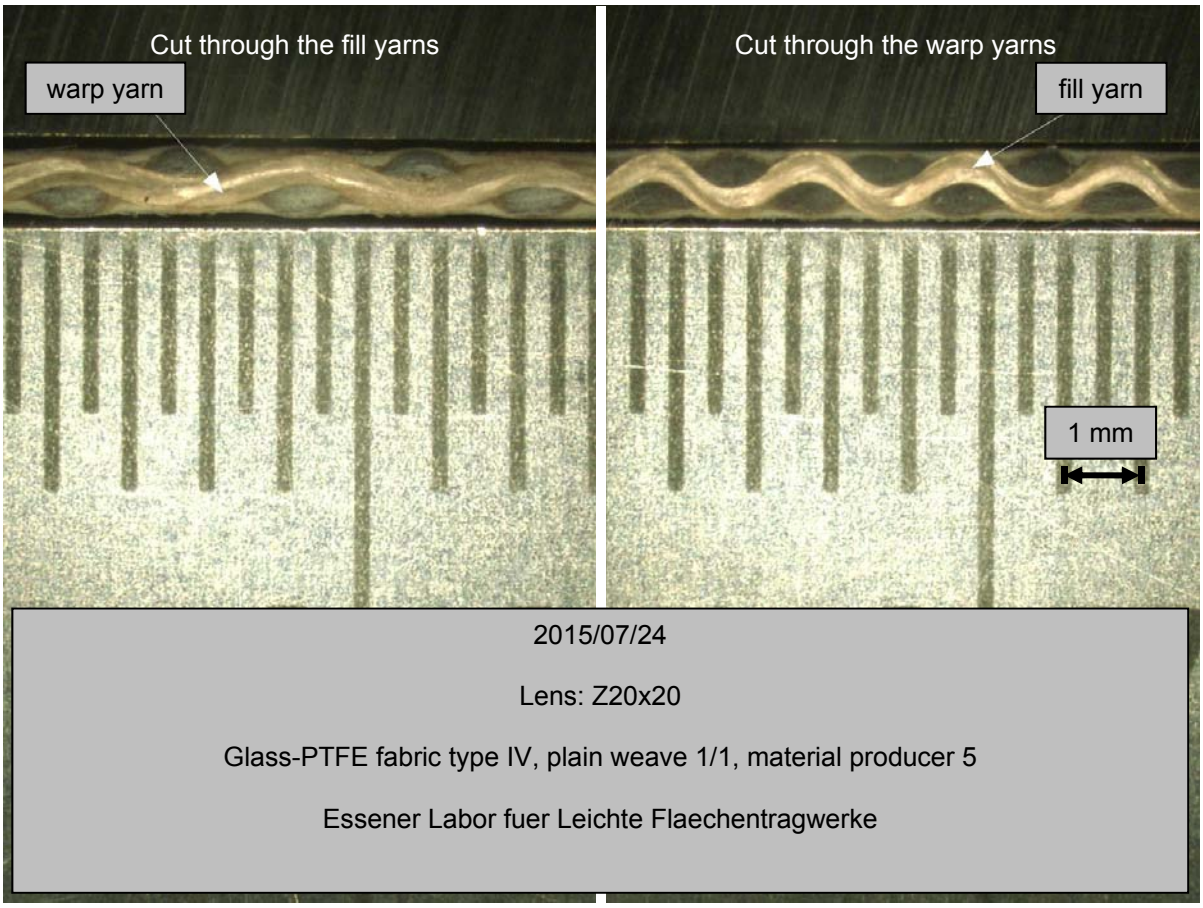

Property		Standard	Measured value	Unit
Tensile strength Warp / Fill	Mean	DIN EN ISO 1421 – strip method	201.6 / 172.7	kN/m
	5%-fractile*		196.4 / 163.8	
Type**		according to [SaP15]	IV	-
Total weight		DIN EN ISO 2286-2	1585	g/m^2
Thickness		DIN EN ISO 2286-3	0.94	mm
Weave		-	Plain weave 1/1	-
Yarn density Warp / Fill		DIN EN 1049	10.1 / 6.7	yarns/cm
Yarn size Warp / Fill		DIN EN ISO 2060	4080 / 4080***	dtex

* according to EN 1990 with a fractile factor k_n = 2.33

** according to proposed classification in [SaP15] based on the measured tensile strength

*** manufacturer information

Annex B

Fictitious elastic constants from MSAJ biaxial tests on PES-PVC and glass-PTFE fabrics

Table B1 Fictitious elastic constants from one MSAJ biaxial test on a PES-PVC fabric type II obtained using different determination options[1),2)]

Determination option (DO)		Tensile modulus [kN/m]		Poisson's ratio [-]		$\nu_{xy} \cdot \nu_{yx}$ [-]	Note
		E_x	E_y	ν_{xy}	ν_{yx}		
Material producer 1 – traditionally coated PES-PVC							
1	All stress ratios – 8 stress-strain paths	738	456	0.13	0.21	0.03 < 1 ✓	MSAJ original
2	All stress-ratios – 10 stress-strain paths	570	376	0.43	0.65	0.28 < 1 ✓	MSAJ modified
3	Two stress ratios: 1:1 / 2:1 – 4 stress-strain paths	696	444	0.14	0.22	0.03 < 1 ✓	practical approach (synclastic)
4	Two stress ratios: 1:1 / 1:2 – 4 stress-strain paths	736	466	0.12	0.19	0.02 < 1 ✓	practical approach (synclastic)
5	Two stress ratios: 1:0 / 2:1 – 4 stress-strain paths	656	256	0.30	0.77	0.23 < 1 ✓	practical approach (anticlastic)
6	Two stress ratios: 0:1 / 1:2 – 4 stress-strain paths	224	388	0.75	0.43	0.32 < 1 ✓	practical approach (anticlastic)
Material producer 2 – traditionally coated PES-PVC							
1	All stress ratios – 8 stress-strain paths	699	523	0.09	0.12	0.01 < 1 ✓	MSAJ original
2	All stress-ratios – 10 stress-strain paths	563	440	0.40	0.51	0.20 < 1 ✓	MSAJ modified
3	Two stress ratios: 1:1 / 2:1 – 4 stress-strain paths	623	475	0.13	0.17	0.02 < 1 ✓	practical approach (synclastic)
4	Two stress ratios: 1:1 / 1:2 – 4 stress-strain paths	680	522	0.10	0.13	0.01 < 1 ✓	practical approach (synclastic)
5	Two stress ratios: 1:0 / 2:1 – 4 stress-strain paths	646	307	0.28	0.59	0.17 < 1 ✓	practical approach (anticlastic)
6	Two stress ratios: 0:1 / 1:2 – 4 stress-strain paths	265	454	0.76	0.44	0.33 < 1 ✓	practical approach (anticlastic)

Table B1 continued (PES-PVC type II)

Material producer 3 – traditionally coated PES-PVC							
1	All stress ratios – 8 stress-strain paths	720	542	0.03	0.04	0 < 1 ✓	MSAJ original
2	All stress-ratios – 10 stress-strain paths	542	432	0.40	0.50	0.20 < 1 ✓	MSAJ modified
3	Two stress ratios: 1:1 / 2:1 – 4 stress-strain paths	614	482	0.11	0.14	0.02 < 1 ✓	practical approach (synclastic)
4	Two stress ratios: 1:1 / 1:2 – 4 stress-strain paths	720	542	0.03	0.04	0 < 1 ✓	practical approach (synclastic)
5	Two stress ratios: 1:0 / 2:1 – 4 stress-strain paths	628	298	0.27	0.57	0.15 < 1 ✓	practical approach (anticlastic)
6	Two stress ratios: 0:1 / 1:2 – 4 stress-strain paths	218	448	0.87	0.42	0.37 < 1 ✓	practical approach (anticlastic)
Material producer 4 – PES-PVC with biaxially prestressed coating system							
1	All stress ratios – 8 stress-strain paths	609	612	0.02	0.02	0 < 1 ✓	MSAJ original
2	All stress-ratios – 10 stress-strain paths	503	501	0.35	0.35	0.12 < 1 ✓	MSAJ modified
3	Two stress ratios: 1:1 / 2:1 – 4 stress-strain paths	591	591	0.02	0.02	0 < 1 ✓	practical approach (synclastic)
4	Two stress ratios: 1:1 / 1:2 – 4 stress-strain paths	550	552	0.10	0.10	0.01 < 1 ✓	practical approach (synclastic)
5	Two stress ratios: 1:0 / 2:1 – 4 stress-strain paths	549	359	0.30	0.46	0.14 < 1 ✓	practical approach (anticlastic)
6	Two stress ratios: 0:1 / 1:2 – 4 stress-strain paths	315	542	0.59	0.34	0.20 < 1 ✓	practical approach (anticlastic)

[1)] Fictitious elastic constants given in terms of the inverse stiffness formulation of the constitutive law

[2)] Least Squares Method minimising the strain error was used for evaluation

Table B2 Fictitious elastic constants from one MSAJ biaxial test on a PES-PVC fabric type III obtained using different determination options[1),2)]

Determination option (DO)		Tensile modulus [kN/m]		Poisson's ratio [-]		$\nu_{xy} \cdot \nu_{yx}$ [-]	Note
		E_x	E_y	ν_{xy}	ν_{yx}		
Material producer 1 – traditionally coated PES-PVC							
1	All stress ratios – 8 stress-strain paths	972	646	0.10	0.15	0.01 < 1 ✓	MSAJ original
2	All stress-ratios – 10 stress-strain paths	738	516	0.47	0.67	0.31 < 1 ✓	MSAJ modified
3	Two stress ratios: 1:1 / 2:1 – 4 stress-strain paths	882	566	0.16	0.25	0.04 < 1 ✓	practical approach (synclastic)
4	Two stress ratios: 1:1 / 1:2 – 4 stress-strain paths	1044	644	0.08	0.13	0.01 < 1 ✓	practical approach (synclastic)
5	Two stress ratios: 1:0 / 2:1 – 4 stress-strain paths	822	292	0.33	0.93	0.31 < 1 ✓	practical approach (anticlastic)
6	Two stress ratios: 0:1 / 1:2 – 4 stress-strain paths	300	554	0.82	0.44	0.36 < 1 ✓	practical approach (anticlastic)
Material producer 2 – traditionally coated PES-PVC							
1	All stress ratios – 8 stress-strain paths	963	644	0.06	0.09	0.01 < 1 ✓	MSAJ original
2	All stress-ratios – 10 stress-strain paths	725	529	0.41	0.56	0.23 < 1 ✓	MSAJ modified
3	Two stress ratios: 1:1 / 2:1 – 4 stress-strain paths	871	601	0.09	0.13	0.01 < 1 ✓	practical approach (synclastic)
4	Two stress ratios: 1:1 / 1:2 – 4 stress-strain paths	972	650	0.06	0.09	0.01 < 1 ✓	practical approach (synclastic)
5	Two stress ratios: 1:0 / 2:1 – 4 stress-strain paths	819	309	0.29	0.77	0.22 < 1 ✓	practical approach (anticlastic)
6	Two stress ratios: 0:1 / 1:2 – 4 stress-strain paths	286	553	0.82	0.42	0.34 < 1 ✓	practical approach (anticlastic)

Table B2 continued (PES-PVC type III)

Material producer 3 – traditionally coated PES-PVC							
1	All stress ratios – 8 stress-strain paths	972	646	0	0	0 < 1 ✓	MSAJ original
2	All stress-ratios – 10 stress-strain paths	708	478	0.42	0.62	0.26 < 1 ✓	MSAJ modified
3	Two stress ratios: 1:1 / 2:1 – 4 stress-strain paths	886	544	0.08	0.13	0.01 < 1 ✓	practical approach (synclastic)
4	Two stress ratios: 1:1 / 1:2 – 4 stress-strain paths	906	602	0.06	0.09	0.01 < 1 ✓	practical approach (synclastic)
5	Two stress ratios: 1:0 / 2:1 – 4 stress-strain paths	776	228	0.32	1.09	0.35 < 1 ✓	practical approach (anticlastic)
6	Two stress ratios: 0:1 / 1:2 – 4 stress-strain paths	256	520	0.86	0.42	0.36 < 1 ✓	practical approach (anticlastic)
Material producer 4 – PES-PVC with biaxially prestressed coating system							
1	All stress ratios – 8 stress-strain paths	826	720	0.07	0.08	0.01 < 1 ✓	MSAJ original
2	All stress-ratios – 10 stress-strain paths	660	594	0.47	0.52	0.24 < 1 ✓	MSAJ modified
3	Two stress ratios: 1:1 / 2:1 – 4 stress-strain paths	750	747	0.09	0.09	0.01 < 1 ✓	practical approach (synclastic)
4	Two stress ratios: 1:1 / 1:2 – 4 stress-strain paths	720	718	0.14	0.14	0.02 < 1 ✓	practical approach (synclastic)
5	Two stress ratios: 1:0 / 2:1 – 4 stress-strain paths	777	496	0.28	0.44	0.12 < 1 ✓	practical approach (anticlastic)
6	Two stress ratios: 0:1 / 1:2 – 4 stress-strain paths	249	600	1.00	0.41	0.41 < 1 ✓	practical approach (anticlastic)

[1)] Fictitious elastic constants given in terms of the inverse stiffness formulation of the constitutive law

[2)] Least Squares Method minimising the strain error was used for evaluation

Table B3 Fictitious elastic constants from one MSAJ biaxial test on a PES-PVC fabric type IV obtained using different determination options[1),2)]

Determination option (DO)		Tensile modulus [kN/m]		Poisson's ratio [-]		$\nu_{xy} \cdot \nu_{yx}$ [-]	Note
		E_x	E_y	ν_{xy}	ν_{yx}		
Material producer 1 – traditionally coated PES-PVC							
1	All stress ratios – 8 stress-strain paths	1274	786	0.08	0.13	0.01 < 1 ✓	MSAJ original
2	All stress-ratios – 10 stress-strain paths	926	620	0.47	0.70	0.33 < 1 ✓	MSAJ modified
3	Two stress ratios: 1:1 / 2:1 – 4 stress-strain paths	1130	712	0.12	0.19	0.02 < 1 ✓	practical approach (synclastic)
4	Two stress ratios: 1:1 / 1:2 – 4 stress-strain paths	1260	776	0.08	0.13	0.01 < 1 ✓	practical approach (synclastic)
5	Two stress ratios: 1:0 / 2:1 – 4 stress-strain paths	1036	332	0.32	1.00	0.32 < 1 ✓	practical approach (anticlastic)
6	Two stress ratios: 0:1 / 1:2 – 4 stress-strain paths	332	658	0.90	0.45	0.41 < 1 ✓	practical approach (anticlastic)
Material producer 3 – traditionally coated PES-PVC							
1	All stress ratios – 8 stress-strain paths	1222	812	0.02	0.03	0 < 1 ✓	MSAJ original
2	All stress-ratios – 10 stress-strain paths	890	596	0.45	0.67	0.30 < 1 ✓	MSAJ modified
3	Two stress ratios: 1:1 / 2:1 – 4 stress-strain paths	1116	742	0.06	0.09	0.01 < 1 ✓	practical approach (synclastic)
4	Two stress ratios: 1:1 / 1:2 – 4 stress-strain paths	1222	812	0.02	0.03	0 < 1 ✓	practical approach (synclastic)
5	Two stress ratios: 1:0 / 2:1 – 4 stress-strain paths	980	296	0.32	1.06	0.34 < 1 ✓	practical approach (anticlastic)
6	Two stress ratios: 0:1 / 1:2 – 4 stress-strain paths	266	642	1.05	0.43	0.45 < 1 ✓	practical approach (anticlastic)

Table B3 continued (PES-PVC type IV)

Material producer 4 – PES-PVC with biaxially prestressed coating system							
1	All stress ratios – 8 stress-strain paths	951	955	0.13	0.13	0.02 < 1 ✓	MSAJ original
2	All stress-ratios – 10 stress-strain paths	691	715	0.70	0.68	0.48 < 1 ✓	MSAJ modified
3	Two stress ratios: 1:1 / 2:1 – 4 stress-strain paths	833	772	0.24	0.26	0.06 < 1 ✓	practical approach (synclastic)
4	Two stress ratios: 1:1 / 1:2 – 4 stress-strain paths	900	898	0.16	0.16	0.03 < 1 ✓	practical approach (synclastic)
5	Two stress ratios: 1:0 / 2:1 – 4 stress-strain paths	712	272	0.45	1.18	0.53 < 1 ✓	practical approach (anticlastic)
6	Two stress ratios: 0:1 / 1:2 – 4 stress-strain paths	399	839	0.85	0.40	0.34 < 1 ✓	practical approach (anticlastic)

[1)] Fictitious elastic constants given in terms of the inverse stiffness formulation of the constitutive law

[2)] Least Squares Method minimising the strain error was used for evaluation

Table B4 Fictitious elastic constants from one MSAJ biaxial test on a PES-PVC fabric type V obtained using different determination options[1),2)]

Determination option (DO)		Tensile modulus [kN/m]		Poisson's ratio [-]		$\nu_{xy}\cdot\nu_{yx}$ [-]	Note
		E_x	E_y	ν_{xy}	ν_{yx}		
Material producer 2 – traditionally coated PES-PVC							
1	All stress ratios – 8 stress-strain paths	1437	955	0.10	0.15	0.02 < 1 ✓	MSAJ original
2	All stress-ratios – 10 stress-strain paths	1067	676	0.61	0.96	0.59 < 1 ✓	MSAJ modified
3	Two stress ratios: 1:1 / 2:1 – 4 stress-strain paths	1390	844	0.14	0.23	0.03 < 1 ✓	practical approach (synclastic)
4	Two stress ratios: 1:1 / 1:2 – 4 stress-strain paths	1600	928	0.11	0.19	0.03 < 1 ✓	practical approach (synclastic)
5	Two stress ratios: 1:0 / 2:1 – 4 stress-strain paths	1118	490	0.49	1.12	0.55 < 1 ✓	practical approach (anticlastic)
6	Two stress ratios: 0:1 / 1:2 – 4 stress-strain paths	357	727	1.11	0.54	0.60 < 1 ✓	practical approach (anticlastic)

[1)] Fictitious elastic constants given in terms of the inverse stiffness formulation of the constitutive law

[2)] Least Squares Method minimising the strain error was used for evaluation

Table B5 Fictitious elastic constants from one MSAJ biaxial test on a glass-PTFE fabric type II obtained using different determination options[1),2)]

Determination option (DO)		Tensile modulus [kN/m]		Poisson's ratio [-]		$\nu_{xy} \cdot \nu_{yx}$ [-]	Note
		E_x	E_y	ν_{xy}	ν_{yx}		
Material producer 5 – glass-PTFE							
1	All stress ratios – 8 stress-strain paths	1060	529	0.60	1.20	0.72 < 1 ✓	MSAJ original
2	All stress-ratios – 10 stress-strain paths	701	414	0.90	1.52	1.37 > 1 ↯	MSAJ modified
3	Two stress ratios: 1:1 / 2:1 – 4 stress-strain paths	1440	660	0.49	1.07	0.52 < 1 ✓	practical approach (synclastic)
4	Two stress ratios: 1:1 / 1:2 – 4 stress-strain paths	1038	544	0.62	1.18	0.73 < 1 ✓	practical approach (synclastic)
5	Two stress ratios: 1:0 / 2:1 – 4 stress-strain paths	799	195	0.49	2.01	0.98 < 1 ✓	practical approach (anticlastic)
6	Two stress ratios: 0:1 / 1:2 – 4 stress-strain paths	208	431	1.34	0.64	0.86 < 1 ✓	practical approach (anticlastic)

[1)] Fictitious elastic constants given in terms of the inverse stiffness formulation of the constitutive law

[2)] Least Squares Method minimising the strain error was used for evaluation

Table B6 Fictitious elastic constants from one MSAJ biaxial test on a glass-PTFE fabric type III obtained using different determination options[1),2)]

Determination option (DO)		Tensile modulus [kN/m]		Poisson's ratio [-]		$\nu_{xy}\cdot\nu_{yx}$ [-]	Note
		E_x	E_y	ν_{xy}	ν_{yx}		
Material producer 5 – glass-PTFE							
1	All stress ratios – 8 stress-strain paths	1292	816	0.57	0.90	0.51 < 1 ✓	MSAJ original
2	All stress-ratios – 10 stress-strain paths	914	610	0.83	1.24	1.03 > 1 ↯	MSAJ modified
3	Two stress ratios: 1:1 / 2:1 – 4 stress-strain paths	1870	1024	0.45	0.82	0.37 < 1 ✓	practical approach (synclastic)
4	Two stress ratios: 1:1 / 1:2 – 4 stress-strain paths	1336	824	0.60	0.97	0.58 < 1 ✓	practical approach (synclastic)
5	Two stress ratios: 1:0 / 2:1 – 4 stress-strain paths	878	228	0.48	1.85	0.89 < 1 ✓	practical approach (anticlastic)
6	Two stress ratios: 0:1 / 1:2 – 4 stress-strain paths	318	680	1.34	0.62	0.83 < 1 ✓	practical approach (anticlastic)

[1)] Fictitious elastic constants given in terms of the inverse stiffness formulation of the constitutive law

[2)] Least Squares Method minimising the strain error was used for evaluation

Table B7 Fictitious elastic constants from one MSAJ biaxial test on a glass-PTFE fabric type IV obtained using different determination options[1),2)]

Determination option (DO)		Tensile modulus [kN/m]		Poisson's ratio [-]		$\nu_{xy}\cdot\nu_{yx}$ [-]	Note
		E_x	E_y	ν_{xy}	ν_{yx}		
Material producer 5 – glass-PTFE							
1	All stress ratios – 8 stress-strain paths	1451	679	0.53	1.13	0.60 < 1 ✓	MSAJ original
2	All stress-ratios – 10 stress-strain paths	976	550	0.77	1.37	1.05 > 1 ↯	MSAJ modified
3	Two stress ratios: 1:1 / 2:1 – 4 stress-strain paths	2207	791	0.42	1.17	0.49 < 1 ✓	practical approach (synclastic)
4	Two stress ratios: 1:1 / 1:2 – 4 stress-strain paths	1458	678	0.55	1.18	0.65 < 1 ✓	practical approach (synclastic)
5	Two stress ratios: 1:0 / 2:1 – 4 stress-strain paths	964	209	0.47	2.17	1.02 > 1 ↯	practical approach (anticlastic)
6	Two stress ratios: 0:1 / 1:2 – 4 stress-strain paths	400	604	1.08	0.71	0.77 < 1 ✓	practical approach (anticlastic)

[1)] Fictitious elastic constants given in terms of the inverse stiffness formulation of the constitutive law

[2)] Least Squares Method minimising the strain error was used for evaluation